

**The impact of surfaces on the self-assembly and other
molecular interactions of the amyloid β peptide**

Liam Aubrey

A thesis submitted for the degree of Doctor of Philosophy

September 2018

Department of Molecular Biology and Biotechnology

University of Sheffield

Abstract

The self-assembly of the amyloid β peptide ($A\beta$) into amyloid fibrils results in amyloid plaques in the brains of patients with Alzheimer's disease (AD). Other molecular interactions by $A\beta$ have been identified as contributing to toxicity in AD.

The human protein Cystatin C (hCC) has previously been identified as an inhibitor of both fibril formation and toxicity by $A\beta$ using *in vitro* and *in vivo* experiments. Previous work *in vitro* however indicated that hCC would bind $A\beta$ only when $A\beta$ was immobilised at a surface. It was therefore hypothesised that hCC interacts primarily with $A\beta$ *in vivo* when at a surface. The most likely surface available *in vivo* was suggested to be lipid bilayers in the cell membrane.

In this study, the self-assembly by $A\beta$ to form amyloid fibrils was shown to be dependent on the available surfaces. Fibril formation time course data show that commonly used commercial microplates catalyse the formation of fibrils. In more inert glass and quartz glass surfaces, the reaction was slower but involved a rate-determining saturable process in which fibril formation was catalysed by the air water interface, the removal of which resulted in no fibril formation. The specific interactions between $A\beta$ and these surfaces was probed further by atomic force microscopy (AFM) revealing specific mechanisms of catalysis in the commercial microplates.

The interaction between $A\beta$ and lipid bilayers was investigated using fibril formation and bilayer permeation time courses, transmission electron microscopy (TEM) and asymmetric flow field flow fractionation (AF4) coupled with ultra-violet (UV) absorbance spectroscopy and multi-angled light scattering (MALS). These data revealed catalysis of $A\beta$ fibril formation by lipid bilayers using a mechanism involving an increased rate of nucleation.

Using a combination of fluorescence spectroscopy and AFM, hCC was shown to inhibit fibril formation as well as $A\beta$ induced lipid bilayer permeation independently of lipid bilayers, suggesting a mechanism by which it can inhibit toxicity *in vivo*. Inhibition of fibril formation by hCC was shown to be dependent on conditions where $A\beta$ fibril formation is either slow or $A\beta$ is immobilised for a significant amount of time at a surface. Therefore, hCC likely interacts with a transient $A\beta$ species.

Finally, TEM studies show that the fibril morphologies formed by $A\beta$ species are dependent on the ionic strength of the solution in which they are formed. Ionic strength can significantly affect the rate of different processes involved in the self-assembly reaction resulting in different observable morphologies.

Acknowledgements

The very first person I would like to acknowledge is Dr Rosie Staniforth for giving me this opportunity and for all of the support over the last 4 years. I was fortunate to find a supervisor that I will only ever have good things to say about.

Secondly, Professor Arwen Pearson, my former supervisor for my final year undergraduate project at the university of Leeds. I haven't had any direct contact with Arwen recently but the belief that she showed in me is the reason I was able to write this thesis and that belief will always be something I can remember with fondness.

Dr Jeremy Craven and Dr Pat Baker were instrumental in leading me in the right direction. Their advice often came at critical moments during my PhD which I greatly appreciate.

Professor Jamie Hobbs who was my co-supervisor, and Dr Nic Mullins have been excellent resources of guidance, especially for anything AFM related.

Everybody needs friends and I think that, after 4 years of working together and 3 years of living together, I have developed a solid friendship with Gus Robertson. Thank you, Gus, for the occasional useful advice and the fun times, but also the awful jokes and the ever present unnecessary pedantry. We all need someone to vent at sometimes.

Thank you also to the other previous inhabitants of 11 melbourn road. Jake, Helen and Henry have all been ideal housemates and I have had the best time living in that house.

It has been an absolute joy to have worked with Alex Taylor over the last few years, it will be to nobody's surprise if Alex goes on to do some amazing work. Abi, Sirwan, Pete and Amy as Staniforth group members have all contributed advice which has helped in many ways. I would also like to acknowledge the contributions of the many undergraduate students that I have supervised in the lab, In particular Josh and Zoe. The NMR group members that I haven't already mentioned elsewhere Claire, Nicky, Mike, Andrea, Callum, Luke, Mahreen, Maryam, Aaron and Yash also deserve praise for their contributions to lab talk and Friday cake.

Probably the most important contributions came from the unconditional, ever-loving support of my Mum, Wendy and my Dad, Keith, as well as the support from my sister and brother in-law Ami and James. Thank you all for being terrific. I couldn't ask for a better family.

Last and most certainly not least, I would like to thank Sarah Nibloe. Thank you, Sarah, for making me happier than I have ever been.

Contents

| | |
|---|----|
| Chapter 1: Introduction | 1 |
| 1.1 Alzheimer's Disease | 1 |
| 1.2 The role of the amyloid β peptide in Alzheimer's disease. | 1 |
| 1.2.1 Amyloid formation in Alzheimer's disease | 1 |
| 1.2.2 The amyloid hypothesis of Alzheimer's disease | 2 |
| 1.2.3 Structural models of A β amyloids | 3 |
| 1.2.4 A kinetic model for the assembly of A β amyloid fibrils. | 6 |
| 1.2.5 Oligomers in Alzheimer's disease | 8 |
| 1.3 Toxicity in Alzheimer's disease | 10 |
| 1.3.1 Membrane Permeation | 10 |
| 1.3.2 Receptor mediated toxicity | 15 |
| 1.3.3 Tau hyperphosphorylation | 18 |
| 1.3.4 Intracellular A β activity | 20 |
| 1.4 Cell membrane constituents and AD | 21 |
| 1.4.1 Cholesterol | 21 |
| 1.4.2 Gangliosides | 24 |
| 1.4.2 Cell membrane structure and AD | 25 |
| 1.5 Human Cystatin C and AD | 26 |
| 1.5.1 <i>In vivo</i> hCC and AD | 27 |
| 1.5.2 <i>In vitro</i> hCC and A β | 27 |
| 1.6 Conclusions | 34 |
| 1.7 Thesis overview | 35 |
| | |
| Chapter 2: Materials and Methods | 36 |
| 2.1 Buffers and Reagents | 36 |
| 2.2 Aβ1-42 preparation | 36 |
| 2.2.1 Monomer protocol 1 | 36 |
| 2.2.2 Monomer protocol 2 | 36 |
| 2.3 Human Cystatin C preparation | 36 |
| 2.3.1 Growth media and solutions | 36 |
| 2.3.2 Preparation of competent cells | 39 |
| 2.3.3 Transformations | 39 |
| 2.3.4 Plasmid production | 39 |
| 2.3.5 DNA sequencing | 39 |
| 2.3.6 Over-expression | 40 |
| 2.3.7 Periplasmic extraction | 40 |
| 2.3.8 Cation exchange chromatography | 40 |
| 2.3.9 Size exclusion chromatography | 40 |
| 2.3.10 SDS polyacrylamide gel electrophoresis | 42 |
| 2.3.11 Determination of protein concentration | 43 |
| 2.4 Lipid handling | 43 |
| 2.4.1 Preparation of lipid stocks | 43 |
| 2.4.2 Preparation of LUVs and SUVs | 43 |
| 2.4.3 SLB formation | 44 |
| 2.5 Transmission electron microscopy | 44 |
| 2.6 Atomic force microscopy | 44 |

| | |
|--|----|
| 2.7 Asymmetric force field flow fractionation (AF4) | 44 |
| 2.8 Vesicle quality control | 46 |
| 2.9 Thioflavin T assays | 47 |
| 2.10 Dye release assays | 49 |
| 2.11 Data analysis | 50 |
| | |
| Chapter 3: Aβ1-42 interactions are surface dependent. | 51 |
| 3.1 Introduction | 51 |
| 3.2 Methods | 52 |
| 3.2.1 Dye release assay | 52 |
| 3.2.2 Thioflavin T assay | 52 |
| 3.2.3 Electron Microscopy | 53 |
| 3.2.4 Atomic force microscopy | 53 |
| 3.3 Results | 54 |
| 3.3.1 A β 1-42 doesn't damage lipid bilayers in a polystyrene microplate | 54 |
| 3.3.2 Amyloid fibril formation in a polystyrene microplate results in a loss of roughly 1 μ M of monomer equivalent A β 1-42 | 58 |
| 3.3.3 A β 1-42 amyloid formation is catalysed by polystyrene and low-binding microplates | 60 |
| 3.3.4 Removing the air water interface slows the rate of amyloid formation. | 63 |
| 3.3.5 A β 1-42 forms a nucleated film on a polystyrene surface | 64 |
| 3.3.6 Different nuclei of A β 1-42 form on different surfaces | 65 |
| 3.3.7 A β 1-42 amyloid fibril formation can nucleate on the surface of lipid bilayers in a polystyrene microplate | 70 |
| 3.3.8 A β 1-42 can disrupt a supported lipid bilayer | 72 |
| 3.4 Discussion | 74 |
| 3.4.1 LUVs could rupture to form a supported lipid bilayer in a low-binding microplate | 74 |
| 3.4.2 A β fibrillisation occurs independently of lipid bilayer damage in polystyrene microplates | 74 |
| 3.4.3 A β fibrillisation is dependent on the surface | 76 |
| | |
| Chapter 4: Investigating methods for observing the impact of lipid bilayers on Aβ interactions, whilst mitigating the effects of competing surfaces. | 78 |
| 4.1 Introduction | 78 |
| 4.2 Methods | 80 |
| 4.2.1 CF encapsulating LUV preparation | 80 |
| 4.2.2 A β 1-42 peptide preparation | 80 |
| 4.2.3 CF leakage | 81 |
| 4.2.4 Imaging the base of a microplate well by AFM | 81 |
| 4.2.5 A β 1-42 peptide fibrillisation on a lipid coated microplate | 82 |
| 4.2.6 A β 1-42 and buffer as washes for a lipid coated microplate | 82 |
| 4.3 Results and discussion | 82 |
| 4.3.1 Dye release profiles show rapid vesicle rupture in low binding microplates | 82 |
| 4.3.2 Removing the base of a microplate well resulted in debris on the surface making it unusable for AFM | 84 |

| | |
|--|-----|
| 4.3.3 Further additions of LUVs suggest SLB formation in low binding microplates | 84 |
| 4.3.4 Washing the microplate with A β 1-42 does not result in the disruption of the SLB | 89 |
| 4.3.5 A β 1-42 peptide fibrillisation is not affected by apparently SLB coated microplates | 91 |
| 4.4 Discussion | 92 |
| | |
| Chapter 5: Lipid bilayer composition and Aβ-lipid bilayer interactions | 94 |
| 5.1 Introduction | 94 |
| 5.2 Methods | 95 |
| 5.2.1 Thioflavin T assays | 95 |
| 5.2.2 Dye release assays | 96 |
| 5.2.3 Electron microscopy | 96 |
| 5.2.4 AF4-MALs | 97 |
| 5.3 Results | 97 |
| 5.3.1 Batch variation in A β 1-42 results in seeded reactions | 97 |
| 5.3.2 Fibril formation is catalysed by LUVs | 97 |
| 5.3.3 Catalysis of fibril formation by LUVs is saturable | 100 |
| 5.3.4 GM1 and Cholesterol containing LUVs do not catalyse fibril formation more than DOPC only LUVs | 102 |
| 5.3.5 GM1 and cholesterol do promote A β 1-42 induced LUV permeation | 103 |
| 5.3.6 A β 1-42 fibrils and oligomers associate with LUVs | 107 |
| 5.3.7 Neither A β 1-42 nor LUV populations significantly change in response to incubation together | 108 |
| 5.4 Discussion | 113 |
| 5.4.1 A β 1-42 fibril formation is promoted by LUVs and salt possibly in a nucleation independent manner | 113 |
| 5.4.2 A β 1-42 induced permeation of lipid bilayers is promoted independently of fibril formation by cholesterol and GM1 | 114 |
| 5.4.3 A β 1-42 does not remain bound to the bulk of lipid bilayers in solution yet is capable of inducing permeation in lipid bilayers | 115 |
| | |
| Chapter 6: The surface dependence of hCC activity as an inhibitor of normal Aβ behaviour | 116 |
| 6.1 Introduction | 116 |
| 6.2 Methods | 117 |
| 6.2.1 Thioflavin T assays | 117 |
| 6.2.2 AFM | 117 |
| 6.2.3 Dye release assays | 118 |
| 6.3 Results | 118 |
| 6.3.1 The inhibition of fibril formation can be dependent on the order in which it interacts with A β 1-42 and lipid bilayers in the presence of polystyrene | 118 |
| 6.3.2 HCC cannot inhibit fibril formation in a low-binding microplate | 120 |
| 6.3.3 LUVs do not impact upon hCC inhibition of fibril formation in glass | 122 |
| 6.3.4 HCC might stabilise the formation of films of A β 1-42 on polystyrene | 124 |
| 6.3.5 HCC can inhibit the A β 1-42 induced permeation of lipid bilayers. | 126 |

| | |
|---|-----|
| 6.4 Discussion | 127 |
| 6.4.1 HCC inhibits fibril formation by interactions with short lived oligomers of A β 1-42 | 127 |
| 6.4.2 HCC inhibits fibril formation in polystyrene by interacting with A β 1-42 that deposits as a film | 127 |
| 6.4.3 HCC modulates A β 1-42 by preventing the formation of lipid membrane permeating oligomers | 128 |
| | |
| Chapter 7: The ionic strength dependency of amyloid fibril formation | 129 |
| 7.1 Introduction | 129 |
| 7.2 Methods | 130 |
| 7.2.1 A β 1-42 preparation | 130 |
| 7.2.2 Electron Microscopy | 130 |
| 7.2.3 AF4 MALS | 130 |
| 7.2.4 Circular dichroism | 130 |
| 7.2.5 Dye release | 131 |
| 7.2.6 Thioflavin T | 131 |
| 7.3 Results | 132 |
| 7.3.1 TEM reveals a salt dependent change in morphology in amyloid fibrils | 132 |
| 7.3.2 AF4-MALS confirms the size distributions for A β 1-42 aggregates formed at physiological salt concentrations | 138 |
| 7.3.3 Salt induced protofibrils have β -structure | 139 |
| 7.3.4 Protofibrils can disrupt lipid bilayers | 140 |
| 7.3.5 High salt concentrations are required to form protofibrils when monomeric A β 1-42 is diluted to neutral pH from high pH | 141 |
| 7.3.6 Salt concentrations can affect the size of amyloid fibrils | 144 |
| 7.4 Discussion | 146 |
| 7.4.1 A β 1-42 nucleates fibrils and protofibrils in a salt dependent manner | 146 |
| 7.4.2 Monomeric A β 1-42 reacts less strongly to salt than small oligomers of A β 1-42 | 147 |
| | |
| Chapter 8: Conclusions and future work | 149 |
| 8.1 Vesicles and the low-binding microplates | 149 |
| 8.2 A β fibril formation and lipid bilayer permeation are surface dependent processes | 149 |
| 8.3 Human Cystatin C can inhibit A β 1-42 induced lipid bilayer permeation and also inhibits fibril formation in a surface dependent manner | 151 |
| 8.4 LUVs catalyse seeded fibril formation reactions and unseeded reactions differently | 151 |
| 8.5 A β 1-42 forms differently sized aggregates when nucleation is increased or decreased by the presence of different ionic strength buffers | 152 |
| | |
| References | 154 |

List of tables

Chapter 5

| | |
|-----------|----|
| Table 5.1 | 96 |
|-----------|----|

List of equations

Chapter 2

| | |
|--------------|----|
| Equation 2.1 | 49 |
| Equation 2.2 | 49 |

List of figures

Chapter 1

| | |
|--|----|
| Figure 1.1 A β Amyloid fibril basic structure | 4 |
| Figure 1.2 High resolution structures of A β amyloid fibrils | 5 |
| Figure 1.3 Polymorphism in A β fibrils | 6 |
| Figure 1.4 A suggested reaction scheme for amyloid fibril formation | 7 |
| Figure 1.5 A β pore formation in a supported lipid bilayer | 10 |
| Figure 1.6 One possible structure of a A β pore forming oligomer | 12 |
| Figure 1.7 Pore forming oligomers modelled by molecular dynamics | 14 |
| Figure 1.8 Colocalization of A β oligomers and synaptic marker proteins | 16 |
| Figure 1.9 A β signalling pathways | 17 |
| Figure 1.10 Cryo-TEM determined structures of AD Tau filaments | 19 |
| Figure 1.11 Cholesterol facilitating A β binding to GM1 | 24 |
| Figure 1.12 hCC colocalises with APP in mouse neuroblastoma cells | 28 |
| Figure 1.13 A β binds tightly to both wild type and variants of hCC | 29 |
| Figure 1.14 hCC inhibits A β fibril formation in a concentration dependent manner | 30 |
| Figure 1.15 Mutations in hCC reduce its ability to inhibit fibril formation | 32 |
| Figure 1.16 A surface plot of hCC | 33 |
| Figure 1.17 Agitation prevents hCC from inhibiting fibril formation | 34 |
| Chapter 2 | |
| Figure 2.1 The purity of hCC analysed by SDS-PAGE | 41 |

| | |
|--|----|
| Figure 2.2 A diagram of how fractionation is achieved by AF4 | 45 |
| Figure 2.3 LUVs form two populations; lone vesicles and clustered vesicles | 47 |
| Figure 2.4 Analysis of thioflavin T data | 48 |
| Chapter 3 | |
| Figure 3.1 A β 1-42 cannot damage LUVs in a polystyrene microplate | 55 |
| Figure 3.2 A β 1-42 can cause dye release depending on external surfaces | 57 |
| Figure 3.3 Less than 1 μ M A β 1-42 does not form amyloid fibrils in a polystyrene microplate | 59 |
| Figure 3.4 The rate of A β 1-42 fibrillisation is surface dependent | 62 |
| Figure 3.5 A β fibril formation is affected by the air water interface | 63 |
| Figure 3.6 A β 1-42 forms a film on a polystyrene surface | 65 |
| Figure 3.7 A β 1-42 does not interact with a quartz glass surface | 67 |
| Figure 3.8 A β 1-42 aggregates nucleate on a hydrophilic surface | 69 |
| Figure 3.9 Lipid bilayers can catalyse fibril formation in a polystyrene microplate | 71 |
| Figure 3.10 A β 1-42 causes the removal of a SLB from a mica surface before aggregating | 73 |
| Figure 3.11 A model for fibril formation on polystyrene | 75 |
| Chapter 4 | |
| Figure 4.1 Dye release occurs in a low binding microplate | 83 |
| Figure 4.2 An image of the detached base of a microplate well | 84 |
| Figure 4.3 Multiple additions of fresh LUVs to a low binding microplate results in changing profiles of dye release | 85 |
| Figure 4.4 The models representing multiple dye release events upon multiple additions of fresh LUVs | 86 |
| Figure 4.5 Addition of fresh LUVs and exchanging the buffer by pipetting results in a different dye release profile | 88 |
| Figure 4.6 Addition of fresh LUVs and exchanging the buffer with no chance of exposing the surface of the well to air results in dye release profiles similar to that in Figure 4 | 89 |
| Figure 4.7 Washing with A β 1-42 results in membrane damage that is lipid dependent | 90 |
| Figure 4.8 The rate of A β 1-42 fibrillisation is independent of surface treatment | 92 |
| Chapter 5 | |

| | |
|--|-----|
| Figure 5.1 DOPC LUVs catalyse fibril formation | 98 |
| Figure 5.2 A β 1-42 fibril formation is catalysed by LUVs with minimal effect on the concentration dependence | 99 |
| Figure 5.3 LUVs catalyse the growth rate of fibril formation | 101 |
| Figure 5.4 Catalysed fibril formation by LUVs can be saturated | 102 |
| Figure 5.5 GM1 and cholesterol do not impact on the rate or concentration dependence of fibril formation by A β 1-42 | 103 |
| Figure 5.6 A β 1-42 can induce some permeation in DOPC LUVs | 104 |
| Figure 5.7 A β 1-42 induced permeation of LUVs is promoted when GM1 and cholesterol are incorporated in the LUVs | 106 |
| Figure 5.8 TEM reveals that fibrils form in association with LUVs in a glass microplate | 107 |
| Figure 5.9 Oligomer formation in a small population of LUVs | 108 |
| Figure 5.10 SUV distributions contain clumped SUVs | 109 |
| Figure 5.11 A small population of large oligomers and fibrils are detected in an A β 1-42 sample after 3 hours in glass | 110 |
| Figure 5.12 The population of SUVs did not change when incubated together | 111 |
| Figure 5.13 Small amounts of A β 1-42 bound to SUVs that fouled the regenerated cellulose membrane | 112 |
| Figure 5.14 Seeded fibril reactions lose their lag phase | 113 |
| Chapter 6 | |
| Figure 6.1 Fibril formation is inhibited in a manner which is dependent on the accessibility of a lipid bilayer to A β 1-42 | 119 |
| Figure 6.2 HCC cannot inhibit fibril formation by A β 1-42 in low-binding microplates | 121 |
| Figure 6.3 HCC inhibits fibril formation in glass independently of LUVs | 123 |
| Figure 6.4 A β 1-42 film deposition and hCC | 125 |
| Figure 6.5 HCC can inhibit A β 1-42 induced permeation of lipid bilayers | 126 |
| Chapter 7 | |
| Figure 7.1 Salt dependent fibril morphology | 133 |
| Figure 7.2 Salt induced protofibrils are less than 100 nm in length | 134 |
| Figure 7.3 Method for measuring the “end to end” length and the actual length of a fibril | 136 |
| Figure 7.4 Protofibrils are 2 orders of magnitude less stiff than fibrils | 137 |

| | |
|--|-----|
| Figure 7.5 Quantification of aggregates formed at physiological salt concentrations reflects the distribution observed by TEM | 139 |
| Figure 7.6 Protofibrils have a β signal by CD | 140 |
| Figure 7.7 Protofibrils can disrupt LUVs | 141 |
| Figure 7.8 When the sample is prepared in 10 mM NaOH there is no lag phase for the reaction | 142 |
| Figure 7.9 Protofibrils form after 30 minutes in high salt conditions | 143 |
| Figure 7.10 A time course of fibril formation detected by MALS | 144 |
| Figure 7.11 Amyloid fibrils formed at low salt are larger than those at high salt | 146 |

List of abbreviations

| | |
|-----------|---|
| AD | Alzheimer's disease |
| ADDL | Amyloid- β derived diffusible ligands |
| AF4 | Asymmetric flow field flow fractionation |
| AFM | Atomic force microscopy |
| APOE | Apolipoprotein E |
| APP | Amyloid precursor protein |
| AWI | Air water interface |
| A β | Amyloid- β peptide |
| CF | Carboxyfluorescein |
| CHOL | Cholesterol |
| CSF | Cerebrospinal fluid |
| DLPC | 1,2-dilauroyl-sn-glycero-3-phosphocholine |
| DLS | Dynamic light scattering |
| DNA | Deoxyribonucleic acid |
| DOPC | 1,2-dioleoyl-sn-glycero-3-phosphocholine |
| DOPG | 1,2-Dioleoyl-sn-glycero-3-phosphoglycerol |
| EDTA | Ethylenediaminetetraacetic acid |
| ELISA | Enzyme-linked immunosorbent assay |
| ER | Endoplasmic reticulum |
| GM1 | Ganglioside 1 |
| GM3 | Ganglioside 3 |
| HCC | Human Cystatin C |
| HFIP | Hexafluoroisopropanol |
| HPLC | High performance liquid chromatography |
| LB | Luria-Bertani media |
| LDL | Low density lipoprotein |
| LUV | Large unilamellar vesicle |
| MALS | Multi-angle light scattering |
| MD | Molecular dynamics |
| NaOH | Sodium Hydroxide |
| NMR | Nuclear magnetic resonance |
| PAGE | Poly acrylamide gel electrophoresis |
| POPG | 1-palmitoyl-2-oleoyl-sn-glycero-3-phospho-(1'-rac-glycerol) |
| RAGE | Receptor for advanced glycation end products |
| SDS | Sodium dodecyl sulfate |

| | |
|-----------|--|
| SEC | Size exclusion chromatography |
| SLB | Supported lipid bilayer |
| ssNMR | Solid state NMR |
| SUV | Small unilamellar vesicle |
| $T_{1/2}$ | Half time |
| TEM | Transmission electron microscopy |
| TIRF | Total internal reflection fluorescence |

Chapter 1: Introduction

1.1 Alzheimer's disease

Alzheimer's disease is a neurodegenerative condition affecting millions of people worldwide, including over half a million in the UK ¹. Initially the disease affects the hippocampal region of the brain, the region responsible for short term memory causing the symptoms of memory loss ². The disease can then spread throughout the brain causing mass disfunction of mental capabilities. There is currently no cure for Alzheimer's disease ³. Multiple drugs have been trialled, including recently the monoclonal antibody Solunzumab, which failed due to a lack of efficacy in phase 3 ⁴. This is a recurring theme with drugs targeting Alzheimer's disease. The drugs are mostly safe (in the sense that they lack strong negative side effects) and so they pass phase 1 of trials but they are not effective in humans so fail at phase 2 and 3 ⁵. The question as to why this is the case, when all experimentation prior to trials suggest that these drugs should work in humans is the focus of current research. Some piece must be missing that will inform us about how Alzheimer's works in humans which makes it different to the research done *in vitro* or in various animal models.

1.2 The role of the amyloid β peptide in Alzheimer's disease.

1.2.1 Amyloid formation in Alzheimer's disease

There is a common theme amongst a range of neurodegenerative diseases in that the formation of amyloid fibrils is a fundamental process resulting in the onset of the disease. Alzheimer's disease, Huntington's disease and Parkinson's disease, to name but a few, all involve the formation of amyloid fibrils ⁶. Amyloid fibrils, their protein precursors and the processes that lead to their formation are the most promising targets for the development of first line treatments of neurodegenerative diseases.

Amyloid fibrils are a specific type of protein aggregate and any protein is capable of forming amyloid fibrils given appropriate conditions ⁶. For many proteins, this involves some form of destabilisation or conditions that promote unfolding. However, a protein is only considered to be amyloidogenic if it is the precursor to amyloid fibril formation resulting in a disease state. In Alzheimer's disease, the most abundant precursor to amyloid fibrils is the amyloid β peptide ($A\beta$) ^{6,7}. $A\beta$ is the result of the degradation of the amyloid precursor protein (APP) by the enzymes β and γ secretase ⁸⁻¹⁰. APP is a transmembrane protein, the function of which is not known. When APP is knocked out in mice, the majority of the mice die within the first week and the rest present with debilitating symptoms ¹¹. In order for $A\beta$ to be formed, the APP must be exposed to β and γ secretase. This happens when sections of cell membrane are routinely transformed into endosomes to be processed. Depending on the

requirements of the cell, the protein content of these endosomes can be processed by enzymes, such as β and γ secretase, with the intention of recycling the amino acids. Alternatively, the endosomes can be returned to the cell membrane, a process which is dependent on the retromer protein complex. Retromer has been linked to numerous neurodegenerative disease states including Alzheimer's disease and, as a result, has been suggested as a potential drug target^{5,12}. When endosomes containing APP are exposed to β and γ secretase however, the protein is fragmented into numerous peptides including $A\beta_{1-40}$ and $A\beta_{1-42}$ ¹³. β and γ secretase have also been suggested and indeed trialled as drug targets for Alzheimer's disease^{14,15}. $A\beta_{1-40}$ and $A\beta_{1-42}$ peptides that result from the fragmentation of APP by β and γ secretase are both amyloidogenic. Whilst $A\beta_{1-40}$ is found at higher concentrations in the cerebral spinal fluid of patients with Alzheimer's disease, it is $A\beta_{1-42}$ that is thought to be more potent in terms of both amyloid fibril formation and toxicity^{16,17}.

1.2.2 The amyloid hypothesis of Alzheimer's disease

The relationship between the generation of $A\beta$ and the initiation of symptoms of Alzheimer's disease has been the foundation of a large body of research over the last 3 decades. For example, multiple drugs that have been used in clinical trials have been anti amyloid agents¹⁸. This is due to initial evidence of the involvement of $A\beta$ ¹⁹ that developed over the best part of a decade into what is now known as the amyloid (or $A\beta$) hypothesis²⁰ of Alzheimer's disease. The amyloid hypothesis indicates a central involvement for $A\beta$ in causing the eventual symptoms of Alzheimer's disease²¹. In the years subsequent to the genesis of the amyloid hypothesis the ideas surrounding it have evolved as evidence has accumulated supporting the role of $A\beta$ in Alzheimer's disease.

Some ideas have been presented that seem to contradict the amyloid hypothesis such as evidence that the presence of neurofibrillary tangles associated with the Tau protein correlates better with cognitive impairment than amyloid plaques. However, these contradictions are not enough to discount the hypothesis and can even be included. For example, there is evidence that neurofibrillary tangles can be a downstream effect of widespread $A\beta$ activity.

Importantly, all dominant mutations which result in early onset (familial) Alzheimer's disease occur in proteins related to the generation of $A\beta$, namely, presenilin and APP.

Mutations in presenilin, a protease which acts as the catalytic site in γ -secretase can result in familial Alzheimer's disease²². Mechanistically, in wild type cases, APP is cleaved multiple times by presenilin acting as a carboxypeptidase, with 3-4 residues being removed from the c-terminus each time (this is subsequent to an initial endopeptidase cleavage at the N-terminus) starting from residue 48 or 49. Mutations in presenilin result in this activity being less efficient and resulting in longer peptides such

as A β ₁₋₄₂²³. Arguably the simplest explanation for the mutations in presenilin resulting in early onset Alzheimer's disease is that the lack of presenilin activity is the cause of the symptoms. However, the majority of Alzheimer's disease patients have wild type presenilin suggesting that it must be involved in a larger process that is not dependent on mutated presenilin¹⁸.

The APP gene is located on chromosome 21²⁴ and in some individuals, it is possible to have microduplications of the APP gene but not the rest of chromosome 21. Normally duplication of chromosome 21 results in Down's syndrome. However, individuals with microduplications of the APP gene do not present with symptoms of Down's syndrome but instead present with early onset Alzheimer's disease²⁵. Furthermore, mutations in APP have been presented with can either increase or decrease the risk of Alzheimer's disease. The Swedish mutation in APP (K670M/N671L) impacts on cleavage by β -secretase resulting in an increase in A β levels and is known to result in familial Alzheimer's disease²⁶. Similarly, the Arctic mutation in APP (E693G or E22G when referring to A β) has been shown to result in familial Alzheimer's disease through a suggested mechanism of enhanced protofibril formation²⁷. In contrast to this, a missense mutation in APP (A673T or A2T in the A β region) has been identified. Carriers of A673T have been shown to have a lower risk of Alzheimer's disease as there is a lifelong decrease in cleavage by β -secretase²⁸. A2T mutant A β also displays a lower propensity for aggregation.

Altogether, the evidence in support of a central role for A β in the onset of Alzheimer's disease is strong.

1.2.3 Structural models of A β amyloids

X-ray fibre diffraction has shown that A β Amyloid fibrils have a distinctive cross- β structure as shown in figure 1.1²⁹. More recent developments in cryo-electron microscopy have deepened our understanding of fibril structure³⁰. Some of these data may seem contradictory to previous models collected using solid-state NMR³¹ but can be explained by the observation that A β forms a range of different fibrillar structures.

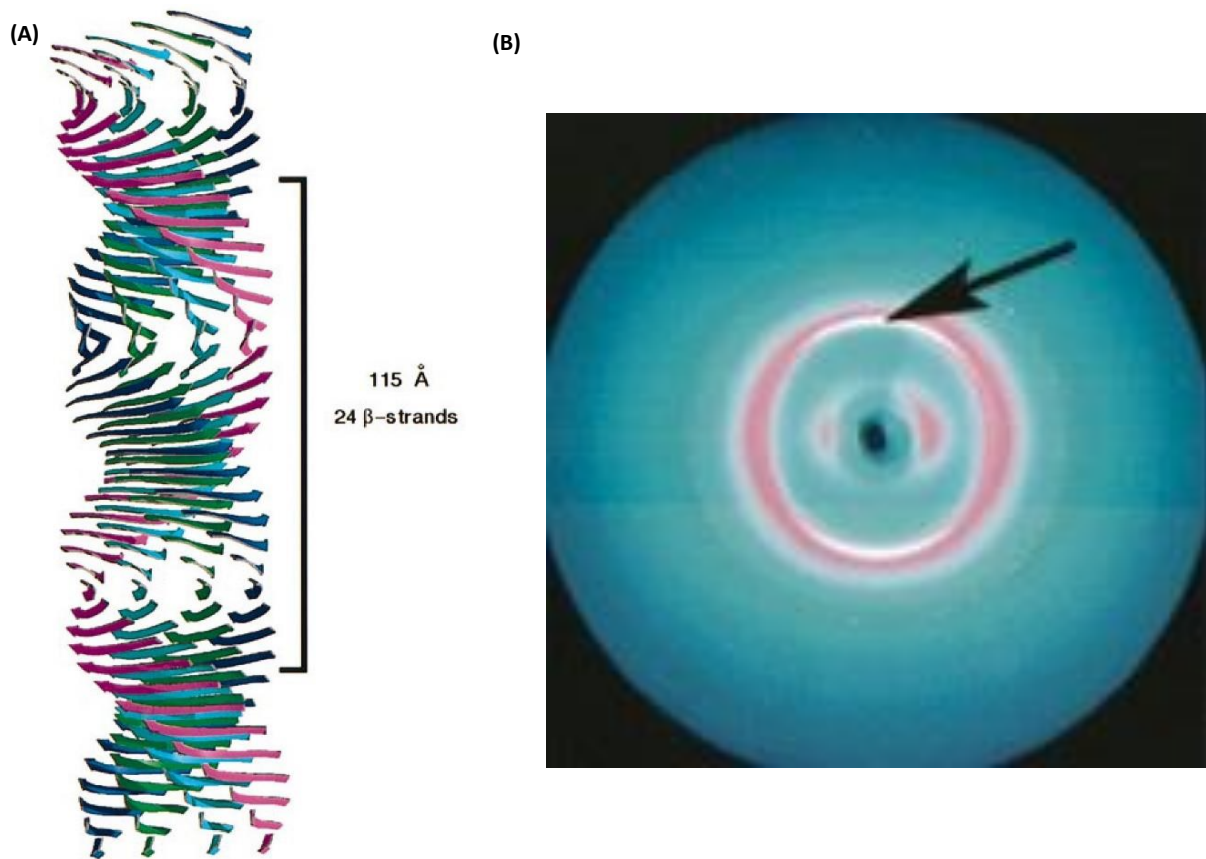


Figure 1.1. A β Amyloid fibril basic structure. A model of the cross β fibril structure (A) from X-ray fibre diffraction data (B) showing β -strands running perpendicular to the fibre axis taken with permission from Sunde et al 1997²⁹. The vertical axis in (B) runs perpendicular to the fibril axis. The arrow indicates the intense reflection at 4.7-4.8 Å that relates to the distance between β strands. The weaker reflections in the horizontal axis reflect the inter-sheet distance which in this case is between 10 and 11 Å. This is displayed as a model in (A).

There is considerable polymorphism in amyloid fibrils as can be seen in figure 1.2^{32 33}. One criticism of fibril structure determination is that the methods used require several rounds of seeding in order to obtain the required homogeneity for techniques such as solid-state NMR and cryo-TEM. Further examples of atomic resolution A β fibril structures show different internal structures, most highlighting a lack of structure in the N-terminus³⁴.

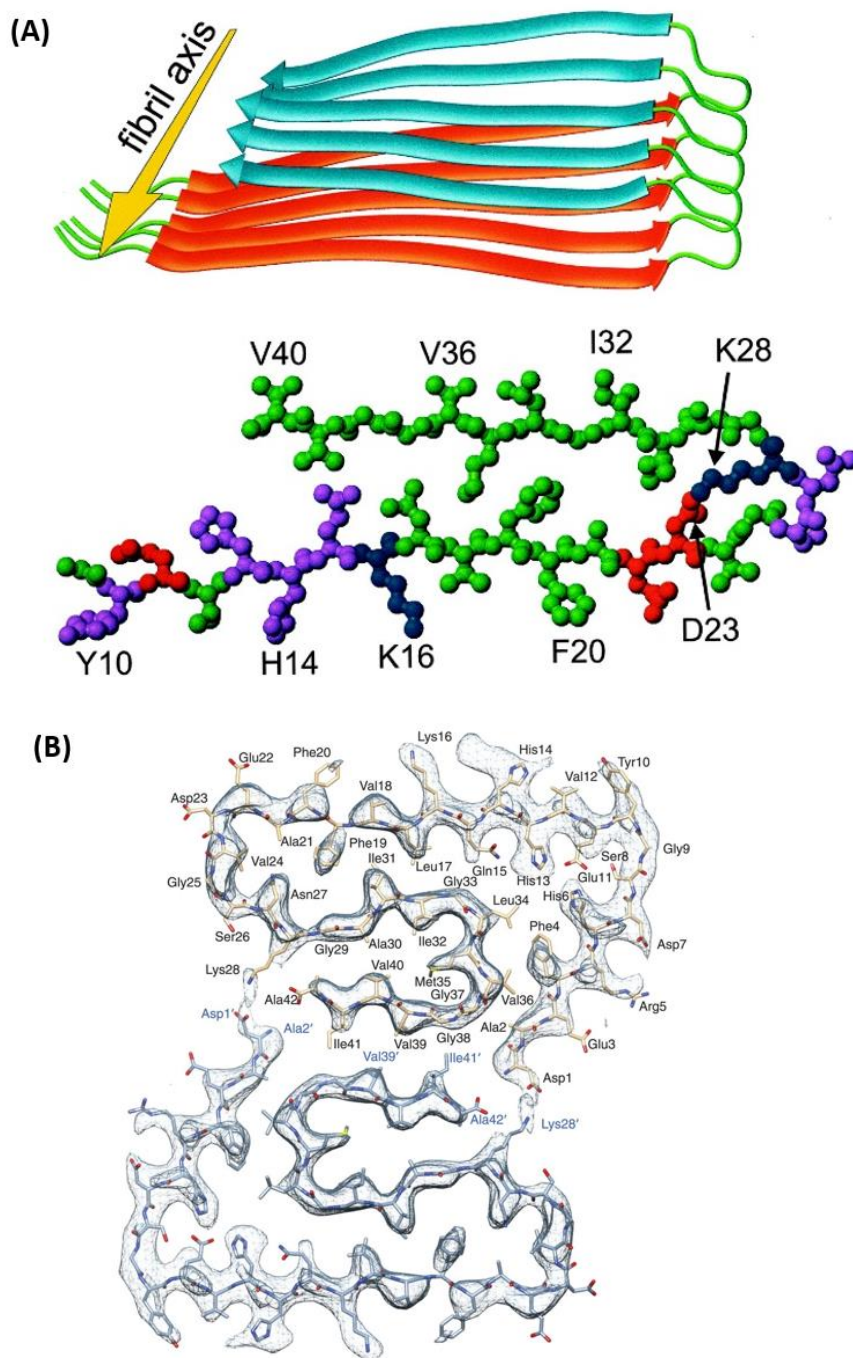


Figure 1.2 High resolution structures of A β amyloid fibrils. A β amyloid fibrils display numerous different polymorphic structures. A model for an A β ₁₋₄₀ fibril structure based on ssNMR data is shown in (A) taken from petkova et al 2002³¹ which is markedly different from the A β ₁₋₄₂ structure obtained using cryo-TEM shown in (B) taken with permission from Gremer et al 2017³⁰. This could be due to different A β precursors being used, different fibrillisation conditions such as the pH or that these fibrils show one structure that exists in a heterogeneous sample.

As there are a number of polymorphs that result from amyloid fibril formation, even from within the same sample (figure 1.3), enforced homogeneity can result in missed information. It is important therefore to consider all of the possible structures observed so far (and the ones that haven't been observed at high resolution) when discussing amyloid fibrils. It is not accurate to consider one model more correct than any other, given the methods required to obtain any given structural model.

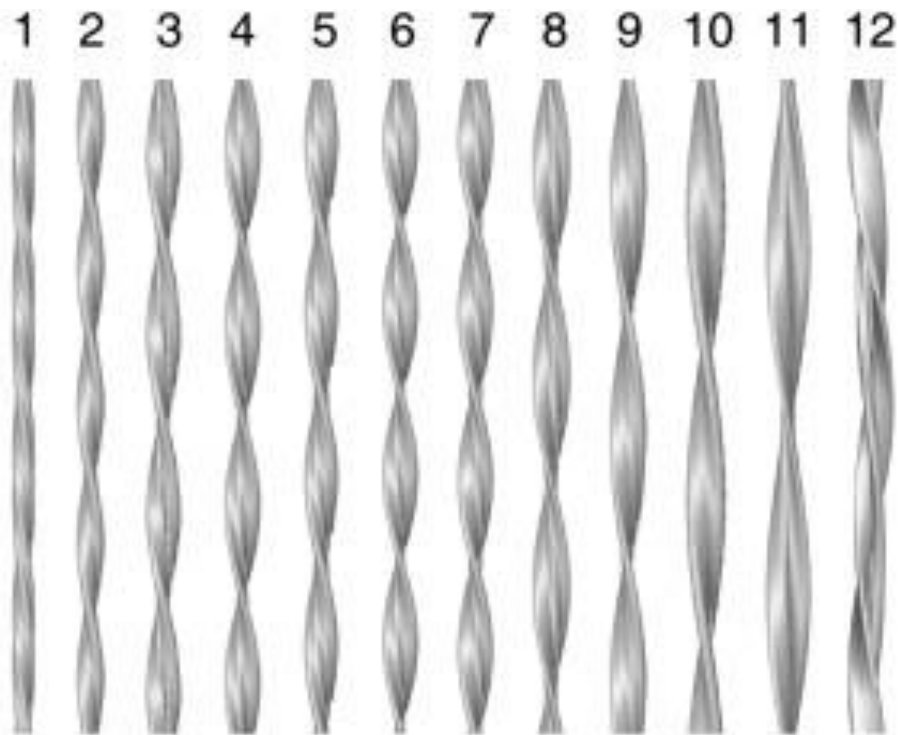


Figure 1.3 Polymorphism in A β fibrils. 12 distinct polymorphs of A β ₁₋₄₀ fibrils modelled from the same cryo-TEM sample. Taken from Meinhardt et al 2009³³.

1.2.4 A kinetic model for the assembly of A β amyloid fibrils

A model for the kinetic assembly mechanism of A β ₁₋₄₂ is as depicted in figure 1.4²⁴. Fibrillisation time courses, where fibrillar mass was quantified using the binding of the fluorescent probe thioflavin T, were used to determine a model for amyloid fibril formation. The presence of a lag phase in the time courses followed by a rapid exponential increase in the observed fibrillar mass was interpreted using a model where early primary nucleation events are rapidly superseded by secondary nucleation events where an existing population of fibrils catalyses the formation of further fibrils. In this model, primary nucleation refers to a nucleation event resulting in a 'fibril competent' species (one that can elongate into a full fibril). Secondary nucleation is a term used to describe the apparent positive feedback loop in which there is an increased rate of fibril formation in the presence of already formed fibrils (figure

1.4). Secondary nucleation is presented ³⁵ as separate from elongation, the process of adding monomer to the end of an amyloid fibril, a process which has been shown to be polarised (one end elongates faster than the other) using total internal reflection fluorescence microscopy ³⁶. How secondary nucleation occurs and whether it is distinguishable from elongation is a contentious subject. It is suggested that secondary nucleation occurs from an interaction between oligomeric species and fibrils resulting in a conformational change in the oligomeric species ³⁵. This has not been directly observed. One alternative model includes the acceleration of fibril formation as a result of fragmentation and the subsequent increase in fibril ends ^{37,38}.

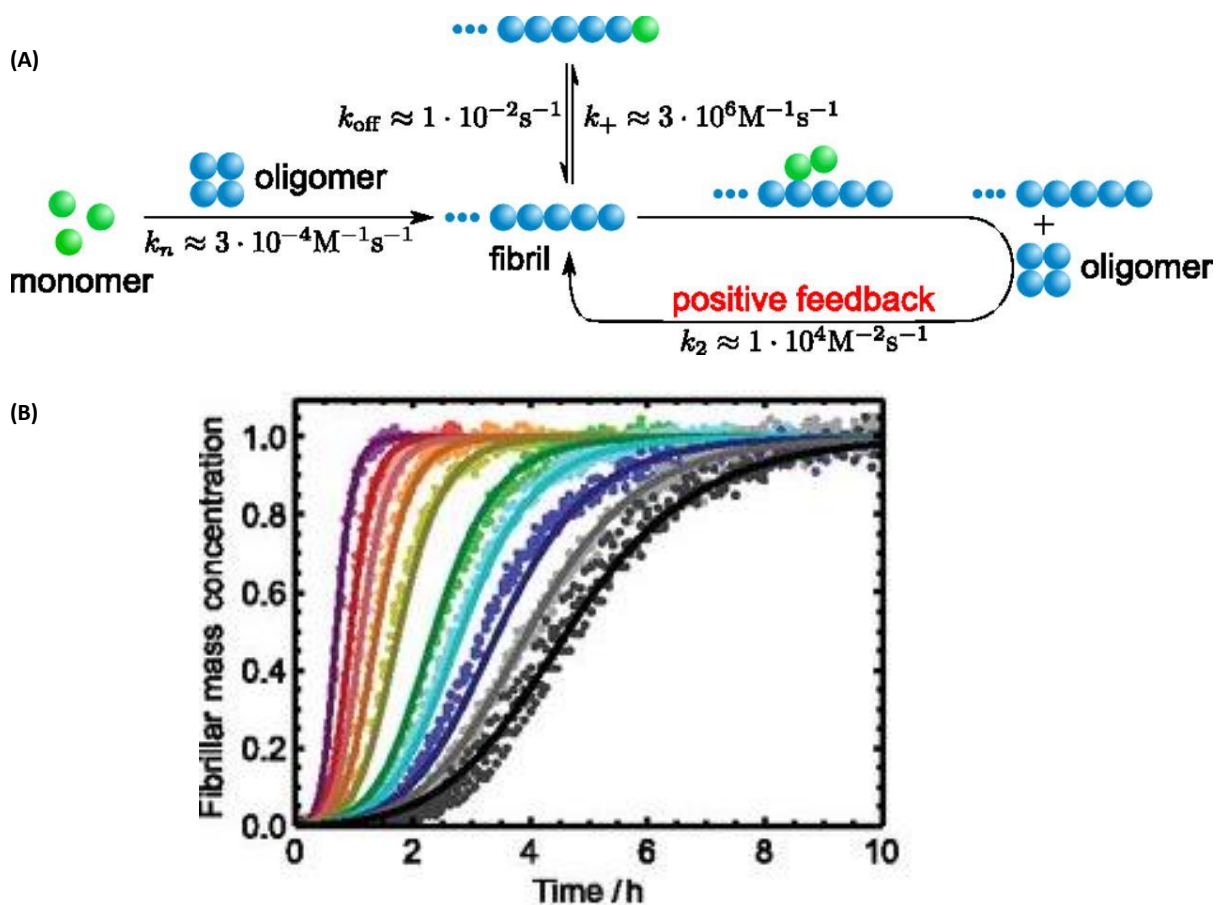


Figure 1.4. A suggested reaction scheme for amyloid fibril formation. A schematic diagram showing the progression from a sample of monomers to a sample of mostly fibrils (A) and an example of thioflavin T data (B) taken from Cohen et al 2013 ³⁵. The rate constants shown were either calculated by Cohen et al 2013 using thioflavin T data (k_n and k_2) or taken from previous work (k_{off} and k_+) ³⁹⁻⁴¹. The colours represent the initial concentrations of $A\beta_{1-42}$ ranging from 0.5 μM (black) to 6 μM (purple).

The presented analysis of thioflavin T data shown in figure 1.4 has the advantage of great simplicity ³⁵. The dependence of fibrillation time courses on the initial $A\beta$ monomer concentration (m) was

analysed then expressed using half-times for fibrillisation ($t_{1/2}$), and the parameter γ was used as an exponent to define the concentration dependence of $t_{1/2}$ on the A β monomer concentration where $t_{1/2} = \alpha m^\gamma$.

The resulting γ observed from the thioflavin T data was a combined result of two macroscopic rate parameters λ and κ . These parameters controlled proliferation through primary (λ) and secondary (κ) pathways in the presented model. By fitting new thioflavin T data to this model it is possible to determine values for λ and κ for each reaction and to plot these values against the initial monomer concentrations used. The contributions of primary and secondary pathways according to this model of fibril formation can be estimated from the contributions of λ and κ to the overall concentration dependence. This method of determining the contributions of primary and secondary pathways is only reliable if the model fits to the data. One contentious point here is the use of primary pathways and secondary pathways as these are not well defined terms. As can be seen in figure 1.4 all processes that occur between the initiation of the reaction and the formation of amyloid fibrils are considered primary events. This includes the reversible formation of any oligomers. Any contribution to the positive feedback loop observed in figure 1.4 after the initial formation of fibrils (excluding elongation) is considered a secondary event although how this process occurs is not explained.

A criticism of this model is that only elongation is presented as an equilibrium and this does not necessarily reflect reality. Also, under many conditions, monomeric A β will rapidly aggregate into larger species such as dimers, trimers and oligomers. These initial nucleation events are not necessarily the same as the nucleation events referred to as primary nucleation when discussing fibril formation. The existence and formation of oligomers is acknowledged but this is not represented in the calculated rate constant k_n which is the rate constant for the formation of fibril from monomer. When fibril presence is measured by thioflavin T fluorescence which is sensitive to some oligomers as well as fibrils, it can be argued that this is an unreliable measure of k_n .

The relationship between toxicity and amyloid fibrils has been well studied with one major conclusion being that amyloid fibrils do not directly contribute to toxicity *in vivo* ⁴². There are however, still assertions that specific polymorphs of amyloid fibril could directly result in toxicity ⁴³. For example, the suggestion that ganglioside GM1 containing lipid bilayers contribute to the formation of fibrils with structures which are toxic (discussed in section 1.4.2), whilst the regular variety of fibrils formed in the absence of GM1 are not ⁴⁴.

1.2.5 Oligomers in Alzheimer's disease

The term oligomer, using the prefix oligo meaning 'few', refers to a small number of monomers forming a non-fibrillar aggregate. Whilst, with regard to A β and Alzheimer's disease, amyloid fibrils are generally considered to not contribute directly to toxicity, oligomers *are* often associated with toxicity^{42,45-47}. The literature surrounding oligomeric species refers to numerous different species. Dimers and trimers are referred to as oligomers but so are A β -derived diffusible ligands (ADDLs)⁴⁸ and protofibrils⁴⁵ which are much larger polymers and can be up to 100 nm in length. The stability of oligomeric species with low monomer numbers has been studied using a number of methods including molecular dynamics (MD) simulations. MD simulations have also described A β dimer formation⁴⁹. These species are often short lived due to the rapid formation of larger aggregates, unless they are stabilised in specific conformations such as pores in lipid bilayers⁵⁰. At the other end of the scale, protofibrils, which are distinct from fibrils despite having a similar appearance are commonly observed. ADDLs which are roughly 5 nm diameter globulomers are observed under specific conditions⁵¹. All of these structures often exist temporarily due to a rapidly shifting equilibrium thus making it difficult to determine structures at high resolution.

Importantly, A β can be manipulated in numerous ways *in vitro* to form oligomers as opposed to fibrils. One such method is to incubate monomeric A β at low temperatures such as 4 °C. This suggests that, on an energy landscape, certain oligomeric species can be energy wells which 'trap' the A β in that state⁵². These species aren't often observed at higher temperatures as there is enough energy to overcome the well and thus form even more stable species such as fibrils. This would suggest that some species of oligomer are 'on pathway' to forming fibrils, in that during the process of forming fibrils there is a point at which these oligomers exist. However due to the polymorphism observed in fibril formation this may not always be true. It could be true that specific oligomer species are always present during the formation of a specific fibril polymorph. It doesn't follow that the same species of oligomer will always be present in the formation of a different fibril polymorph. It is important to consider that different fibril polymorphs exist within the same sample and will likely have different oligomeric precursors.

Oligomers can also form in a surface dependent manner. Numerous reports show that interactions between A β and lipid bilayers can result in specific oligomers, some of which appear to form pores in the lipid bilayers (figure 1.5)⁵³⁻⁵⁵. It could be argued that these pore-forming species could contribute to toxicity in Alzheimer's disease.

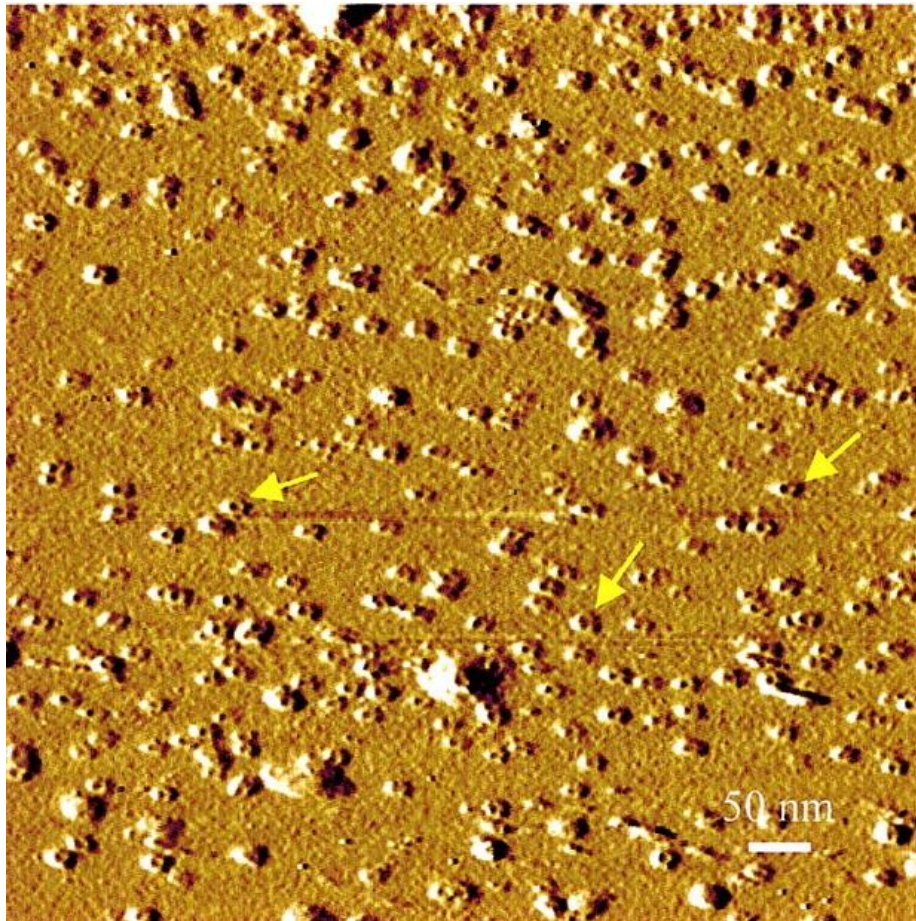


Figure 1.5. A β pore formation in a supported lipid bilayer. An AFM amplitude mode image depicting numerous pore-like structures in a supported lipid bilayer taken from Lin et al 2001⁵³. A β was mixed with lipids in an organic solvent in order to incorporate the A β into the lipid bilayer. The yellow arrows indicate examples of pore forming species.

1.3 Toxicity in Alzheimer's disease

There are a number of ways in which A β is thought to induce toxicity *in vivo*. The most popular explanations include membrane permeation by A β oligomers, receptor mediated cell death as a result of A β oligomerisation, the triggering of Tau hyperphosphorylation resulting in loss of cell structure and finally, toxicity attributed to intracellular A β .

1.3.1 Membrane permeation

It has long been thought that A β oligomers can directly damage lipid bilayers resulting in the disruption of cell function^{6,53}. In particular, the disruption of calcium ion homeostasis is important, and it has been hypothesised that this is the primary toxic event in Alzheimer's disease⁵⁶.

One mechanism by which membrane permeability can be increased by A β is pore formation. Pore formation has been observed in numerous experiments using supported lipid bilayers (SLBs). The pores observed in figure 1.5 used AFM to image pores in an artificial supported lipid bilayer⁵³. A major criticism of this work with regard to implied toxicity is the method chosen to investigate the interaction between A β and the SLB. The A β was mixed with lipids in an organic solvent before being dried and resuspended in a water-based solvent to form vesicles. These vesicles were then incubated on freshly cleaved mica to form a supported lipid bilayer. The decision to mix the lipids and the A β in an organic solvent prior to the formation of a lipid bilayer removes possibly the most important step in any pore formation that would occur *in vivo*, the insertion of the A β into the lipid bilayer. The lipid bilayers already have A β inserted into them making it easy to observe apparent pores. Whether or not these pores would be observed, especially in the amounts seen in figure 1.5, if the A β was to be added after SLB formation is not clear from this work.

However, there is evidence from other sources that A β can indeed insert into a lipid bilayer followed by the formation of pores or channels⁵⁷⁻⁵⁹. In fact, one compelling piece of evidence that pore formation is important is the finding that pore-like structures were observed in Alzheimer's disease brain tissue⁶⁰. Fluorescently labelled antibodies were used to show that annular protofibrils are capable of forming pores in lipid bilayers. The term 'annular protofibrils' in this case refers to spherical oligomers as opposed to 'protofibrils' which generally refers to oligomers which resemble short fibrils. The conclusion that these annular protofibrils are forming pores in the membrane *in vivo* relies on the assumption that the structures observed by electron microscopy at high resolution are actually inserted into the membrane in the low resolution images. Co-localisation of these annular protofibrils and the cell membrane is not enough to guarantee that there is pore formation *in vivo*.

Further evidence of pore formation by A β is presented in another study⁶¹. Molecular dynamics simulations are used to suggest a viable model for the structure of a pore. This is presented alongside electrical recording data measuring the change in electrical potential on one side of a planar lipid bilayer. A β_{1-42} was used to collect the electrical recording data and A β_{p3-42} for both the electrical recording and the molecular dynamics simulations. A β_{p3-42} is formed by the post translational cleavage of the first two residues at the N-terminus leaving an exposed glutamate residue. Pyroglutamate is then formed when glutaminyl cyclase catalyses the formation of a lactam ring. The authors argue that A β_{p3-42} is found at high concentrations in the brains of AD patients. Mass spectrometry data showed that A β_{p3-42} is present but both A β_{1-40} and A β_{1-42} are more prominent¹³. In the molecular dynamics study it was shown that A β_{1-42} and A β_{p3-42} were capable of forming ion channels. The molecular dynamics simulations showed 2 different conformers of A β_{p3-42} in dodecameric barrel structures inserted into a lipid bilayer (figure 1.6).

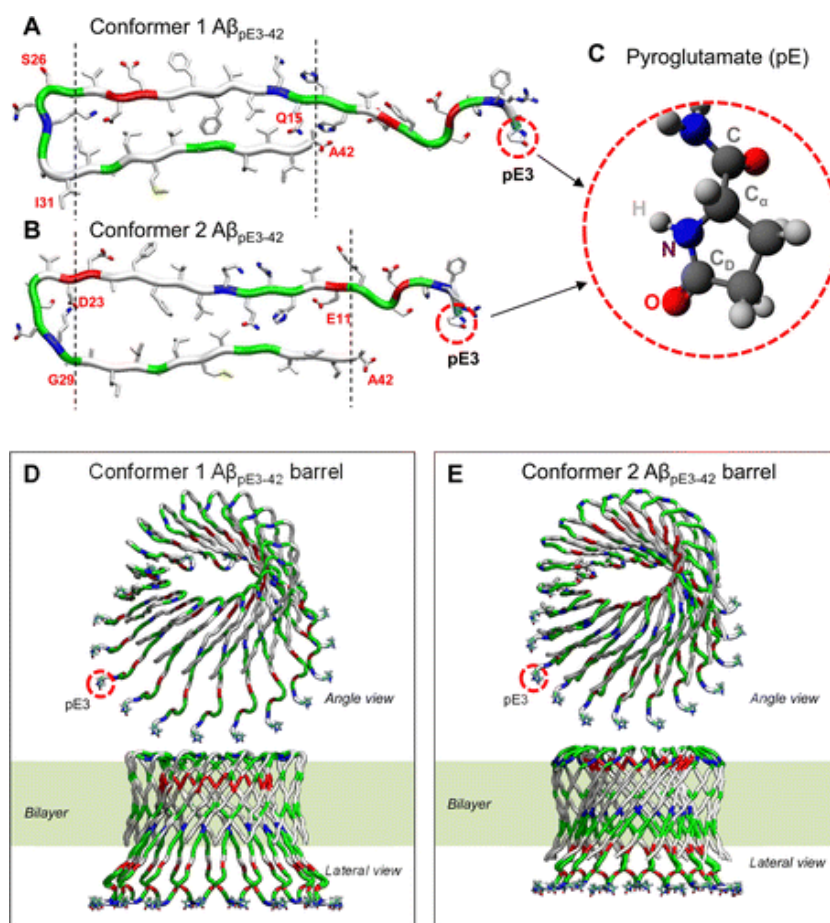


Figure 1.6 One possible structure of a A β pore forming oligomer. Models of A β pores from molecular dynamics simulations using two different A β _{p3-42} conformers taken from Gillman et al 2014⁶¹. (A) and (B) show the two different conformers of A β _{p3-42}. In (A) the turn occurs between S26 and I31 and in (B) the turn occurs between D23 and G29. (C) highlights the location and structure of the pyroglutamate. (D) and (E) are the initial barrel structures used in MD simulations. The areas between the dotted lines in (A) and (B) represent the sections of each monomer that are inserted into the lipid bilayer.

Another method of detecting pores is to use single molecule fluorescence studies⁶². Single molecule fluorescence was combined with measuring conductivity across a planar “black lipid membrane”. The term black lipid membrane refers to the method of forming a model lipid bilayer. In brief, this involves forming a monolayer of lipids on either side of a hydrophobic substrate with an aperture in the middle. The sections of monolayer that form at the aperture fuse to form a bilayer. A β was shown to have a concentration dependent range of behaviours. At less than 10 nM, the A β deposited onto the surface but did not aggregate or permeabilise the membrane in any way. Between 10 and 100 nM the A β

formed oligomeric species, the larger of which were capable of forming pores in the lipid bilayer. Above 100 nM large scale damage to the lipid bilayer was observed.

The phenomenon that A β ₁₋₄₂ produces more toxicity *in vivo* has not always been reflected by studies observing pore formation of A β aggregates *in vitro*. In one study⁶³ patch clamp technology was used to detect the permeability of a lipid bilayer in the presence of A β monomers, oligomers and fibrils⁶⁴. Thioflavin T fluorescence was used to determine at which stage of aggregation the A β was at and this was confirmed by negative stain TEM. Importantly, cell membrane extract was taken from neuronal cells to form the lipid bilayer. A β ₁₋₄₂ oligomers were shown to be the only species tested that resulted in an increased permeability in the membrane. The exact species of A β oligomer was not determined. However, based on the channel conductance, the size of the pores formed were separated into 3 size ranges. These were roughly 1.7 nm, 2.1 nm and 2.4 nm. Molecular dynamics simulations of 16-mer, 20-mer and 24-mer pores result in pore diameters of roughly the same length suggesting that these are potentially viable structures⁶⁵. Figure 1.7 shows the structure of these pores. This contrasts with the 12-mer presented elsewhere⁶¹ and showed that there was a significant interaction between physiologically relevant membrane constituents and A β ₁₋₄₂.

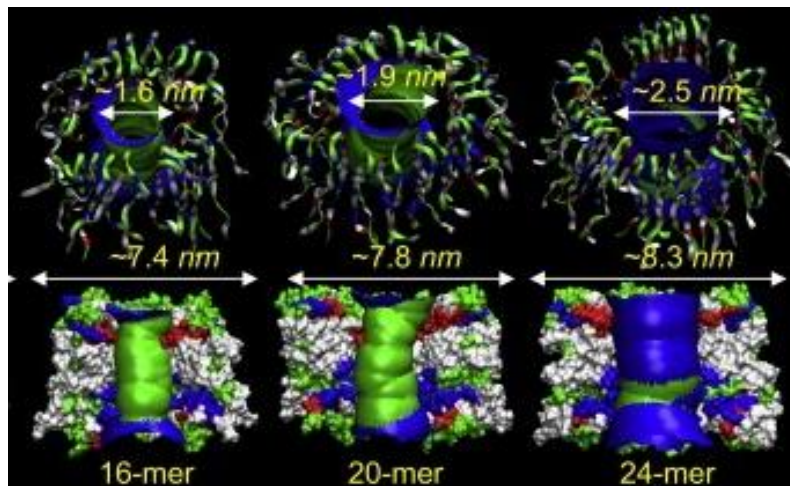


Figure 1.7 Pore forming oligomers modelled by molecular dynamics. 16-mer, 20-mer and 24-mer pores of $A\beta_{9-42}$ were examined using molecular dynamics simulations taken with permission from Jang et al 2009⁶⁵. $A\beta_{9-42}$ monomers were based on previous solid state NMR work using $A\beta_{1-40}$ ⁶⁶. These 16, 20 and 24-mer models predict pore sizes of roughly 1.6, 1.9 and 2.5 nm respectively. In a separate study using patch clamped membranes and $A\beta_{1-42}$ oligomers, pores were observed and calculated to be in 3 subgroups with pore diameters of 1.7, 2.1 and 2.4 nm suggesting that these 16-mer, 20-mer and 24-mer pore structures may be viable⁶⁴.

The impact of metal ions on $A\beta$ induced membrane permeation has also been investigated⁶⁷⁻⁶⁹. In one study copper ions were introduced to monomeric $A\beta_{1-42}$ incubations⁶⁹. This resulted in the inhibition of fibril formation observed by thioflavin T fluorescence and the reported promotion of oligomer formation observed by TEM. Due to the nature of TEM, only the material that has adsorbed onto the grid and in particular the grid squares observed can be recorded. Complementary techniques are needed such as SEC-MALS or AF4-MALS (discussed in chapter 2 section 2.7) which fractionate, quantify and determine the range of sizes present in the whole sample. Nevertheless, it was also shown using a dye release assay that copper ions can elevate the permeabilisation of lipid bilayers by $A\beta_{1-42}$ supporting the idea that copper promotes the formation of toxic species. Only a 5% difference in total fluorescence was observed however, between the control and the sample containing $A\beta_{1-42}$ and less than a 5% increase was observed when copper was added along with $A\beta_{1-42}$ suggesting that whilst this impact may be statistically significant, it is not a large effect. The fluorescence was also recorded after 280 hours of incubation which is just over 11 days. Compared to other studies^{70,71} (in which the reaction can be over in a matter of seconds) this is a long incubation. However, presumably due to the use of synthetic $A\beta$ as opposed to recombinant $A\beta$, the time courses of fibril formation observed in this study by thioflavin T also require much longer incubation periods than is reported elsewhere^{35,41}. TEM images of deformed LUVs in the presence of $A\beta_{1-42}$ and copper ions were also presented in which phosphotungstic acid was used to stain the samples, as opposed to the commonly used uranyl

formate, in order to alleviate the LUVs from being damaged by the heavy metal. All in all, this study supports the role of copper ions in the formation of toxic oligomers.

Pore formation is not necessarily the only method by which an increase in lipid bilayer permeability may be compromised. A model that includes pore formation but also an initial membrane fragmentation step has been presented ⁷¹. Structural changes in the lipid bilayer such as membrane thinning have also been observed ⁷². Another alternate hypothesis is that the aggregation process itself is responsible for lipid bilayer disruption ⁷³. Finally, increased permeabilisation of lipid bilayers that was originally not believed to be due to channel formation has also been observed ⁷⁴. In this latter study the evidence that channel formation was not involved was that the increased conductance across the bilayer was not inhibited by the calcium channel inhibitor cobalt. This conclusion assumed that any channel was specific to calcium ions which, as presented later ⁶⁴ was not correct. More recently, TIRF has allowed for direct observation of the A β related ion channels ⁷⁵.

1.3.2 Receptor mediated toxicity

Another popular explanation as to how A β aggregation results in toxicity is the binding of A β to various receptors associated with neurons. Binding to these receptors triggers downstream effects that result in a loss of synaptic activity and cell death. Confocal immunofluorescence has shown that it is possible for extracellular A β oligomers to accumulate at the synapse ⁷⁶. In this work immunofluorescently labelled oligomeric species were formed *in vitro* and added to cultured rat hippocampal neurons. Imaging showed that the oligomeric species colocalised with synaptic marker proteins (figure 1.8). An assumption was made that oligomers were specifically bound to sites at the synapse. Another convincing argument from the same work is that A β oligomers were selective to particular neurons suggesting that there was a specific receptor for A β oligomers to bind to.

Another argument in favour of the importance of receptor mediated toxicity is that the disruption of synapse is readily observed at nanomolar concentrations of A β ⁷⁷. This is important as the concentration of A β oligomers reported to be found in AD brains is at a similar concentration ⁷⁸. With regard to the specific binding of A β oligomers to sites located on the synapse of neurons it can be concluded that there must be a high affinity receptor for A β oligomers.

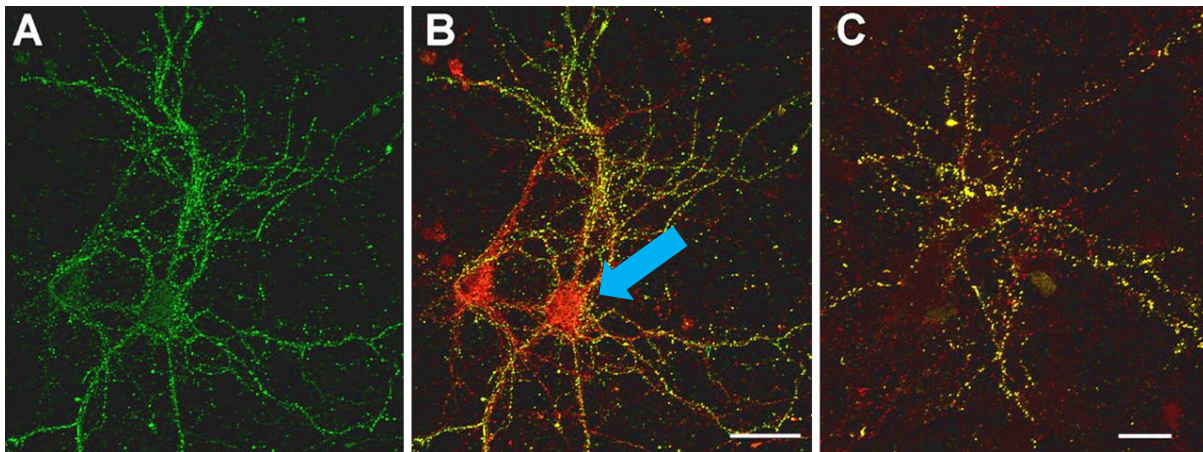


Figure 1.8 Colocalization of Aβ oligomers and synaptic marker proteins. Immunofluorescent tags were used to identify the locations of Aβ oligomers (green) and the synaptic marker proteins αCaM Kinase II and PSD-95 (both red). Image A shows the location of Aβ oligomers only. Images B and C show the colocalization with αCaM Kinase II and PSD-95 respectively. Overlap of the two tags produces a yellow colour. Interestingly in image B only one (blue arrow) out of the 2 neurons present appears to show colocalization between Aβ oligomers and αCaM kinase II, suggesting that this behaviour is specific to neurons expressing a receptor for Aβ oligomers. Taken with permission from Lacor et al 2004 ⁷⁶.

Cellular prion protein has been identified as an example of a high affinity receptor for Aβ oligomers ⁷⁹ by comparing the binding of Aβ to hippocampal neurons with the binding of Aβ to non-neuronal cells expressing prion. It was shown that in both cases Aβ displayed the same binding affinity for the cells at nanomolar concentrations. In the same work it was shown that the inhibition of long term potentiation in hippocampal cells by Aβ oligomers required an interaction with prion protein. Anti-prion protein antibodies were used to prevent Aβ oligomers from binding to prion and this resulted in the recovery of long term potentiation in hippocampal cells. Further evidence that memory impairment requires prion protein was obtained in transgenic mice. Mice lacking cellular prion protein but containing APP with the Swedish mutation (known to increase Aβ formation *in vivo* ⁸⁰) lack memory impairment ⁸¹.

There are a number of reported downstream effects of Aβ oligomers binding to cellular prion protein. The glutamate receptor metabotropic glutamate receptor 5 (mGluR5) has been implicated by showing that Aβ facilitates long term depression in AD models in an mGluR5 dependent manner which is inhibited by anti-prion protein antibodies ⁸². This suggests that long-term depression in AD requires all three components. The same work showed that an antagonist of mGluR5 was able to recover long

term potentiation in the presence of A β . The mechanism by which mGluR5 contributes to AD toxicity has been investigated using quantum dot labelling⁸³. This showed that upon addition of A β to hippocampal neurons, mGluR5 became clustered resulting in elevated levels of intracellular calcium ions. This describes an alternative mechanism for the disruption of calcium homeostasis discussed in section 1.3.1.

Another downstream effect of A β oligomers binding to prion is the activation of intracellular kinases such as Fyn kinase⁸⁴. Fyn kinase is a protein tyrosine kinase that is associated with apoptosis and is found at elevated levels in AD⁵¹. It has been shown to activate subunits of N-methyl-D-aspartate receptors (NMDA receptors). NMDA receptors have also been extensively linked to loss of synaptic function in AD models where specific attention was not paid to the contribution of prion protein^{56,85,86}. NMDA receptors are also ion channels and their hyperactivation can result, once again, in disruption to calcium homeostasis⁸⁷. Fyn kinase activation can also lead to dendritic spines not growing in an A β dependent manner⁸⁴. Finally, it has been shown that Fyn kinase, when complexed with prion protein and activated in an A β dependent manner can result in the hyperphosphorylation of Tau, the toxicity of which is discussed in section 1.3.3.

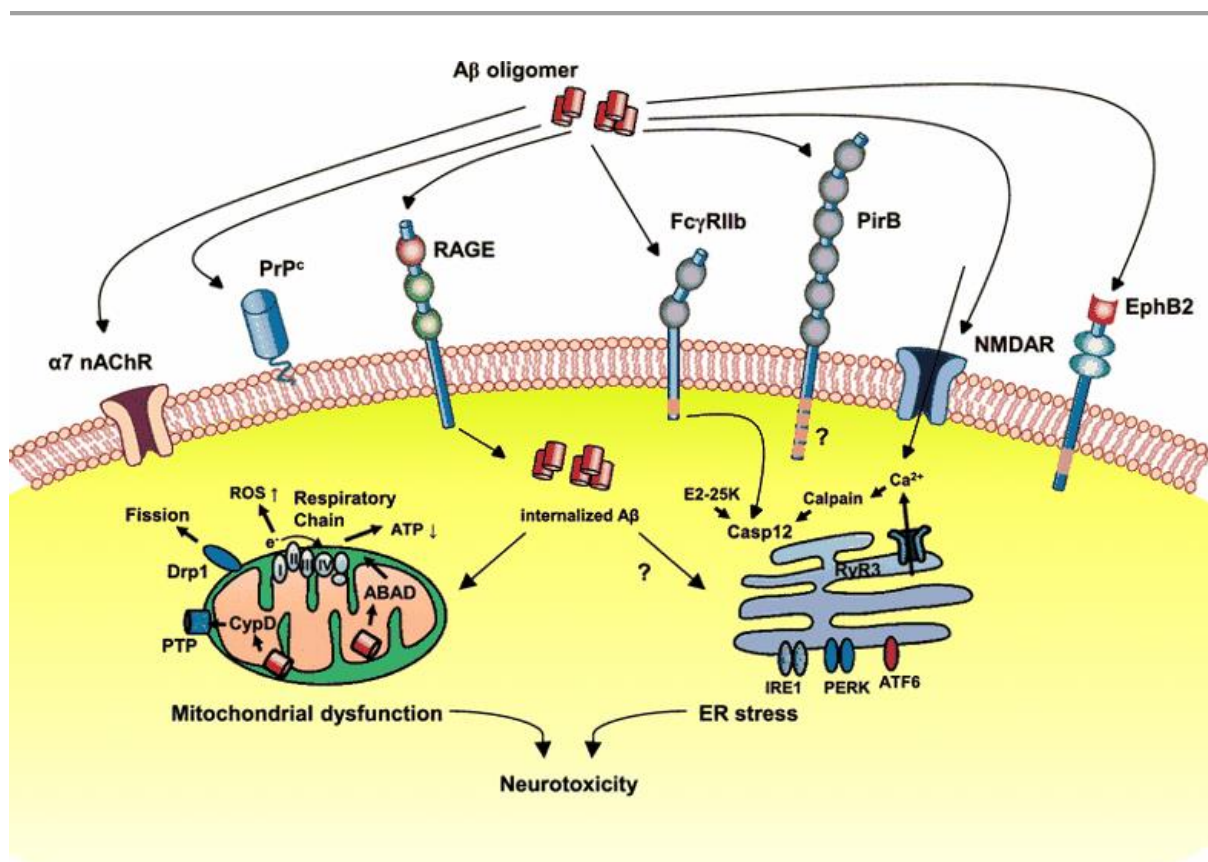


Figure 1.9 A β signalling pathways. A diagram taken from Kam *et al*⁸⁸. The receptors for A β oligomers and their specific downstream signalling pathways are indicated.

There are a number of other potential receptors for A β oligomers. A diagram of potential receptors for A β (figure 1.9) shows some of them. The majority of receptors for A β are only tenuously linked to toxicity but are useful in explaining the overall behaviour of A β in the brain. For example, the export of A β from the brain is mediated by low density lipoprotein receptors including LDL receptor related protein 1⁸⁹. The expression of this receptor is decreased at the blood brain barrier in AD⁹⁰. This behaviour is observed in concurrence with receptors for advanced glycation end products (RAGE) which mediate A β uptake into the brain from the blood^{91,92}. APP processing into A β is dependent on cholesterol levels⁹³, the transport of which is reliant on APOE, which binds to A β ⁹⁴ (discussed further in section 1.4.1).

1.3.3 Tau hyperphosphorylation

Tau is a microtubule-associated protein that helps to maintain the stability and dynamics of microtubules⁹⁵. By regulating microtubule behaviour, Tau can ensure that neurites (an all-encompassing term used to describe the structures protruding from the ends of neuronal cells, such as dendrites and axons) grow out correctly. Post translational phosphorylation of Tau is a means by which Tau can be regulated.

In Alzheimer's disease, the hyperphosphorylation of Tau results in intracellular neurofibrillary tangles as the Tau aggregates into paired helical filament and straight filament structures^{96,97}. Figure 1.10 shows the internal structure of the aggregated Tau filaments determined by cryo-TEM⁹⁶.

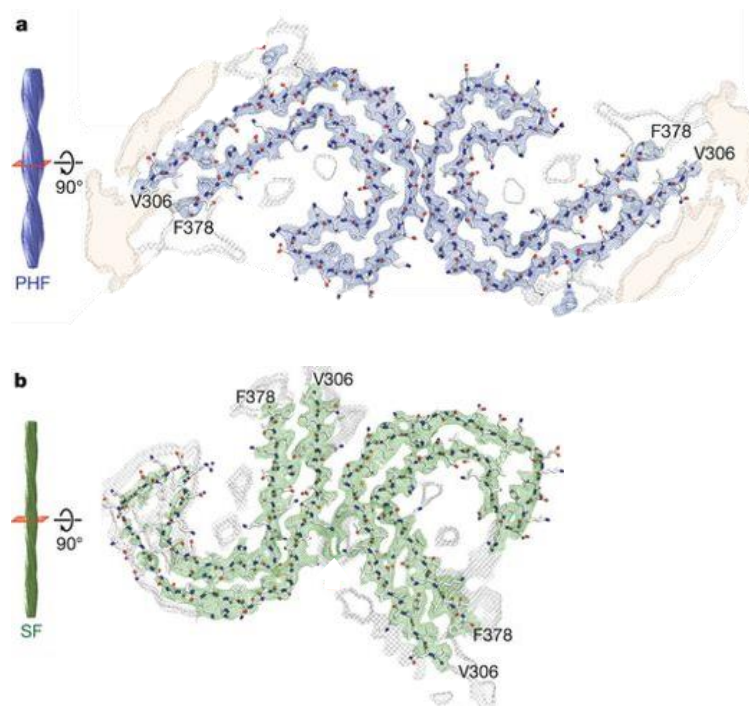


Figure 1.10 Cryo-TEM determined structures of AD Tau filaments. Tau filaments from neurofibrillary plaques found in an AD brain were used to seed Tau aggregation in a cell culture environment. This produced populations of paired helical filaments (A) and straight filaments (B) which were imaged using cryo-TEM. The internal structures of the two types of filament were then determined. Adapted with permission from Fitzpatrick et al 2017 ⁹⁶.

As a result of Tau aggregation, microtubules become destabilised and neurites lose structure. The loss of structure in neurites contributes to a loss of function which promotes cell death. Loss of cerebral function in Alzheimer's disease is most strongly related to the hyperphosphorylation and aggregation of Tau ⁹⁸. More accurately, the loss of cerebral function and the presence of intracellular neurofibrillary tangles are most closely correlated ⁹⁹. However, as the main constituent of the neurofibrillary tangles is Tau filaments, there is little reason to distinguish between Tau hyperphosphorylation and aggregation, and neurofibrillary tangle presence.

The relationship between A β and Tau is often referred to as a relationship between extracellular plaques (A β -related) and intracellular tangles (Tau related). Evidence points to the formation of tangles occurring subsequently to the formation of plaques ^{98,100,101}. This order of events has led to the hypothesis that A β related plaque formation is the primary contributor to AD with Tau related tangle formation being a downstream consequence ²¹. Evidence from *in vivo* models suggests that there is a

specific mechanism that results in tangles and is instigated by plaque formation¹⁰⁰⁻¹⁰². An example of this is the characterisation of Tau aggregates from transgenic mouse models expressing both APP with the Swedish mutation and mutants of Tau that are more prevalent in frontotemporal dementia¹⁰². This resulted in the phosphorylation of serine residues in Tau that were not observed in the Tau only transgenic model controls. This example highlights the insufficiency of discussing the interaction between Tau and A β in terms of plaques and tangles as, in particular with regards to A β plaques, the constituent populations of plaques and tangles are not exclusively A β fibrils and Tau filaments. Typically, however, the observation that an increase in the presence of A β results in an increase in not only Tau aggregation but also pathology is made when different transgenic models are characterised^{98,103,104}. As discussed in section 1.3.2 it has been shown that oligomeric A β can bind to the prion protein-Fyn kinase complex resulting in the activation of Fyn kinase and the subsequent hyperphosphorylation of Tau. This provides one pathway by which this can occur.

Another interesting result is that, when specific sites are phosphorylated in Tau, A β toxicity is inhibited in transgenic mouse models¹⁰⁵. The authors of this work concluded that this could be evidence that Tau does not contribute to AD pathology as much as originally believed. An alternate hypothesis is that the initiation of Tau hyperphosphorylation and toxicity could be part of an attempt at a response to regulate A β related pathology. If Tau, when phosphorylated at a specific site, regulates A β pathology, then this would promote the phosphorylation of Tau. Unfortunately, too much of a good thing could potentially result in the hyperphosphorylation of Tau and the related pathologies.

1.3.4 Intracellular A β activity

Intracellular A β is also capable of resulting in toxicity in AD. When induced pluripotent stem cells were taken from AD patients and developed into neuronal cells, oxidative stress and endoplasmic reticulum stress were observed suggesting an intracellular mechanism of toxicity¹⁰⁶. It has also been shown that in transgenic mice containing both the Swedish mutation and the arctic mutation (which enhances 'protofibril' formation²⁷), intracellular A β and observed toxicity precede the observation of extracellular A β species. This suggests that the enhancement of oligomer formation related to the arctic mutation results in intracellular toxicity or an inhibition of A β secretion or both. Another example is the observation that triple transgenic mice, containing the Swedish mutant APP and mutated Tau, showed the regular progression of plaque and tangle related pathologies but also displayed inhibited long-term potentiation and synaptic plasticity before either was established¹⁰⁷. These latter symptoms instead correlated with the accumulation of intracellular A β .

In order to accumulate extracellularly A β must first be secreted from the cell, therefore it may be possible that intracellular A β could accumulate without ever being exported. Alternately extracellular A β oligomers have been shown to be taken up by endosomes ¹⁰⁸.

Another argument in support of toxicity caused by intracellular A β is that at concentrations found in human cerebral spinal fluid and brain tissue, A β is capable of causing toxicity in an intracellular fashion ⁷⁷. This often isn't true for experiments investigating extracellular A β toxicity. Intracellular uptake of A β it therefore fundamental to the pathology.

An investigation using Swedish mutant transgenic mice to identify the impact of intracellular A β on the mitochondria revealed significant mechanisms by which intracellular A β related toxicity could be occurring ¹⁰⁹. General mitochondrial dysfunction was observed and more specifically a reduction in cytochrome c oxidase activity which correlated with intracellular A β . This suggests that mitochondrial metabolism is impacted by intracellular A β which would have significantly toxic downstream effects. In the same study, increasing hydrogen peroxide levels were also shown to correlate with intracellular A β .

Calcium homeostasis can also be impacted by intracellular A β ¹¹⁰. When A β oligomers were injected into *Xenopus* oocytes and the calcium ion response was recorded, calcium ion release was observed. Some of this release was inhibited by antagonists of the endoplasmic reticulum membrane receptor inositol triphosphate, suggesting that intracellular A β oligomers were causing calcium release from the ER.

1.4 Cell membrane constituents and AD

Apart from receptors and sites for pore formation for A β oligomers the cell membrane and its constituents play an important role in AD. In particular cholesterol and ganglioside GM1 have been implicated in exacerbating A β activity.

1.4.1 Cholesterol

To say that cholesterol plays an important role in Alzheimer's disease is possibly an understatement. It has been implicated in a number of pathways involved in both A β peptide production and toxicity.

In some forms of familial Alzheimer's disease, a mutation in the ApoE4 gene results in mutant apolipoprotein Epsilon-4 (APOE4) ¹¹¹ and early disease onset. APOE4 has a role in redistributing cholesterol in order to aid membrane repair and facilitate synaptic plasticity (new connections being made by neurons), the disruption of which is commonly referred to as one of the early symptoms involved in AD. It has been proposed that the tight binding of APOE4 to A β induces a conformational

change contributing to A β aggregation ¹¹². However, conflicting evidence as to how APOE4 affects A β has surfaced. It is implicated in both promoting plaque formation and failing to inhibit it as effectively as other APOE isoforms ⁹⁴. Whether or not it is a promotor or a weak inhibitor of plaque formation, APOE4 has also been shown to be less capable of clearing A β from the brain than other APOE isoforms.

The ApoE4 genotype correlates with an accumulation of intracellular A β ¹¹³. APOE4 is speculated to perturb intracellular trafficking, in particular of cholesterol. This is because the higher affinity of A β for APOE4 reduces the lipoprotein's ability to transport cholesterol. However, because cholesterol is implicated in APP processing ⁹³ this lack of cholesterol leads to increased levels of intracellular A β , generating a positive feedback loop for creating more intracellular A β

Cholesterol levels typically correlate with A β levels in both cellular and animal models of AD ¹¹⁴. Mouse models of AD with diet-induced high cholesterol displayed altered APP processing, resulting in increased A β accumulation ¹¹⁵. In the inverse of this experiment, adding statins to remove cholesterol from hippocampal neurons in cell culture inhibited A β formation via APP processing ⁹³. It was proposed that the mechanism by which cholesterol prevents APP processing is by enabling lipid rafts containing the appropriate secretases to localise with APP for processing. Contrasting evidence points to a role where increased cholesterol reduces the amount of APP processing into toxic A β , by modulating α -secretase cleavage of APP. α -secretase does not produce pathological A β peptides as there is no cleavage at the β site ¹¹⁶. The β secretase BACE 1 has also been shown to display higher levels of co-localisation with APP in hippocampal neuronal cell culture when levels of cholesterol are reduced ¹¹⁷. However, cholesterol activity also modulates BACE 1 activity and depleting cholesterol levels led to inhibited APP processing by BACE 1 when it was targeted to lipid rafts using a GPI anchor in human neuroblastoma cells ¹¹⁸. There are numerous contradicting conclusions regarding the effect of cholesterol on APP processing. Clearly however, cholesterol levels have an impact on lipid raft formation which is important in the processing of APP by secretases. By causing an imbalance in either cholesterol levels, for example through diet, or by affecting the transport of neuronal cholesterol, such as by A β binding to APOE4, the processing of APP can be affected, which in AD results in higher levels of A β pathology. Recent work has shown that, conversely, full length APP is required for proper cholesterol homeostasis ¹¹⁹ providing further evidence that APP, cholesterol and A β interactions in AD participate in a vicious cycle resulting in further A β production:

A summary of the relationship between A β and cholesterol is as follows. The processing of APP results in A β . This simultaneously disrupts cholesterol homeostasis (by reducing APP levels) ¹¹⁹ and transport (as A β binds to APOE4) ⁹⁴. This results in an imbalance in cholesterol which is no longer being relocated, resulting in disrupted lipid raft colocalization with existing APP ¹¹⁸. This results in lower alpha-secretase

activity ¹¹⁶ and higher beta-secretase-APP colocalization ¹¹⁷ and activity ¹¹⁸. All this leads to higher levels of APP cleavage to form A β peptides.

However, cholesterol's activity in AD is not only limited to indirect interactions with A β but as a cell membrane constituent it interacts directly with A β ¹²⁰⁻¹²². It has been argued that, as cholesterol can impact on local lipid bilayer compositions, it can facilitate the accumulation of extracellular A β at the cell membrane surface ¹²⁰. It has also been shown that A β oligomers can bind to cholesterol, in preference to other more generic lipids ¹²³.

By using surface plasmon resonance to identify A β interactions, binding of A β to lipid bilayers either made synthetically or derived from vascular smooth muscle cells was shown to be cholesterol dependent ¹²¹. Toxic effects with regard to those bilayers were also measured and these effects were also shown to be cholesterol dependent. Arguably, in AD, the effects of A β on non-neuronal cell types are not as interesting due to the differences in cell membrane constituents. However, this clearly showed the importance of the A β -cholesterol interaction independently of specific neuronal receptors.

Recent work has shown that by impacting on the fluidity of the cell membrane cholesterol can impact on the ability of A β to both localise at the cell membrane and disrupt it ¹²². Neuronal cell membrane fluidity was measured using generalized polarisation imaging with a small percentage of fluorescently labelled lipids. A β association with the membrane was measured using immunocytochemistry and electrophysiological techniques were used to measure membrane perforation. In conditions where cholesterol content was low, the lipid bilayers showed higher fluidity resulting in less accumulation of A β at the surface but higher levels of perforation with respect to the control cells. Contrastingly, at high cholesterol levels membrane rigidity was enhanced, as was A β accumulation at the surface, however, perforation was inhibited. This data showed that, by controlling the fluidity of the cell membrane, cholesterol can regulate the perforation of lipid bilayers by A β . It also suggests that in order to insert into the lipid bilayer, A β requires a low density, highly fluid environment otherwise it will accumulate and cluster onto the surface but not insert and perforate.

Numerous studies show a link between cholesterol and ganglioside GM1 with regard to A β toxicity ^{124,125}. The effects of A β binding to GM1 will be discussed further in section 1.4.2 however, the method by which cholesterol binds to GM1 and facilitates binding to A β is of interest here. Figure 1.11 shows a structure for A β ₅₋₁₆ bound to a GM1-cholesterol complex tested using molecular dynamics simulations ¹²⁴.

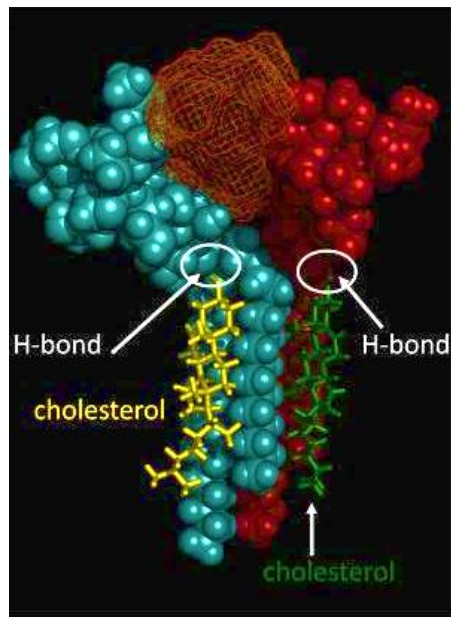


Figure 1.11 Cholesterol facilitating A β binding to GM1. Cholesterol forms a hydrogen bond with GM1 (blue and red models) inducing a 'head tilt' conformation allowing for the binding of A β ₅₋₁₆. Complementary experimental data showed that A β ₅₋₁₆ peptide (orange cage model) more rapidly bound to GM1 in the presence of cholesterol but not in the presence of other lipids. Taken from Fantini et al 2013 ¹²⁴.

Cholesterol was modelled hydrogen bonded with GM1 establishing an altered conformation of the GM1 head group allowing for a stable complex of cholesterol, GM1 and A β ₅₋₁₆. A β ₅₋₁₆ was used as this was the region predicted to bind to GM1. A complementary *in vitro* assay was performed to show that binding of A β ₅₋₁₆ to GM1 was in fact accelerated in the presence of cholesterol.

Finally, cholesterol is one of a number of molecules that has been shown to produce hydrogen peroxide in a copper ion dependent manner in the presence of A β ¹²⁶. Cell culture models of AD were used to show that A β -copper complexes were capable of increasing levels of hydrogen peroxide which in turn correlated with high levels of toxicity. Also implicated in this work as substrates for A β -Cu catalysed conversion resulting in hydrogen peroxide were vitamin C and dopamine.

1.4.2 Gangliosides

Gangliosides are sialic acid containing glycosphingolipids with a single hydrophobic tail and an oligosaccharide hydrophilic head group. They are commonly found in neurons.

Discussions of gangliosides in Alzheimer's disease mostly refer to either a direct interaction with A β resulting in cell membrane perforating oligomers ¹²⁷ or the formation of toxic fibrils ^{128,129}. Either way the work of the Matsuzaki group strongly point to beta-sheet rich toxic aggregates ^{44,128} of A β that are

formed in the presence of the ganglioside GM1, cholesterol and sphingomyelin model membranes that simulate the behaviour of lipid rafts ¹²⁷. An interesting finding is that A β ₁₋₄₀ fibrils prepared in the presence of GM1-cholesterol-sphingomyelin and isolated from the membranes and soluble aggregates were capable of reducing cell viability to 50% ¹²⁹ which is a similar effect to adding 0.2 mM hydrogen peroxide ¹³⁰. It could be argued that as the fibrils were left for at least 7.5 hours some soluble aggregates would begin to repopulate as the sample returned to its equilibrium state. Overall, this result contrasts with two popular ideas, firstly that fibrils cannot be toxic ¹³¹, but also that A β ₁₋₄₀ does not contribute as heavily to toxicity as A β ₁₋₄₂ ⁶³. Fourier transform infrared spectroscopy also showed that A β ₁₋₄₀ fibrils, when formed in the presence of a GM1-cholesterol-sphingomyelin lipid bilayer, contain anti-parallel β sheets as opposed to the exclusively parallel β sheet containing fibrils formed apart from lipid bilayers. However, the authors were not entirely confident in these particular data and therefore concluded that some fibrils formed in the presence of a GM1-cholesterol-sphingomyelin lipid bilayer *may* contain anti-parallel β sheets ¹²⁸.

Recent work has shown that ganglioside nanoclusters found in reconstituted synaptosomal lipid bilayers from aged mouse brain facilitated the formation of spherical assemblies of A β aggregates ¹³². In this context synaptosomal refers to isolated vesicles formed by light homogenisation of the synaptic ends of neurons. It was also shown that these nanoclusters were capable of initiating A β assembly and that the oligosaccharide structures of the gangliosides mediated the generation and elongation of amyloid fibrils. A follow up study showed the differences in compositions of synaptosomal lipid bilayers and non-synaptosomal lipid bilayers. GM1 was equally abundant in both bilayers although the ratio of GM1:GM3 (0.6:1 and 0.3:1 respectively) and cholesterol was higher in synaptosomal lipid bilayers than in non-synaptosomal lipid bilayers ¹³³. The importance of GM3 is that, of the gangliosides tested, it was the only one that didn't facilitate fibril formation. The concentration of GM1 in ganglioside nanoclusters was also shown to be higher in those that readily interacted with A β .

Interestingly, given the specificity of GM1 as the contributor to toxic A β activity, a lipidomic analysis of mouse and human brain with Alzheimer's disease showed that there is an enrichment in GM3 in AD but not GM1. The authors also presented anomalies in ganglioside metabolism however and they did not present a reduction in GM1 levels ¹³⁴.

1.4.3 Cell membrane structure and AD

Whilst the majority of the literature focuses on pore forming species of A β with regards to membrane disruption, a number of studies describe a more general characterisation of membrane disruption. In particular, membrane thinning is often mentioned ¹³⁵⁻¹³⁸. The evidence of potential membrane thinning in AD comes from an experiment measuring changes in conductance across patch clamped

mammalian cells as a response to A β species¹³⁹. It was shown that only oligomers can increase this conductance and the authors concluded that localised defects or membrane thinning could contribute to the observed dielectric constant increase. Further evidence presented in this work showed that A β could be rapidly removed from model lipid bilayers and the cell membrane of mammalian cells which the authors argued was due to a lack of insertion into the bilayer. They also argued that these results suggested that A β oligomers could increase the area per molecule of the bilayer due to membrane thinning.

More recent work using molecular dynamics simulations of A β trimers showed localised thinning of lipid bilayers on POPG bilayers (a lipid with a negatively charged headgroup commonly found in mammalian cells)¹³⁵. There have been little to no reported instances of the direct observation of membrane thinning of either model lipid bilayers or cell membranes either *in vitro* or *in vivo*.

Despite this, a recent study investigated the inverse relationship, how a thin lipid bilayer affects A β behaviour¹³⁶. The authors argue that membrane thinning is relevant to AD as lipid peroxidation, which is reported to occur in AD^{140,141}, can result in changes to the physical properties of lipid bilayers such as thinning¹⁴². The A β related activity of DLPC (a short chain lipid with a zwitterionic headgroup) model lipid bilayers was compared with that of DOPC (a “normal” chain length lipid with the same headgroup as DLPC) bilayers. A combination of fluorescence assays, circular dichroism, AFM, TEM and NMR was used to determine that thin DLPC lipid bilayers were able to more rapidly instigate aggregation of toxic A β species. The authors suggested that more favourable hydrophobic matching in thinner membranes would allow for the insertion of A β into the lipid bilayer. It was also shown that preformed amyloid fibrils, when in contact with DLPC lipid bilayers, were remodelled into protofibril like structures that presented similar toxicity to aggregates prepared directly from monomeric A β . These data suggest that lipid bilayer thickness, regulated by lipid peroxidation, could in turn regulate A β aggregation and toxicity in AD.

1.5 Human cystatin C and AD

Attempts at the discovery of biomarkers for the identification of AD has provided valuable information. The most common strategy is to identify proteins that exist at higher levels in the CSF in AD patients. A number of binding partners for A β have been discovered this way including transthyretin and human cystatin C (hCC)¹⁴³⁻¹⁴⁵. Although levels of hCC and transthyretin have also been shown to be reduced in the brains of some Alzheimer’s patients¹⁴⁶, hCC has been suggested as a possible drug target in AD^{147,148}. The activity of hCC in AD will be discussed here and in chapter 6 where the interaction between hCC and A β will be examined further.

1.5.1 *In vivo* hCC and AD

Separate studies have identified polymorphisms in the CST3 gene, which is the hCC gene, as being an associated risk factor for late onset Alzheimer's disease ^{149,150}. Coupled with evidence that hCC is observed at elevated levels in AD ¹⁵¹, two potential hypotheses emerge: Mutated hCC directly contributes to AD toxicity or hCC can inhibit AD toxicity and this activity is reduced in mutants.

Evidence for the direct contribution of hCC to toxicity in AD is that neuronal cell death was observed in rats when hCC was injected into the hippocampus of rats ¹⁵². However, hCC is a cysteine protease inhibitor and the observed cell death was inhibited by cathepsin B which is a cysteine protease. Neuronal cell death could therefore be attributed to the cysteine protease inhibitory activity of hCC. This does not exclude hCC from directly contributing to toxicity in AD but, given the numerous ways in which A β and Tau can cause toxicity it appears unlikely that toxicity attributed to hCC plays an important role.

A positive role for the activity of hCC has also been displayed *in vivo* ¹⁴⁸. Transgenic mouse models expressing hCC and overexpressing APP showed that extracellular A β deposition was substantially diminished. A similar study in which hCC was overexpressed in mouse models expressing APP reported reduced deposition of extracellular A β but also showed co-immunoprecipitation of hCC and A β ¹⁴⁷. Given the numerous ways in which cystatin C can affect cell death, the authors use this experiment to show that the activity of hCC is predominantly down to its direct interaction with A β .

1.5.2 *In vitro* hCC and A β

Further evidence for the positive role of hCC in AD has been shown by adding hCC alongside various preformed A β aggregates extracellularly to hippocampal neuronal cells ¹⁵³. Once again, it was shown that hCC prevented A β toxicity although in this experiment it was possible to also examine the direct impact of hCC on the A β structures present. HCC was not able to dissolve A β fibrils or insoluble oligomers indicating that this is not part of its inhibitory mechanism of action.

Another study using Immunofluorescence showed the colocalisation of hCC this time with APP in kidney cells and mouse neuroblastoma cells shown in figure 1.12 ¹⁵⁴.

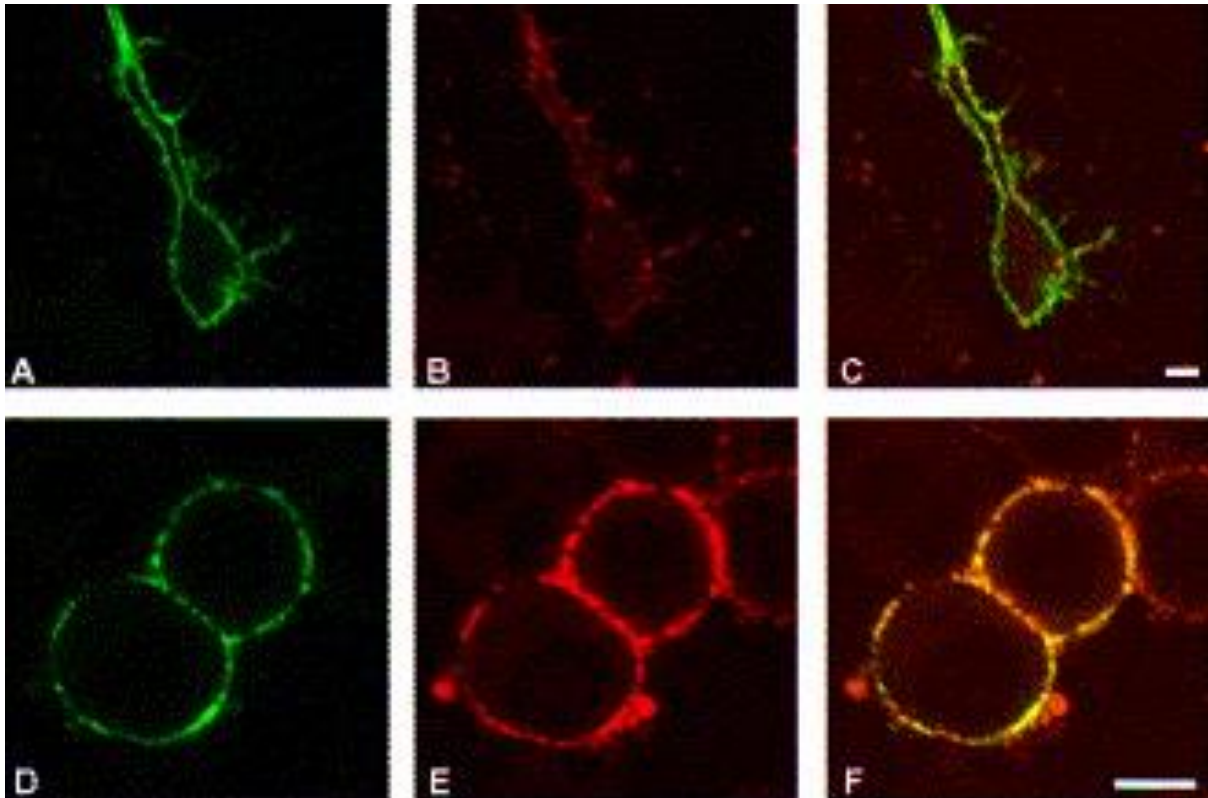


Figure 1.12 hCC colocalises with APP in mouse neuroblastoma cells. Fluorescently labelled anti-APP (green) was imaged in A and D and fluorescently labelled anti-hCC was imaged in B and E (red) with the overlap shown in C and F. Colocalisation of hCC and A β can be observed and is represented by the yellow colour. Taken with permission from Sastre et al 2004¹⁵⁴.

In the same study, an ELISA assay was performed to determine how strongly hCC bound to monomeric A β and the results are shown in figure 1.13. For A β_{1-40} a binding constant of 16.4 nM was determined for binding to wild type hCC. The binding constant for the binding of A β_{1-42} to wild type hCC was determined to be 10.6 nM. Tight binding of hCC to A β was therefore reported.

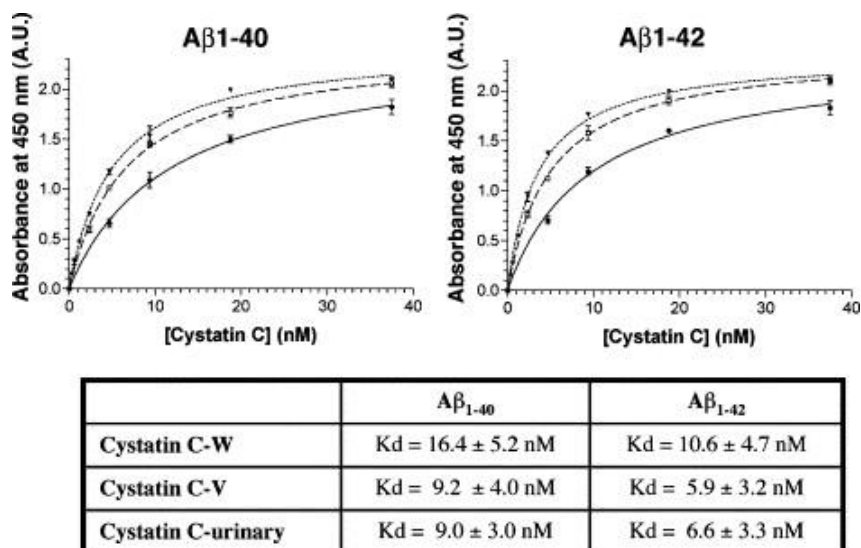


Figure 1.13 A β binds tightly to both wild type and variants of hCC. Wild type (solid line), variant (dashed line) and urinary (dotted line) hCC were incubated for 3 hours with immobilised A β ₁₋₄₀ and A β ₁₋₄₂. Anti-hCC was added followed by anti-IgG labelled with horseradish peroxidase. The amount of bound hCC was therefore determined by measuring the absorbance at 450 nm. Binding constants were calculated from this data and were tabulated. Taken with permission from Sastre et al 2004¹⁵⁴.

In mouse primary neurons, hCC is secreted from the cell by both the classical secretory pathway as determined by the signal peptide sequence of hCC and also in association with exosomes¹⁵⁵. The association of hCC with exosomes was reduced in mice overexpressing 2 familial AD-associated presenilin mutations. Presenilin is one of the core proteins in the gamma secretase complex⁹. A reduction of APP metabolites associated with exosomes was also reduced suggesting that hCC bound A β no can no longer be secreted from the cell in an exosome associated manner. This could result in an increase in intracellular A β .

A recent study has investigated the interaction between oligomeric hCC and A β . Overexpression of hCC in *E. coli* produced not only monomeric hCC but also oligomeric hCC as detected by DLS¹⁵⁶. Oligomeric hCC was purified and incubated with monomeric A β ¹⁵⁷. Fibril formation was measured by thioflavin T fluorescence. Monomeric and dimeric hCC were also tested and showed moderate inhibition of fibril formation. Oligomeric hCC however showed total inhibition of A β fibril formation. Arguably, as prior to the detection of oligomeric hCC the sample is concentrated to 1 mg/ml, there is a potential for micellar like hCC structures to form from unfolded hCC rather than oligomeric as unfolded proteins have a critical micellar concentration¹⁵⁸. Furthermore, micellar hCC may appear to be a similar size to the oligomeric hCC presented. This would provide an obvious explanation as to

why the apparent oligomeric hCC would be a more potent inhibitor of fibril formation as in micellar hCC, there would be exposed hydrophobic residues that would readily bind A β . Importantly then, the cysteine protease inhibitory activity of oligomeric hCC was determined to be as good as that of monomeric hCC. In domain swapped dimeric cystatin, the loss of an exposed hydrophobic loop from the active site results in a lack of enzyme inhibition. Therefore, the oligomeric hCC was judged to maintain the secondary and tertiary structure of hCC suggesting that it is not unfolded hCC forming micelle like structures. Whether or not oligomeric hCC exists in AD is yet to be determined.

In our laboratory in Sheffield, an investigation into the manner in which monomeric hCC interacts with monomeric A β was carried out using thioflavin T fluorescence, high-performance liquid chromatography (HPLC) and NMR spectroscopy¹⁵⁹. Thioflavin T fluorescence showed a concentration dependent inhibition of fibril formation by monomeric hCC (figure 1.14). As hCC concentration increased, fibril formation was reduced up to the point at which fibril formation was totally inhibited at ratio of [hCC]:[A β] at 2:1. Interestingly, in cases where fibril formation was not totally inhibited, the rate of fibril formation was not modified by hCC.

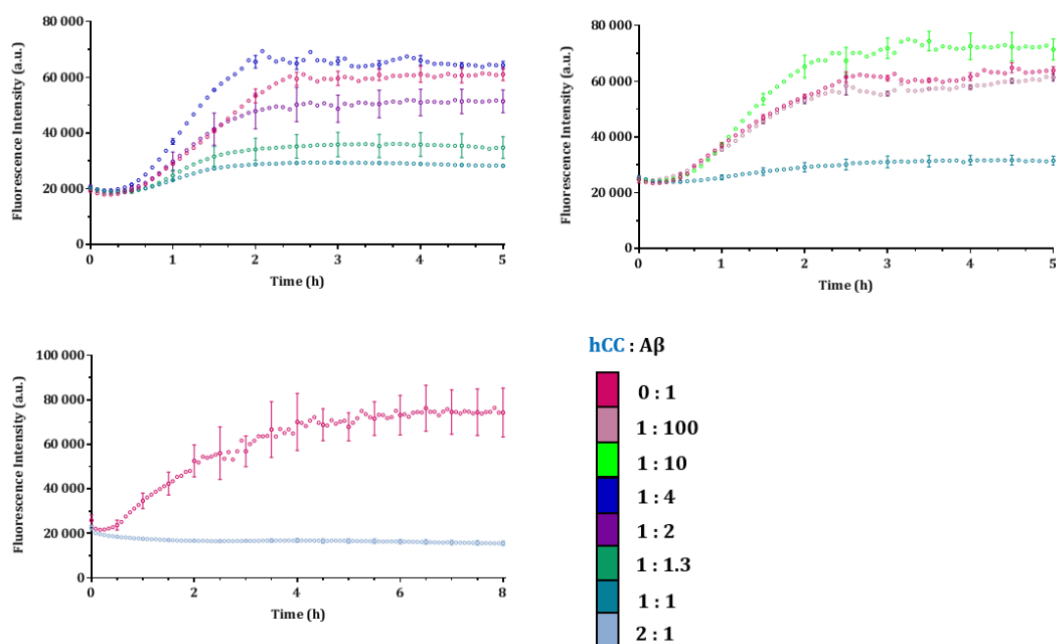


Figure 1.14 hCC inhibits A β fibril formation in a concentration dependent manner. Time courses of A β fibril formation were measured by thioflavin T fluorescence in the presence of increasing concentrations of hCC. As the concentration of hCC increased the amount of fibril formation was reduced. At an [hCC]:[A β] ratio of 2:1 no thioflavin T fluorescence was measured suggesting complete inhibition of A β fibril formation. Taken from Williams 2014¹⁵⁹

HPLC analysis of A β fibril formation in the presence of hCC showed only a small change in the presence of monomeric hCC ¹⁵⁹. The monomeric peak for hCC was observed to be 25% smaller from the beginning to the end of a 24 hour time course and no peak was observed that could be identified as an hCC-A β complex. This result contradicts results obtained in a previous study where a shift in the hCC peak is observed ¹⁶⁰. This is most likely due to the difference in gel filtration columns used to attempt to separate the A β bound hCC from the rest. In the study where binding was observed a superdex 75 gel filtration column was used which would not be able to resolve bound and unbound hCC ¹⁶¹. The more likely explanation is that A β aggregates were responsible for the shift in the observed peak.

Monomeric A β was titrated into a sample of hCC at 50 μ M for analysis by NMR spectroscopy ¹⁵⁹. Chemical shift changes in hCC were tracked as A β was added but no significant shifts were observed. This was still the case when hCC and A β had been left at a 1:1 ratio for 24 hours at 30 °C. There was however a significant change in amide peak intensity across hCC suggesting a change in the chemical environment of these residues, potentially due to A β interaction. One explanation is that the amount of soluble hCC is reduced as it is incorporated into aggregates. This would also explain the loss of 25% of monomeric hCC observed by HPLC.

These results presented a conundrum. Previous work showed that hCC binds tightly to A β with a nanomolar binding constant ¹⁵⁴. Other works show the impact of the interaction between hCC and A β , colocalised to cell membranes ¹⁵³. Yet in this study, despite showing that hCC can inhibit fibril formation in a concentration dependent manner, little significant interaction was observed between hCC and A β . It was speculated that maybe A β species were catalytically converted by a transient hCC interaction to a species that were not on pathway to forming fibrils.

Finally, a more recent study from our laboratory in Sheffield investigating the ability of various hCC mutants the inhibition of A β fibril formation using thioflavin T showed that certain mutations caused a reduction in hCC inhibitory activity as shown in figure 1.15 ¹⁶².

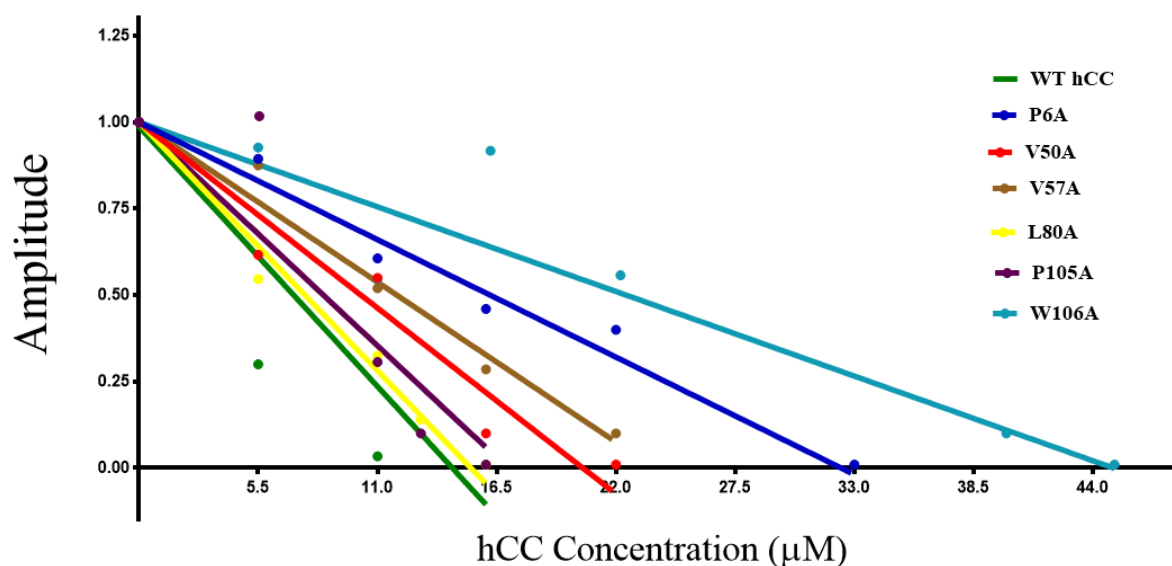


Figure 1.15 Mutations in hCC reduce its ability to inhibit fibril formation. The final amplitude of fibril formation from thioflavin T time courses was plotted against the concentration of hCC. The concentration of A β was always 11 μ M. The data were fitted to a linear regression model. In some instances, significantly more mutant hCC was required to totally inhibit fibril formation with the W106A mutant requiring a [hCC]:[A β] at 4:1. Taken from Al-Jaff 2016 ¹⁶².

Candidate residues for mutations were chosen due to their location in hydrophobic patches on the surface of hCC as it was hypothesised that these were likely binding sites for A β . The W106 residue is located in the cysteine protease inhibitory active site loop that undergoes a conformational change in the domain swapped dimer ¹⁵⁷. The W106A mutant showed the most change in behaviour suggesting that A β -hCC interactions take place at the active site loop. The P105A mutant which is adjacent to W106 showed a moderate change in behaviour. Another significant change in behaviour is when the N-terminally located P6 residue is substituted for an alanine residue. These residues are highlighted in figure 1.16.

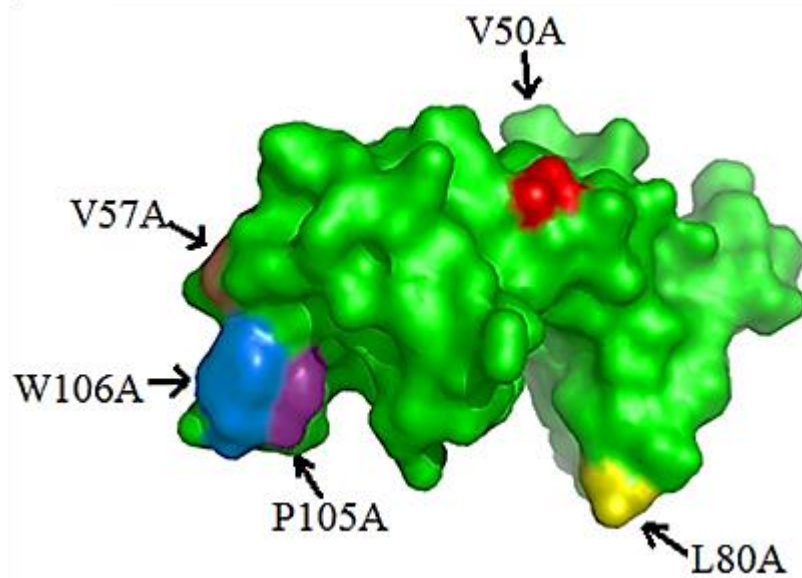


Figure 1.16 A surface plot of hCC. Examples of the locations of some of the mutations made to hCC for the experiment detailed in figure 1.15 are shown. The mutated residues are highlighted in different colours. Taken from Al-Jaff 2016 ¹⁶².

From the same study ¹⁶² the effects of agitation on the ability of hCC to inhibit A β fibril formation were investigated (figure 1.17). It was shown that, in conditions where the sample was continually agitated, 4 times more hCC was required to totally inhibit fibril formation. This suggests that the interaction between A β and hCC is affected by agitation which could have potential implications in AD and other neuropathologies. For example, Parkinson's disease is associated with high contact sports such as rugby and American football in which high levels of agitation are exerted on neuronal cells.

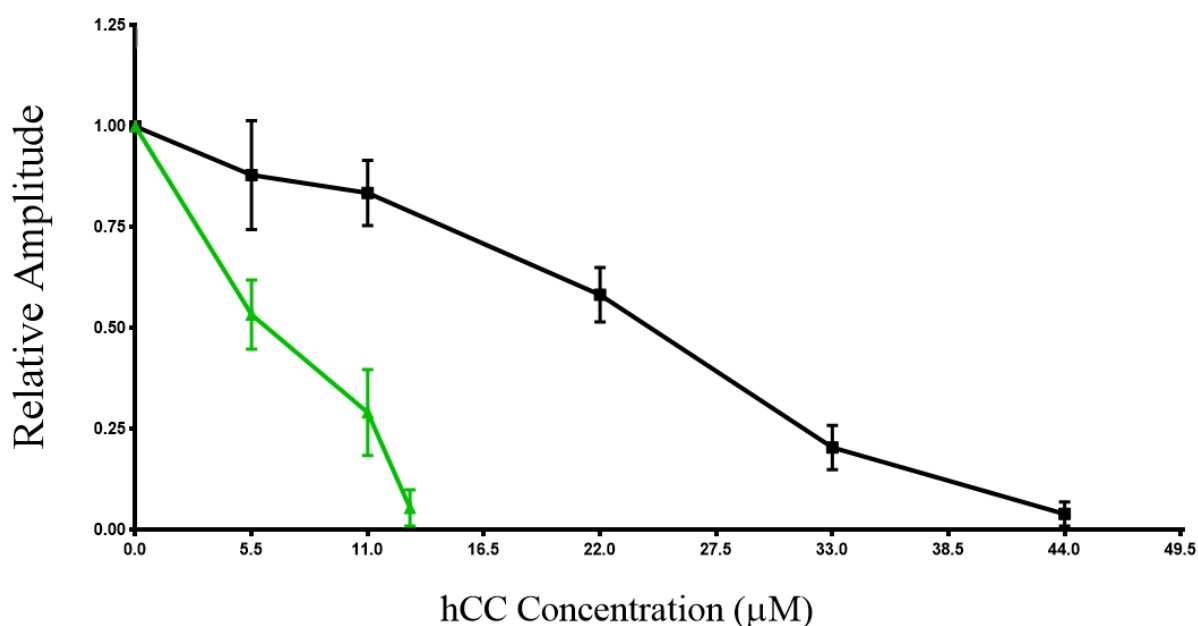


Figure 1.17 Agitation prevents hCC from inhibiting fibril formation. The final amplitude of fibril formation (relative to the amplitude of fibril formation in the absence of any hCC) was plotted against the concentration of hCC in the sample. Minimally agitated samples are presented in green and agitated samples are presented in black. Taken from Al-Jaff 2016 ¹⁶².

1.6 Conclusions

There is a wealth of data regarding the intricate methods by which A β can cause havoc in the brains of people with AD. The majority of studies so far however, have focused on the effects caused by A β on various systems rather than the effects of those systems on A β behaviour. The studies that do focus on how A β is affected are mostly focused on fibril formation which is indeed a useful indicator of normal A β behaviour. In order to be able to better understand A β behaviour *in vivo*, *in vitro* experiments should be performed in a range of conditions that mimic disease states in AD such as those involving different model cell membranes ^{128,132,133,136,163}. This will allow us to find the information required in order to better design drugs that will be effective in AD.

The mechanism of *how* hCC inhibits A β toxicity remains a mystery. Evidence shows that it inhibits normal A β behaviour *in vitro* ^{154,159,162} but this doesn't fully explain the data from *in vivo* experiments ^{147,148,153}. This is because inhibiting fibril formation is not the same as inhibiting toxicity ⁴². Human cystatin C has also displayed contradictory results, in seemingly identical experiments different behaviours are observed with regard to A β interactions. In order to obtain the full picture, experiments should be examined in the context of how A β behaves in a range of conditions as this might impact on how hCC interacts with it and thus provide a mechanism for how A β behaviour might be modulated.

1.7 Thesis overview

The aim of this study was to investigate if and how lipid bilayers altered the interaction between A β ₁₋₄₂ and hCC. Evidence that A β can induce permeation in lipid bilayers as a mechanism by which they are toxic combined with evidence that hCC inhibits A β toxicity led to the hypothesis that hCC might prevent permeation in lipid bilayers.

In testing this hypothesis, an observation was made about the general effects of different surfaces on A β behaviour in the absence of hCC. In chapter 3, the results of testing different surfaces using AFM, thioflavin T assays and dye release from lipid vesicles will indicate a strong surface dependence of A β behaviour.

In chapter 3, it will be shown that lipid vesicles rupture upon addition to low-binding microplates. This interaction was investigated in more depth, using dye release assays, with the intent to determine whether the rupturing was due to the formation of functional supported lipid bilayers coating the surface of the microplates. The results of this investigation will be presented in chapter 4 as well as an analysis of the usefulness of the potential new technology in performing thioflavin T assays.

Previous studies investigating the interactions between A β and lipid bilayers have not accounted for third party surfaces that are necessary to contain any given reaction. Therefore, in chapter 5, the results of an investigation into the effect that lipid bilayers have on various A β behaviours will be presented. It will be shown that, in a manner dependent on the lipid bilayer constitution, A β induced permeation of lipid bilayers can be promoted independently of fibril formation.

Finally, the impact of surfaces in general, but also lipid bilayers, on the interaction between hCC and A β was investigated. Chapter 6 will show the results of an investigation into how hCC can interact strongly with A β in the presence of some surfaces but not others.

It was decided that further examination of how different conditions can affect the behaviour of A β was required. Specifically, the effects of different concentrations of salt on the behaviour of A β were investigated. TEM and AF4-MALS data will be presented in chapter 7, revealing that the resulting fibril morphologies can be salt dependent.

Chapter 2: Methods and Materials

2.1 Buffers and Reagents

All reagents were purchased from Fisher (USA), Melford (UK) or Sigma-Aldrich (DE), unless stated otherwise. Water was purified and deionised (18.2 Ω) from an Elga Purelab 611 Classic UVF. This was used for all experiments. Buffers were prepared as per Sambrook *et al* 1989¹⁶⁴ and filtered through a 0.2 μ m filter. Except those used for bacterial growth, 1 mM sodium azide (NaN₃) was added to all buffers.

2.2 A β ₁₋₄₂ preparation

2.2.1 Monomer protocol 1

Lyophilised, HFIP treated, monomeric A β ₁₋₄₂ and monomeric A β ₁₋₄₀ was purchased from rPeptide (USA). 1 mg vials were received and stored at -20 °C. The A β was resuspended to 1 mg/ml in HFIP and sonicated for 10 minutes to resuspend all the material. The resuspended material was then aliquoted into 100 μ l volumes. The HFIP solvent was then removed using a stream of nitrogen gas. The remaining HFIP was removed by freeze drying. The lyophilised material was stored again at -20 °C. For use, each aliquot of lyophilised material was resuspended to 1 mg/ml in 10 mM NaOH with 30 minutes of sonication. The monomeric A β was then diluted into the experimental buffer to the desired concentration.

2.2.2 Monomer protocol 2

As before A β was purchased from rPeptide (USA). However, rather than resuspending the A β in HFIP, it was resuspended to 1 mg/ml in 50 mM NaOH with 30 minutes of sonication. The resuspended material was then aliquoted into 100 μ l volumes, flash frozen in liquid nitrogen and stored at -80 °C. For use the aliquots were defrosted and the monomeric A β was diluted into the experimental buffer to the desired concentration.

2.3 Human Cystatin C preparation

2.3.1 Growth Media and Solutions

Luria-Bertani Media (LB)

Per litre of deionised water:

- tryptone 10 g

- yeast extract 5 g
- NaCl 10 g

The solution was adjusted to pH 7.0, made up to 1 litre with deionised water and sterilised by autoclaving. Antibiotic was added after cooling. If LB-agar was required, 28 g Nutrient Agar (Oxoid Ltd, UK) was made up to 1 litre with deionised water and autoclaved.

RF1 Buffer

- 30 mM KCH₃CO₂
- 100 mM RbCl
- 10 mM CaCl₂
- 50 mM MnCl₄
- 15% glycerol

The buffer was adjusted to pH 5.8 and was stored at 4 °C.

RF2 Buffer

- 10 mM MOPS
- 10 mM RbCl
- 75 mM CaCl₂
- 15% glycerol

The buffer was adjusted to pH 6.5 and was stored at 4 °C.

M9 Minimal Media

Per litre of deionised water:

- Na₂HPO₄ 6 g
- KH₂PO₄ 3 g
- NaCl 0.5 g

The solution was adjusted to pH 7.4 and the volume made up to 1 litre before sterilisation by autoclaving.

The following were added to the media immediately before use (per litre):

- trace elements 650 µl (autoclaved)
- glucose 2g
- 10 mg/ml thiamine 0.1 ml

- 0.5 mg/ml (NH₄)₂SO₄ 2 ml
- 1 M MgSO₄ 1 ml (autoclaved)
- 1 M CaCl₂ 0.1 ml (autoclaved and added last)

All solutions were 0.2 µm filter-sterilised before use except where autoclaved as indicated. The flask was swirled immediately to disperse precipitate; if precipitate did not disperse then the preparation was abandoned.

Trace Elements

Per 100 ml deionised water:

- CaCl₂·2H₂O 550 mg
- MnSO₄·H₂O 140 mg
- CuSO₄·5H₂O 40 mg
- ZnSO₄·H₂O 220 mg
- CoCl₂·6H₂O 45 mg
- Na₂MoO₄·2H₂O 26 mg
- H₃Bo₄ 40 mg
- KI 26 mg

The above solutions were added to 70 ml of deionised water and the pH adjusted to 8.0 before adding:

- EDTA 500 mg

The pH was again adjusted to 8.0 before adding:

- FeSO₄·7H₂O 375 mg

The solution was made up to 100 ml with deionised water before autoclaving.

Ampicillin

100 mg/ml ampicillin sodium salt was dissolved in water to produce a 1000 x stock solution, and 0.2 µm filter-sterilised. Aliquots were stored at -20°C, then gently thawed and added to growth media to a final concentration of 100 µg/ml as required.

Isopropyl-β-D-galactosidase (IPTG)

120 mg/ml isopropyl-β-D-galactosidase was dissolved in water to produce a 1 M stock solution, and 0.2 µm filter-sterilised. Fresh solution was added to growth media as required to induce protein over-expression.

2.3.2 Preparation of competent cells

Two strains of *E. coli* were prepared BL21 for expression and XL10 blue for plasmid production.

Nutrient agar plates were made and non-competent cells from glycerol stocks (stored at -80 °C) were streaked onto the plates. The plates were then incubated overnight at 37 °C. 5 ml of LB was inoculated with a single colony from the streak plate and this was incubated again at 37 °C with shaking at 200 rpm overnight. 200 µl of the overnight culture was used to inoculate a further 10 ml of LB and the new culture was grown at 37 °C until the OD₆₀₀ reached 0.6. The culture was then incubated on ice for 5 minutes. The cells were pelleted by centrifugation at 1663 x g for 10 minutes at 4 °C. 3.3 ml of RF1 buffer was used to re-suspend the pellet. This was then re-pelleted using the same centrifugation method. The pellet was resuspended in 1 ml of RF2 buffer and incubated on ice for 30 minutes. 200 µl aliquots were stored at -80 °C.

2.3.3 Transformations

A 200 µl aliquot of competent cells was defrosted and transferred to a 14 ml falcon tube. 1.5 µl of plasmid DNA was added to the tube and the sample was incubated on ice for 30 minutes. The cells were incubated for 90 seconds at 42 °C followed by incubation for 2 minutes on ice. The solution was made up to 1 ml using LB and this was incubated at 37 °C for 90 minutes with shaking. The cells were serially diluted into fresh LB and plated out onto agar plates containing ampicillin. These were grown overnight

Wild type hCC cloned into the pIN-III-ompA periplasmic expression system was provided by Dr Abi Williams. 1.5 µl of plasmid DNA was added to 200 µl of competent cells in a 14 ml polypropylene Falcon tube on ice and incubated for 30 minutes. The cells were heat shocked at 42°C for 90 seconds and then incubated on ice for 2 minutes. 800 µl of non-selective LB was added and incubated at 37°C with shaking for 90 minutes. Aliquots of 100 µl, 10 µl and 1 µl (diluted in fresh LB) were plated out on selective plates and grown overnight at 37°C.

2.3.4 Plasmid production

Plasmid production was carried out using the *E. coli* XL10 blue strain. Extra plasmids were produced following the protocol acquired with the Qiagen midi prep kit. The final step involved eluting the plasmid into water rather than buffer to allow for sequencing of the resulting plasmids.

2.3.5 DNA Sequencing

Sequencing was carried out by GATC-Biotech (DE) using the following primer sequence:

| | | | |
|--------------|----------------|-------------|--------------------|
| hCC-F | GCTAGAGAGGCTTT | TM = 51.2°C | Forward sequencing |
| | ACAC | | primer |

2.3.6 Over-Expression

Expression was carried out in *E. coli* BL21 strain. Previous work had removed the rare codons found in genes for human proteins to allow expression in this strain.

Single colonies of *E. coli* BL21 carrying the hCC plasmid DNA were used to inoculate 10 ml of LB broth. Cultures were grown overnight at 37°C. 8 x 600 ml (4.8 L total) of M9 minimal media was inoculated with overnight cultures. Cultures were grown at 37 °C with shaking at 200 rpm. Cell growth was monitored by measuring the OD₆₀₀. When the OD₆₀₀ was between 0.4 and 0.6 the cultures were induced with IPTG which was diluted into the cultures to a concentration of 75 µM. The cultures were then incubated once more at 37 °C with shaking at 200 rpm for 5 hours.

2.3.7 Periplasmic Extraction

The cultures were divided into centrifuge tubes and pelleted by centrifugation at 18,592 x g for 15 minutes. The pelleted cells were re-suspended in 14 ml of 20 % sucrose, 0.2 M Tris at pH 8.0 by shaking gently at 30 °C. The resuspended cells were centrifuged at 48,384 x g for 15 minutes. These pellets were resuspended in 28 ml of 2 mM EDTA pH 8.0 at 4 °C using pasteur pipettes. The solution was once again centrifuged at 48,384 x g for 15 minutes, this time at 4 °C, and the supernatant was collected. Roche EDTA-free protease inhibitors (1 tablet per 50 ml of supernatant), 0.1 mg/ml DNase and 20 mM MgCl₂ were added. The sample was left in dialysis tubing overnight to dialyse into 10 mM sodium phosphate buffer at pH 7 at 4°C.

2.3.8 Cation Exchange Chromatography

A 100 ml SP-Sepharose (GE healthcare, USA) cation exchange column was equilibrated with cold 10 mM sodium phosphate buffer pH 7.0, at a rate of 2 ml/min. The dialysed periplasmic extract was kept on ice before being loaded onto column. 10 mM sodium phosphate pH 7.0 was washed down the column until the A₂₈₀ of the eluent had peaked and then reached the baseline. The buffer was then substituted for 10 mM sodium phosphate buffer pH 7.0, 0.2 M NaCl. 5 ml fractions were collected until the A₂₈₀ of the eluent reached the baseline. The buffer was once again substituted, this time for sodium phosphate buffer pH 7.0, 1 M NaCl. Again, 5 ml fractions were collected until the A₂₈₀ of the eluent reached the baseline. The fractions were analysed by SDS-PAGE (see section 2.3.7) and those containing hCC were pooled and stored at 4°C overnight.

2.3.9 Size-Exclusion Chromatography

The pooled sample was concentrated to a volume of 10 ml using a vivaspin (sartorius) with a 5000 KDa molecular weight cut off using a PES membrane. The sample was loaded onto either a 400 ml or 500 ml Superdex 75 gel filtration column (GE Healthcare, USA). The column had been equilibrated with a running buffer that was 10 mM sodium phosphate buffer pH 6.0, 0.1 M NaCl overnight. Running buffer was run into the column at 3 ml/min and 6 ml fractions were collected. Once again, the fractions were analysed using SDS-PAGE to determine hCC content shown in figure 2.1. The average yield of pure hCC was 1-2 mg per litre of culture.

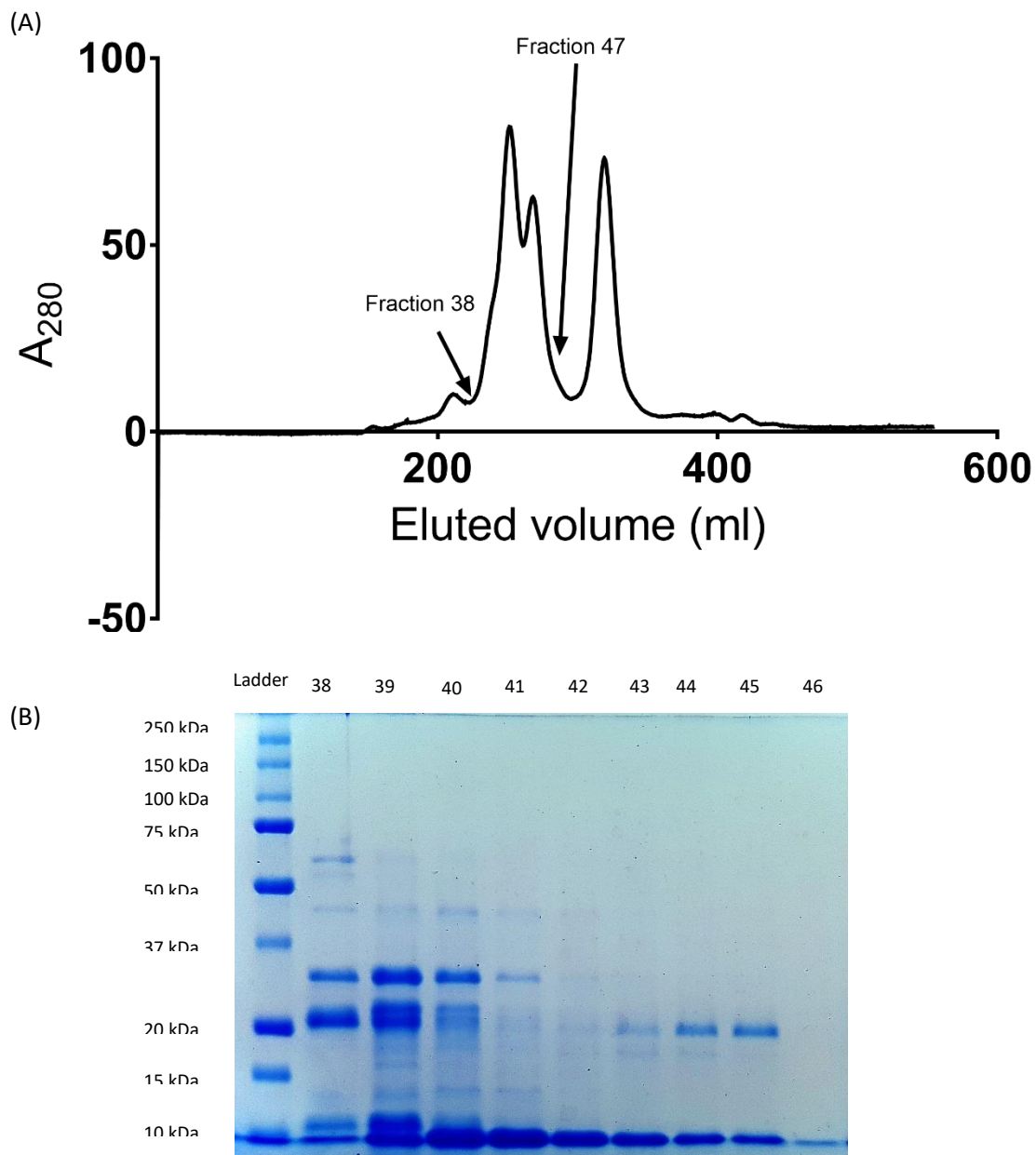


Figure 2.1 The purity of hCC analysed by SDS-PAGE. Human Cystatin C was over-expressed in *E.coli* and purified using ion exchange and size exclusion chromatography. The elution profile from size exclusion chromatography showed four peaks. Analysis by SDS-PAGE revealed that hCC (13.5 kDa) eluted between fractions 38 and 46 with fraction 42 containing pure hCC.

2.3.10 SDS Polyacrylamide Gel Electrophoresis

All electrophoresis was carried out using a Bio-Rad (USA) Mini Protean II apparatus.

SDS-PAGE Buffers

4x Upper Buffer

- 0.5 M Tris HCl pH 6.8
- 0.4% (w/v) SDS

4x Lower Buffer

- 1.5 M Tris HCl pH 8.8
- 0.4% (w/v) SDS

Running Buffer

- 25 mM Tris HCl pH 8.3
- 190 mM glycine,
- 0.1% (w/v) SDS

2x Loading Buffer

- 100 mM Tris HCl pH 6.8
- 200 mM DTT
- 4% (w/v) SDS
- 0.2% (w/v) bromophenol blue
- 30% (v/v) glycerol.

200µl aliquots were frozen at -20°C and defrosted as required.

Instant blue (Generon)

Gel Preparation

4% stacking gels were cast above 16% resolving gels as described below:

16% Resolving gel (per gel):

- 2.5 ml 4x Lower Buffer
- 4 ml 40% acrylamide (acrylamide: bisacrylamide ratio 37.5:1) (Bio-Rad)
- Make up to 10 ml and shake before adding:
- 100 µl 10% (w/v) ammonium persulphate (APS)

- 10 μ l N, N, N', N'-tetramethylethylenediamine (TEMED) (Bio-Rad)

4% Stacking gel (per gel):

- 2.5 ml 4x upper buffer
- ml 40% acrylamide (acrylamide: bisacrylamide ratio 37.5:1) (Bio-Rad)
- Make up to 10 ml and shake before adding:
- 100 μ l 10% (w/v) ammonium persulphate (APS)
- 10 μ l N, N, N', N'-tetramethylethylenediamine (TEMED) (Bio-Rad)

Samples were prepared with a 1:1 ratio of 2x loading buffer to protein solution, and 20 μ l were loaded onto the gel. Gels were run with running buffer at 180 V for 55 minutes. Gels were then stained on a rotating platform for 20 minutes using instant blue. Bio-Rad (USA) pre-stained Precision Plus Protein Dual Standards were used.

2.3.11 Determination of Protein Concentration

The concentration of protein was determined by measuring the UV absorption spectra at 280 nm using a Varian Cary 50-Bio UV-Visible spectrophotometer. Protein concentration was calculated using the Beer-Lambert law:

$$A = \epsilon l c$$

where A is the absorbance, c is the concentration (M), ϵ is the molar extinction coefficient ($M^{-1} cm^{-1}$) and l is the pathlength (cm). Human Cystatin C had an extinction coefficient of 11050.

2.4 Lipid Handling

2.4.1 Preparation of Lipid Stocks

All lipids were purchased from Avanti Polar Lipids (USA). Using all glass equipment, 5 ml of chloroform was added into a vial containing 100 mg of lyophilised lipid (DOPC, DOPG, GM1 or cholesterol) and this was added to a further 5 ml of chloroform in a separate glass beaker. This solution was then aliquoted out into 1 ml aliquots (10 mg) and stored at -20 °C. Alternately if lipids were received in chloroform they were poured into a glass beaker and aliquoted out before storage at -20 °C.

2.4.2 Preparation of large unilamellar vesicles (LUVs) and small unilamellar vesicles (SUVs)

A suitable mixture of lipids was dispensed into a glass round bottomed flask and the the chloroform was removed with a stream of nitrogen gas to create a lipid film. 1 ml of 50 mM sodium phosphate buffer at pH 7.4 was added to the lipid film. The films were resuspended by vortexing vigorously until

the solution became cloudy and the lipid film had disappeared. The samples were then passed through the Avanti Polar Lipids mini-extruder with a 200 nm membrane for LUVs and a 50 nm membrane for SUVs at least 11 times. The LUVs were filtered through a PD-10 mini-column (GE Scientific, USA) and eluted in 50 mM sodium phosphate buffer. This process diluted the LUVs to a final concentration of between 2.5 and 3 mg/ml. Quality control of these preparations was performed using a range of techniques and is presented below (section 2.8).

2.4.3 SLB formation

10 mg/ml of SUV solution was incubated onto freshly cleaved mica for 30 minutes at room temperature.

2.5 Transmission Electron Microscopy (TEM)

Carbon-coated copper grids (Agar Scientific, UK) were glow-discharged for 1 minute using a Cressington (UK) 208 glow-discharge unit. 10 μ l of sample material were adsorbed onto a freshly glow-discharged grid for 1 minute. The grids were washed in two drops of water and two drops of 0.75% uranyl formate and blotted between each wash. The grids were held in the final drop of 0.75% uranyl formate for 20 seconds. Finally, the grids were dried with gentle vacuum suction after blotting. A Philips (UK) CM-100 electron microscope, equipped with a 1024 x 1024 pixel Gatan CCD camera, was used to record micrographs. The microscope was operating at 100 KV using a LaB6 filament.

2.6 Atomic Force Microscopy (AFM)

Samples were prepared on either freshly cleaved mica (Agar Scientific, UK) or a silicon wafer with dust removed by N₂ gas. The mica and silicon substrates were glued to a glass microscope slide using green glue (JPK) and were positioned on the MFP-3D (Asylum Research, UK) microscope stage prior to being incubated with the sample. MLCT chips were purchased from Bruker (DE). All tips except for tip E were broken off using a pair of tweezers. The spring constant for each tip was recorded and was usually between 150 and 200 nN/m. Data was collected in tapping mode with the sample submerged in liquid.

2.7 Asymmetric flow field flow fractionation (AF4)

Asymmetric flow field flow fractionation (AF4) is a method that can separate molecules by size. A diagram of how the AF4 system achieve fractionation is shown in figure 2.2. It works by using a parabolic flow combined with a cross flow (running asymmetric to the parabolic flow) that forces molecules against a membrane. As the cross flow is reduced, the molecules diffuse away from the membrane. Small molecules diffuse faster than large molecules. Due to the parabolic flow the

molecules that move away from the membrane the furthest move faster through the field resulting in fractionation. Combined with multi angled light scattering (MALS) and UV detection the size of the molecules in a given sample can be determined. This is a useful technique for determining the size distribution of samples.

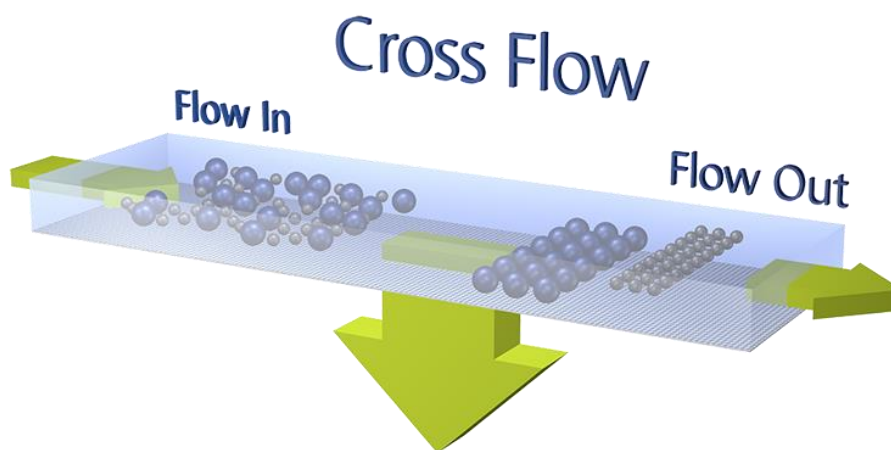


Figure 2.2 A diagram of how fractionation is achieved by AF4. The box in blue represents a contained solution with the sample to be separated represented by the blue and silver spheres. The arrow pointing from left to right represents the parabolic flow which forces molecules through the separation field. Molecules further from the membrane, which is represented by the dark blue shaded area, move faster through the separation field than those held close to the membrane. The cross flow which is represented by the large arrow pointing downwards, forces molecules towards the membrane. To begin with, a high cross flow is used and all molecules are forced towards the membrane. As this cross flow is reduced, small molecules diffuse faster away from the membrane than large molecules which remain close to the membrane. Small molecules therefore move faster through the separation field than large molecules. Taken from the Postnova website ¹⁶⁵.

Buffers were prepared fresh for each session and passed through a 0.1 μm filter. The AF4 system was equilibrated with the fresh buffer before each run. Asymmetric field flow fractionation was performed with a metal-free Postnova (UK) AF2000 system using an analytical channel, 350 μm spacer and 1 kDa MWCO regenerated cellulose membrane. Separation was performed with a detector flow of 0.2 ml/min with linear cross-flow being reduced to 0 ml/min according to specific protocols. Samples were injected with a PN5300 autosampler and detection performed with a Shimadzu (JP) UV detector at

280 nm and Postnova (UK) MALS detector. Data was analysed using Postnova (UK) AF2000 software and light scattering data was typically fitted to a Zimm plot.

2.8 Vesicle quality control

An analysis of LUVs was performed and is shown in figure 2.2. A 15 μg sample of LUVs prepared by extrusion using a 100 nm membrane were injected into the AF4 system. An initial cross-flow of 4.5 ml/min which ran for 30 minutes was reduced to 2 ml/min over 15 minutes and then down to 0.8 ml/min over 15 minutes and finally to 0 ml/min over 30 mins at which it was left for an additional 30 mins to ensure the whole sample was eluted. Two regions of interest (ROIs) were determined which contained two distinct populations (data not shown). One population that fit to a hollow sphere model with sizes that were distributed with a radius between 10 and 50 nm and one population that fit to a random coil model with radii of gyration between 200 and 250 nm. As both of these populations eluted together when the cross flow was significantly reduced the protocol was changed. An initial cross flow of 2 ml/min which ran for 15 minutes was reduced to 0.8 ml/min over 15 minutes and then down to 0.2 ml/min over 20 minutes and finally down to 0 ml/min over 30 minutes followed by an additional 30 minutes in order to elute the whole sample. Figure 2.3 (A) shows a time course of the UV signal at 280 nm collected over time. Lipids were not expected to absorb at 280 nm in the same manner as a protein but were expected to scatter the light significantly enough to give a signal which enabled the detection of when the sample was eluting and quantification of how much of the total sample was accounted for by each population. 2 regions of interest were again identified. The first region of interest was a broad peak that eluted between 15 and 50 minutes. When analysed this region contained a population of LUVs that fit to a hollow sphere model with radii distributed between 10 and 50 nm shown in figure 2.3 (B). This population accounted for 60 % of the total UV signal at 280 nm. The second region of interest eluted between 55 and 80 minutes and contained a population that fit to a random coil model with radii of gyration between 50 nm and 350 nm shown in 2.3 (C). This population accounted for the rest of the UV signal at 280 nm. The random coil model here is not particularly informative as a lot of species fit to a random coil model. However, it is not unusual for LUVs to cluster together as shown in figure 2.3 (D) which is likely to be the cause of this population.

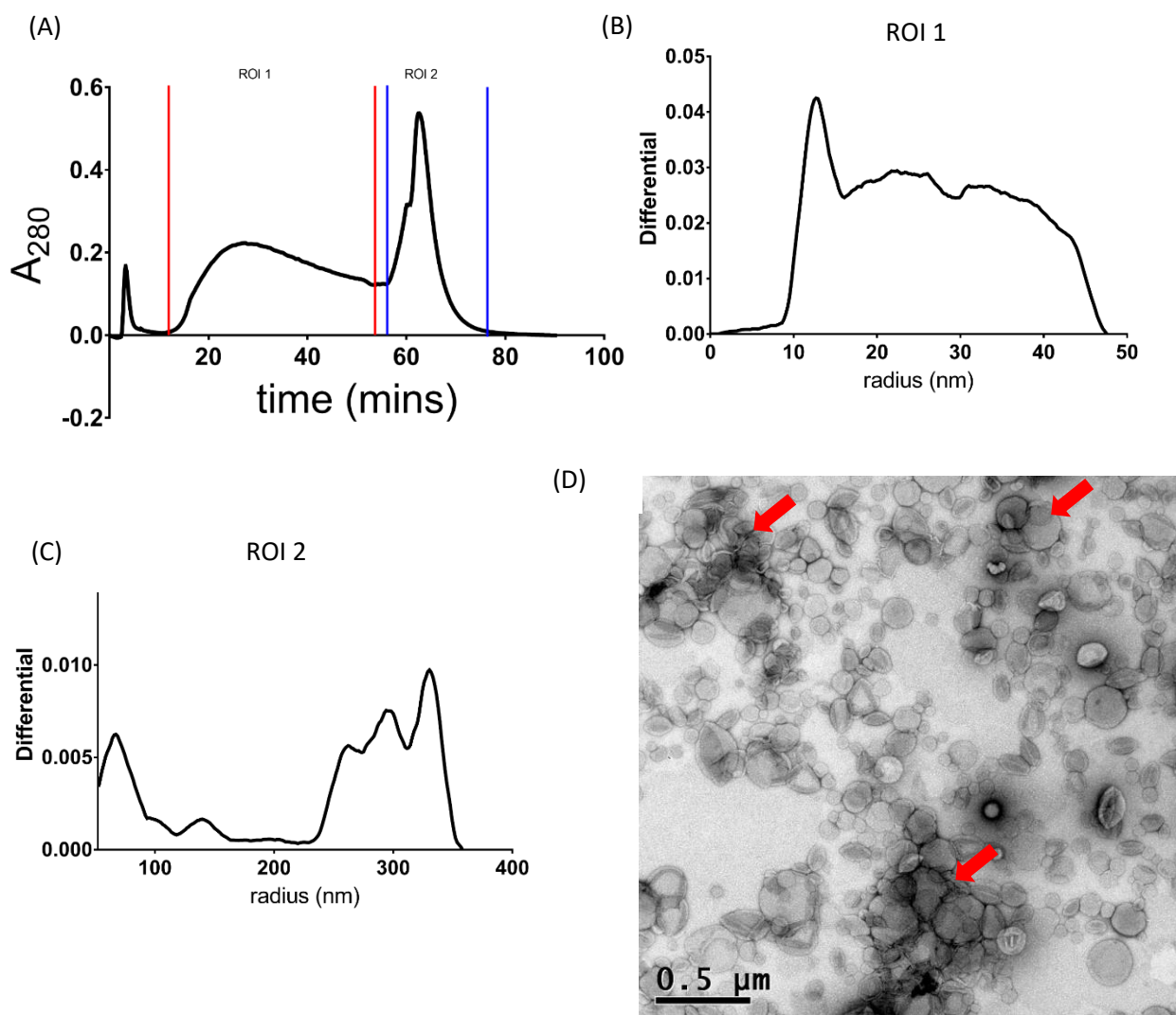


Figure 2.3 LUVs form two populations; lone vesicles and clustered vesicles. LUVs prepared by extrusion through a 100 nm membrane were injected into the AF4 system. The UV at 280 nm was recorded and a time course of the signal is shown (A). Two regions of interest were observed. In the first region (B) a population of LUVs that fit to a hollow sphere model were observed with radii between 10 and 50 nm. In the second region (C) clusters of LUVs which fit to a random coil model were observed with radii of gyration between 50 and 350 nm. LUVs prepared by extrusion through a 200 nm membrane were imaged by TEM (D). The arrows indicate examples of clustered LUVs.

2.9 Thioflavin T assays

Thioflavin T was purchased as dry stock from Sigma-Aldrich (DE). 2 mM stock solutions were stored at 4 °C prior to use. Thioflavin T was always diluted to a final concentration of 10 μM . Visible light emission was recorded at regular intervals at a wavelength of 485 nm after excitation at a wavelength of 435 nm using a BMG Labtech (UK) microplate reader.

Data was collected using the MARS analysis software (BMG Labtech, UK) and exported into Microsoft Excel where the data were normalised, and half times were calculated. A summary of typical thioflavin T data analysis is as follows:

The minimum y value from each set of raw data (figure 2.4 (A)) was subtracted from every y value in that data set. This generated a new set of curves that had been baseline adjusted (figure 2.4 (B)). The 95th percentile of the y values was obtained from each new set of data. These values represented the fibrillar yield from each reaction. The 95th percentile was used as variation in behaviour was often observed at the end of a reaction making it difficult to determine an exact maximum. Each data set was then divided by its 95th percentile to produce a data set normalised to this value (figure 2.4 (C)). This allowed for comparisons between the shape and relative position of the curves.

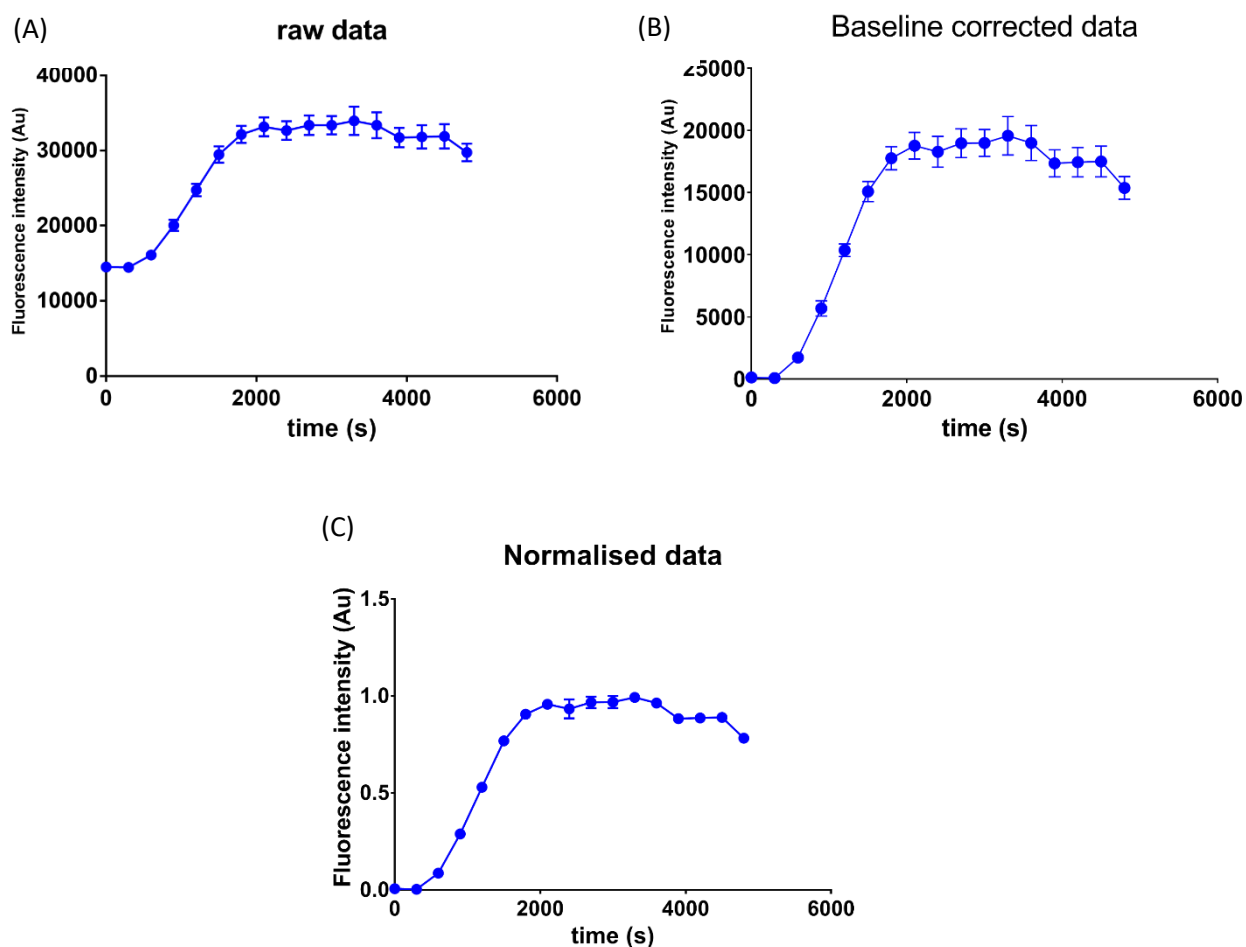


Figure 2.4 Analysis of thioflavin T data. Raw data (A) is baseline corrected (B) by subtracting the minimum y value from all of the y values. The data set is then normalised (C) by dividing each y value by the 95th percentile of the data.

The half time was collected by using the match and index formulae in Excel (Microsoft, USA) to identify the timepoint at which the reaction had reached half way to the 95th percentile. This method produced the timepoint at which the reaction had almost reach half way to the 95th percentile. For example, if at the timepoint 1800 seconds the reaction was 0.49 of the way to completion and at the next timepoint of 1920 seconds the reaction was 0.51 of the way to completion then 1800 seconds would be returned as the half time. Therefore, to determine half times more accurately equation 2.1 was used where t_i is the value in time found by the above method and a_i is the corresponding value from the normalised data (in the example above $t_i = 1800$ s, $t_{i+1} = 1920$ s, $a_i = 0.49$ and $a_{i+1} = 0.51$). The half time for the example would be calculated to be 1860 s.

Equation 2.1

$$t_{1/2} = t_i + ((t_{i+1} - t_i)(0.5 - a_i)) / (a_{i+1} - a_i)$$

If a range of concentrations of A β were used further analysis of the half times revealed information about the concentration dependence by calculating the exponent γ as discussed in chapter 1 section 1.2.3 using equation 2.2 where x is initial monomer concentration.

Equation 2.2

$$t_{1/2} = ax^\gamma$$

2.10 Dye release assays

5-6-carboxyfluorescein was purchased from Sigma-Aldrich (DE) as a dry stock. 50 mM stock solutions of carboxyfluorescein were prepared in varying buffers dependent on the specific experiment. Using a conductivity meter (Jenway, UK), the ionic strength of each solution was adjusted to match a corresponding buffer. This was to maintain the stability of the LUVs by ensuring that, when LUVs were made using these solutions, the difference in osmotic potential on either side of the bilayer was minimal. The LUVs were made as per section 2.4.2 with the caveat of using the prepared solutions of 50 mM carboxyfluorescein to resuspend the lipid films.

Samples to be tested were mixed with the carboxyfluorescein dye containing LUVs in quartz glass cuvettes. Emission was recorded at regular intervals at a wavelength of 515 nm after UV excitation at a wavelength of 485 nm using a Cary Eclipse spectrophotometer (Agilent, USA).

2.11 Data analysis

Data were typically analysed using Excel (Microsoft, USA) or Prism software (GraphPad, USA).

Chapter 3: A β ₁₋₄₂ interactions are surface dependent.

3.1 Introduction

Upon investigating the mechanisms and interactions of A β regarding Alzheimer's disease, it quickly becomes apparent that the interaction between A β and the lipid bilayer is important^{44,166-169}. There is a lot of evidence that A β will damage a lipid bilayer^{170,171} and mechanisms such as membrane thinning^{135,172} and pore formation^{173,174} have been put forward. Another way of observing this interaction is from the perspective of what happens to A β in the presence of a lipid bilayer. There have been studies that have investigated this with a range of results and conclusions. One conclusion is that the bilayer surface facilitates the formation of mature amyloid fibrils⁷³. Another is that the aggregation and cytotoxicity of A β is regulated by membrane thinning¹³⁶. The morphology of amyloid fibrils formed in the presence of lipid bilayer surfaces has also been investigated. One group has suggested that the mature fibrils formed in the presence of a lipid bilayer containing the ganglioside GM1 have an anti-parallel β structure rather than the classically defined parallel β structure of mature amyloid fibrils and have increased cytotoxicity^{163,168,175}. It is clear from all these studies that the presence of a lipid bilayer has an impact diversity and quantity of A β aggregates.

The diversity of aggregates, also produces a range of possible binding partners for proteins such as hCC which are known to interact with A β . The mechanism of how hCC interacts with A β is not known and importantly it is not known in what state of aggregation the A β is when the interaction is taking place. There is evidence that hCC interacts with A β at a surface¹⁵⁴ as well as evidence that it is an effective inhibitor of A β activity *in vivo*^{147,148}. Combined, these two conclusions suggest that an interaction between A β and hCC occurs at the lipid bilayer surface and this could be important in Alzheimer's disease. Therefore, one of the aggregates that form at the lipid bilayer might bind specifically to hCC.

Without knowing the species that hCC binds to and how to isolate it, it is impossible to investigate a specific interaction between hCC and A β . It is however possible to investigate the extent to which hCC impacts on A β interactions with a lipid bilayer surface. To investigate whether hCC impacts on A β – lipid bilayer interactions, the interaction between A β and lipid bilayer surfaces must first be investigated. Whilst the literature on this subject is vast, it is not particularly consistent due to the range of conditions used by different researchers including varying concentrations, stoichiometries, pHs and ionic strengths. The source of this variation is often the need to change conditions to suit an experimental technique at the expense of consistency. An investigation that uses a range of

techniques that all provide information about the interaction between A β and lipid bilayers in the same sample conditions would therefore be useful and informative.

Here it is shown that not only does the *lipid bilayer* surface have an impact on A β aggregation, but that a wide range of surfaces have a significant impact. Using a dye release assay, it will be shown that a polystyrene surface can outcompete lipid bilayer surfaces for monomeric A β . AFM experiments will show that different types of aggregates form on different surfaces. It will also be shown using thioflavin T assays that different surfaces result in different rates of formation of amyloid fibrils. The data presented in this chapter will provide evidence that A β aggregation is highly surface dependent.

3.2 Methods

3.2.1 Dye release assay

LUVs were prepared by the protocol described in chapter 2 (sections 2.4.2 and 2.10).

A β_{1-42} was prepared as per protocol 1 discussed in chapter 2 (section 2.2).

A β_{1-42} was diluted to 11 μ M into buffer solutions containing the carboxyfluorescein encapsulating LUVs and rapidly aliquoted out into wells in the polystyrene microplates (Corning 3694). The microplate was then covered with a clear plastic film and incubated in an BMG Labtech (UK) Omega Fluostar fluorimeter at 37 °C. Measurements were taken every 5 minutes with excitation at 485 nm and emission recorded at 515 nm.

Alternatively, A β_{1-42} was diluted to 2 μ M into a HEPES buffer containing carboxyfluorescein encapsulating LUVs in a quartz cuvette which was incubated in a Cary Eclipse fluorimeter (Agilent, UK). The cuvettes were incubated at 37 °C and measurements were taken every 5 minutes with excitation at 485 nm and emission recorded at 515 nm.

3.2.2 Thioflavin T assays

Thioflavin T was prepared as described in chapter 2 (section 2.9).

A β_{1-42} was prepared as per protocol 2 described in chapter 2 (section 2.2).

A β_{1-42} was diluted into a solution of 50 mM sodium hydroxide to 20 times the final concentrations (for a 1 μ M final concentration a 20 μ M solution) and these stock solutions were kept in separate Eppendorf tubes. Thioflavin T was diluted to 10 μ M into a solution of 20 mM phosphate 2 mM EDTA 2mM sodium azide pH 8.0. Then, 95 μ l of the thioflavin T solution was aliquoted into wells in a polystyrene or low-binding microplate (Corning 3694 & 3686 respectively). 5 μ l of A β_{1-42} was added per well and the microplate was covered with a clear plastic cover. The microplate was then incubated

in the Omega fluostar fluorimeter at 37 °C with shaking before measurements. Measurements were taken every 5 minutes with excitation at 445 nm and emission recorded at 485 nm. This was repeated in the presence of DOPC LUVs, which were prepared as per the protocol described in chapter 2 (section 2.4.2) and A β_{1-42} prepared as per protocol 1 described in chapter 2 (section 2.2).

Thioflavin T was diluted to 10 μ M in a degassed solution of either 50 mM phosphate 150 mM sodium chloride 2 mM sodium azide pH 7.4 or . Either 450 μ l or 1.8 ml of these solutions were added to clean quartz glass cuvettes. A β_{1-42} , prepared as per protocol 2 described in chapter 2 (section 2.2), was added to these solutions to a final concentration of 22 μ M in each cuvette. In the cuvettes with a total of 2 ml of solution a clean glass coverslip was placed over the top of the cuvette causing a slight overflow to remove the air water interface. The cuvettes were then incubated in a Cary fluorimeter at 37 °C with no shaking and measurements were taken every 15 minutes. This was repeated using 11 μ M A β_{1-42} and 20 mM phosphate 2 mM EDTA 2mM sodium azide pH 8.0.

3.2.3 Electron microscopy

Monomeric A β_{1-42} was diluted to 80 μ M in a 1.5 ml polypropylene microfuge tube in 50 mM HEPES, 150 mM NaCl 2mM sodium azide pH 7.4 overnight at 4 °C. A grid was prepared as per the protocol for negative stain EM described in chapter 2 and imaged using a CM100 electron microscope at varying magnification.

After 24 hours of incubation in the Omega Fluostar fluorimeter an EM grid of the solution of A β_{1-42} , LUVs and thioflavin T used in the thioflavin T assay described above was prepared. The grid was prepared as per the protocol for negative stain EM described in chapter 2. This was then imaged using a CM100 electron microscope (Phillips, UK) at varying magnification.

3.2.4 Atomic force microscopy

A flat polystyrene surface was prepared by spin coating 2 % polystyrene (molecular weight 200,000 KDa) in toluene onto a clean silicon wafer. The polystyrene surface was incubated in a solution of 20 mM phosphate 2 mM sodium azide pH 8 at room temperature. The surface of the polystyrene was then imaged by AFM in contact mode with a set point of 0 using cantilever E from a Bruker MLCT AFM chip. While the surface was being imaged, monomeric A β_{1-42} was injected to a concentration of 11 μ M and the surface was continually imaged for 12 hours.

Similarly, a quartz glass plate and a mica surface were incubated in 20 mM phosphate 2 mM EDTA 2mM sodium azide pH 8.0 and imaged in the same fashion before and after injection with a final concentration of 11 μ M A β_{1-42} .

A supported lipid bilayer was formed by the addition of SUVs to a mica surface as described in chapter 2. This surface was incubated in 20 mM phosphate 2 mM EDTA 2mM sodium azide pH 8.0 and imaged in the same fashion before and after injection with a final concentration of 11 μ M A β ₁₋₄₂.

3.3 Results

3.3.1 A β ₁₋₄₂ doesn't damage lipid bilayers in a polystyrene microplate

A β ₁₋₄₂ is known to damage lipid bilayers. A dye release assay is a simple method of determining the effect of external factors on the integrity of a lipid bilayer. 50 mM carboxyfluorescein was encapsulated in large unilamellar vesicles. Carboxyfluorescein is a self-quenching dye and once diluted below 50 mM, carboxyfluorescein produces a large emission signal. Therefore, if the lipid bilayer of the LUVs is damaged the carboxyfluorescein will leak out and be diluted below 50 mM producing an increased fluorescence signal.

LUVs were utilised here as a simple mimic of a biological membrane. The lipids used to form the LUVs were chosen due to their experimental relevance. DOPC is a zwitterionic lipid and is commonly used in mimicking biological membranes whereas DOPG has a negatively charged head group and has been used previously to promote an interaction between lipid bilayers and A β ₁₋₄₂^{170,176}. 1,2-dioleoyl-sn-glycero-3-phosphocholine (DOPC) and 1,2-Dioleoyl-sn-glycero-3-phosphoglycerol (DOPG) were used in either a 1:1 or 4:1 mix (50 % or 20 % DOPG).

By incubating monomeric A β ₁₋₄₂ with carboxyfluorescein encapsulating LUVs, the lipid bilayers of the LUVs were expected to be damaged by the A β ₁₋₄₂ and the carboxyfluorescein leak out, resulting in an increased fluorescence. Experiments were initially carried out in standard polystyrene untreated microplates (Corning 3694). Figure 3.1(A) shows that, in comparison to LUVs that were incubated alone, LUVs incubated in the presence of 11 μ M of monomeric A β ₁₋₄₂ did not significantly release more carboxyfluorescein. This suggested that monomeric A β ₁₋₄₂ was not able to damage the LUVS sufficiently to cause significant dye release.

If monomeric A β ₁₋₄₂ would not damage the lipid bilayers enough to result in dye release then it was hypothesized that significant dye release would then be observed if small aggregates such as oligomeric species were pre-formed and then incubated with the LUVS. One method for forming small aggregates is by incubating monomeric A β ₁₋₄₂ at a high concentration (80 μ M was used here) at 4 °C overnight. This results in a range of small aggregates often described as amyloid derived diffusible ligands (ADDLs). Figure 3.1(B) shows a representative electron micrograph of a sample of ADDLs formed this way. Interestingly figure 3.1(C) shows that incubating an 11 μ M monomer equivalent sample of ADDLs with LUVs also lacked any significant dye release.

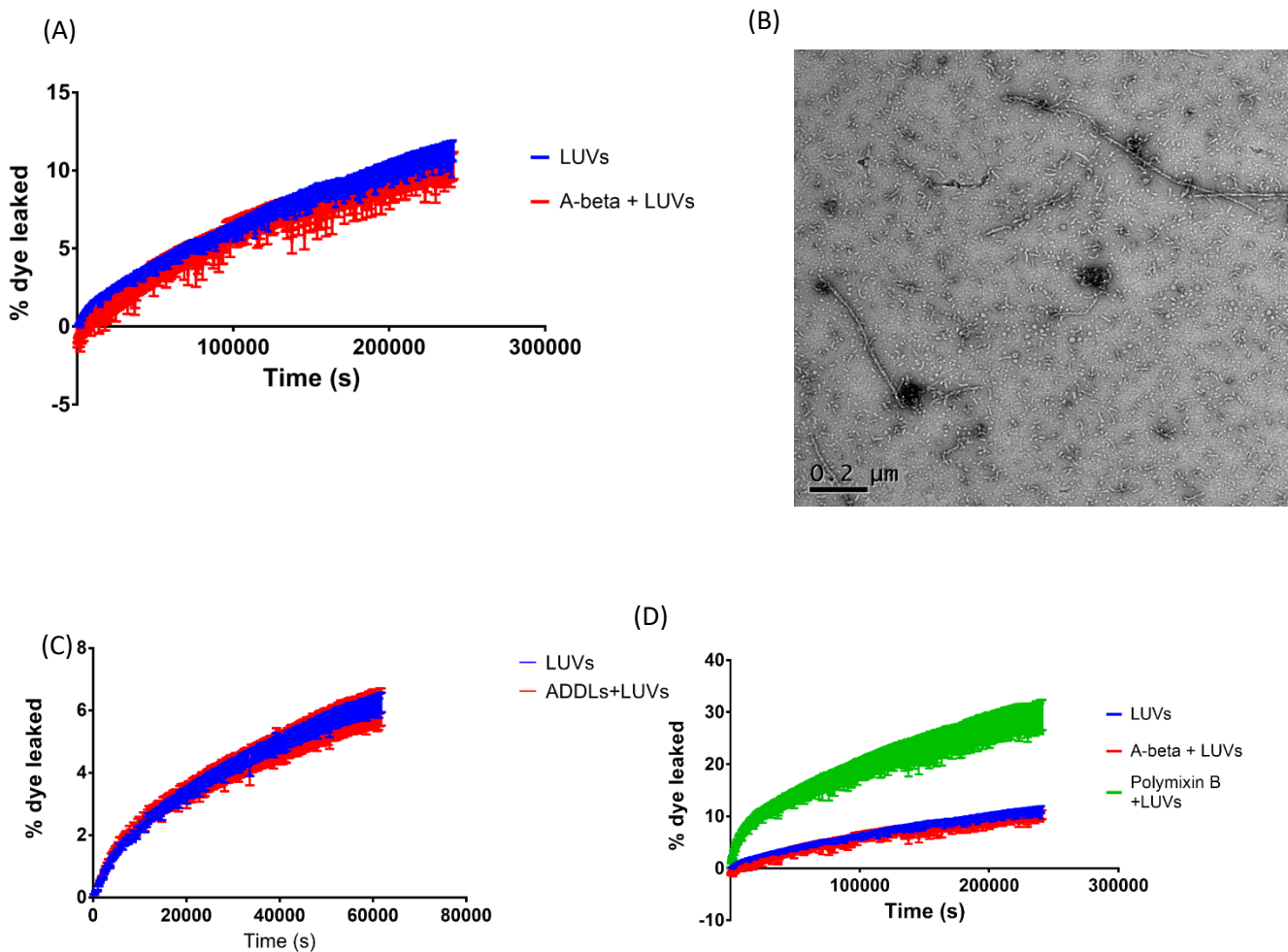


Figure 3.1 $A\beta_{1-42}$ cannot damage LUVs in a polystyrene microplate. (A) shows the percentage dye leakage from LUVs encapsulating a 50 mM carboxyfluorescein solution in the presence (red) and absence (blue) of monomeric $A\beta_{1-42}$. Over a time-course of 80 hours no significant dye release is observed in the presence of $A\beta_{1-42}$. (B) shows an electron micrograph of a range of amyloid aggregates including fibrils prepared using a protocol previously used for forming ADDLs. (C) shows that when the aggregates observed in (B) are diluted and incubated with LUVs (red) and compared with a LUV only control (blue), in a polystyrene microplate there is still no significant dye release observed. (D) shows that by adding polymyxin B, a known pore forming protein (green), and comparing to the LUVs with (red) and without (blue) $A\beta_{1-42}$, significant dye release can be observed suggesting that it is the $A\beta_{1-42}$ that is incapable of causing dye release. Error bars represent the standard error about the mean from at least 2 repeats of 5 replicate reactions.

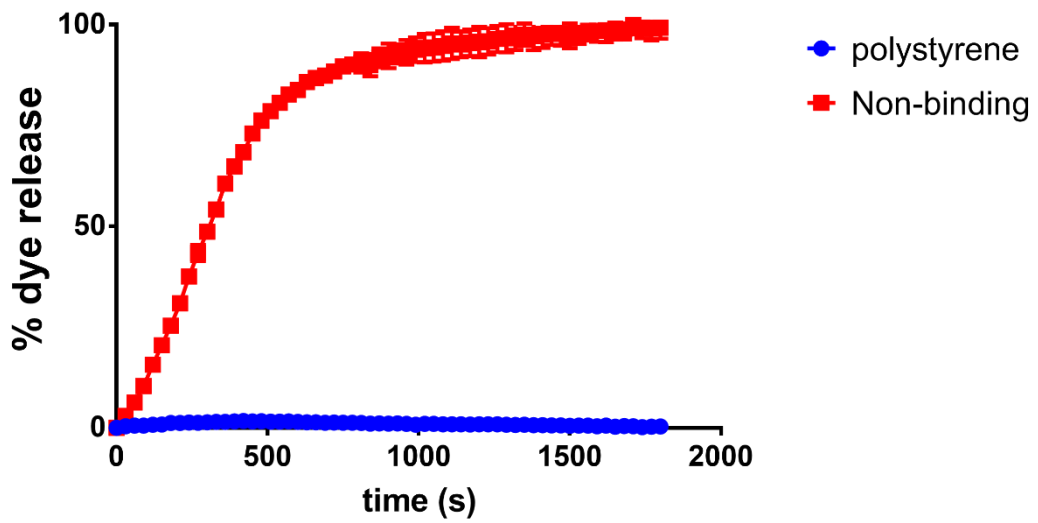
It was then hypothesised that the species of $A\beta_{1-42}$ aggregate wasn't the reason for the lack of dye release but that the conditions didn't promote an interaction between the peptide and the lipid

bilayers or that the large unilamellar vesicles were not forming optimally. In order to optimise the experiment, HEPES buffer was used as opposed to phosphate as HEPES is a zwitterionic buffer which shouldn't impact on the rate of carboxyfluorescein diffusion from the LUVs. Similarly, EDTA was added as an attempt to prevent any contaminating metal ions from impacting on the dye release reaction. Finally, copper ions had been reported as an important factor in the formation of $A\beta_{1-42}$ aggregates that would damage a lipid bilayer^{69,177}. Therefore, $CuCl_2$ was added to the reaction to promote $A\beta_{1-42}$ induced membrane damage. All three of these modifications to the original method were attempted both in isolation and combined yet the outcome was unchanged in all cases: there was no significant increase in dye release observed upon the addition of any species of $A\beta_{1-42}$ to the LUVs when compared to the LUVs alone (data not shown).

A positive control using polymixin B, a known pore forming protein, was performed to determine whether the vesicles were correctly forming and were capable of releasing the carboxyfluorescein. Figure 3.1(D) shows that polymixin B was able to immediately cause a significant amount of dye release.

All the aforementioned experiments were performed in an untreated polystyrene microplate (Corning 3694). Repeating the experiment described above in a low-binding microplate (Corning 3686) rather than a polystyrene plate resulted in rapid dye release. Rapid dye release was also observed however, in the negative control performed in the absence of $A\beta_{1-42}$ as shown in figure 3.2(A). When 2 μM of monomeric $A\beta_{1-42}$ was incubated with LUVs in a quartz cuvette significant dye release was observed. Figure 3.2(B) shows the difference in signal after 16 hours of incubation of LUVs with monomeric $A\beta_{1-42}$ at 37 °C in a quartz cuvette and resembles data from other sources^{69,170}. The nature of the experimental surface clearly has a significant impact on the outcome of the experiment.

(A)



(B)

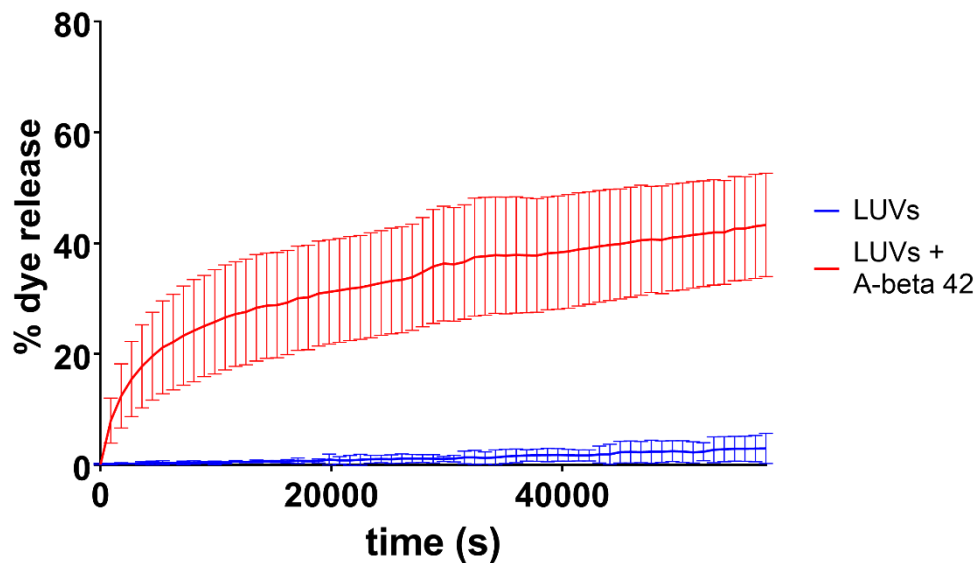


Figure 3.2 A β 1-42 can cause dye release depending on external surfaces. (A) shows that, when incubated in a low-binding microplate (red) LUVs rupture and a significant dye release signal is rapidly observed compared to the same LUVs incubated in a polystyrene microplate (blue). (B) shows that in a quartz glass cuvette A β 1-42 can cause significant dye release (red) when incubated for 16 hours (57600 s) at 37 °C compared to the control (blue). Error bars represent the standard error about the mean from 2 repeats of 5 replicates per repeat.

3.3.2 Amyloid fibril formation in a polystyrene microplate results in a loss of roughly 1 μ M of monomer equivalent $A\beta_{1-42}$

One possible hypothesis that would explain the lack of lipid bilayer damage by $A\beta_{1-42}$ in polystyrene microplates is that the $A\beta_{1-42}$ peptide binds to the polystyrene surface. This is likely because monomeric $A\beta_{1-42}$ has exposed hydrophobic residues and polystyrene is a hydrophobic surface. Alternatively, the surface could affect the population of aggregates available in such a manner that those capable of damaging a lipid bilayer is either reduced substantially or removed entirely. If $A\beta_{1-42}$ were binding to the polystyrene surface it would be expected that any observed yield of amyloid fibrils would be reduced. The standard method for observing amyloid fibrils is to monitor the fluorescence of the amyloid sensitive dye thioflavin T ($\lambda_{ex} = 445 \text{ nm}$, $\lambda_{em} = 485 \text{ nm}$).

Thioflavin T can be used to measure a change in the mass of amyloid fibrils over time. When measured with the readings set to the same gain, the relative amount of amyloid fibril formed once fibril formation has plateaued can also be measured.

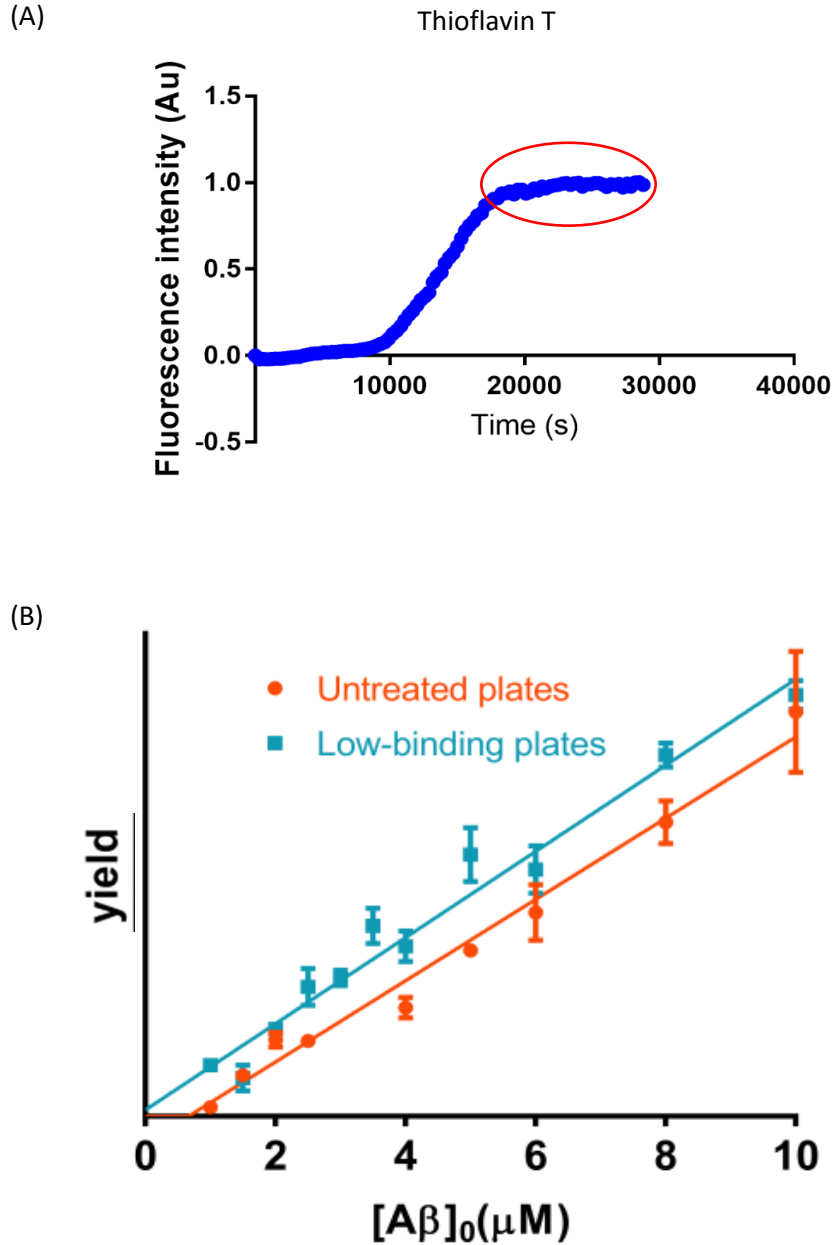


Figure 3.3 Less than 1 μM $A\beta_{1-42}$ does not form amyloid fibrils in a polystyrene microplate. (A) A representative thioflavin T curve on a polystyrene microplate showing the change in signal intensity over time. The red circle highlights the plateau phase at which the maximum intensity is observed. This can be collected from each curve and plotted against the initial monomeric $A\beta_{1-42}$ concentration of that curve as seen in (B). The relationship between maximum signal and concentration is linear. Data from a low-binding surface (blue) passes through (0,0) whereas in a polystyrene microplate (red), the x-intercept is just below 1 μM suggesting that at least this amount is required before fibrils can be formed in polystyrene. In (B) the x-intercept was calculated from 5 repeat experiments and the average values were 0.7 in the untreated microplates and -0.34 in the low binding microplates which were determined to be statistically significant using a Student's t-test.

Monomeric $A\beta_{1-42}$ was incubated in both low-binding (Corning 3686) and polystyrene microplates (Corning 3694) at a range of concentrations from 2 μM to 6 μM . Figure 3.3(A) shows a representative curve of thioflavin T signal over time and highlights the plateau phase at which maximum signal is observed. The maximum signal and therefore relative amount of fibril formed is plotted against each concentration of initial $A\beta_{1-42}$ monomer in figure 3.3(B). This is plotted against the same data recorded in polystyrene plates coated in a low-binding surface (Corning 3686). If all (or almost all as the monomer must exist in equilibrium with other aggregate species) of the monomeric $A\beta_{1-42}$ is used in making fibrils it would be expected that, when extrapolated, the observed straight line would intercept the x-axis at 0. This is the case for the data recorded in the low-binding microplates shown in figure 3.3 (B). For the data recorded in the polystyrene plates shown in figure 3.3 (C) however, the x-intercept is around 1 μM suggesting that this amount of $A\beta_{1-42}$ is “lost” at the end of each reaction. This contradicts the hypothesis discussed previously that the $A\beta_{1-42}$ cannot damage a lipid bilayer in a polystyrene plate due to all of the $A\beta_{1-42}$ binding to the polystyrene surface. This is because 11 μM of monomeric $A\beta_{1-42}$ was used in the experiments described in section 3.3.1. If only 1 μM of monomeric $A\beta_{1-42}$ at most remains bound to the polystyrene surface, then 10 μM of $A\beta_{1-42}$ must at some point be free to interact with the lipid bilayers. The most likely hypothesis becomes that the mechanism of amyloid formation in a polystyrene microplate is sufficiently different to the mechanism of amyloid formation in the presence of other surfaces that $A\beta_{1-42}$ becomes incapable of damaging a lipid bilayer in a polystyrene microplate. This could be because all or most of the $A\beta_{1-42}$ species adhere to the polystyrene at one point or another and are then diverted to fibrils without ever interacting with the LUVs.

3.3.3 $A\beta_{1-42}$ amyloid formation is catalysed by polystyrene and low-binding microplates.

In order to investigate the surface dependence of the mechanism of amyloid formation, a powerful method is to look into the concentration dependence of the assembly kinetics.

Monomeric $A\beta_{1-42}$ at concentrations ranging from 2 to 7 μM was incubated in either glass coated, quartz glass, polystyrene or low-binding surface microplates. Figure 3.4(A-D) shows the normalised fibrillisation curves at a range of concentrations for each different surface. In the polystyrene microplates there is a concentration independence shown by the curves mostly overlapping in figure 3.4 (A). In low-binding surface microplates a concentration dependence is observed. The concentration dependence observed is close to those observed in Cohen et al ¹⁷⁸ which was discussed in chapter 1 section 1.2 and is expected here as the same experimental conditions are used. It could be assumed here that $A\beta$ binds to the polystyrene microplates and that the rate of fibrillisation is dependent on the dissociation of $A\beta$ from the surface hence the concentration independence.

However, figure 3.4 (C) shows that in a glass coated microplate fibrillisation is also concentration independent. Furthermore figure 3.4 (E), which shows the average normalised fibrillisation curve at 4 μM for all four different surfaces, reveals that the rate of fibril formation in glass or quartz glass is an order of magnitude slower than in either polystyrene or low-binding microplates. This suggests that polystyrene microplates actually catalyse the formation of A β amyloid fibrils. Figure 3.4 (D) shows that in quartz glass microplates, the reaction is somewhat stochastic. Each replicate is shown individually as averaging them would provide meaningless seemingly randomly positioned curves. This is expected when the impact of the surface is limited as homogenous nucleation should be spontaneous and ultimately stochastic¹⁷⁹. Figure 3.4 (F) shows the half times for amyloid formation plotted against the initial monomer concentration for the different surfaces. The different concentration dependencies are observed as a flat line and suggest concentration independence. The difference in rate can also be observed across the entire concentration range.

The observation that polystyrene catalyses the fibrillisation process has implications for studies using polystyrene surfaces. In particular, cell culture models of Alzheimer's disease often use polystyrene surfaces^{180,181}. Without the knowledge that polystyrene surfaces catalyse fibril formation the results of experiments performed in polystyrene could be misinterpreted. The same argument can be made for low-binding microplate surfaces which have been used for the analysis of fibrillisation kinetics without the realisation that the low-binding surface catalyses fibrillisation^{35,41,182}.

Thioflavin T

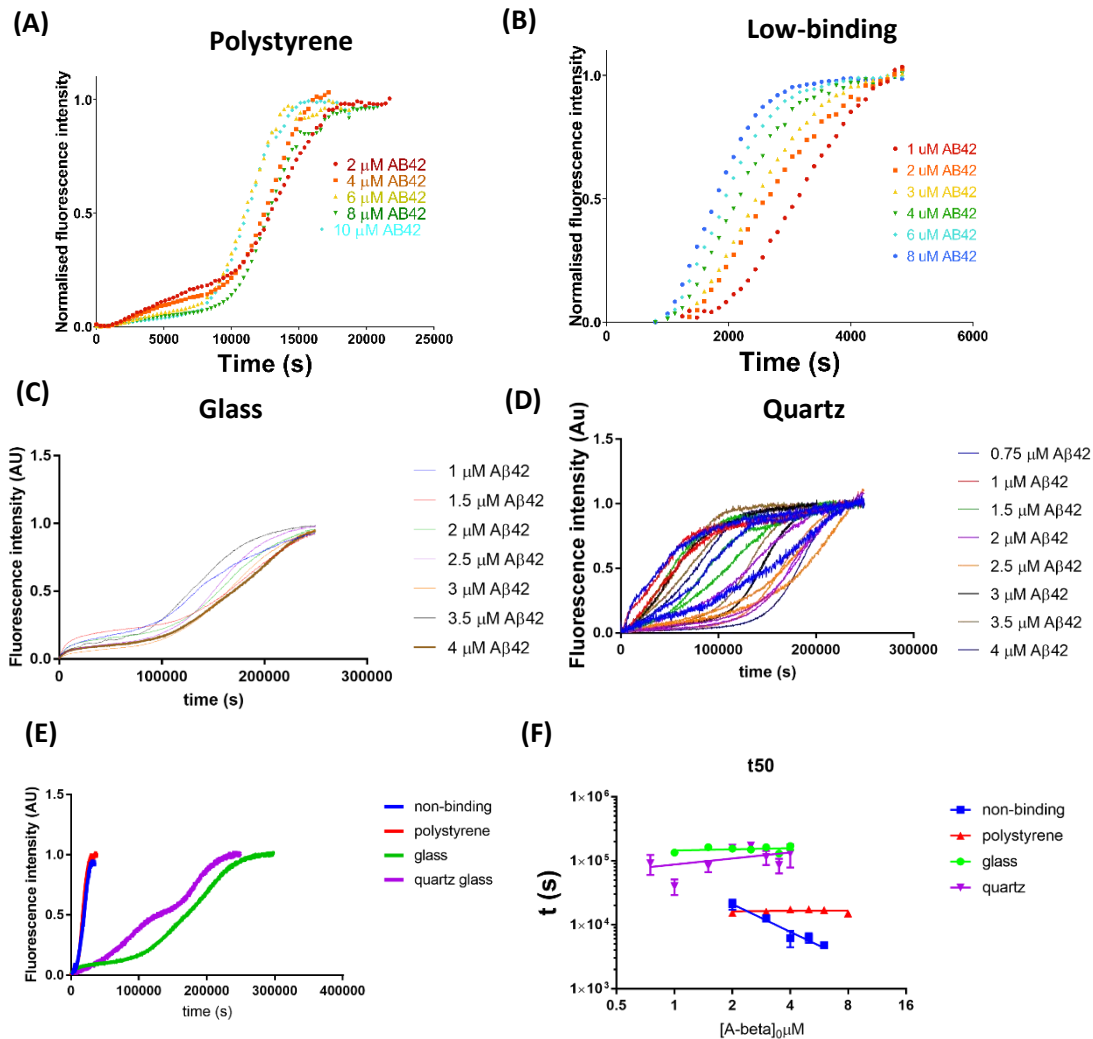


Figure 3.4 The rate of Aβ₁₋₄₂ fibrillisation is surface dependent. Aβ₁₋₄₂ was incubated with thioflavin T in 4 different microplates; glass coated, low-binding, polystyrene and quartz glass. The fibrillisation curves were then normalised according to the protocol in chapter 2. The fibrillisation curves from polystyrene (A) are concentration independent which contrasts with the curves from low-binding microplates (B). The curves in glass coated microplates (C) were also concentration independent. In the quartz glass microplate (D) the curves were stochastic suggesting more dependence on homogeneous nucleation. When the average normalised curve at 4 μM Aβ₁₋₄₂ from each surface are plotted together (E) it becomes clear that the rate of fibril formation is much faster in polystyrene and low-binding microplates than in glass coated or quartz glass microplates. The half times to reach the maximum thioflavin T signal were plotted against the initial monomer concentration on a log log graph (F). These data were then fit to the equation $y = a(x)^\gamma$ where γ is a scaling factor that can be used as a measure of the concentration dependence. Due to the stochastic nature of the data from the quartz glass microplate γ could not be measured. In the glass coated microplate and in the polystyrene microplate $\gamma=0$ suggesting concentration independence. In contrast in the low-binding microplate $\gamma= -1.4$ suggesting a high concentration dependence.

3.3.4 Removing the air water interface slows the rate of amyloid formation.

Given the impact of hydrophobic surfaces like polystyrene on amyloid formation, the next question was clearly whether the non-physiological air-water interface present in all *in vitro* assays may be having a similar impact. Jean *et al*¹⁸³ have shown that in the absence of an air water interface $A\beta_{1-40}$ does not form amyloid fibrils in glass containers until the initial monomer concentration reaches a critical assembly concentration, which was estimated to be between 0.6 and 4 μM . Therefore, the impact of the air water interface on the fibrillisation of the more amyloidogenic $A\beta_{1-42}$ was of interest.

22 μM of monomeric $A\beta_{1-42}$ was incubated in quartz cuvettes with thioflavin T. The air water interface was removed by degassing the solutions used and filling the cuvettes to the brim followed by placing a clean glass coverslip over the top. Figure 3.5 shows that in the absence of an air water interface there was no amyloid formation.

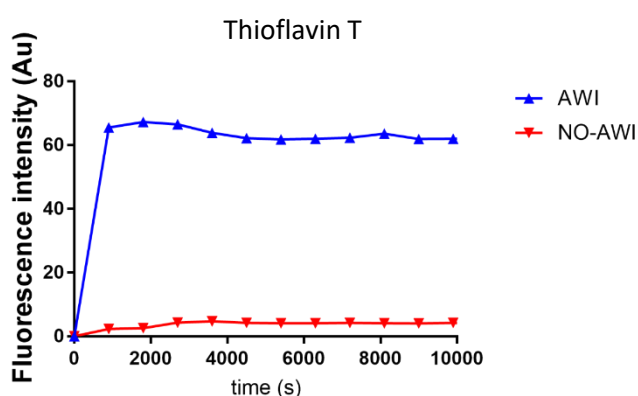


Figure 3.5 $A\beta$ fibril formation is affected by the air water interface. Thioflavin T assays were performed in the presence and absence of the air water interface in a quartz glass cuvette and the half time to achieve maximum signal was recorded. The fibrillisation curves of 22 μM $A\beta_{1-42}$ in the presence (blue) and absence (red) of an air water interface are shown. There is no change in signal over the course of 24 hours (the first 3 hours are shown) in the absence of the air water interface. Timepoints were every 15 minutes to increase the amount of continuous measurements as the software used could only take 200 measurements at a time. This is the reason that no lag phase was observed for fibril formation in the presence of an air water interface. A single reaction time course is shown, however, the same phenomenon was observed upon repeated attempts although the time courses themselves were different.

The reproducibility of this phenomenon suggests that $A\beta_{1-42}$ fibril formation is strongly influenced by interactions with surfaces and interfaces including the air water interface.

3.3.5 A β ₁₋₄₂ forms a nucleated film on a polystyrene surface

Since there is a dependence on surface interactions with regard to A β fibrillisation, the events that take place at the surface were examined next. The first surface of interest was polystyrene. Flat polystyrene surfaces were prepared by spin coating polystyrene onto a silicon wafer. 11 μ M A β ₁₋₄₂ was incubated on the surface and imaged by AFM. A 20 μ m by 20 μ m area was imaged at a rate of 1 scan per 4 minutes and 15 seconds. Figure 3.6(A) shows a time course of AFM images. After 1-hour large aggregates can be seen on the surface. After 2 hours the majority of the surface is covered by multiple large aggregates on the surface that despite the appearance in figure 3.6 are actually much wider (10 μ m or 10,000 nm) than they are tall (100-200 nm) hence resembling a film. The film continues to grow up to the 3-hour time point. After 3 hours the film begins to lose mass which is clear after 4 hours. The size of height irregularities (roughness), is plotted in figure 3.6(B). It can be seen that the film's mass decreases after 3 hours. An explanation for this is that as the monomer concentration reaches a steady state, presumably as fibrils are also forming, it can no longer support the growth of the film on the surface and thus the film subsequently deteriorates.

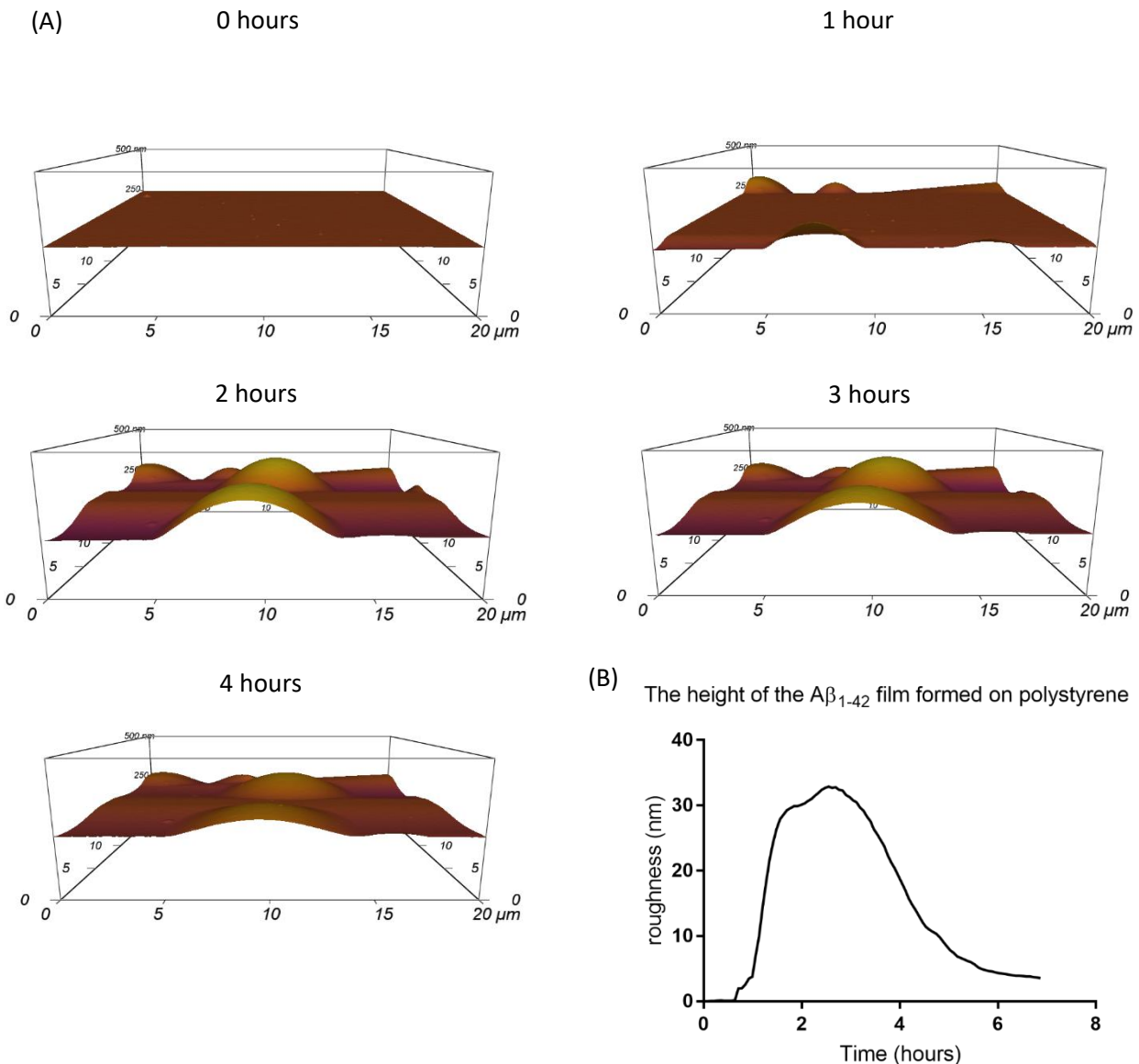


Figure 3.6 $A\beta_{1-42}$ forms a film on a polystyrene surface. 11 μM $A\beta_{1-42}$ was incubated on a polystyrene surface. A time course of AFM images depicting $A\beta_{1-42}$ film growth on a polystyrene surface is shown in (A). The use of the term film is appropriate as the observed aggregates are about 500 to 1000 times wider than they are tall. These films grow in size until about 3 hours at which point they begin to lose mass. The surface roughness at each time point was plotted in (B) highlighting the peak and trough of film formation. This suggests that once the monomer concentration reaches a steady state the presence of the film is no longer supported to the point at which it deteriorates. A single reaction is shown; however, this reaction was observed over 5 repeated experiments.

3.3.6 Different nuclei of $A\beta_{1-42}$ form on different surfaces

The types of aggregates that form on other surfaces that aren't polystyrene are also of interest. Low binding microplates catalyse fibril formation in a specific and reliable manner. Unfortunately, while

the surface chemistry can be assumed to be “PEG-like” the exact surface is unknown (discussed further in chapter 5). PEG is a hydrophilic compound hence its low binding nature with regard to proteins and peptides. Mica is also a hydrophilic compound and that property alone makes it a useful mimic of the low binding surface used previously. Mica is also often used in AFM experiments due to the ease of creating a clean, flat surface. Glass and quartz glass do not appear to catalyse fibril formation but that does not necessarily mean that there is no interaction between $A\beta_{1-42}$ aggregates and a glass or quartz glass surface.

A flat quartz glass plate was imaged by AFM. 11 μM of monomeric $A\beta_{1-42}$ was then incubated on the quartz glass plate. Figure 3.7 shows a time course of AFM images. The surface remains flat with no apparent aggregates settling on the surface. This suggests that any aggregation including any fibrillisation that occurs in the presence of a quartz glass surface does not occur at the surface. However, as shown previously, nucleation of aggregates could occur at the air water interface.

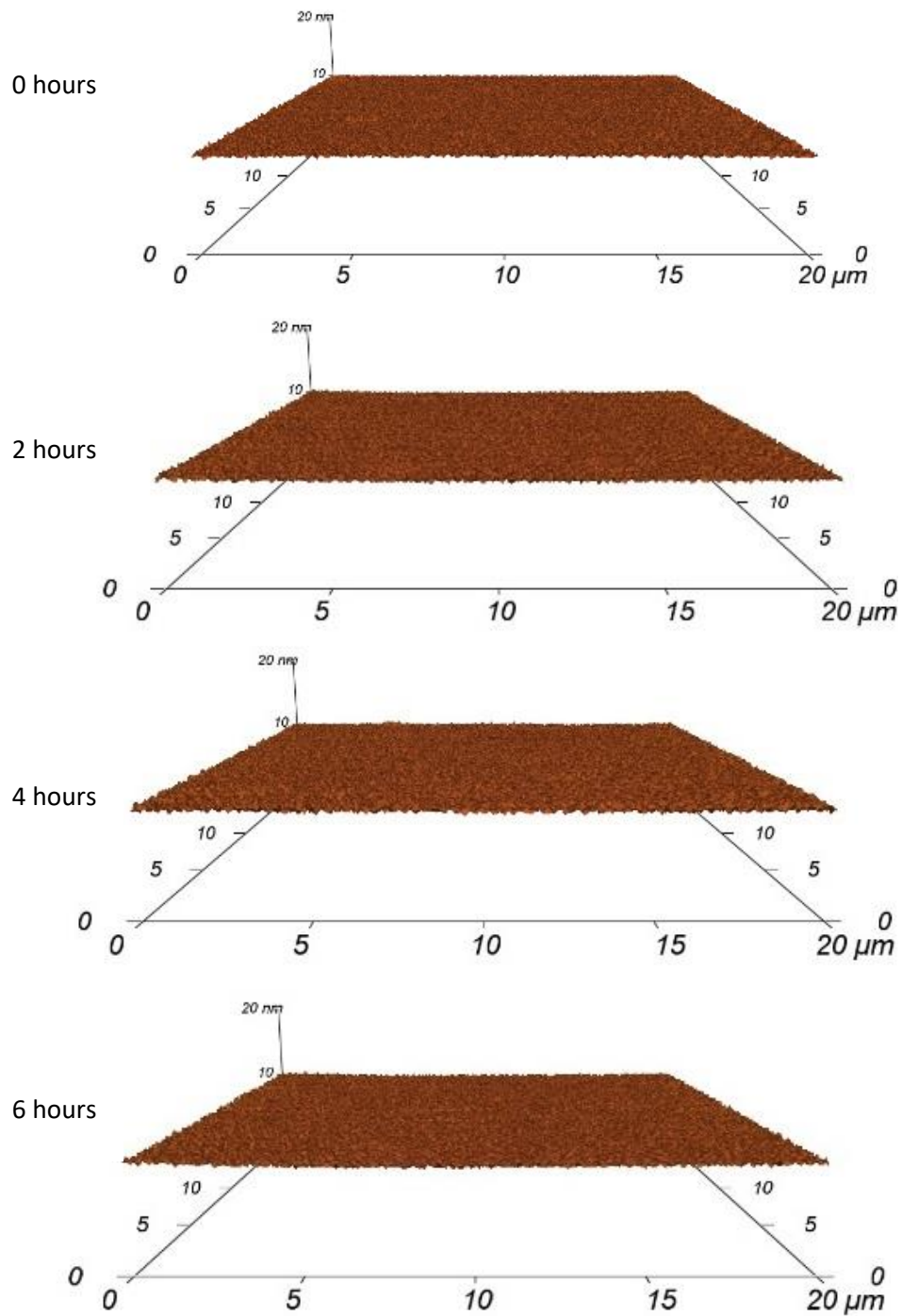


Figure 3.7 Aβ1-42 does not interact with a quartz glass surface. Aβ was incubated on a quartz glass surface. The surface was continually imaged using AFM. Nothing was observed as can be seen in the above time course. The same result was observed upon repeat.

Figure 3.8 shows a similar time course observed on a hydrophilic mica surface. $A\beta_{1-42}$ forms aggregates that interact transiently with the surface. Despite fresh images being taken every 4 minutes and 15 seconds and the same area being imaged for hours, no two images from the time course were alike. Interestingly there were periods during the time course at which larger aggregates appear at the surface. This suggests that transient nucleation reactions occur at the surface sporadically which could increase the rate of fibril formation. Due to the hydrophilic nature of mica this data could be compared to the fibrillisation time courses monitored using thioflavin T in the hydrophilic low-binding microplates.

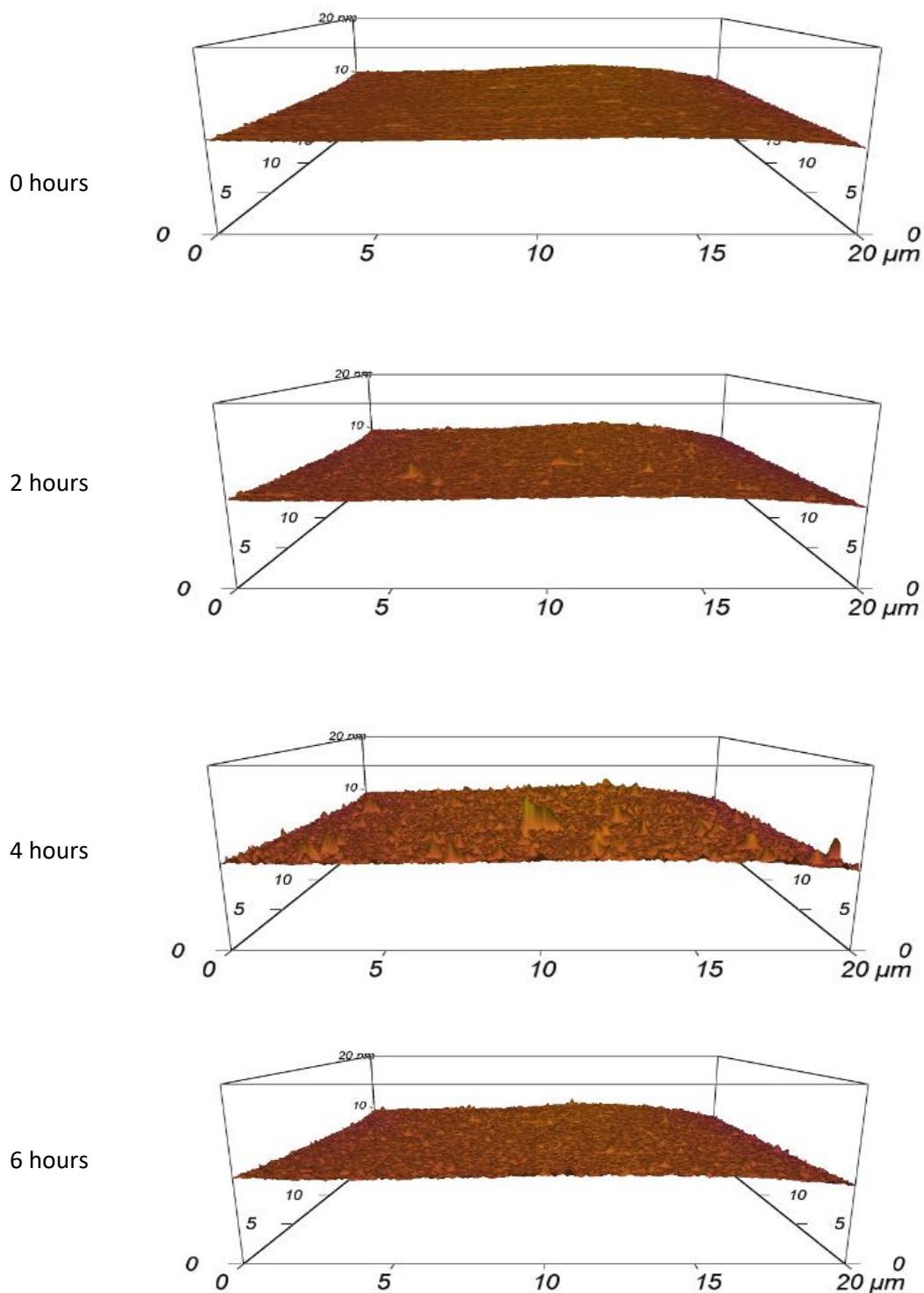
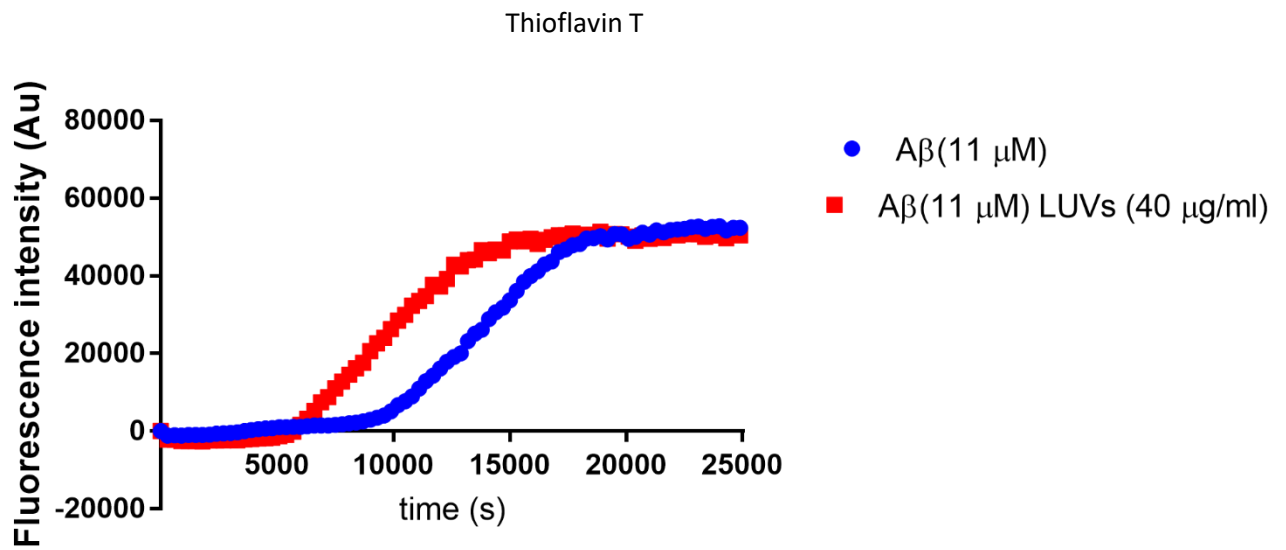


Figure 3.8 $A\beta_{1-42}$ aggregates nucleate on a hydrophilic surface. $A\beta_{1-42}$ was incubated on a freshly cleaved mica surface and imaged by AFM. A time course of images were collected and revealed a continuously shifting landscape of aggregates at the surface as can be seen in the above time course. Notably at 4 hours there are a number of large aggregates observed however these moved off of the imaged surface as can be seen at the 6 hour time point. Whether the aggregates observed moved away laterally or returned to the bulk solution is unknown. This was repeated and the same result was observed.

3.3.7 A β ₁₋₄₂ amyloid fibril formation can nucleate on the surface of lipid bilayers in a polystyrene microplate

Evidence from the previous sections suggests that in order to investigate A β ₁₋₄₂ interactions *in vitro* the impact of the surface must be considered. The next obvious step would be to investigate more physiologically relevant surfaces such as lipid bilayers. Ideally this would be done in an environment where the only surface that had an impact was the lipid bilayer such as in quartz glass or glass. However, despite a film of A β ₁₋₄₂ forming on the polystyrene surface as shown in section 3.3.5, the fibril yield analysis in section 3.3.2 shows that there is possibly an excess of A β ₁₋₄₂ available that could still interact with lipid bilayers. The impact of lipid bilayers on the process of amyloid fibrillisation was therefore investigated using a thioflavin T assay in a polystyrene microplate.

(A)



(B)

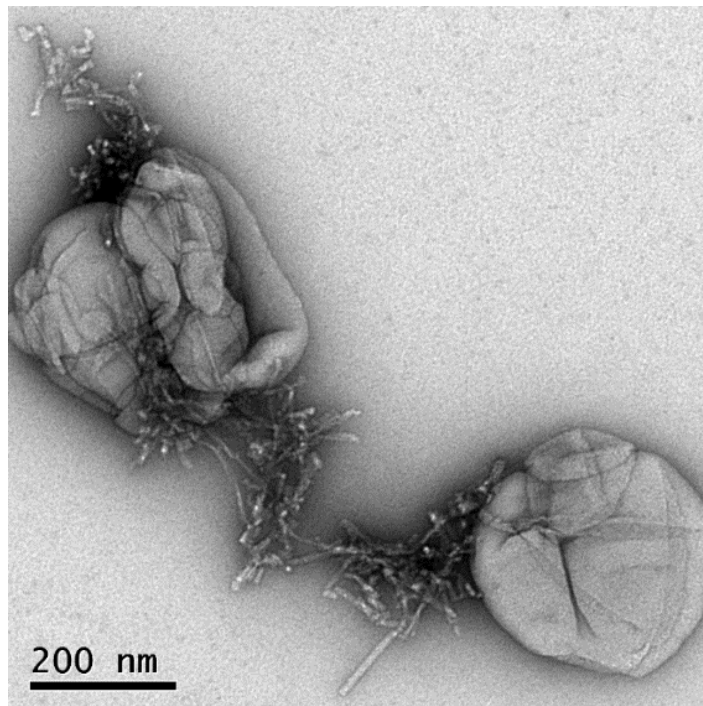


Figure 3.9 Lipid bilayers can catalyse fibril formation in a polystyrene microplate. Aβ1-42 was incubated with thioflavin T in the presence and absence of LUVs in a polystyrene microplate (A). It can be seen that the lag phase for amyloid formation is reduced in the presence of LUVs suggesting that they provide a nucleation site for amyloid formation. Some of this sample was then imaged by electron microscopy (B) and indeed it can be observed that fibrils grow in close proximity to the LUVs. The average half times of the reactions in A were determined to be 13800 s in the absence of LUVs and 9800 s in the presence of LUVs. The half times were determined to be significantly different using a Student's t-test where $p < 0.05$.

Monomeric A β ₁₋₄₂ was incubated in a polystyrene microplate at 11 μ M with 40 μ g/ml of LUVs. Figure 3.9(A) shows that in the presence of LUVs there is a reduced lag phase for amyloid formation. This clearly demonstrates that the presence of lipid bilayers results in an increased rate of nucleation.

Figure 3.9(B) shows an electron micrograph of the same sample with amyloid fibrils appearing to grow from nucleation sites around the LUVs. This suggests that lipid bilayer surfaces do interact with A β ₁₋₄₂ to provide a surface for the formation of amyloid fibrils. Alternatively, the fibrils may interact with LUVs after formation, however the data in figure 3.9 (A) suggests that the initiation of fibril formation is impacted by interactions with LUVs. Unfortunately, due to the use of uranyl formate to negatively stain the samples the impact of A β ₁₋₄₂ on the LUVs cannot be observed by negative stain TEM. Ideally another method would be used to investigate this such as cryo-TEM¹⁸⁴ or AFM.

A simple DOPC lipid bilayer can further catalyse fibril formation in a polystyrene microplate as shown here. However, as discussed in chapter 1 there is evidence that lipid bilayers play a substantial role in Alzheimer's disease and the interaction between A β and lipid bilayers is far more complex than an increase in the rate of fibril formation.

3.3.8 A β ₁₋₄₂ can disrupt a supported lipid bilayer.

One method of investigating the interaction between a lipid bilayer and A β ₁₋₄₂ is to continuously image a supported lipid bilayer (SLB) using AFM. This allows for the direct measurement of surface interactions between A β ₁₋₄₂ aggregates and the lipid bilayer.

A SLB was formed on a mica surface. The SLB used does not completely cover the surface of the mica substrate but large patches of SLB are observed. The observed SLB was consistently present for at least 3 hours before the addition of A β ₁₋₄₂ which served as the negative control for this experiment. Figure 3.10 shows a time course of A β ₁₋₄₂ incubated on the SLB surface. After about 1 hour of incubation, as a direct consequence of the addition of A β ₁₋₄₂ the SLB began to lose its structure and was eventually removed entirely from the surface. Once the SLB had been removed, the molecules interacting with the mica surface remain small and highly mobile with no two-consecutive images (each 4 minutes and 15 seconds apart) being the same. After 6 hours the average size of the molecules interacting with the surface began to continuously increase in size including the eventual formation of an aggregate that appeared on the left-hand side and was mostly out of frame. As the aggregates increased in size, they began to become less mobile and stayed put on the surface, showing behaviour that is distinct from when A β ₁₋₄₂ is incubated on mica alone. Large aggregates could have been forming from interactions with the displaced lipids that eventually settled on the mica surface. The data collected here support a model in which A β ₁₋₄₂ is able to disrupt an SLB within a relatively short

timescale of 2 hours and where the $A\beta_{1-42}$ species themselves form large deposits that settle onto the surface after 8 hours.

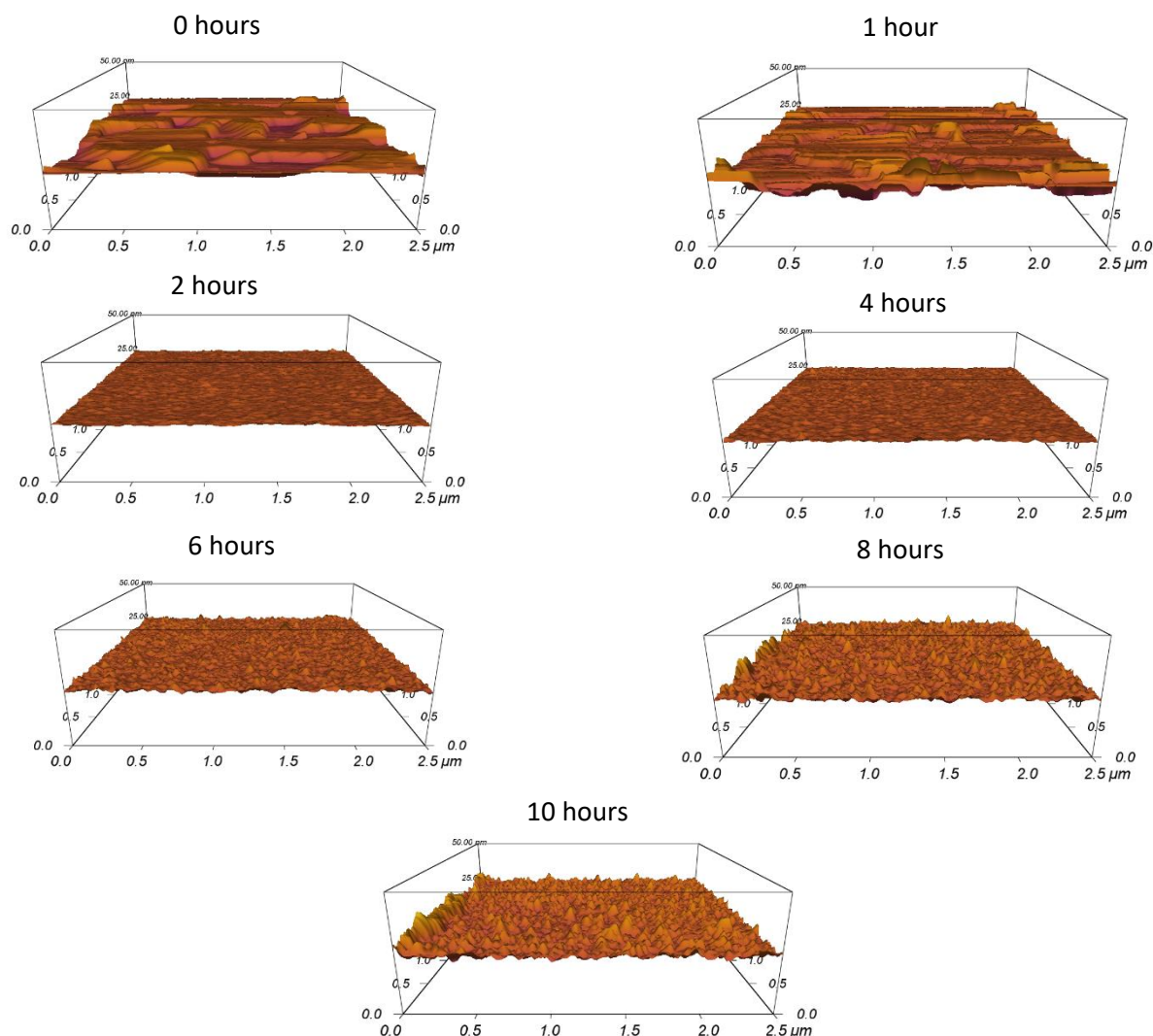


Figure 3.10 $A\beta_{1-42}$ causes the removal of a SLB from a mica surface before aggregating. SUVs were incubated on a freshly cleaved mica surface and imaged by AFM until consistent patches of SLB were observed. $A\beta_{1-42}$ was added and a time course of images were collected. After 1 hour of incubation the morphology of the SLB becomes perturbed and after 2 hours it is completely removed from the surface of the mica substrate. There is then minimal interaction with the surface by aggregated species until about 6 hours into the time course at which point large aggregates begin to settle onto the surface. After 8 hours a large aggregate appears (mostly out of frame to the left). This aggregate and some of the smaller aggregates remain in place and are observed at 10 hours. This is distinctly different behaviour to the mica surface alone. These aggregates could therefore be either large aggregates of $A\beta_{1-42}$ formed in solution after coming into contact with the displaced lipids, or just the displaced lipids resettling onto the mica surface. Before the addition of $A\beta_{1-42}$ the SLB was incubated for 3 hours and no disruption was observed.

3.4 Discussion

3.4.1 LUVs could rupture to form a supported lipid bilayer in a low-binding microplate

As part of the investigation into the conditions upon which $A\beta_{1-42}$ can and can't cause dye release from LUVs, changes to the "test tube" surface were made. Figure 3.2(A) shows that when a hydrophilic low-binding surface was used, all the dye encapsulated in the LUVs was immediately released, including in the absence of any $A\beta_{1-42}$. This suggests that the LUVs were rupturing when they encountered the surface. An investigation into the low-binding surface reveals that the exposed surface is polyethylene oxide (PEO) which, with regards to the exposed regions at the surface of the monolayer, is chemically the same as polyethylene glycol (PEG). There are examples of PEG being used as a support for supported lipid bilayers (SLBs). It is therefore possible to form a SLB by incubating LUVs or SUVs in a low-binding microplate. This would be a useful tool as it would be a simple method for forming a SLB in a microplate which could then be used for further experimentation such as a thioflavin T assay to determine how the rate of fibril formation changes in the presence of different lipid bilayers. The presence of a SLB could be tested by AFM. This phenomenon is investigated further in chapter 5.

3.4.2 $A\beta$ fibrillisation occurs independently of lipid bilayer damage in polystyrene microplates

As discussed in section 3.3.1, the ability of $A\beta_{1-42}$ to cause enough damage to the integrity of LUVs to observe significant dye release is dependent on the surface of the "test tube". Polystyrene microplates prevent dye release caused by $A\beta_{1-42}$ whereas quartz glass cuvettes do not.

Further investigation into the polystyrene surface in section 3.3.5 by AFM shows that large deposits of $A\beta$ form there. This occupation of the $A\beta_{1-42}$ could be the reason that there is no dye release observed in a polystyrene microplate. This would suggest that the bulk of the $A\beta_{1-42}$ binds to the polystyrene surface.

Examination of fibril yields on polystyrene (section 3.3.2) shows that only 1 μM of monomer equivalent of $A\beta_{1-42}$ does not form amyloid fibrils when the starting solution contained 11 μM monomeric $A\beta_{1-42}$. Therefore $A\beta_{1-42}$ does not *just* bind to the surface in a polystyrene microplate. In fact, as shown by the time courses collected in section 3.3.3, amyloid formation is catalysed by the polystyrene microplate. If the polystyrene microplate catalyses fibrillisation but inhibits dye release caused by $A\beta_{1-42}$, then this suggests that dye release and by extension damage to LUVs is caused by an aggregate that is either not formed or prevented from interacting with LUVs in a polystyrene microplate. The most likely scenario is that most of the $A\beta_{1-42}$ is sequestered onto the film observed

in figure 3.6, including potential permeation inducing species, which catalyses fibril formation and then depletes.

Figure 3.11 shows a diagram of a possible model for fibril formation on polystyrene. Monomeric $A\beta_{1-42}$ monomers are injected in solution. Initially these monomers form a film on the polystyrene surface. Fibril formation is then catalysed by the accumulation of $A\beta_{1-42}$ as a film at the polystyrene surface. As both fibrils and the film grow simultaneously, the monomer concentration in solution becomes depleted. Once the monomer concentration in solution is sufficiently low, the deposited film begins to deteriorate.

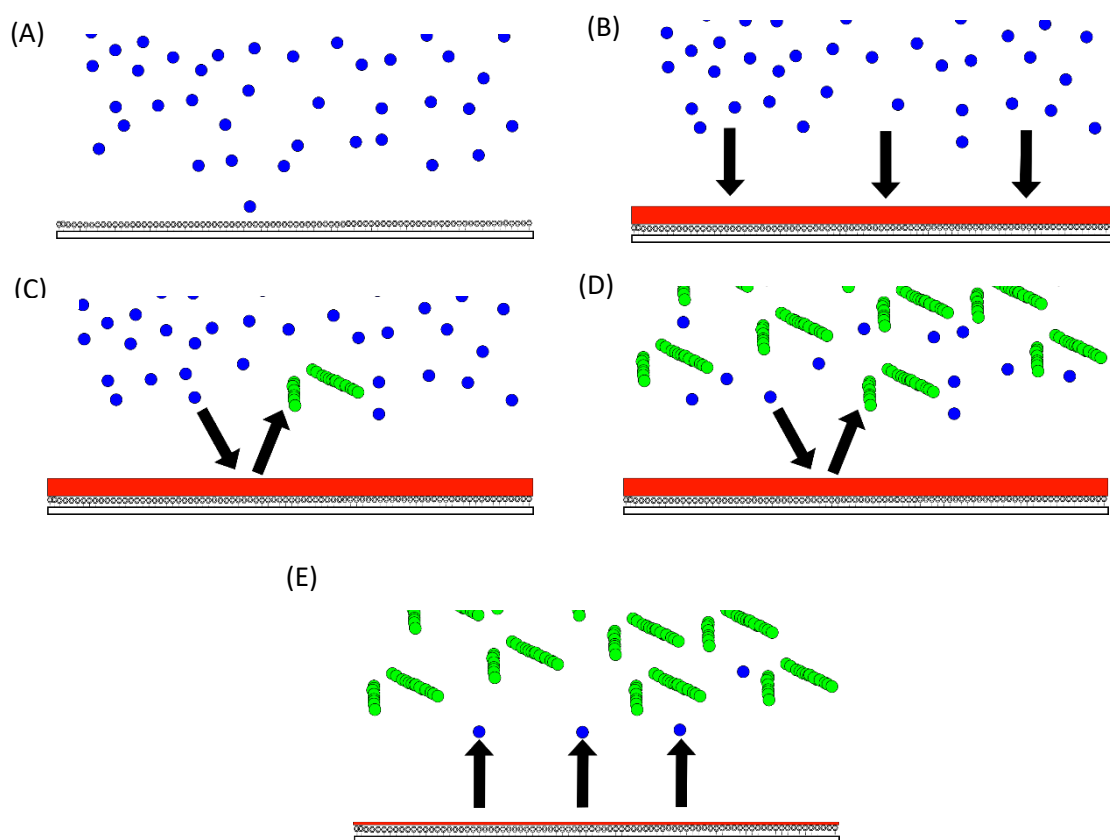


Figure 3.11 A model for fibril formation on polystyrene. Monomers in solution (A) (or non-fibrillar aggregates/oligomers) (blue circles) initially form a film (red rectangle) on the polystyrene surface (B). In this diagram, only a section of the polystyrene surface is depicted. The formation of fibrils (green circles) is catalysed by the formation of the film as the accumulation of $A\beta_{1-42}$ is promoted (C). As film deposition and fibril formation occur the monomer concentration in solution drops (D). At a critically low monomer concentration the film is no longer supported and deteriorates (E).

Section 3.3.6 shows that LUVs can reduce the lag phase for forming amyloid fibrils in a polystyrene microplate. This shows that the $A\beta_{1-42}$ can interact directly with the LUVs in a polystyrene microplate but as per the dye release data shown in section 3.3.1, not in a manner that induces lipid bilayer

permeation. The fact that the lag phase is reduced suggests that the LUVs catalyse the initiation (possibly nucleation) of fibril formation in this case. Amyloid fibrils could therefore nucleate more rapidly in the presence of LUVs in a polystyrene microplate, independently of the lipid bilayers of those LUVs becoming permeable. This is a major conclusion. A lack of $A\beta_{1-42}$ induced lipid bilayer permeation might be observed upon promoting this pathway, which could be an alternative explanation as to why there is a lack of toxicity in some cell culture experiments where polystyrene microplates are used.

This data could be helpful in better understanding which $A\beta_{1-42}$ aggregates are capable of damaging lipid bilayers. If monomeric $A\beta_{1-42}$ was to be incubated in a polystyrene microplate and the resulting species separated by size, using technology such as size exclusion chromatography or asymmetric flow field flow fractionation, they could then be analysed by multi angle light scattering. This would give a distribution of different sized aggregates found after the incubation of $A\beta_{1-42}$ in a polystyrene microplate. A time course analysed in this manner would provide information about the shifting populations of aggregates over time. A comparative time course could be performed in a quartz cuvette. By comparing the two conditions it could be inferred that any aggregates that appear in the quartz cuvette incubation but not the polystyrene incubation could be responsible for causing damage to LUVs. Both conditions would have to be tested with and without the presence of LUVs.

3.4.3 $A\beta$ fibrillisation is dependent on the surface

Section 3.3.3 highlights the fact that $A\beta_{1-42}$ fibrillisation is catalysed when monomeric $A\beta_{1-42}$ is incubated in either a polystyrene or a low-binding microplate when compared to a quartz glass or glass coated microplate. This catalysis includes a reduced lag phase which suggests a mechanism of heterogeneous nucleation of amyloid fibrils. The apparent concentration dependence displayed only in low binding microplates across the concentration range tested suggests that detailed kinetic analysis of data collected in low binding microplates may restrict the analysis of fibril formation to specific behaviours that are not necessarily present in other conditions including physiological ones^{35,41,178,182}. The concentration independence observed in polystyrene suggests that the rate of fibril formation is limited by the formation of the film observed by AFM in section 3.3.5.

To determine whether amyloid formation is totally dependent on heterogeneous nucleation, the air water interface was removed. In a quartz glass cuvette, the only heterogeneous surface for $A\beta$ to interact with is the air water interface. Section 3.3.7 shows that when incubated on a quartz glass surface no aggregates form on the surface. Therefore, if there was no heterogeneous surface at which $A\beta$ can interact, then it must nucleate in a homogeneous manner if at all. It has previously been shown that $A\beta_{1-40}$ cannot nucleate and form amyloid fibrils in these conditions¹⁸³. Section 3.3.4 shows that if the conditions are controlled to the point where there is highly limited nucleation of amyloid fibrils

before the air water interface can be cut off, the rate of fibril formation is drastically reduced. It is likely therefore that, given the entire absence of a heterogeneous surface, amyloid formation would not occur.

In vivo, there are several surfaces that could act as heterogeneous nucleation sites for amyloid formation. A β is deposited extracellularly however, the behaviour of A β when encapsulated within endosomes at low pH is also of interest. One notable surface therefore, is the extracellular matrix which has a large surface area and if it binds A β even transiently, as seen in section 3.3.7 with the hydrophilic mica surface, it could provide a nucleation site for amyloid formation.

Another surface that has been shown to provide a heterogeneous nucleation site for amyloid formation is the lipid bilayer¹⁸⁵. As shown in 3.3.6 the lag phase for amyloid formation can be reduced by incubating monomeric A β with LUVs suggesting that the LUVs provide a heterogeneous nucleation site for amyloid formation. Importantly lipid bilayers *in vivo* have varying compositions, some of which may be important in Alzheimer's disease. An investigation into the different lipid compositions that affect amyloid formation is therefore useful as is discussed in chapter 5.

Chapter 4: Investigating methods for observing the impact of lipid bilayers on A β interactions, whilst mitigating the effects of competing surfaces.

4.1 Introduction

It was shown in chapter 3 (section 3.3.1) that LUVs become permeable when introduced to a low binding microplate (Corning 3686). It was hypothesised that these LUVs were forming a supported lipid bilayer on the hydrophilic surface of the microplates.

Cell membranes are important in both a biophysical and a biochemical context¹⁸⁶. The biophysical properties of cell membranes (size, curvature) have a strong bearing on our understanding of disease states such as the structural changes to the cell membrane that occur in cancerous cells¹⁸⁷ and the effects of protein and peptide interactions with the cell membrane in Alzheimer's disease¹⁸⁸. In studies of microbes and plants these factors affect processes such as photosynthesis, protein lipid interactions and structural properties such as the periplasmic space in Gram negative bacteria¹⁸⁹⁻¹⁹². Biochemically, cell membranes provide a large surface area of chemically active ingredients for interactions to occur¹⁹³. This largely includes membrane proteins¹⁹⁴⁻¹⁹⁶ however the activity of the lipids within the lipid bilayer should not be overlooked¹⁹⁷⁻¹⁹⁹. In addition, where bimolecular interactions between soluble species occur, *in vivo* surfaces can and in many instances do, have a significant impact. As a result, when investigating specific interactions between biomolecules *in vitro*, model cell membranes can and should be used to provide further context into the nature of the interaction¹⁸⁶.

In several studies, the use of model cell membranes is hampered by the presence of third party surfaces. This particularly affects systems in which the biomolecules interact in a surface dependent manner. The use of vesicles as model cell membranes in some assays can result in competition between the interaction of the biomolecules at the lipid bilayer surface and the interaction of the biomolecules at the surface of the 'test tube'^{170,182,200-202}. In these scenarios it is difficult to determine the extent to which the vesicles are impacting upon the bimolecular interactions of interest. This includes examples of high throughput screening experiments^{201,202}, which could be improved by the inclusion of a membrane model of known size and curvature.

In other studies cell membranes are modelled by supported lipid bilayers (SLBs)^{186,203,204}. In these systems lipid bilayers are deposited onto a solid substrate, typically mica²⁰⁵ or silicon dioxide²⁰⁶, by

one of a number of methods²⁰⁷⁻²⁰⁹. These can be used in experiments such as atomic force microscopy^{205,210}, surface plasmon resonance²¹¹ and ellipsometry²⁰⁵ to measure bimolecular interactions at or with a lipid bilayer surface. However, many experimental techniques rely on equipment that are not considered optimal for SLB formation.

In vitro assays often utilise the efficiency of 96 well microplates. In situations where a model membrane is of interest, these assays tend to use vesicles as the model system^{182,201,202}. In most experiments, the role of the microplate surface is not defined. Indeed, this is very rarely presented although, in theory, measurements could be made on a range of surfaces to ensure the neutrality of the microplate surface. It will always be the case that where the impact of vesicles on the interaction between biomolecules is being investigated, the vesicle surface will be competing with the surface of the microplate and the relative effects will not be easily quantifiable. This becomes even more complex in systems where one of the biomolecules of interest is incorporated into the vesicle^{201,202}: any of the three components may still be affected by weak interactions with the microplate surface and controls become extremely difficult to design. One way of getting around this is to probe the impact of the microplate surface on the lipid vesicles. For example, in dye release assays^{170,200} the effect of the microplate on the vesicles can be directly measured. Another way would be to coat the surface of a microplate with a SLB. This would be a useful tool when a bimolecular interaction is being investigated that may be influenced by the presence of a highly complex lipid bilayer. Example applications include the way chaperones interact with bilayers when the trans-membrane domains of proteins are inserted into the lipid bilayer²¹² and the behaviour of membrane anchored proteins that are involved in binding structural proteins²¹³ or signalling pathways²¹⁴. Viral proteins such as hepatitis C²¹⁵ and glycoproteins from Herpes simplex virus²¹⁶ are also known to interact at the bilayer surface and many biochemical assays have been excluded due to the lack of model lipid bilayers available in a microplate.

In this chapter it is shown that low binding microplates (named non-binding surface by the manufacturer) (Corning 3686) cause the rupture of LUVs. This could result in the microplate surface becoming coated with SLBs with a range of different lipid compositions. As an approach for forming SLBs this would be easy to use, provide a membrane model of known size and curvature and would be remarkably simple compared to SLB formation on glass as it wouldn't require a wash step²¹⁷. The ability to form SLBs of complex lipid compositions on a microplate surface would be extremely useful²¹⁸. For example, the binding of the cholera toxin to the ganglioside GM1²¹⁹ could only be modelled in a complex SLB. Equally, modelling the behaviour of the anthrax toxin requires a complex lipid bilayer model as it interacts with cholesterol and glycosphingolipids²²⁰. The most commonly used methods for detecting a SLB such as AFM^{205,221}, quartz crystal microbalance^{205,207} and fluorescence microscopy

²⁰⁹ were not applicable here due to the size and shape of a microplate. It was also not possible to mimic the surface due to the commercial nature of the coating on the low binding microplates. The patent referring to the non-binding surface displays a range of coatings ²²², any one of which could be used in practice. Attempts to excavate the wells will be shown not to be useful. Therefore, a method that was possible within the wells of a microplate that could determine the presence of a SLB was required. By using the self-quenching fluorescent dye 5-6 carboxyfluorescein (CF) it was shown that addition of large unilamellar vesicles (LUVs) to the microplates causes the rupture of the LUVs. Further addition of fresh LUVs results in a change in the profile of dye release which indicates that the lipids are forming bilayers on the surface.

These microplates were then used to carry out a thioflavin T assay in which the formation of amyloid fibrils by A β ₁₋₄₂ ²²³, a process which is known to occur in the brains of patients with Alzheimer's disease ^{21,224}, is measured. It will be shown that the observed rate of fibril formation is not strongly affected by the presence and composition of a SLB in a lipid coated microplate.

4.2 Methods

4.2.1 CF encapsulating LUV preparation

1,2-dioleoyl-sn-glycero-3-phosphocholine (DOPC) (850375) (> 99 % purity), Cholesterol (ovine) (700000) (> 98 % purity) and GM1 Ganglioside (Brain, Ovine-Sodium Salt) (860065) (> 99 % purity) were purchased from Avanti polar lipids, (Alabaster Alabama), as a lyophilised powder. Stocks of 10 mg/ml lipid solutions were created by dissolving 100 mg of powdered lipid in 10 ml of chloroform (Sigma-Aldrich). Lipids were mixed in the ratios listed according to their molar concentration.

1 ml of each mixed lipid solution was exposed to a stream of nitrogen until all of the chloroform had been removed. The resulting lipid film was re-suspended in CF solution: 50 mM 5-6 carboxyfluorescein (Sigma-Aldrich) 10 mM HEPES pH 7.4 (adjusted with NaOH) by vortexing to make large multi-lamellar vesicles (LMVs). To make LUVs, the LMVs were passed through a mini-extruder (Avanti polar lipids) with a 200 nm polycarbonate filter. The LUVs were run down a PD-10 desalting column (GE healthcare) that had been equilibrated with 10 mM HEPES 125 mM NaCl pH 7.4 to remove any excess CF solution. 0.6 ml of LUV solution containing 10 mg/ml lipid solution was allowed to enter the packed bed of the column. This was immediately followed by 1.9 ml of 10 mM HEPES 125 mM NaCl pH 7.4 buffer. Once this had all entered the packed bed of the column 3 ml of 10 mM HEPES 125 mM NaCl pH 7.4 buffer was added and the eluent from the bottom of the column was collected. This resulted in stock 2 mg/ml LUV solutions.

4.2.2 A β ₁₋₄₂ peptide preparation

A β_{1-42} peptide (HFIP treated, lyophilised product number A-1163-2) was purchased from rPeptide (Bogart, GA). Each 1 mg aliquot of peptide was resuspended in 1 ml 10 mM NaOH by sonicating in a sonicating water bath for 30 minutes. The resulting 220 μ M solution was aliquoted into 10 microfuge tubes each containing 100 μ l. These aliquots were frozen in liquid nitrogen and stored at -80 °C for up to 2 weeks.

4.2.3 CF leakage

LUVs in polystyrene microplates. Stock LUV solutions were diluted to 50 μ g/ml. 110 μ l of each 50 μ g/ml solution was added to wells in a Corning® “96 Well half area black flat bottom polystyrene not treated microplate” (corning product number 3694) (polystyrene microplate). The wells were subjected to excitation at a wavelength of 485 nm and emission was recorded at 515 nm using a FLUOstar Omega microplate reader (BMG labtech) every 30 seconds at 37 °C for 30 minutes with 1 second of agitation per reading.

LUVs added to low binding surface microplates. As above, using Corning® 96 Well Half Area Black Flat Bottom Polystyrene NBS™ Microplate (Corning product number 3686) (low binding microplate).

LUVs added in steps to low binding surface microplates. Initially, LUVs were added to low binding microplates as above and fluorescence was recorded every 5 minutes at 37 °C for 30 minutes. The microplate was then emptied of most of its solution by inverting, 150 μ l of water was then added before emptying once more. 110 μ l of fresh 50 μ g/ml LUV solution was added. The fluorescence signal was recorded every 5 minutes at 37 °C for 30 minutes with 10 second of agitation per reading. This was repeated 3 times to give a total of 4 profiles of dye release.

Alternatively, after the first 30 minutes, 55 μ l of solution was taken out of the wells and 55 μ l of fresh buffer was added. This was repeated 6 times. Finally, 55 μ l of 100 μ g/ml LUV solution was added and the fluorescence signal was recorded every 30 seconds at 37 °C for 30 minutes with 1 second of agitation per reading. This was repeated 3 times to give 4 total profiles of dye release.

To avoid any possible exposure to air, 75 μ l of LUV solution was added initially and after 30 minutes of recording fluorescence signal 75 μ l of fresh buffer was added to the wells. This was followed by the removal of 75 μ l of solution from the wells. This was repeated 6 times and finally 75 μ l of 100 μ g/ml LUV solution was added to the wells and 75 μ l of solution was removed from the wells before the fluorescence signal was recorded every 30 seconds at 37 °C for 30 minutes with 1 second of agitation per reading. This was repeated 3 times to give 4 total profiles of dye release.

4.2.4 Imaging the base of a microplate well by AFM

To investigate the presence of a SLB by AFM a flat substrate was required. A pair of scissors and a sharp blade were used with caution to break a low-binding surface microplate to expose the wells. Individual wells were removed from the rest of microplate and the walls were removed using a sharp blade. This substrate was then glued to the base of a petri dish using green glue and imaged in buffer using the MFP-3D AFM (Asylum research) with cantilever E of the MLCT AFM tips (Bruker).

4.2.5 A β ₁₋₄₂ peptide fibrillisation on a lipid coated microplate

100 μ l of each 50 μ g/ml LUV solution was added to wells in a low binding surface microplate and was left at 37 °C for 1 hour. The solution in each well was exchanged (without exposing the SLB to air) for 97.7 μ l of 50 mM phosphate 150 mM NaCl 2mM sodium azide pH 7.4 along with 0.5 μ l of 2 mM thioflavin T (Sigma-Aldrich) giving a final thioflavin T concentration of 10 μ M. A β ₁₋₄₂ at a range of concentrations was added to each well. The wells were subjected to excitation at a wavelength of 445 nm and emission was recorded at 485 nm by a FLUOstar Omega microplate reader (BMG Labtech) every 5 minutes at 37 °C for 24 hours with 10 seconds of agitation per reading.

4.2.6 A β ₁₋₄₂ and buffer as washes for a lipid coated microplate

90 μ l of each 50 μ g/ml LUV solution was added to wells in a low binding surface microplate. The wells were subjected to excitation at a wavelength of 485 nm and emission was recorded at a wavelength 515 nm every 30 seconds at 37 °C for 30 minutes. The solution in the well was exchanged for either 90 μ l or 86.5 μ l of 50 mM phosphate 150 mM NaCl 2mM sodium azide pH 7.4 without exposing to air. To the wells containing 86.5 μ l of buffer 3.5 μ l of 220 μ M A β ₁₋₄₂ solution was added. The microplate was left at 37 °C for 5 minutes. The solution in the microplate was then exchanged back to 10 mM HEPES buffer pH 7.4 125 mM NaCl. 90 μ l of fresh 50 μ g/ml LUV solution was added and 90 μ l of solution was removed from the well. The fluorescence signal was then recorded every 30 seconds at 37 °C for 30 minutes with 1 second of agitation per reading.

4.3 Results and Discussion

4.3.1 Dye release profiles show rapid vesicle rupture in low binding microplates

CF solution was encapsulated within LUVs made using lipids with a variety of compositions, reflecting standard membrane mimics such as 1,2-dioleoyl-sn-glycero-3-phosphocholine (DOPC) but also more complex mixtures such as those associated with neuronal cells by including cholesterol and GM1¹⁷⁰. The assay relies on the observation that CF self-quenches above a threshold concentration and will fluoresce strongly upon release from the vesicles, i.e. dilution. Addition of 110 μ l of 50 μ g/ml LUV solution to a half area polystyrene microplate results in a very small change in fluorescent signal

(Figure 4.1) suggesting that the vesicles are intact and still encapsulating the dye after 30 mins (1800 s) at 37 °C.

However, addition of the same 110 μ l of 100 μ g/ml LUV solution to a half area low binding surface microplate and incubation at 37 °C for 30 mins results in a significant change in fluorescence signal (Figure 4.1) suggesting that the vesicles are no longer able to contain the dye to keep it above the required concentration threshold. Low binding surface microplates are coated in a “PEO-like” substance (polyethylene oxide) which is hydrophilic. LUVs adhere to hydrophilic surfaces. When LUVs adhere to a surface above a critical concentration they undergo vesicle fusion to form a SLB²¹⁷. The initial rate of dye release is a direct measure of vesicle rupture which is a process involved in SLB formation.

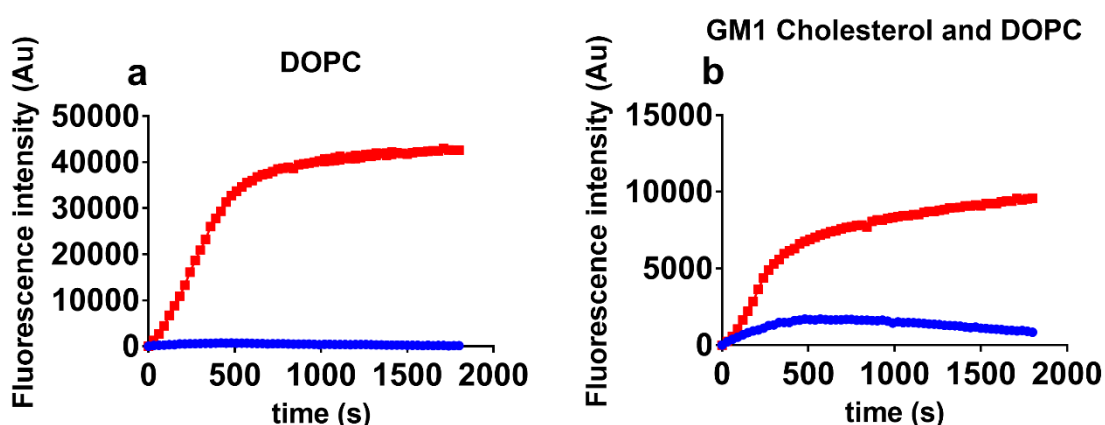


Figure 4.1: Dye release occurs in a low binding microplate. In blue data collected in a polystyrene microplate and in red data collected in a low binding microplate. Release of CF dye, which is fully self-quenching above 50 mM and was encapsulated within LUVs at 50 mM, occurs to a greater extent over 30 minutes in a low binding microplate than in a polystyrene microplate. This is independent of the composition of lipids in the LUVs as shown with (a) DOPC (b)DOPC Cholesterol and GM1. This suggests that LUVs adsorb to the hydrophilic surface of the low binding microplate and form a SLB by vesicle fusion. Error bars represent the standard error about the mean and are covered by the data points.

In support of SLB formation, a calculation of the theoretical mass of lipids required to cover the surface of the well suggests the additions made here would be saturating. In a 50 μ g/ml solution of DOPC LUVs, the concentration of lipids equals 63.6 μ M. This is equal to 4.2135×10^{15} lipid molecules in a 110 μ l volume. The surface area of a DOPC headgroup is estimated to be 0.5 nm²²²⁵. The accessible surface

area of the well containing 110 μl of solution is 1.11 cm^2 and for the DOPC molecules to cover this area given that they each have a surface area of 0.5 nm^2 means that 2.22×10^{14} molecules are required. This suggests that there are about 10 times more lipids in each addition than are necessary to cover the surface area of the well, given that the lipids exist in a bilayer (2 lipids per 0.5 nm^2) and at least 10% of these vesicles are seen to rupture upon addition to the microplate (10% of the maximum signal as confirmed by triton x-100 addition, accounting for the change in volume and therefore signal upon triton x-100 addition, data not shown).

4.3.2 Removing the base of a microplate well resulted in debris on the surface making it unusable for AFM.

Ideally, direct measurement by AFM would be the best way to determine the presence or absence of a SLB.

A sharp blade was used in order to remove the base of one of the wells from the rest of the microplate with the intention of using this for AFM. Figure 4.2 shows the resulting base of the well after it had been removed from the microplate. The base was placed in a small petri dish and held in place with a small amount of green glue.

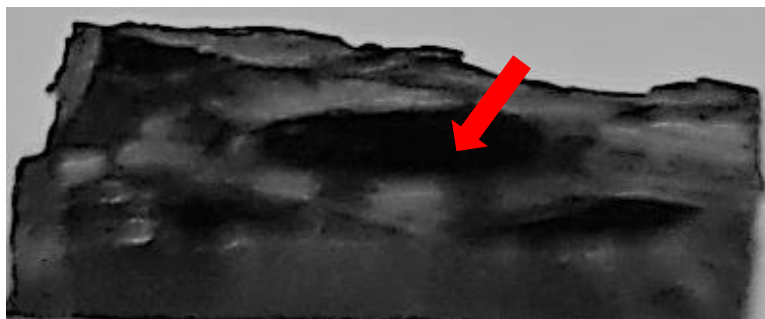


Figure 4.2 An image of the detached base of a microplate well. An image of the base of a microplate well on a benchtop. The red arrow indicates the region that was originally the base of the well. The lighter areas are where the walls of the well used to be.

The surface of the base of the microplate was then imaged in buffer by AFM with the intention being to obtain a set of force distance curves on the surface before and after exposure to LUVs to determine whether a SLB was formed. Unfortunately, the surface of the base was covered in debris which would obscure the results. Blow drying the surface with air and/or nitrogen did not remove the debris to a level sufficient for analysis of the surface by AFM.

4.3.3 Further additions of LUVs suggest SLB formation in low binding microplates

In order for the SLB to be useful as a surface for bimolecular interactions, total surface coverage would be ideal. One way of establishing whether the SLB coverage is complete would be to repeat the above process by removing the buffer solution and all excess LUVs from the microplate then adding a fresh solution of dye-containing LUVs and measuring whether any further changes occur. This has the added benefit of testing whether the SLB remains stable during buffer changes.

Figure 4.3 shows such an experiment. While the initial rate of dye release upon the first addition of LUVs is rapid followed by either a slower rate or a tailing off of dye release (blue circles, Figure.2 (A-H)), following the removal of solution from the wells, it can also be seen that further addition of LUVs results in a slower initial rate of dye release. This trend repeats after further rounds of addition of fresh LUVs to previously coated wells suggesting that while the LUVs are rupturing and coating the wells after the first addition, further additions of LUVs cannot access the low binding microplate surface in the same way. However, since the first addition is more than enough to fully coat the wells, an explanation for why successive additions still lead to dye release is required here.

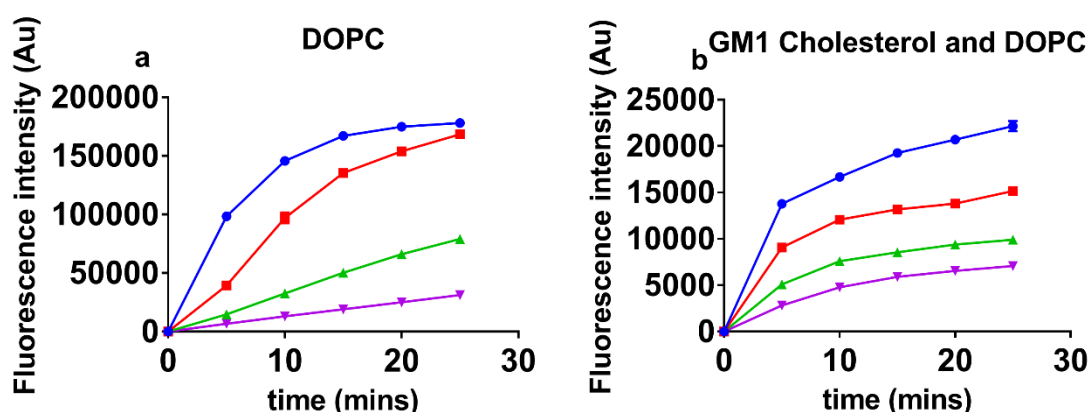


Figure 4.3: Multiple additions of fresh LUVs to a low binding microplate results in changing profiles of dye release. In blue 1st addition, in red 2nd addition, in green 3rd addition and in purple 4th addition. Release of CF dye from LUVs occurs at a slower rate in microplates that have been pre-treated with LUVs and emptied of solution. This is independent of the composition of lipids in the LUVs as shown with (a) DOPC (b) DOPC Chol and GM1. This suggests that there is formation of a SLB after the initial addition of LUVs to the microplate followed by a less favourable interaction between the LUVs and the surface of the microplate upon further additions.

Four distinct models may describe the phenomenon where multiple dye release events are observed upon successive wash/LUV addition cycles and are considered here (Figure. 4.4). The favoured model after further experimentation is shown in Figure 4.4(A) where a SLB is formed and then undergoes an exchange process with LUVs that adsorb onto the SLB. This model assumes that initial addition of LUVs

forms a SLB covering most, if not all, of the surface. Washing and further addition of fresh LUVs results in an exchange between the lipids in the SLB and those in the LUVs. This behaviour has been observed in other situations by the exchange of charged lipids²²⁶⁻²²⁸.

Alternative models considered here are shown in Figures. 4.4 (B), (C) and (D). In Figure 4.4 (B)(i) layer formation occurs, i.e. the original surface is saturated upon the first addition of LUVs and fresh additions of LUVs form further layers which in Figure 4.4 (B)(ii) are removed during the wash process. In Figure 4.4 (C), the original surface is not saturated upon initial LUV addition and the addition of further fresh LUVs results in saturation of the surface. Finally in Figure. 4.4 (D), a SLB is formed upon first addition and some or all of this is removed during the wash steps (exposure to air could cause this).

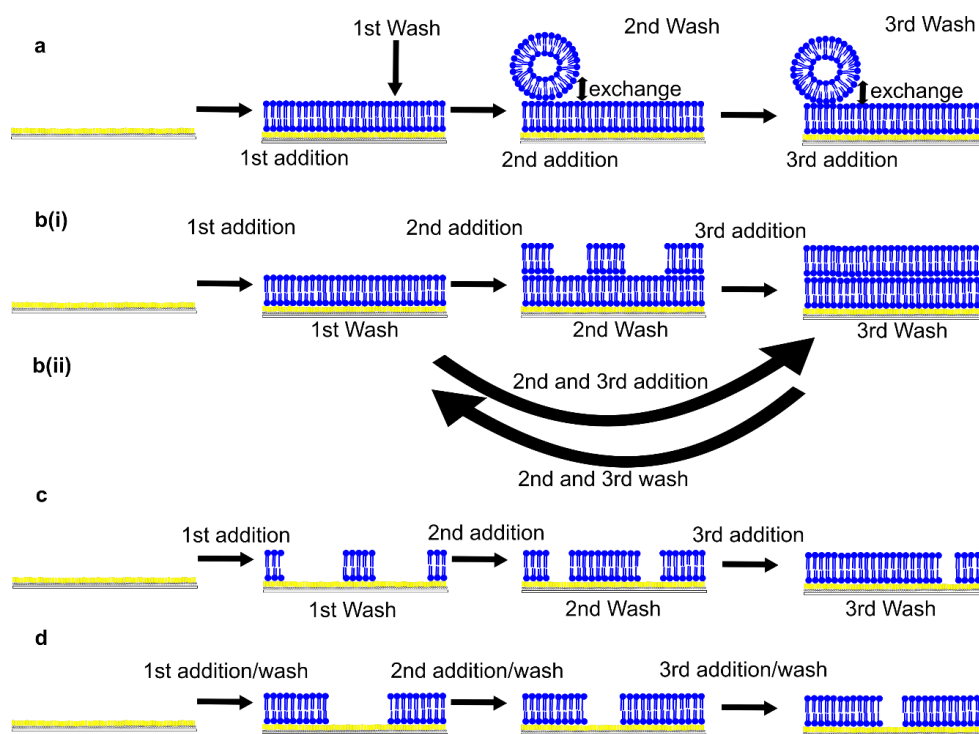


Figure 4.4: The models representing multiple dye release events upon multiple additions of fresh LUVs. In model **a** initial LUV addition results in a complete SLB and further LUV addition results in LUVs adsorbing to the surface and exchanging lipids with those in the SLB. In model **b(i)** an initial SLB is formed and as more LUVs adsorb to the surface further layers are formed. This becomes more unfavourable over time. In **b(ii)** an initial SLB is formed and a second layer is produced upon secondary LUV addition. This is then removed in the wash step. In **c** a partial SLB is formed which upon further LUV addition ‘fills in the gaps’ to complete the SLB. Finally, in **d** a complete SLB is formed upon initial LUV addition however it is partially washed away during the wash steps. This is then ‘filled in’ to create another complete SLB until the next wash step occurs.

It was hypothesised that some of these models could explain the data in Figure 4.3 if the SLB was exposed to air between LUV additions. Therefore, the method of washing between fresh additions of LUVs was changed. Figure 4.3 shows the data obtained after using the initial method for buffer exchange which consisted of microplate inversion with total exposure to air. This was changed to washing by the removal of half the volume of solution in the well followed by careful addition of the same volume of buffer returning the volume of solution in the well to what it was originally. Repeating this at least 6 times before adding fresh LUVs (the final volume and concentration was the same as the initial addition) resulted in less than 1% of the initial solution still being in the well. The data obtained using this method are shown in Figure 4.5. In the LUV composition containing cholesterol, this resulted in the second, third and fourth additions having the same dye release profile. This suggested that by removing half the volume during the wash steps, a large area of the SLB was exposed to air and removed which was then replaced by the next addition of LUVs each time. In the 100% DOPC and in repeats however, the profiles of dye release appear similar to those when the original wash method is used. Washing by first adding buffer to double the volume of solution in the well, followed by removal of the same amount of buffer to return the volume of solution in the well to its original amount was then used. Again, this was repeated 6 times before fresh LUVs were added (some of which were then removed) to a concentration and volume that was the same as the original addition. In this way the coated surface is never exposed to air during buffer exchange. These data are shown in Figure 4.6. This “add and remove” wash method produced extremely similar data to the inverse “remove and add” wash method despite the impossibility of exposing any of the SLB to air using this wash method. This suggests that exposure to air does affect the integrity of the SLB, explaining the data in Figure 4.3, but this doesn’t explain the phenomena observed in Figures 4.5 and 4.6. The only model which predicts these phenomena is the model shown in Figure 4.4 (A) where the SLB lipids are in exchange with those in the freshly added LUVs.

Multi-layering of SLBs, represented by the model shown in Figure 4.4(B)(i), could explain the data shown in Figure 4.3 but not the data shown in Figures 4.5 or 4.6. This is because the dye release profile would be reduced each time depending on the number of patches where the layer was incomplete. Therefore, it would not predict additions 2, 3 and 4 having the same dye release profile, as observed in Figures 4.5 and 4.6. The model shown in Figure 4.4(B)(ii), where a second SLB forms but is removed during the wash step, could explain the data in Figures 4.5 and 4.6 as it would predict additions 2, 3 and 4 being different from the first but the same as each other. However, multi-layer formation of SLBs is not supported in the literature unless a polymer intermediate is deployed in between the layers²²¹. Figure 4.4 (C) shows a model where the surface is only partially coated after each addition. This model predicts that less than the number of LUVs required to saturate the microplate would rupture

upon the first addition, something which is not the case in Figures. 4.3, 4.5 or 4.6. Finally, the model in Figure 4.4(D), where the surface of the well is coated upon each addition but the SLB is partially removed during each wash step, predicts a random dye release profile after each addition (as the amount of damage during each wash step should be stochastic) which is not observed in Figures 4.3, 4.5 or 4.6.

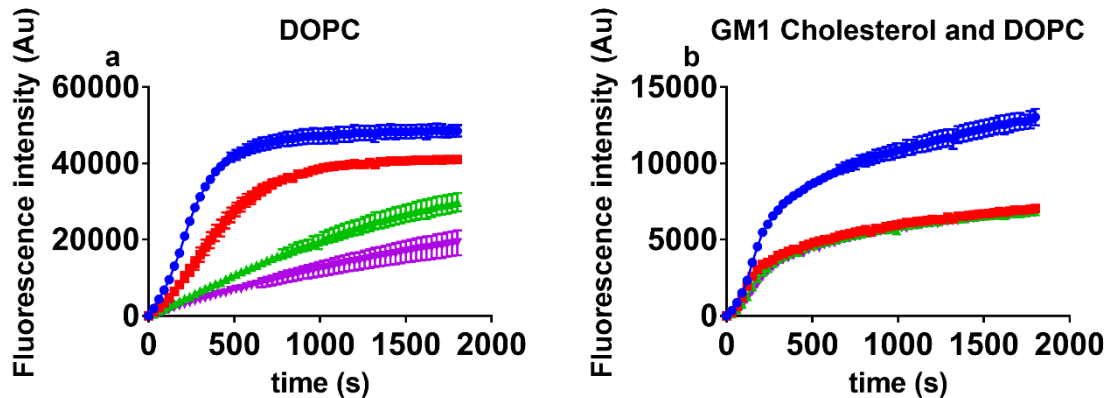


Figure 4.5: Addition of fresh LUVs and exchanging the buffer by pipetting results in a different dye release profile. In blue the 1st addition, in red the 2nd addition, in green the 3rd addition and in purple the 4th addition. Release of CF dye from LUVs occurs at a slower rate in microplates that have been pre-treated with LUVs. The profile of dye release upon the 2nd addition is consistent upon each addition suggesting that the same process occurs after each of these additions. This is dependent on the presence of cholesterol in the LUVs as shown with (a) DOPC (b) DOPC Chol and GM1. This suggests that in all cases there is formation of a SLB after the initial addition of LUVs to the microplate. However, in the absence of cholesterol and GM1 the process that occurs after each addition becomes less favourable each time.

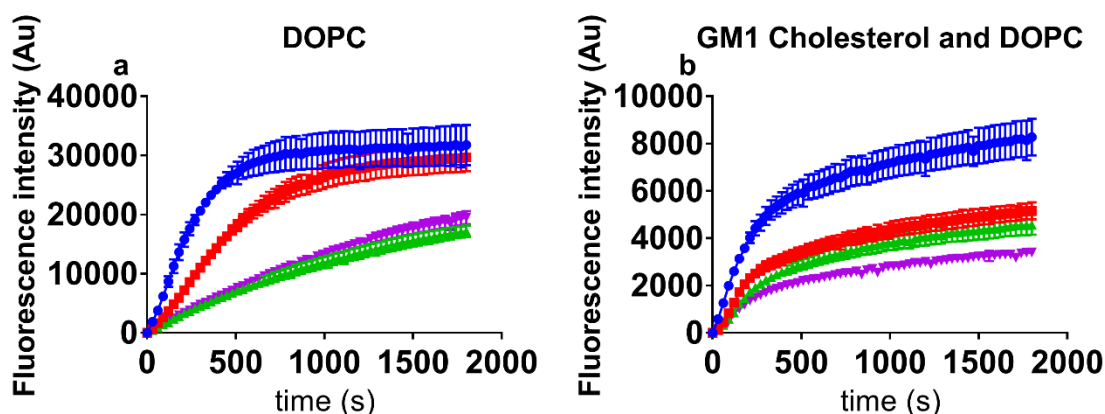


Figure 4.6: Addition of fresh LUVs and exchanging the buffer with no chance of exposing the surface of the well to air results in dye release profiles similar to that in Figure 4.5. In blue the 1st addition, in red the 2nd addition, in green the 3rd addition and in purple the 4th addition. Release of CF dye from LUVs occurs at a slower rate in microplates that have been pre-treated with LUVs. The profile of dye release upon the 2nd addition is consistent upon each addition suggesting that the same process occurs after each of these additions. This is dependent on the presence of cholesterol in the LUVs as shown with (a) DOPC (b) DOPC Chol and GM1. This suggests that in all cases there is formation of a SLB after the initial addition of LUVs to the microplate. However, in the absence of cholesterol and GM1 the process that occurs after each addition becomes less favourable each time.

To conclude, Figure 4.4 (A) shows a diagram of the model which is the most likely explanation for the dye release phenomena shown. Here the SLB lipids are in exchange with those from the freshly added LUVs. If this process occurred, then it would be likely to occur at the same rate each time assuming the original SLB was not damaged. There is also a possibility that the composition of some of the LUVs facilitates this activity by allowing for stronger adhesion to the pre-formed SLBs or easier replacement of SLB lipids. Therefore, under these conditions, the experimental protocol results in the formation of a stable SLB at the surface of a commercial microplate.

These same experiments were repeated with a different batch of the same microplates. Vesicle rupture as observed in Figure 4.1 was still observed. However, the different profiles observed in Figures 4.3, 4.5 and 4.6 were not observed, instead the rupture profile observed was the same as in figure 4.1 for all subsequent additions of LUVs (data not shown). This suggests that there may be some batch variation involved and that the formation of a stable SLB on these microplates is unpredictable.

4.3.4 Washing the microplate with $A\beta_{1-42}$ does not result in the disruption of the SLB

A more in-depth interpretation of the impact of lipids on the $A\beta_{1-42}$ aggregation process requires the proposal and testing of several different molecular models. The literature supports a model where

oligomeric forms of the $A\beta_{1-42}$ peptide can integrate into and disrupt the membrane as well as bind to it reversibly^{125,229,230}. It was hypothesised that, when cholesterol and GM1 were added as components of the SLB, there could be disruption to the SLB by the introduction of $A\beta_{1-42}$ as they have been proposed to aid adhesion of $A\beta_{1-42}$ to lipid bilayers.

To test this, dye release data from LUVs added after the treatment of a SLB with $A\beta_{1-42}$ peptide were compared with dye release data from LUVs added after the treatment of a SLB with buffer (Figure 4.7). The first addition of LUVs to the low binding surface microplate leads to a rapid release of the dye as shown in Figure 4.3, whereas after washing with buffer, a subsequent addition of fresh CF containing LUVs results in a significantly slower release. In this experiment, the SLB established after the first addition of LUVs is either treated with buffer or treated with $A\beta_{1-42}$ peptide before washing and addition of further LUVs. The outcome is that the observed change in dye release profile is, in the case of DOPC LUVs, independent of the addition of $A\beta_{1-42}$. This suggests that the SLB remains intact although there is a different profile of dye release observed to that in the previous buffer only

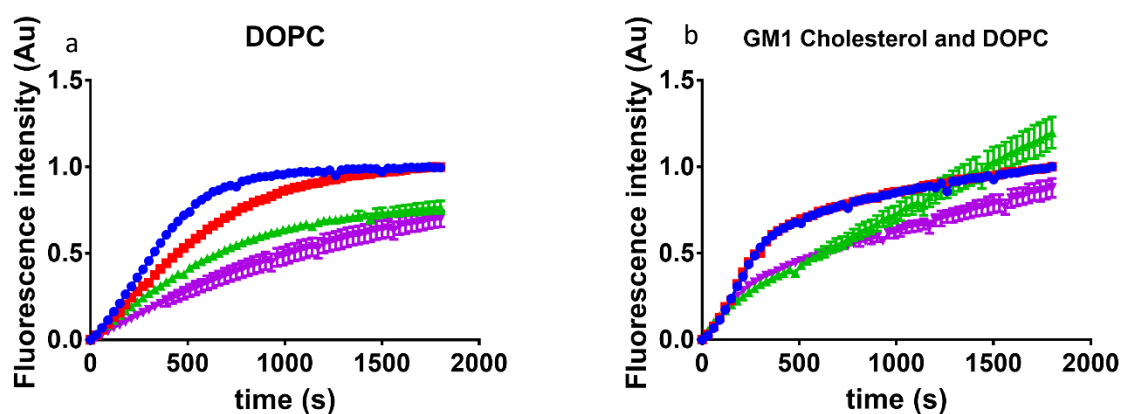


Figure 4.7: Washing with $A\beta_{1-42}$ results in membrane damage that is lipid dependent. In blue the addition before the $A\beta_{1-42}$ wash, in red the addition before the buffer wash, in green the addition after the $A\beta_{1-42}$ wash and in purple the addition after the buffer wash. The initial rate of dye release from LUVs added before (blue and red) is faster than the rate of dye release from LUVs in wells coated with a SLB after being treated with either buffer (purple) or $A\beta_{1-42}$ (green) for 5 minutes at 37 °C when DOPC only LUVs are used (A). This suggests that the presence of the SLB is not affected by treatment with either buffer or $A\beta_{1-42}$ for 5 minutes at 37 °C in these conditions. At low concentrations of GM1 (B) however, the $A\beta_{1-42}$ can sufficiently damage the SLB for additional LUVs to repopulate the surface with a new SLB. Alternatively, enough $A\beta_{1-42}$ might bind to the SLB in these conditions (strongly enough that it is not removed during the wash steps) that when it dissociates it is able to form pores within the fresh LUVs causing dye release. The data is normalised to the maximum signal observed from each addition prior to washing.

washes. This could be due to the change in salt concentration of the buffer during the wash. The buffer was exchanged back to the original before LUV addition suggesting exposure of the SLB to a higher salt concentration does have an impact on the SLB. It is not clear from these data what that impact is. These data do suggest that A β ₁₋₄₂ is unable to displace the SLB from the microplate surface under our conditions fast enough to affect the kinetic profile of amyloid fibril formation. In SLB conditions with 30 % cholesterol and 2 %, GM1 however the A β ₁₋₄₂ had a greater impact than buffer alone suggesting that A β ₁₋₄₂ can damage the SLBs formed here. An alternative explanation could be that A β ₁₋₄₂ peptide could be bound to these compositions of SLB. The low concentrations of GM1 could result in dissociation of A β ₁₋₄₂ from the SLB to directly interact with added vesicles. This is plausible because the dye release observed after the wash with A β ₁₋₄₂ is more linear than sigmoidal. This suggests a direct method of dye release rather than a nucleated one hence the suggestion that A β ₁₋₄₂ might still be present.

4.3.5 A β ₁₋₄₂ peptide fibrillisation is not affected by apparently SLB coated microplates

If a SLB was formed, then this could be applied to experiments in which the impact of different membrane surfaces on the formation of amyloid was observed. The formation of amyloid is readily monitored using the fluorescent dye Thioflavin T²³¹, a small molecule that undergoes a conformational change upon binding to amyloid fibrils resulting in a large change in fluorescent signal^{223,231}. Time courses for the formation of amyloid from A β ₁₋₄₂ peptide were monitored in low binding microplates with and without potential SLBs and the rate of amyloid fibril formation was observed. Figure 4.8 shows that compared with the reaction in non-lipid coated low binding microplates, the reaction in the DOPC coated microplates across a range of concentrations occurred at the same rates. The addition of cholesterol and GM1 at concentrations considered to be physiologically relevant¹⁷⁰ as components of the SLB also resulted in the same rates of fibrillisation. These results are inconsistent with current literature that underlines the importance of surface chemistry, in particular cholesterol and GM1 in the genesis of A β ₁₋₄₂ assembly^{44,125,168,170,232-237}. This indicates that it is unlikely that there is a SLB formed on the microplate surface in this batch of microplates.

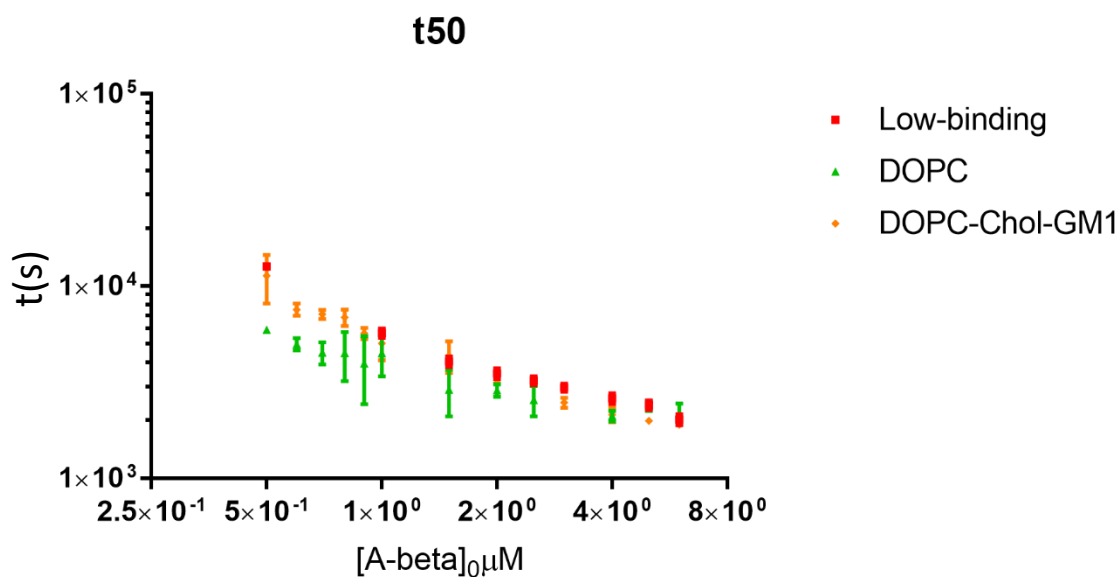


Figure 4.8: The rate of $A\beta_{1-42}$ fibrillisation is independent of surface treatment. The rate of fibrillisation of a range of concentrations of $A\beta_{1-42}$ was measured by thioflavin T fluorescence. Half times were measured and compared on the different surfaces. A difference in rate was not observed when $A\beta_{1-42}$ was incubated in a low binding microplate (red), a DOPC coated microplate (green) and a 2% GM1, 30% cholesterol, 58% DOPC coated microplate (orange) This suggests that $A\beta_{1-42}$ fibrillisation is either independent of the presence and composition of a lipid bilayer or that a SLB has not in fact formed on the surface.

4.4 Discussion

Due to the lack of direct measurement, it is difficult to determine whether the rupture of LUVs in a low binding microplate leads to the formation of a SLB. In support of the formation of a SLB, the rupture of LUVs must lead to something more energetically favourable and as can be seen from figure 4.1 this phenomenon is specific to the surface of the low binding plates. The profiles of dye release after the addition of LUVs to the low binding plates and the subsequent washing also suggests that something about the surface has changed.

However, these techniques are not direct measures of a SLB. Unfortunately, due to the debris formed on the surface any data collected by AFM would be difficult to interpret. Also, due to the incompatibility of plastic for fluorescence microscopy techniques such as FRAP were also impossible. The thioflavin T data suggests that either fibril formation is independent of the presence and composition of a lipid bilayer or that a SLB has not in fact formed on the surface.

In order to investigate the impact of lipid bilayers on the rate of amyloid formation therefore a more reliable technique is to use LUV in a quartz glass or glass surface. This is because these surfaces do not appear to act as a separate nucleating interface for $A\beta_{1-42}$ and the vesicles remain intact in these conditions. While the AWI (air water interface) remains, its activity towards $A\beta_{1-42}$ as a potential hydrophobic surface is slow compared with other experimental surfaces such as treated or untreated polystyrene microplates. As long as the impact of the lipids on the $A\beta_{1-42}$ is significantly greater than the AWI under the chosen experimental conditions, then the impact of different lipid bilayers can be measured.

Chapter 5: Lipid bilayer composition and A β -lipid bilayer interactions

5.1 Introduction

Previous studies have shown that A β behaviour can be modified by lipid bilayer compositions ^{124,128,129,163,168}. Since A β behaviour has been shown to be surface dependent (chapter 3), the importance of these studies has been intensified as lipid bilayers make up a significant proportion of the surfaces available *in vivo*. Therefore, revisiting and expanding upon these ideas could reveal key information about A β activity *in vivo*.

A commonly presented idea is that fibril formation is impacted upon by the presence of lipid bilayers of different compositions ^{132,163,168}. One study showed that in the presence of LUVs A β fibril formation was retarded by an extension of the lag phase ¹⁸². In that study LUVs were mixed with monomeric A β peptide in a low-binding surface microplate which has been shown to catalyse fibril formation in chapter 3 (section 3.3.3). Therefore, fibril formation was not necessarily retarded by LUVs, but they may be interfering instead with the catalysis of fibril formation by the PEG coating used on the low binding microplates. This is especially likely as there is a direct interaction between the low binding microplates and DOPC LUVs (chapter 4). Cholesterol incorporation was shown to reduce the retardation of fibril formation whereas the use of a shorter lipid, DPPC, rather than DOPC increased the lag phase. Again, these data do not distinguish between inhibiting fibril formation directly or by inhibiting the catalysis of fibril formation by the low-binding surface. This is because any interaction between the low-binding surface and the LUVs could also be dependent on the lipid bilayer composition. The same study also revealed that in this system, negatively charged lipids such as DOPS did not impact fibril formation differently to zwitterionic DOPC lipids, despite monomeric A β holding an overall negative charge at pH 8. This further suggests that LUVs in this system are preventing the catalysis of fibril formation rather than directly interacting with A β . More recently analysis of A β fibril formation in the presence of DMPC and cholesterol vesicles revealed that cholesterol catalyses fibril formation by accelerating primary nucleation ¹⁸⁵. Once again in this study, low-binding microplates were used. The impact of the LUVs on fibril formation appeared to be independent of the low-binding surface. However, the impact of the low binding surface on fibril formation was not accounted for. In order to truly investigate the impact of cholesterol, a neutral background surface is required.

Ganglioside GM1 is also often discussed as a lipid bilayer constituent that affects fibril formation ^{129,163}. GM1 has been shown to interact with A β in combination with cholesterol either by a direct interaction,

or by accumulation in lipid raft like regions which are modulated by cholesterol^{124,125}. In these studies, a range of techniques were used to determine that GM1 can impact upon fibril formation with multiple different background surfaces potentially impacting upon the process. An investigation that provides information about the direct impact of GM1 and cholesterol on fibril formation in the presence of a neutral background surface would be a useful contribution.

Another idea that has been presented previously is that the toxicity of A β species is dependent on their formation in the presence of different lipid bilayer compositions^{128,129,170}. GM1 in particular has been shown to induce toxic fibril formation¹²⁹. In one study the impact of the presence of GM1 on the permeation of LUVs by A β was measured by calcein dye release¹⁷⁰. The presence of GM1 was shown to increase the amount and the rate of LUV permeation by A β . Here the interaction took place in the presence of a quartz glass cuvette which, as shown in chapter 3 (section 3.3.3), does not impact upon normal A β fibril formation. This suggests that the impact of GM1 was reliably measured. However, another investigation into the impact of GM1 and cholesterol combined with DOPC rather than DMPC in LUVs would be useful as DOPC is commonly used in model membranes²³⁸.

To truly determine the impact of lipid bilayers and their compositions on fibril formation, they must be tested in an environment that impacts upon fibril formation minimally such as glass surfaces, as displayed in chapter 3 (sections 3.3.3 and 3.3.6). In this chapter A β fibrillisation catalysed by LUVs in glass microplates will be shown, as will the effect of different lipid compositions on fibril formation with a neutral background surface.

Equally, how lipid compositions impact upon A β induced LUV permeation in the presence of a neutral quartz glass background surface will be further explored.

Finally, the distribution of LUVs with different compositions and A β aggregates determined by AF4-MALS after incubation together will be presented. This will determine if the population of LUVs, or A β aggregates changes as a response to lipid bilayer composition.

5.2 Methods

5.2.1 Thioflavin T assays

Different concentrations of A β ₁₋₄₂ were incubated with a variety of different LUVs in the conditions listed in table 5.1. Fluorescent measurements were recorded as per chapter 2 (section 2.9) every 2 minutes with shaking at 100 rpm before each measurement at 37°C.

Table 5.1

| Experiment Set | Corresponding figures | A β ₁₋₄₂ batch | A β ₁₋₄₂ concentration (μ M) | Total lipid concentration (μ g/ml) | LUV composition (% of total lipid) | Buffer composition |
|----------------|-----------------------|---------------------------------|--|---|------------------------------------|---|
| 1 | 5.1, 5.2 | A | 2, 3, 4, 5, 6 | 0, 50 | 100% DOPC | 20 mM NaPO ₄ , pH 7.4 |
| 2 | 5.1, 5.2 | A | 2, 3, 4, 5, 6 | 0, 50 | 100% DOPC | 50 mM NaPO ₄ , 150 mM NaCl, pH 7.4 |
| 3 | 5.2 (C) | A | 2, 3, 4, 5, 6 | 0, 50 | 65% DOPC, 33% Chol, 2%GM1 | 20 mM NaPO ₄ , pH 7.4 |
| 4 | 5.2 (C) | A | 2, 3, 4, 5, 6 | 0, 50 | 65% DOPC, 33% Chol, 2%GM1 | 50 mM NaPO ₄ , 150 mM NaCl, pH 7.4 |
| 5 | 5.3, 5.4 | B | 0.25, 0.5, 0.75, 1.0, 1.25, 1.5, 1.75, 2.0 | 0, 5, 10, 20, 30, 40 | 65% DOPC, 33% Chol, 2%GM1 | 50 mM NaPO ₄ , 150 mM NaCl, pH 7.4 |

The batch of A β ₁₋₄₂ prepared for these experiments varied as indicated in table 5.1. Due to variations between these batches beyond experimental control, direct comparisons could not be made between results obtained using different batches. Results obtained within the same batch of A β ₁₋₄₂ were reproducible and therefore results obtained within a batch of A β ₁₋₄₂ could be compared.

5.2.2 Dye release assays

DOPC LUVs encapsulating 50 mM carboxyfluorescein were prepared as per chapter 2 (section 2.4.2 and 2.10). In a quartz glass cuvette 50 μ g/ml LUVs were incubated at 37 °C in the presence and absence of 2 μ M A β ₁₋₄₂. Fluorescence spectra were recorded every 15 minutes as per chapter 2 (section 2.10).

LUVs made up of 2% GM1 33% cholesterol and 65% DOPC and encapsulating 50 mM carboxyfluorescein were prepared as per chapter 2 (section 2.4.2 and 2.10). In a quartz glass cuvette 50 μ g/ml LUVs were incubated at 37 °C in the presence and absence of 2 μ M A β ₁₋₄₂. Fluorescence spectra were recorded every 15 minutes as per chapter 2 (section 2.10).

In both cases the A β ₁₋₄₂ was from the same batch used in experiments 1, 2, 3 and 4 in table 5.1.

5.2.3 Electron Microscopy

10 μ M A β ₁₋₄₂ was incubated with LUVs made up of 2% GM1, 33% cholesterol and 65% DOPC in a 50 mM sodium phosphate buffer at pH 7.4 with 150 mM sodium chloride for 3 hours in glass coated

microplates. EM grids were prepared and imaged using this sample as described in chapter 2 (section 2.5). In this case the A β_{1-42} was from the same batch (A) used in experiments 1, 2, 3 and 4 in table 5.1.

11 μ M A β_{1-42} was incubated with LUVs made up of 50 % DOPC and 50 % DOPG in a 50 mM sodium phosphate buffer at pH 7.4 with 150 mM sodium chloride for 24 hours. EM grids were prepared and imaged using this sample as described in chapter 2 (section 2.5). In this case the batch of A β_{1-42} used was different to all other batches used in this chapter.

5.2.4 AF4-MALS

22 μ M A β (from the same batch used in experiments 1, 2, 3 and 4 in table 5.1) was incubated in at 37 °C with no agitation for 3 hours in the presence and absence of 100% DOPC LUVs and 2% GM1, 33% cholesterol, 65% DOPC LUVs in a 50 mM sodium phosphate buffer at pH 7.4 with 150 mM sodium chloride. The AF4-MALS system was equilibrated with the same buffer. 15 μ g of sample was injected per run. The eluted sample was measured by A₂₈₀ and MALS. The experiments were performed as per chapter 2 (section 2.7).

5.3 Results

5.3.1 Batch variation in A β_{1-42} results in seeded reactions

The aim of this chapter was to investigate the effects of adding LUVs to monomeric A β_{1-42} in conditions where the surface environment was having a minimal effect. The data sets presented in figures 5.1 to 5.4 (and also when compared to data shown in chapter 3 section 3.3.3) show A β_{1-42} behaviour that is not consistent even in the absence of LUVs. This is due to variation in the quantity of counter ions provided in different batches of A β_{1-42} , discussed further in chapter 7 (section 7.3.5), resulting in reactions that were seeded to different extents between batches. Therefore, data can only be compared directly between A β_{1-42} samples taken from the same batch, the results of which were reproducible. The effects of LUVs can be observed from these data but due to the nature of seeded reactions, it is complex to determine what was happening mechanistically.

5.3.2 Fibril formation is catalysed by LUVs

The catalysis of fibril formation by LUVs was discussed in chapter 3 (section 3.3.7) where DOPC LUVs were shown to increase the rate of A β_{1-42} fibril formation by decreasing the lag phase. These experiments were performed in a polystyrene microplate which as shown in chapter 3 (section 3.3.3) catalyses the fibril formation reaction. To determine the true extent to which LUVs catalyse fibril formation a neutral background surface such as glass microplates must be used.

3 μM monomeric $\text{A}\beta_{1-42}$ was added to 50 $\mu\text{g}/\text{ml}$ DOPC LUVs in a low salt buffer (20 mM sodium phosphate, pH 7.4) containing 10 μM thioflavin T in glass microplates. These microplates were then incubated at 37 $^{\circ}\text{C}$ and fluorescence was measured every 120 seconds with minimal agitation. Figure 5.1 shows a time course of the normalised thioflavin T fluorescence displaying an increase in the rate of fibril formation in the presence of DOPC LUVs.

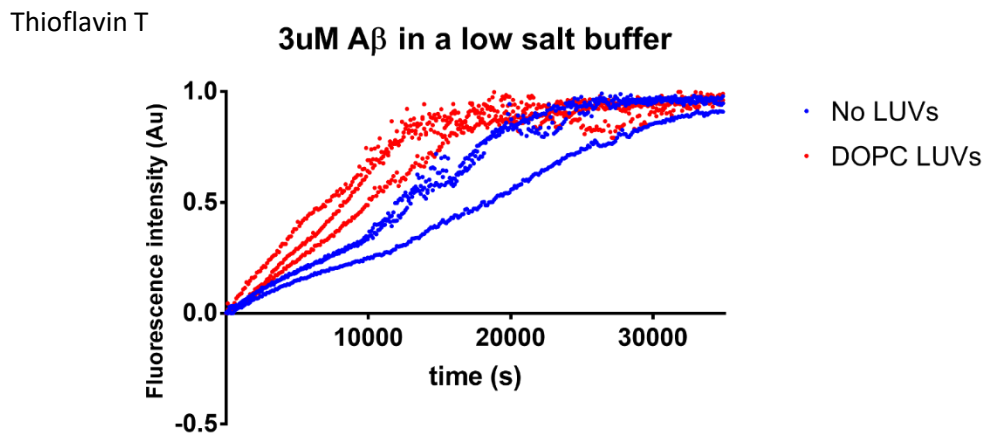


Figure 5.1 DOPC LUVs catalyse fibril formation. 3 μM $\text{A}\beta_{1-42}$ was incubated in the presence (red) and absence (blue) of 50 $\mu\text{g}/\text{ml}$ DOPC LUVs and fibril formation was measured by thioflavin T fluorescence. A short lag phase is observed in both cases however, the growth phase is faster in the presence of DOPC LUVs.

A range of concentrations of $\text{A}\beta_{1-42}$ were also incubated with DOPC LUVs in both the same low salt buffer and a more physiological salt buffer (50 mM sodium phosphate, 150 mM sodium chloride, pH 7.4). The time courses of the normalised data across the range of concentrations in the low salt buffer are shown in figure 5.2 (A and B). The half time for each reaction was recorded and plotted against initial $\text{A}\beta_{1-42}$ monomer concentration in figure 5.2 (C). These data show that fibril formation maintains similar concentration dependences in the presence of LUVs in glass microplates but that, overall it is catalysed by the presence of LUVs.

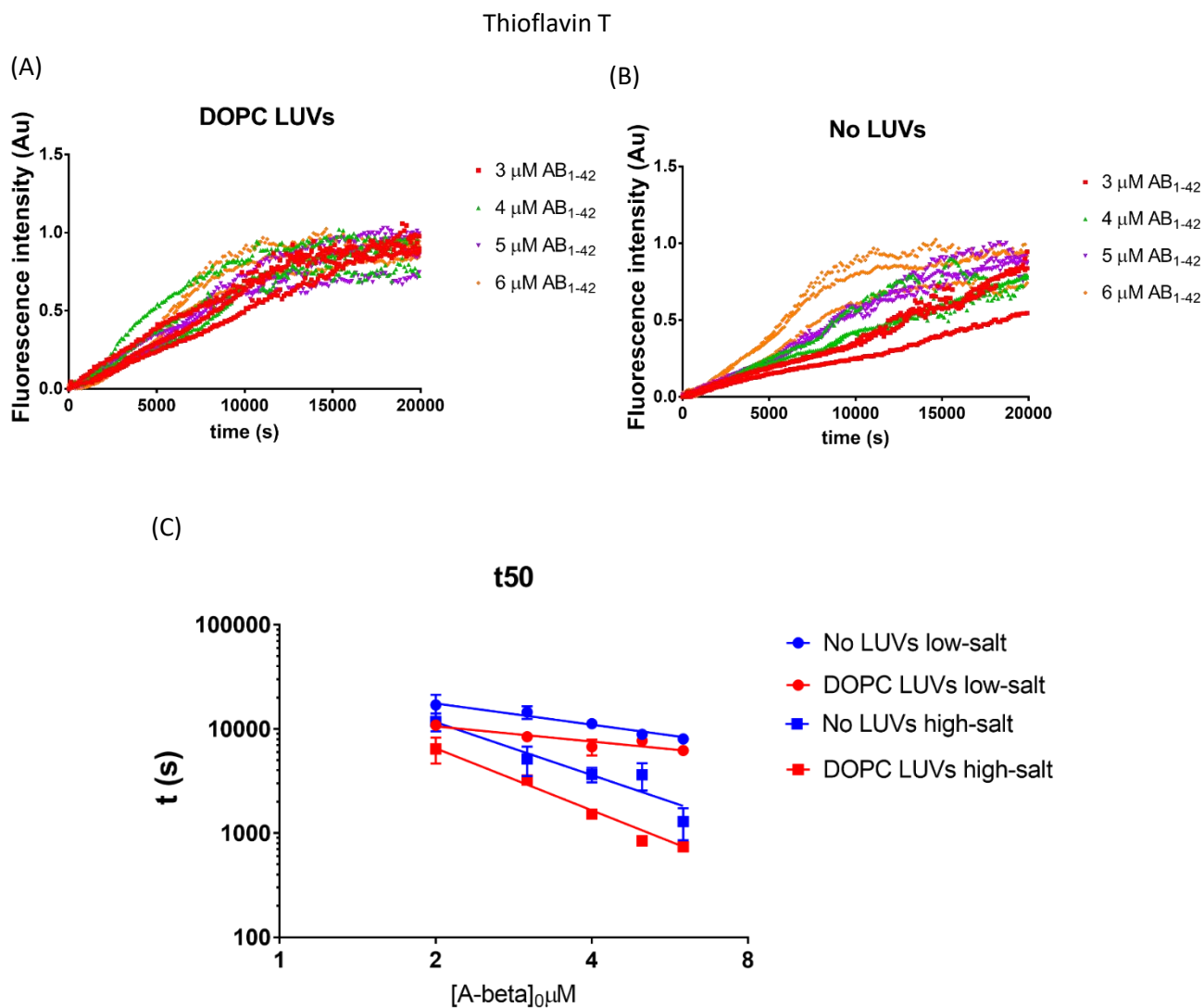


Figure 5.2 $\text{A}\beta_{1-42}$ fibril formation is catalysed by LUVs with minimal effect on the concentration dependence.

Monomeric $\text{A}\beta_{1-42}$ was incubated in the presence (A) and absence (B) of DOPC LUVs at a range of initial monomer concentrations and the normalised change in thioflavin T fluorescence over time was plotted. The data in (B) is cut-off before it reaches maximum in order to better compare the data sets. These experiments were repeated in physiological salt buffer. The half times of the reactions were plotted against the initial concentrations of monomeric $\text{A}\beta_{1-42}$. The concentration dependencies of the reactions (C) in the low-salt (circles) conditions produced γ values of -0.7 in the absence of LUVs and -0.5 (blue) in the presence of LUVs (red) when the data was fit to equation 1 shown in chapter 2 (section 2.8). In the physiological salt conditions the concentration dependencies of the reactions produced γ values of -1.6 in the absence of LUVs (blue) and -1.9 in the presence of LUVs (red). The data in (C) were plotted on a log 10 (y-axis) log 2 (x-axis) scale for the purpose of clarity. The error bars represent the standard error about the mean from 2 repeats of 3 replicates per reaction. Only one of these repeats is shown in (A) and (B).

The values of the exponent γ can be calculated using equation 2.2³⁵.

Equation 2.2

$$t_{1/2} = ax^\gamma$$

These values were calculated to be -0.7 in the absence of LUVs and -0.5 in the presence of LUVs in the low-salt conditions and -1.6 in the absence of LUVs and -1.9 in the presence of LUVs in the high-salt conditions. Generally, it is expected that physiological salt concentrations increase the rate of fibril formation when compared to low salt conditions (discussed further in chapter 7 (section 7.3.5)). Interestingly the overall reaction became more concentration dependent in the presence of salt. With consideration that these reactions are likely seeded this suggests the existence of a concentration dependent process that is promoted at higher salt concentrations which can occur after nucleation has likely become negligible with regard to the overall rate. One possibility is that dimerisation is promoted by high salt concentrations and elongation occurs through both dimer addition and monomer addition. In this case dimer addition as a more concentration dependent mechanism would take over at higher salt concentrations as Debye-Hückel screening promotes dimerisation. At low salt concentrations elongation by monomers would dominate and be less concentration dependent.

Despite no significant changes to the concentration dependencies, the overall rates of the reactions are generally faster in the presence of DOPC LUVs. The LUVs must therefore promote fibril formation in this case without affecting the concentration dependence of the reaction. As these reactions are likely seeded this suggests that the LUVs were capable of promoting fibril formation in conditions where the effect of nucleation on the overall rate of the reaction is negligible and therefore LUVs can likely catalyse other processes as well as the observed impact on nucleation (chapter 3, section 3.3.7).

5.3.3 Catalysis of fibril formation by LUVs is saturable

In section 5.3.2 a single concentration of LUVs was incubated with increasing concentrations of $A\beta_{1-42}$ in which fibril formation was deemed to be catalysed by LUVs. To determine whether the catalytic sites available on the LUVs could be saturated, a range of concentrations of LUVs were applied.

The ability of LUVs to affect the rate of fibril formation at different concentrations is shown in figure 5.3. Various concentrations of monomeric $A\beta_{1-42}$ were incubated in a high salt buffer with various concentrations of LUVs containing 2% GM1, 33% cholesterol and 65% DOPC (percentages represent percentage concentration of lipid and not percentage mass). The GM1/Chol/DOPC LUVs were used

here as they have been previously described as good biomimetic LUVs ¹⁷⁰. Fibril formation was measured by thioflavin T fluorescence. Figure 5.3 shows the normalised fluorescence over time when 1 μM $\text{A}\beta_{1-42}$ was incubated with no LUVs, 5, 10, 20, 30 and 40 $\mu\text{g}/\text{ml}$ LUVs. As the concentration of LUVs increases the initial phase that is observed occurs at the same rate which is maintained for longer as the concentration of LUVs increases.

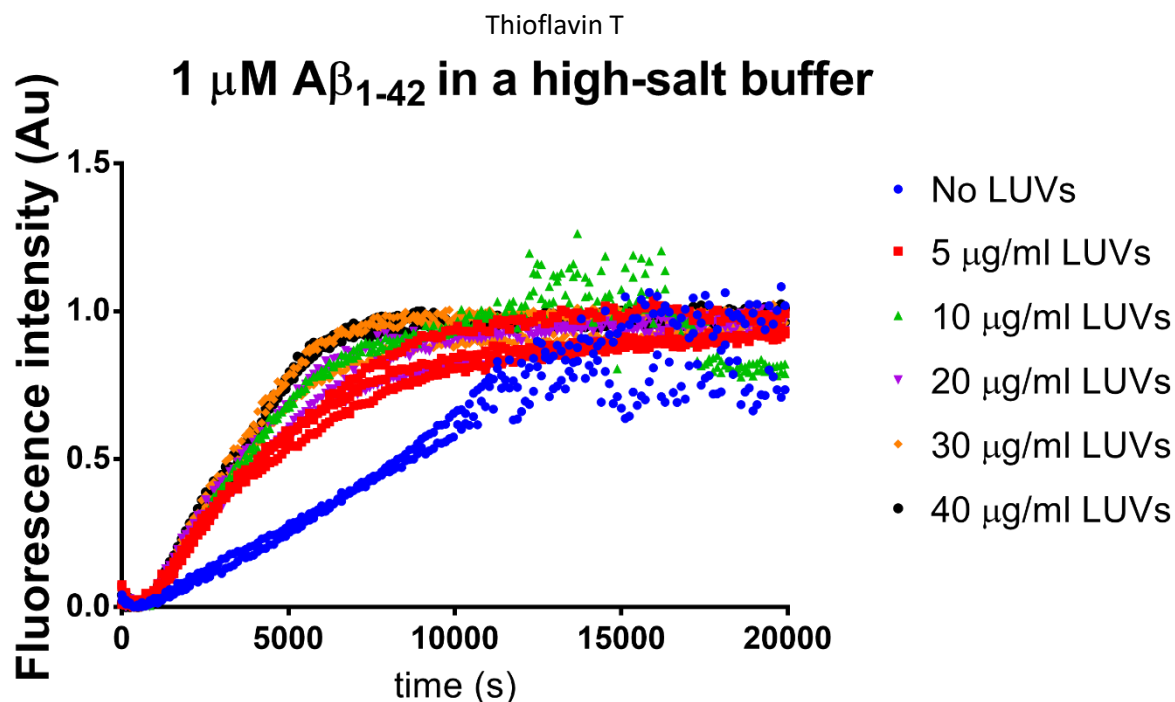


Figure 5.3 LUVs catalyse the growth rate of fibril formation. Various concentrations of $\text{A}\beta_{1-42}$ were incubated in a high salt buffer with increasing concentrations of GM1/Chol/DOPC LUVs. The time courses of normalised fluorescence for the 1 μM $\text{A}\beta_{1-42}$ reactions with increasing concentrations of LUVs were plotted (A). The lag phase for all of the reactions remained the same however the growth phase of the reactions was faster in the presence of LUVs. As the concentration of LUVs increased the longer the fast rate of growth was maintained.

The overall concentration dependences of the reactions were shown in figure 5.4 by plotting the t_{50} against the initial concentration of $\text{A}\beta_{1-42}$ monomers. This shows a concentration independence at low LUV concentrations. The reaction increases in concentration dependency as the concentration of LUVs is increased until it becomes concentration independent again at high LUV concentrations. At low LUV concentrations the reaction is slow, albeit faster than in the absence of LUVs, and concentration independent. This suggests that the $\text{A}\beta_{1-42}$ greatly outnumbers the LUVs. As the concentration of LUVs increases the reaction becomes faster and more dependent on the initial concentration of monomeric $\text{A}\beta_{1-42}$, suggesting that $\text{A}\beta_{1-42}$ no longer saturates the LUVs and the increased fibril growth rate is facilitated as the concentration of $\text{A}\beta_{1-42}$ increases. At a high concentration of LUVs, the reaction

becomes concentration independent again with respect to $A\beta_{1-42}$. At this concentration of LUVs, a concentration independent and also LUV independent process must occur. One possibility is the formation of oligomers catalysed by the air water interface that are more easily converted to fibrils. This would be concentration independent as the air water interface could be saturated and also LUV independent.

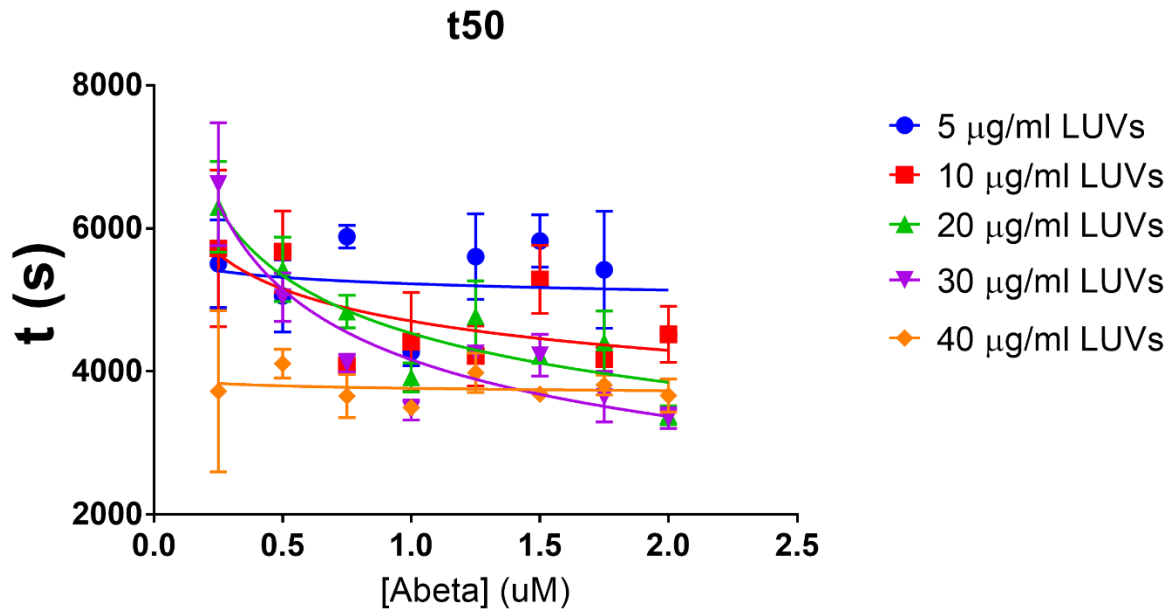


Figure 5.4 Catalysed fibril formation by LUVs can be saturated. $A\beta_{1-42}$ was incubated at various concentrations in a high salt buffer with increasing concentrations of GM1/Chol/DOPC LUVs. The half times of the reactions were measured and plotted against the initial concentrations of monomeric $A\beta_{1-42}$. As the concentration of LUVs increased the reaction moved from concentration independent and slow through concentration dependence to become concentration independent and fast. Error bars represent the standard error about the mean from 3 replicates per reaction.

5.3.4 GM1 and Cholesterol containing LUVs do not catalyse fibril formation more than DOPC only LUVs

In order to determine whether GM1 and cholesterol containing LUVs have an impact on fibril formation, they must be tested using a neutral background surface and compared to DOPC only LUVs using the same batch of $A\beta_{1-42}$.

Monomeric $A\beta_{1-42}$ at various concentrations from the same batch as used to collect the data shown in figures 5.1 and 5.2 were incubated with 50 $\mu\text{g/ml}$ of GM1/Chol/DOPC LUVs in both high and low-salt buffers. The half times of the reaction are plotted in figure 5.5 against the initial $A\beta_{1-42}$ monomer

concentration along with the half times of the reactions in the presence of DOPC LUVs and in the absence of LUVs. These data show that the incorporation into the LUVs of 2 % GM1 and 33% cholesterol make no difference to the rates or concentration dependences of the reaction. This suggests that the interaction between A β ₁₋₄₂ and LUVs that results in catalysed fibril formation under the conditions used here is independent of GM1 and cholesterol. However, as the reaction is likely seeded, any effect of adding GM1 and cholesterol to the nucleation of fibril formation would not be observed because in a seeded reaction the effect of nucleation on the overall rate of the reaction is negligible. To conclude, while LUVs can impact on elongation and/or secondary nucleation in A β ₁₋₄₂ fibril assembly, GM1 and cholesterol do not modulate this activity.

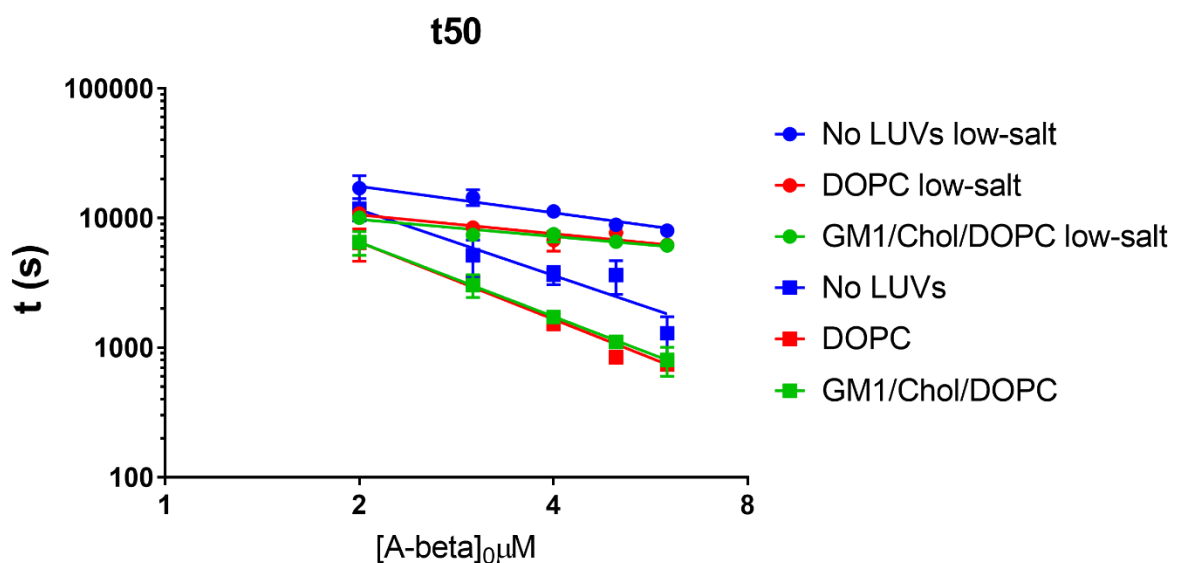


Figure 5.5 GM1 and cholesterol do not impact on the rate or concentration dependence of fibril formation by A β ₁₋₄₂. Monomeric A β ₁₋₄₂ from the same batch was incubated with DOPC (red) and GM1/Chol/DOPC (green) LUVs and in the absence of LUVs (blue) in both high-salt (squares) and low-salt (circles) buffers. In both buffers the effect of adding LUVs was the same independently of adding GM1 and cholesterol. The error bars represent the standard error about the mean from 2 repeats of 3 replicates per reaction. The reproducibility of these data is highlighted by the overlap between the DOPC data and the GM1/Chol/DOPC data.

5.3.5 GM1 and cholesterol do promote A β ₁₋₄₂ induced LUV permeation

Fibril formation by A β ₁₋₄₂ is not traditionally associated with an increase in toxicity⁴². However, fibril formation induced by GM1 has been shown to form toxic fibrils¹²⁹. Therefore, due to the inability of GM1 to impact upon fibril formation in a glass microplate in the seeded conditions, the ability of A β ₁₋₄₂ aggregates to produce effects related to toxicity such as increased lipid bilayer permeation was investigated.

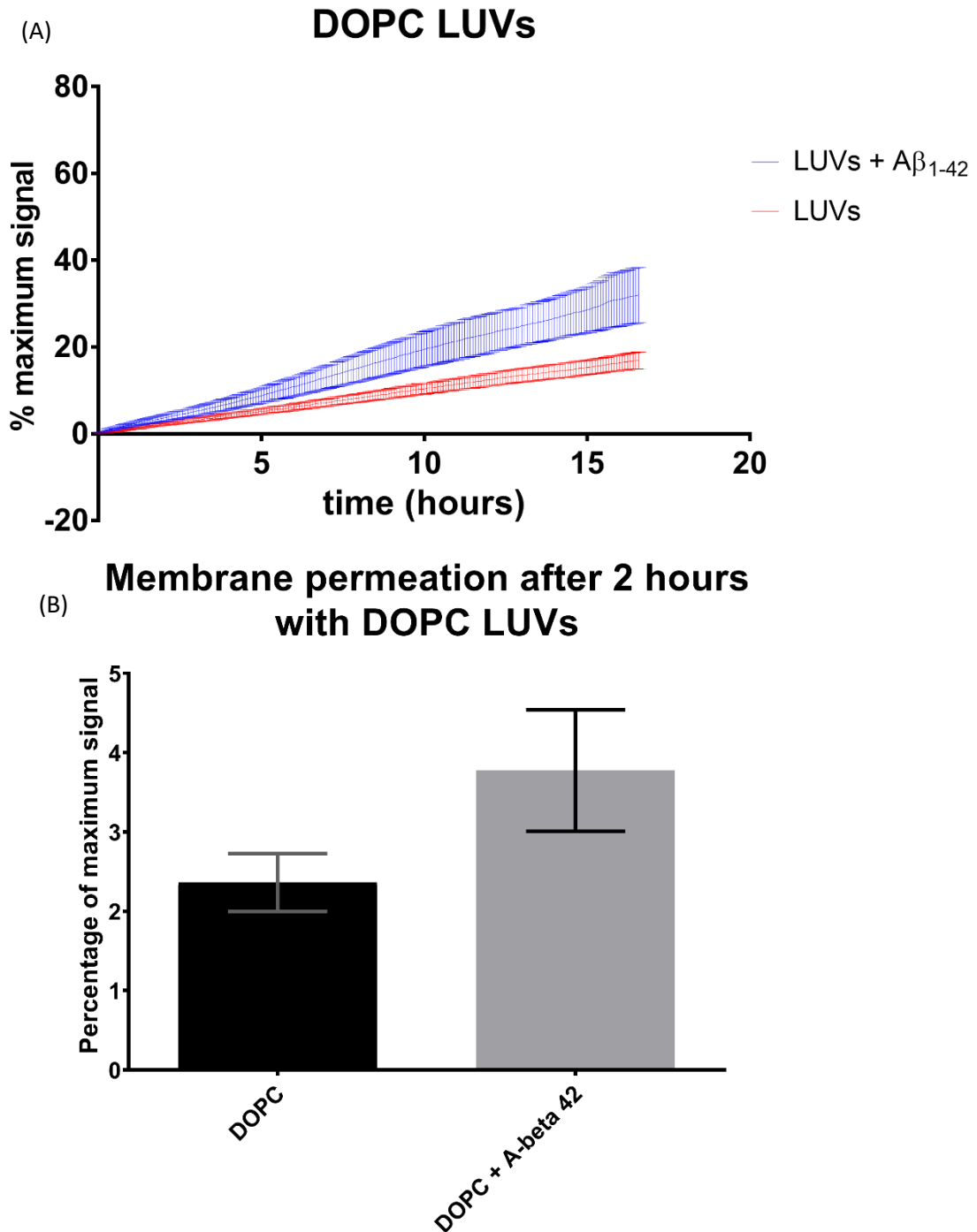


Figure 5.6 A β_{1-42} can induce some permeation in DOPC LUVs. Monomeric A β_{1-42} was incubated with DOPC LUVs encapsulating 50 mM carboxyfluorescein and the change in fluorescence was measured for 16 hours. After 16 hours the maximum signal was obtained and the change in the percentage of the maximum signal was plotted over time (A). The percentage of the maximum signal after 2 hours was also plotted (B). The increase in signal was determined to be insignificant using a Student's t-test.

DOPC LUVs encapsulating 50 mM carboxyfluorescein were incubated for 16 hours with 2 μ M monomeric A β_{1-42} and lipid bilayer permeation was measured by dye release as described in chapter

2 (section 2.9). The experiment was performed in a quartz glass microplate. A normalised fluorescence time course is shown in figure 5.6 (A) and revealed a low level of $A\beta_{1-42}$ induced permeation. Plotting the final percentage of the maximum signal (determined by adding 1 μ l of 20 % Triton X-100 and measuring the fluorescence) after 2 hours in figure 5.6 (B) showed that there was more permeation in the sample containing $A\beta$ than in the control.

In order to determine the ability of $A\beta_{1-42}$ to induce lipid permeation in the presence of GM1 and cholesterol, GM1/Chol/DOPC LUVs were made encapsulating 50 mM carboxyfluorescein. These LUVs were incubated with 2 μ M $A\beta_{1-42}$ for 16 hours in quartz glass cuvettes. The change in fluorescent signal observed over time was plotted in figure 5.7 (A). These data show that, in the presence of $A\beta_{1-42}$, there is a significant increase in initial the rate of dye release that is not observed in the absence of GM1 and cholesterol in figure 5.6 (A). The percentage of the maximum signal achieved after 2 hours was also recorded in figure 5.6 (B) and was shown to be significantly higher in the presence of $A\beta_{1-42}$. The difference between LUV permeation in the presence and absence of $A\beta_{1-42}$ after 2 hours was also significantly larger when GM1/Chol/DOPC LUVs were used as opposed to DOPC LUVs. This shows that, despite an inability to affect fibril formation in a glass microplate, the presence of GM1 and cholesterol promotes lipid bilayer permeation even using our seeded $A\beta_{1-42}$ batches. Generally, the difference in dye leakage in the absence of $A\beta_{1-42}$ is expected to be due to the difference in ionic strength on either side of the lipid bilayer. However, this does not adequately explain why repeats using GM1 and cholesterol were generally less prone to dye leakage than DOPC LUVs in the absence of $A\beta_{1-42}$.

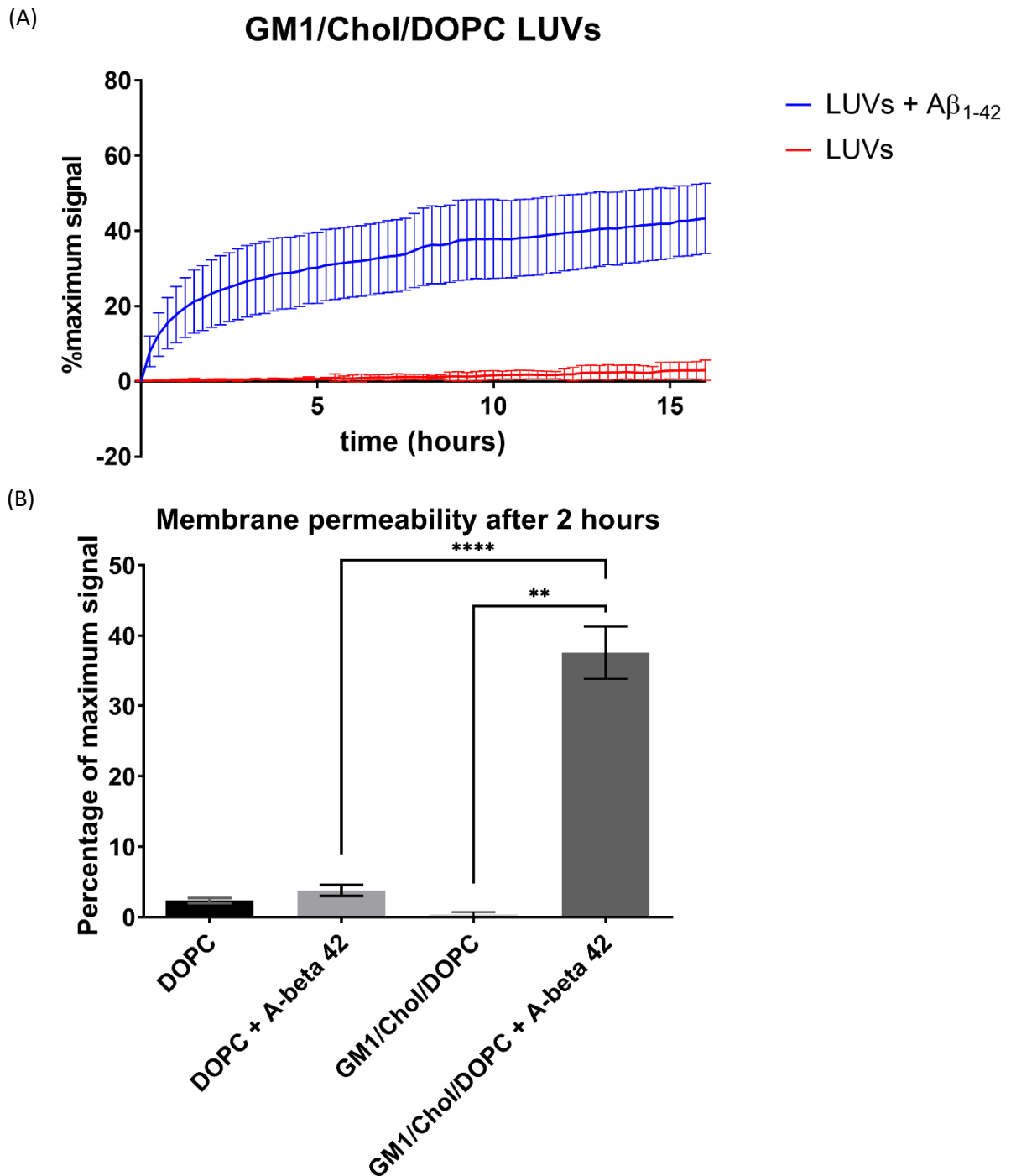


Figure 5.7 $A\beta_{1-42}$ induced permeation of LUVs is promoted when GM1 and cholesterol are incorporated in the LUVs. Monomeric $A\beta_{1-42}$ was incubated with DOPC-cholesterol-GM1 LUVs encapsulating 50 mM carboxyfluorescein and the change in fluorescence was measured for 16 hours. After 16 hours, the maximum signal was obtained and the change in the percentage of the maximum signal was plotted over time (A). The percentage of the maximum signal after 2 hours was also plotted (B) alongside the data plotted in figure 5.6 (B). Significance was determined using a Student's t-test where ** indicates that $p < 0.05$ and **** indicates that $p < 0.0005$.

5.3.6 A β ₁₋₄₂ fibrils and oligomers associate with LUVs

Electron microscopy can be used in order to directly determine the association of A β ₁₋₄₂ aggregates with LUVs of different lipid bilayer compositions. Ideally, cryo-electron tomography would be used as this would allow for a 3 dimensional reconstruction of any interactions between aggregates and LUVs. Due to time constraints and limitations due to the equipment available, negative stain TEM was used here which, while not ideal, was sufficient to identify interactions between aggregates and LUVs.

10 μ M A β ₁₋₄₂ was incubated with 50 μ g/ml of GM1/Chol/DOPC LUVs for 3 hours in a glass microplate with no agitation. EM grids were prepared and imaged. Examples taken from different sections of the grid are shown in figure 5.8. Fibrils formed in association with LUVs are clearly present. One commonly observed phenomenon was that some fibrils appeared to connect to LUVs at one end.

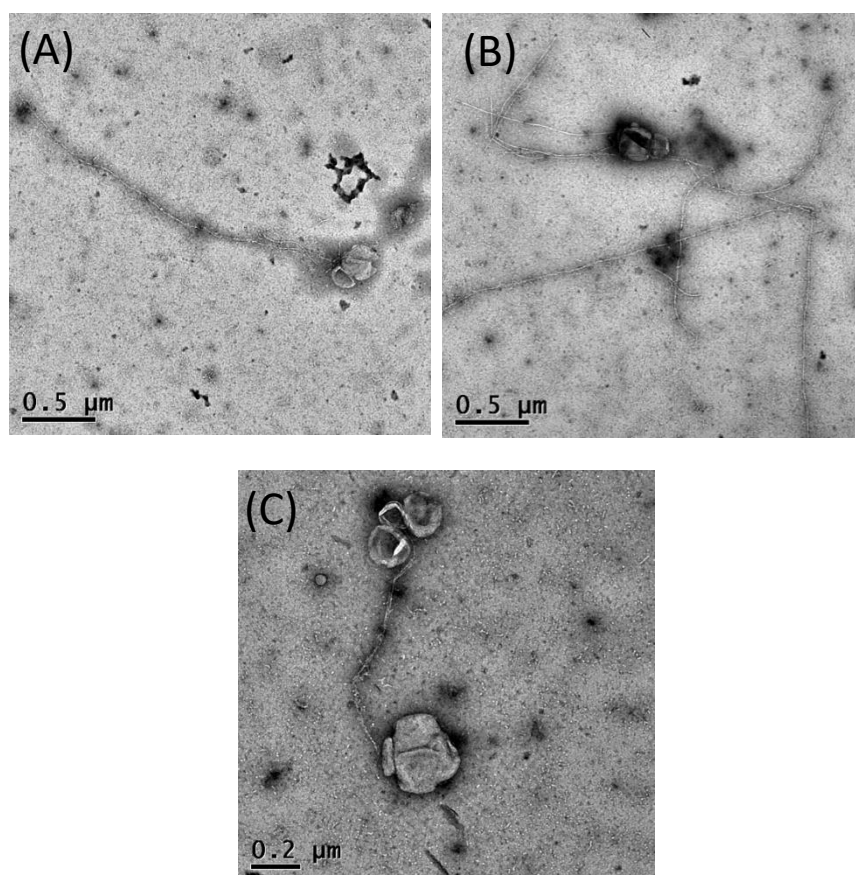


Figure 5.8 TEM reveals that fibrils form in association with LUVs in a glass microplate. 10 μ M A β ₁₋₄₂ was incubated with 50 μ g/ml LUVs for 3 hours at 37 $^{\circ}$ C with no agitation. EM grids were made and imaged at 6600 X (A and B) and 11500 X magnification (C). Fibrils can be seen associated with LUVs. Some of the fibrils appear to end at a LUV.

Furthermore, there is evidence of oligomeric species forming on the surface of LUVs. 11 μM $\text{A}\beta_{1-42}$ was incubated for 24 hours with 50% DOPC and 50% DOPG LUVs. The greater part of the EM grid surface showed the occasional isolated fibril and many isolated LUVs. However, one small section of the grid housed a locally concentrated population of LUVs with a high population of protofibril like aggregates on the surface of the LUVs shown in figure 5.9. This sample was incubated at 37 °C with constant agitation at 300 RPM. The observed oligomeric species could be multiple fibril nuclei that would have otherwise elongated into full length fibrils but didn't due to the constant aggressive agitation. Alternatively, the agitation may have aided the insertion of $\text{A}\beta_{1-42}$ into the bilayer or there is always a small population of oligomeric species formed at the surface of LUVs but due to it being a small population it is unlikely to be observed. The fact that these $\text{A}\beta_{1-42}$ infested LUVs all co-localised suggests a specific behaviour in which the formation of a small amount of these oligomers promotes the formation of more of them. The formation of fibrils would result in the conversion of these species to fibrils. This is because in all other observed conditions, fibrils appear to dominate and that the rarity of these species suggests that their existence is transient.

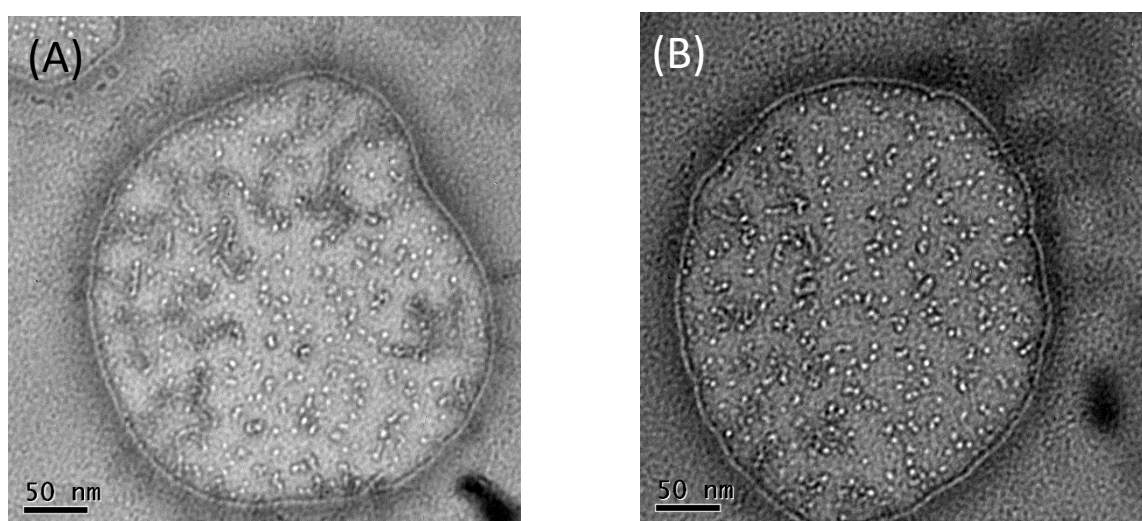


Figure 5.9 Oligomer formation in a small population of LUVs. Oligomeric species of different sizes can be observed in both (A) and (B) where 50% DOPC 50% DOPG LUVs have been incubated with 11 μM $\text{A}\beta$ for 24 hours at 37 °C with constant shaking at 300 rpm. Both (A) and (B) were imaged at 52000 X magnification.

5.3.7 Neither $\text{A}\beta_{1-42}$ nor LUV populations significantly change in response to incubation together

Quantification of how much $\text{A}\beta_{1-42}$ associates with LUVs with different lipid bilayer compositions would provide information about how much of the $\text{A}\beta_{1-42}$ population interacts directly with LUVs. Fractionation of differently sized species followed by characterisation using MALS can allow the

identification of different populations of $A\beta_{1-42}$ aggregates in solution and different populations of LUVs. If some $A\beta_{1-42}$ is bound to the surface of some of the LUVs as seen in figure 5.9 then the distribution of the LUVs population should be split.

The size distribution of a sample of LUVs is shown in chapter 2 (section 2.7). In an attempt to reduce the clustering, a sample of SUVs prepared by extrusion using a 50 nm membrane were injected into the AF4 system. This resulted in a single continuous distribution of SUV populations which could be separated into 2 regions of interest (figure 5.10). The first region contained SUVs that fit to a hollow sphere model and had radii distributed about 35 nm. The second region contained SUVs that fit to a random coil model with radii of gyration distributed between 100 and 300 nm. It was decided that upon the addition of $A\beta_{1-42}$ it would be easier to determine any differences in an apparently single distribution observed across the whole sample using SUVs as opposed to the multiple distributions observed with LUVs.

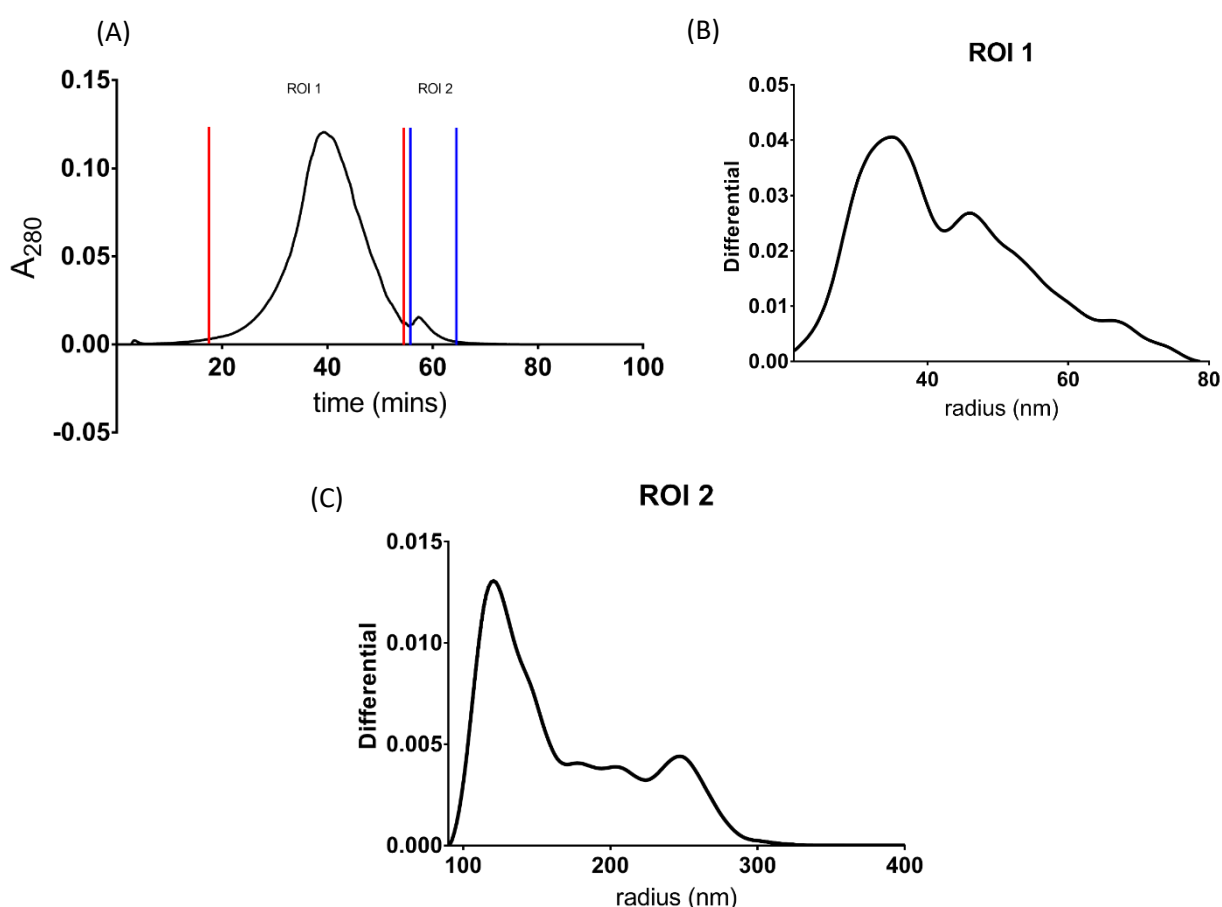


Figure 5.10 SUV distributions contain clumped SUVs. SUVs were injected into the AF4 system. Two regions of interest were identified in the eluogram (A). Region 1 (B) had a corresponding size distribution that matched single vesicles. Region 2 had a corresponding size distribution that matched clumped vesicles similarly to the LUVs discussed in chapter 2 (section 2.7).

22 μM $\text{A}\beta_{1-42}$ was incubated for 3 hours and then injected into the AF4 system. One region of interest was observed when the absorbance at 280 nm was measured over time. A distribution of the sizes of species in this region is shown in figure 5.11. The majority of the sample eluted in this region was of similar size to monomeric or small oligomeric (dimers, trimers etc) $\text{A}\beta_{1-42}$. Small peaks were observed indicating a small population of larger aggregates, possibly including some fibrillar species.

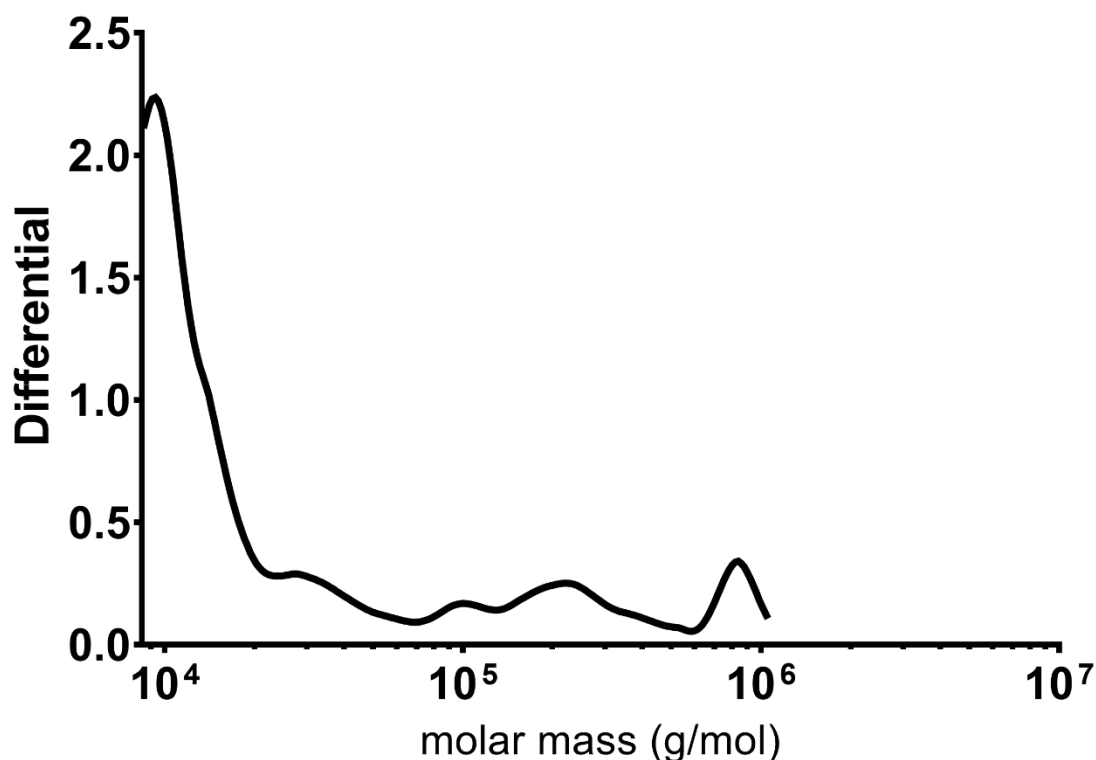


Figure 5.11 A small population of large oligomers and fibrils are detected in an $\text{A}\beta_{1-42}$ sample after 3 hours in glass. 22 μM $\text{A}\beta_{1-42}$ was incubated for 3 hours and then injected into the AF4 system. The $\text{A}\beta_{1-42}$ eluted after 4 minutes. A distribution of the size of the species that eluted was plotted. The largest peak can be observed at roughly 4000 g/mol indicating that most of the sample is monomeric $\text{A}\beta_{1-42}$. The shoulder to the right of this peak indicates the presence of dimer and trimer. Finally, larger aggregates are observed in smaller quantities indicating a small population of larger oligomers or fibrils or both.

22 μM $\text{A}\beta_{1-42}$ was incubated for 3 hours at 37 °C in 50 mM sodium phosphate, 150 mM sodium chloride, pH 7.4 in the presence and absence of both DOPC and GM1/Chol/DOPC SUVs in glass HPLC vials. These samples were injected into the AF4 system. Figure 5.12 shows a time course of the UV signal at 280 nm in which the populations of both $\text{A}\beta_{1-42}$ related species and DOPC SUVs were observed. The $\text{A}\beta_{1-42}$ related species eluted at 4 minutes in both the presence and absence of SUVs. It was not possible to

calculate a size distribution of $A\beta_{1-42}$ in the presence of SUVs as, in the presence of a much larger SUVs peak, in the light scattering data the peak relating to $A\beta_{1-42}$ was difficult to determine. In the eluograms however there is no change in the peak which would indicate a change in size distribution. A slight shift in the peaks relating to the SUVs is observed which could be explained by variation in the amount of sample. When the size distributions of the sample that eluted in these regions were analysed (figures 5.12 (C) and (D)), similar profiles were observed to those in figure 5.10. The same phenomenon was observed when GM1/Chol/DOPC SUVs were used (data not shown). This shows that in the eluted samples, there was only minimal bound $A\beta_{1-42}$ and that the overall populations of $A\beta_{1-42}$ aggregates formed independently of SUVs. It is possible that due to the high concentration focusing step required for AF4, some of the sample may remain bound to the regenerated cellulose membrane rather than eluting.

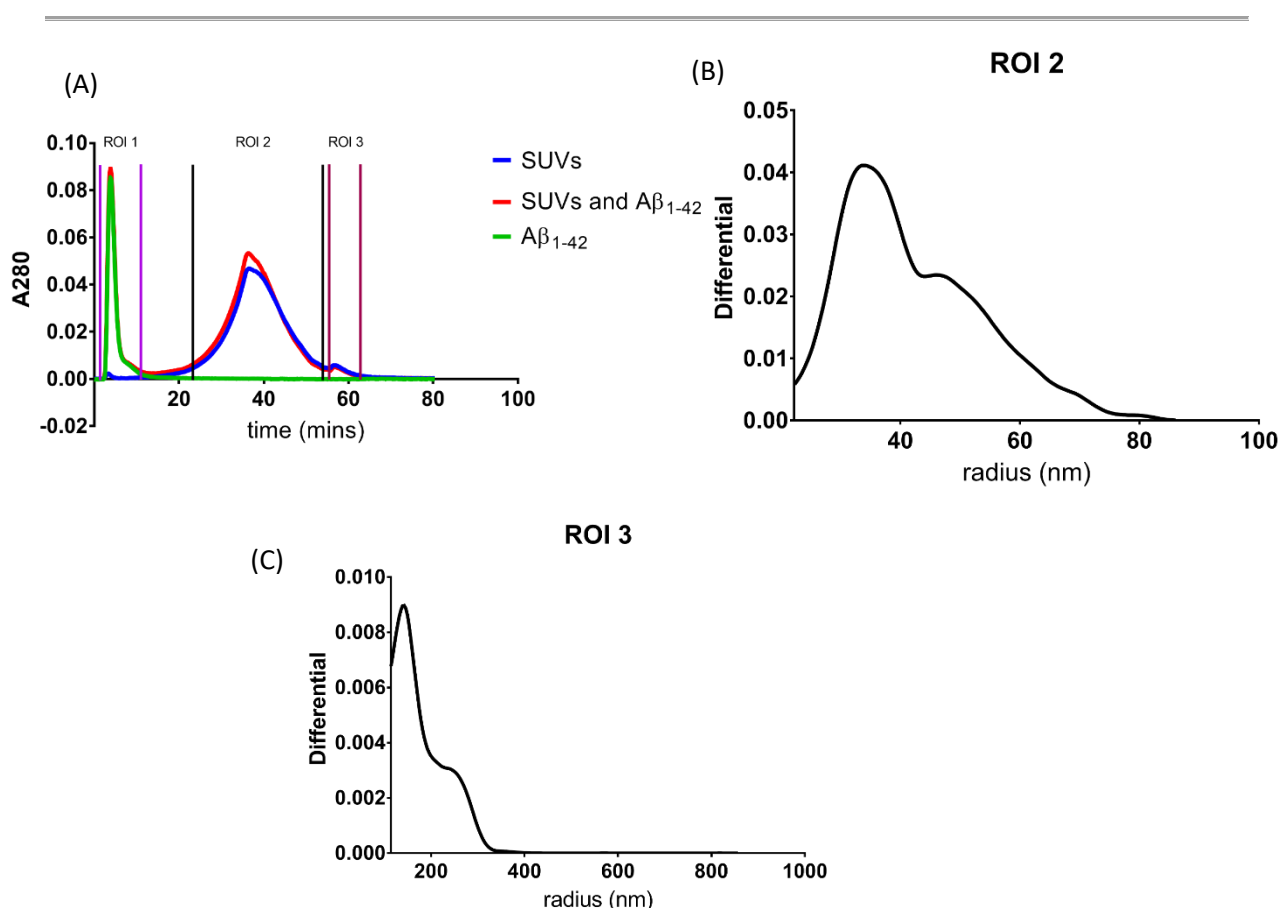


Figure 5.12 The population of SUVs did not change when incubated together with $A\beta_{1-42}$. 22 μ M $A\beta_{1-42}$ was incubated for 3 hours in the presence of DOPC SUVs. The absorbance at 280 nm was recorded and plotted over time (A). The SUVs peaks were observed between 20 and 40 minutes and were largely unchanged in the presence (red) and absence (blue) of $A\beta_{1-42}$. The $A\beta_{1-42}$ peak was observed at 4 minutes and was unchanged in the presence (red) and absence (green) of SUVs. The distributions observed at 2 of the regions of interest (ROIs) are shown. ROI 2 (C) and ROI 3 (D) show the distributions relating to the SUVs and are largely the same as the distributions observed in the absence of $A\beta_{1-42}$ in figure 5.10.

It was observed that not all of the $A\beta_{1-42}$ sample was accounted for in the eluted samples. It was therefore hypothesised that SUVs were fouling the membrane causing a small amount of $A\beta_{1-42}$ to bind. Multiple injections of 50 mM NaOH were made in order to elute the remaining $A\beta_{1-42}$ if it were indeed stuck to the membrane. Figure 5.13 shows the resulting elugrams in which, in the first run, a significant amount of material was observed to elute at both 4 minutes and 60 minutes. The amount of material eluting decreased with each injection suggesting that it was indeed fouling the membrane and not eluting in the previous runs and is also not an artefact of the NaOH or the system in general. This could be evidence therefore that $A\beta_{1-42}$ does bind to lipid bilayers in small amounts however it is impossible to determine whether or not this was an exclusive feature of the DOPC SUVs or the GM1/Chol/DOPC SUVs or whether $A\beta_{1-42}$ might bind to both. This loss of material is not generally observed when $A\beta_{1-42}$ is injected into the AF4 system in the absence of SUVs. However, it is difficult to rule out that the $A\beta_{1-42}$ could be binding to the membrane independently of SUVs.

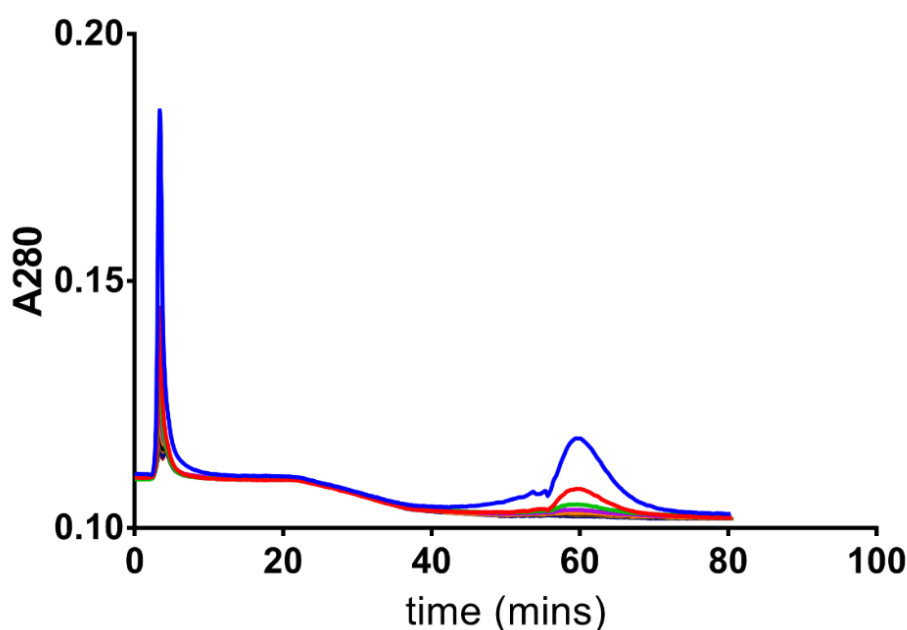


Figure 5.13 Small amounts of $A\beta_{1-42}$ bound to SUVs that fouled the regenerated cellulose membrane. It was hypothesised that SUVs were fouling the membrane rather than eluting and that a small amount of $A\beta_{1-42}$ that was not accounted for in previous experiments was binding to these SUVs. 50 mM NaOH was therefore injected into the AF4 system in 10 separate runs. In the first run (blue) peaks can be observed that correspond to $A\beta_{1-42}$ and SUV populations. The amount of material is reduced in the second run (red) and even more so in the third run (green).

5.4 Discussion

5.4.1 A β_{1-42} fibril formation is promoted by LUVs and salt possibly in a nucleation independent manner

In a seeded reaction, nucleation of fibril formation is expected to impact upon the overall rate and concentration dependence negligibly²³⁹. This is because the reaction should be dependent on the rate of elongation of the already formed seeds. Figure 5.14 shows the effect of adding increasing amounts of seed to monomeric A β_{1-42} . The data shown in figures 5.1 to 5.4 appear to behave similarly to the seeded reactions in figure 5.14.

Despite the likelihood that the reactions in figures 5.1 and 5.2 were seeded the reduction of salt still decreased the rate and concentration dependence of the reaction. The increase in the rate of the overall reaction at the physiological salt concentration suggests that salt induces a nucleation independent mechanism of fibril formation. The increase in concentration dependence suggests that this mechanism is also dependent on monomer concentration and is therefore competing with elongation by monomer addition, a process which is expected to occur in the low salt conditions as well. One potential explanation for this would be elongation by dimers or other small oligomers which form in a salt dependent manner.

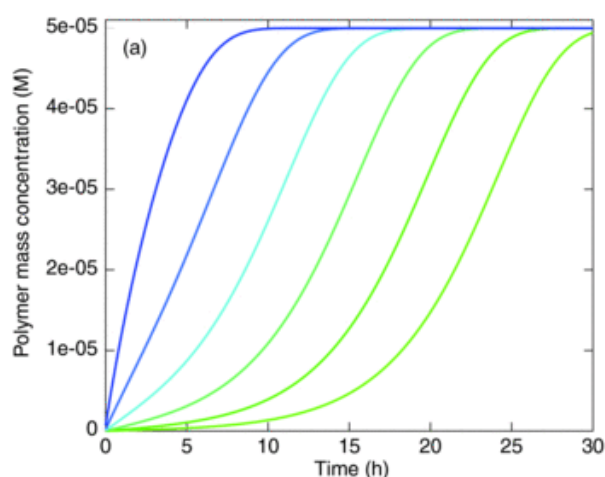


Figure 5.14 Seeded fibril reactions lose their lag phase. Thioflavin T time course data in the presence of increasing amounts of seed taken with permission from Cohen *et al* 2011²³⁹. The light green time course is unseeded and as the reaction becomes more seeded (green to blue) the lag phase is reduced until, in the dark blue reaction it is completely removed.

The addition of LUVs once again increased the rate of fibril formation (figure 5.2) but in the presence and absence of salt, the concentration dependence is unchanged. This suggests that fibril formation can be promoted by LUVs in a manner that is independent of nucleation *and* independent of the mechanism by which salt promotes fibril formation.

The addition of a range of concentrations of LUVs suggests that this mechanism can be saturated when the concentration of A β ₁₋₄₂ is higher than the concentration of catalytic sites available on LUVs. This is shown in figure 5.4 by the concentration independence at 5 μ g/ml of LUVs. At high concentrations of LUVs however, fibril formation also becomes concentration independent. Therefore, the mechanism by which the LUVs are promoting fibril formation could include a step that is LUV independent and also concentration independent. This process could become rate determining once all other mechanisms of the promotion of fibril formation by LUVs, which occur in a monomer dependent fashion, have become maximal. One such monomer concentration independent process could be the formation of oligomers at the air water interface, where they are more easily converted to fibrils. This would therefore increase the rate of fibril formation without affecting the overall concentration dependence. The air water interface would be saturable and therefore this process could be concentration independent. In the cases where the reaction is concentration dependent then this process would not be rate determining as the rate of conversion of species to fibrils by LUVs in a monomer dependent fashion is not maximal. Due to the likely seeding of the discussed reactions, it is difficult to make conclusive insights into the actual mechanisms that result in these behaviours.

5.4.2 A β ₁₋₄₂ induced permeation of lipid bilayers is promoted independently of fibril formation by cholesterol and GM1

Previous work has shown that under certain conditions, GM1 and cholesterol containing lipid bilayers can produce toxic A β fibrils¹²⁹. Specific importance has often been placed on cholesterol and GM1^{44,124,125,129,132,133,163,167,170}. Figure 5.5 however, reveals that in a glass microplate the incorporation of GM1 and cholesterol into a DOPC lipid bilayer does not promote the formation of fibrils any more than DOPC only lipid bilayers (although these reactions are likely seeded).

GM1 and cholesterol containing lipid bilayers did however, promote a distinct A β ₁₋₄₂ induced permeation of LUVs in a quartz glass cuvette compared with DOPC only LUVs (figure 5.7) and as reported previously¹⁷⁰. This suggests that in these conditions the permeation of lipid bilayers by A β ₁₋₄₂ is independent of the formation of fibrils. This could be in part an explanation as to why some drugs that target amyloid formation appear to work in *in vitro* assays and even in *in vivo* models but don't work in humans⁴. Fibrils have been shown to not contribute directly to toxicity²¹, however it has been hypothesised that the fibril formation process could contribute to toxicity either directly⁷³ or by the

production of on-pathway oligomers¹³⁶. In these cases, disrupting amyloid formation at the right step would result in a reduction in A β induced toxicity. However, if fibril formation and A β induced toxicity are independent in some conditions as observed for membrane permeation here, then targeting fibril formation would not result in a reduction in A β induced toxicity.

5.4.3 A β ₁₋₄₂ does not remain bound to the bulk of lipid bilayers in solution yet is capable of inducing permeation in lipid bilayers

A lot of previous studies have shown that A β can interact with lipid bilayers^{53,54,70,174}. A quantification of how much A β ₁₋₄₂ was bound to lipid bilayers in the form of SUVs revealed that little A β ₁₋₄₂ remained bound to the lipid bilayers in a detectable manner (figure 5.12). Figure 5.7 shows that A β ₁₋₄₂ induced permeation of lipid bilayers in this time frame was high. In fact, the majority of dye leakage observed occurred within the first 3 hours which was the time that the A β ₁₋₄₂ and the SUVs were incubated for before injection into the AF4 system. The interaction between A β ₁₋₄₂ must therefore be short lived enough for the bulk of A β ₁₋₄₂ observed in solution to remain unaffected. Also, the population of SUVs must be largely unaffected by the introduction of A β ₁₋₄₂ other than to become more permeable. The size and overall shape of the SUVs must be independent of an increase in permeability. Therefore, an increase in permeability in lipid bilayers could be due to a short lived interaction with A β ₁₋₄₂. Figure 5.9 shows TEM images of oligomeric A β ₁₋₄₂ species embedded into LUVs. If this interaction were short lived, which would explain why these A β ₁₋₄₂ infested LUVs were only found on a small portion of the grid, then this could be a mechanism by which A β ₁₋₄₂ induces increased lipid bilayer permeation. The clustering of LUVs and SUVs identified by AF4 and EM may also explain why dye release upon addition of A β ₁₋₄₂ (and also by polymixin B in chapter 3 section 3.3.1) does not reach 100% as the LUVs in the clusters may be protected.

Chapter 6: The surface dependence of hCC activity as an inhibitor of normal A β behaviour

6.1 Introduction

Human Cystatin C (hCC) is a cysteine protease inhibitor that has been linked with AD¹⁴⁹⁻¹⁵¹. Studies have shown that a polymorphism in the cystatin C gene is a risk factor¹⁴⁹ although there are conflicting reports about whether hCC contributes to AD symptoms¹⁵¹ or plays a more protective role¹⁴⁸. Convincing evidence has shown that hCC can modulate normal A β behaviour^{147,148,154,157} which is often considered to be one of the primary sources of AD symptom progression²¹. How hCC interacts with A β species has yet to be identified and conflicting reports have been presented^{154,159,160,162}.

HCC has been shown to inhibit A β fibril formation in a concentration dependent manner^{159,162}. It has also been shown to bind tightly, with nanomolar binding constants, to monomeric A β_{1-42} ¹⁵⁴. It was hypothesised that this tight binding interaction may result in an inability of A β to aggregate. However, in different conditions, such as in a glass test tube designed for NMR, strong binding was not observed¹⁵⁹.

The fibril formation activity of A β_{1-42} in the presence of different surfaces was discussed in chapter 3 (section 3.3.3). It was shown that in the presence of a glass surface, fibril formation was significantly slower than in a polystyrene microplate where fibril formation was catalysed. Furthermore, in chapter 3 (section 3.3.6), when A β_{1-42} was incubated on a quartz glass microplate no interaction with the surface was observed.

Contrastingly, A β_{1-42} was shown in chapter 3 (section 3.3.5) to form a film on polystyrene surfaces. So far, the inhibition of fibril formation by hCC monomers and the tight binding of hCC to A β_{1-42} have only been presented in conditions where polystyrene surfaces have been used^{154,159,160}. The loss of the inhibition of A β_{1-42} fibril formation by hCC in polystyrene microplates has also been presented when the microplates were agitated¹⁶². This suggests that there may be an interaction between the film formed on polystyrene and hCC.

HCC has also been shown to reduce A β related toxicity in AD models¹⁵³. This could be as a result of the impact that hCC has on APP processing²⁴⁰. Arguably however, the ability of hCC to directly bind A β in some conditions suggests that it may directly inhibit A β related toxicity.

In order to determine the true extent to which hCC can inhibit fibril formation, a comparison of inhibition in the presence of a range of surfaces must be examined. In this chapter, it will be shown

that at low stoichiometries of [hCC]:[A β ₁₋₄₂], the inhibition of fibril formation is ineffective in low-binding microplates. Furthermore, it will be shown by using glass and polystyrene surfaces that fibril formation can be inhibited by hCC.

Since it has been shown in chapter 3 (section 3.3.5) that A β ₁₋₄₂ forms a film on polystyrene surfaces, the interaction between hCC and these films was investigated by AFM. This interaction could inform why hCC can inhibit fibril formation and presents with tight binding in a polystyrene microplate but not in other conditions.

Finally, the interaction between hCC, A β and lipid bilayer surfaces was investigated. It will be shown that LUVs can impact on the inhibition of A β ₁₋₄₂ fibril formation by hCC in a way which is dependent on whether or not the A β ₁₋₄₂ can first interact with the lipid bilayer surface or a polystyrene surface. The ability of hCC to inhibit A β induced lipid bilayer permeation in the presence and absence of cholesterol and GM1 will also be presented.

6.2 Methods

6.2.1 Thioflavin T assays

11 μ M of A β ₁₋₄₂ was incubated in a polystyrene microplate (Corning 3694) in the presence of 40 μ g/ml of DOPC LUVs and hCC at stoichiometries of [hCC]:[A β ₁₋₄₂] at 0.1:1, 0.25:1, 0.5:1 and 1:1 and also in the absence of any hCC.

4 μ M of A β ₁₋₄₂ was incubated in a polystyrene microplate in the presence of hCC at stoichiometries of [hCC]:[A β ₁₋₄₂] at 0.1:1, 0.25:1, 0.5:1, 1:1 and 1.25:1 and also in the absence of any hCC in polystyrene and low-binding microplates (Corning 3694 and 3686). Stoichiometries of 0.5:1, 0.75:1, 1:1, 1.5:1 and 2:1 were used in glass microplates (WebSeal plate+, ThermoScientific) with and without LUVs. Multiple different batches of A β ₁₋₄₂ were used on all surfaces.

Both experiments used a 50 mM sodium phosphate buffer with 150 mM sodium chloride and 10 μ M thioflavin T. Fluorescence measurements were taken every 5 minutes for 8 hours as per chapter 2 (section 2.9).

6.2.2 AFM

11 μ M of A β ₁₋₄₂ was incubated with 11 μ M of hCC on a polystyrene coated silicon substrate formed as described in chapter 3 (section 3.2.4). A 50 mM sodium phosphate buffer with 150 mM sodium chloride was used. A 20 μ m by 20 μ m area was imaged at room temperature by an MFP-3D AFM continuously with each image being acquired every 4 minutes and 15 seconds.

6.2.3 Dye release assays

In separate quartz glass cuvettes 2 μM $\text{A}\beta_{1-42}$ was incubated with 50 $\mu\text{g}/\text{ml}$ of 100% DOPC LUVs and 2% GM1, 33% cholesterol, 65% DOPC LUVs each containing 50 mM carboxyfluorescein. A 50 mM sodium phosphate buffer with 150 mM sodium chloride was used. Fluorescence readings were taken at 37 °C every 15 minutes as described in chapter 2 (section 2.10).

6.3 Results

6.3.1 The inhibition of fibril formation can be dependent on the order in which it interacts with $\text{A}\beta_{1-42}$ and lipid bilayers in the presence of polystyrene.

The ability of hCC to seemingly bind $\text{A}\beta_{1-42}$ in some conditions but not others^{154,159,160} combined with the ability of hCC to modulate $\text{A}\beta$ related toxicity *in vivo*¹⁵³ led to the hypothesis that hCC binding to $\text{A}\beta_{1-42}$ might be affected by the presence of a lipid bilayer. In order to test this, hCC and $\text{A}\beta_{1-42}$ were incubated together in the presence of DOPC LUVs. These experiments were carried out in a polystyrene microplate in order for the data to be directly comparable to a previous study¹⁵⁹.

$\text{A}\beta_{1-42}$ was mixed with hCC in a 1.5 ml polypropylene tube, followed by the addition of LUVs. The sample was then dispensed into a polystyrene microplate. Inhibition was observed as normal as can be seen in figure 6.1(A), but with the addition of catalysis by LUVs. This shows that hCC and $\text{A}\beta_{1-42}$ were interacting independently of the LUVs in this case.

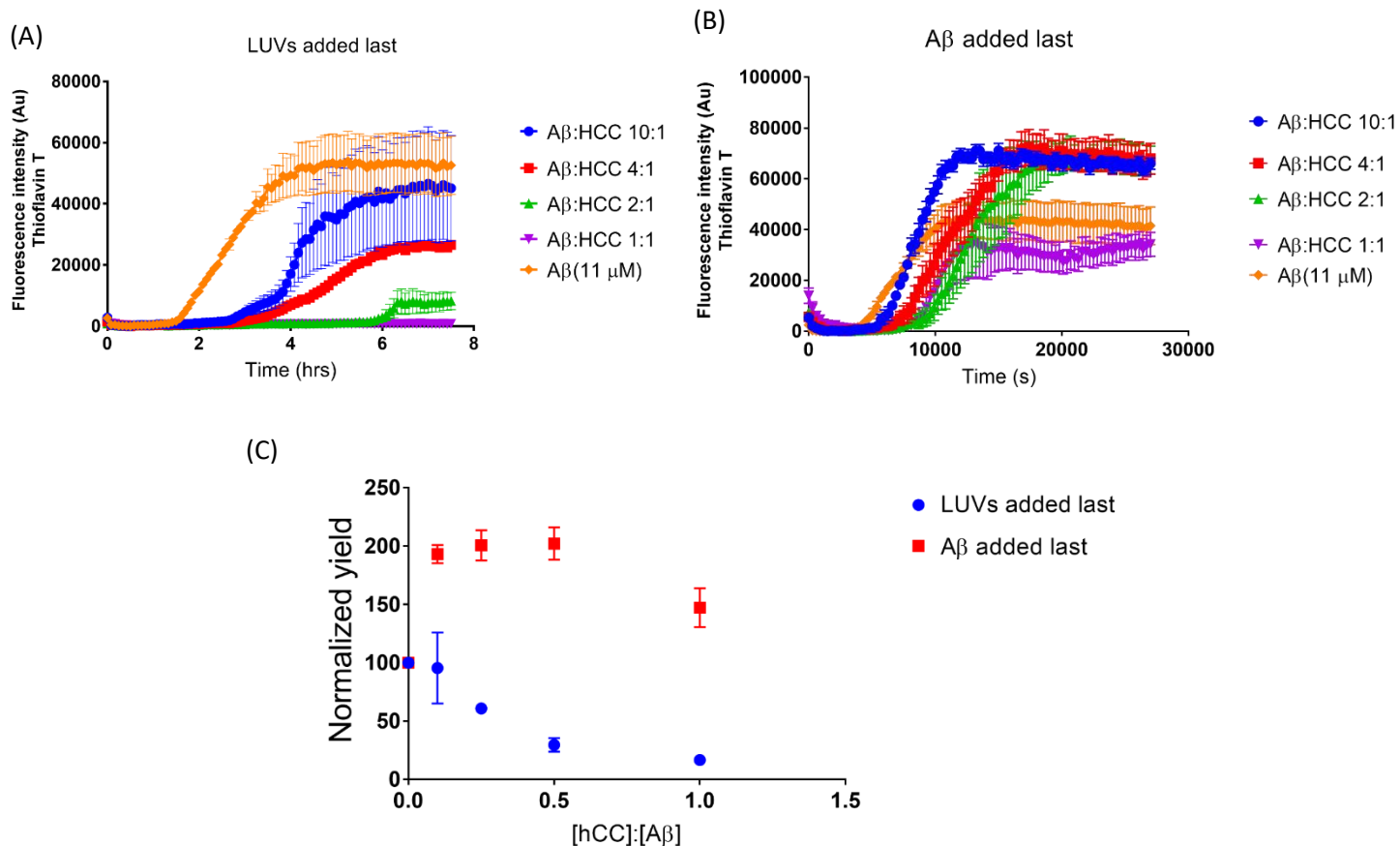


Figure 6.1 Fibril formation is inhibited in a manner which is dependent on the accessibility of a lipid bilayer to $A\beta_{1-42}$. $A\beta_{1-42}$ was incubated with increasing concentrations of hCC and 40 $\mu\text{g}/\text{ml}$ of DOPC LUVs. When LUVs were added last (A) concentration dependent (with respect to hCC) inhibition of fibril formation was observed using thioflavin T. When the $A\beta$ was added last however (B), fibril formation was not inhibited by hCC. The yields from each reaction were normalised by dividing the maximum fluorescence signal of each run by the average maximum yield in the absence of hCC in each condition (C). These data show a direct comparison between when the LUVs were added last (blue) where fibril formation is inhibited with increasing concentrations of hCC and when $A\beta_{1-42}$ was added last (red) where fibril formation is not inhibited. Error bars represent the standard error about the mean from 2 repeats of 5 replicates per reaction.

HCC and LUVs were then mixed in a 1.5ml polypropylene tube. $A\beta_{1-42}$ was then added, and the sample was divided into a polystyrene microplate. In this case, as shown in figure 6.1(B), inhibition of fibril formation was not observed. A comparison of the fibril yields observed after 8 hours in the presence of increasing hCC concentrations in the two experiments can be seen in figure 6.1 (C). In a previous study it was concluded that hCC was binding to an oligomeric species and reduced the pool of “on-pathway” aggregates in order to reduce the total amount of fibrils¹⁵⁹. These data suggest that the species that is bound by hCC are not present when $A\beta_{1-42}$ fibril formation is catalysed by LUVs but form

rapidly in the absence of LUVs. Alternatively, when the $A\beta_{1-42}$ is bound to the LUVs, it becomes inaccessible to hCC.

In the conditions where LUVs are added last, the observed inhibition by hCC not only impacts the yield but also the rate of fibrillisation. This is contrary to previous studies^{159,162} where the rate of fibrillisation is not affected by hCC. This suggests that in the presence of LUVs, the inhibition of fibril formation is distinct from that in polystyrene microplates alone.

6.3.2 HCC cannot inhibit fibril formation in a low-binding microplate

It has been shown in chapter 3 (section 3.3.3) that $A\beta_{1-42}$ fibril formation is surface dependent. It was subsequently hypothesised that different surfaces would impact on the ability of hCC to inhibit fibril formation by $A\beta_{1-42}$. In order to test how surfaces impact on the inhibition of $A\beta_{1-42}$ fibril formation by hCC, thioflavin T assays were performed in three different microplates.

In chapter 5, it was shown that different batches of $A\beta_{1-42}$ were seeded to different amounts. Therefore, for these experiments, multiple batches were compared against all conditions in order to determine whether the differences observed were due to batch variation in $A\beta_{1-42}$ or the differences in surface conditions. Independent of the batch of $A\beta_{1-42}$ used, the following phenomena were observed.

In glass microplates, fibril formation is observed to be slower than in polystyrene and low-binding microplates as shown in chapter 3 (section 3.3.3). In order to determine whether this would facilitate or prevent the inhibition of $A\beta_{1-42}$ fibril formation by hCC, a thioflavin T assay was performed in which $A\beta_{1-42}$ was incubated with increasing concentrations of hCC. The data are presented in figure 6.2 (A) which shows that, as the concentration of hCC increases, fibril formation is inhibited. Two effects were observed; the rate of fibril formation was slower, and the final yield was reduced as the concentration of hCC was increased. This shows that fibril formation is inhibited by hCC in glass microplates. The inhibition of fibril formation by hCC on polystyrene microplates was repeated here and is shown in figure 6.2 (B) where hCC and $A\beta_{1-42}$ were incubated together in a polystyrene microplate. As reported in previous studies, the rate of fibril formation was independent of hCC regardless of whether or not the final yield was affected^{159,162}.

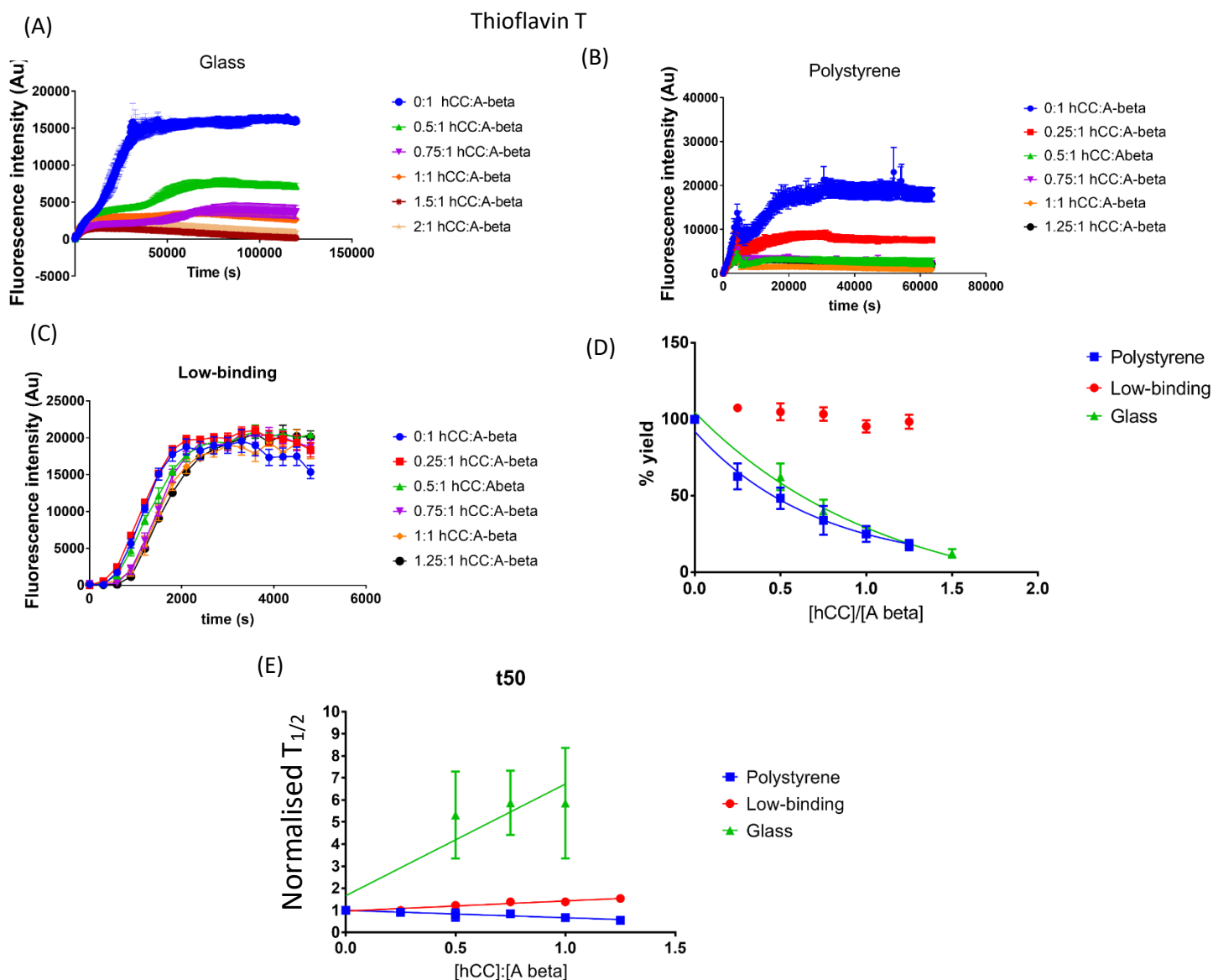


Figure 6.2 HCC cannot inhibit fibril formation by $A\beta_{1-42}$ in low-binding microplates. $A\beta_{1-42}$ was incubated with increasing concentrations of hCC in 3 different microplate conditions. In glass (A) and polystyrene (B) lower fibril yields were observed as hCC concentrations were increased. Furthermore, in glass (A) as hCC concentrations were increased the rate of fibril formation was reduced. In low-binding microplates (C) however, fibril formation is comparably unaffected by increasing hCC concentrations. The yields from each reaction were normalised by dividing the maximum fluorescence signal of each run by the average maximum yield in the absence of hCC in each condition (D). The yield in polystyrene (blue) and glass (green) was greatly reduced as the concentration of hCC was increased whereas in the low-binding surface (red) the yield was only minimally reduced. The t_{50} of each reaction was calculated and was normalised in the same manner as the yields. These data are plotted in (E) which shows that the rate of fibril formation is largely unaffected by hCC in polystyrene, slowly increases in low-binding microplates and is drastically slower in glass. Error bars in (D) and (E) represent the standard error for 3 repeats of 4 replicates per reaction in polystyrene and low binding and 2 repeats of 3 replicates per reaction in glass.

In chapter 3 (section 3.3.3), it was shown that low binding microplates catalyse $A\beta_{1-42}$ fibril formation. Increasing concentrations of hCC were incubated with $A\beta_{1-42}$ in a low-binding microplate in order to determine whether or not the inhibitory activity of hCC was affected. Figure 6.2 (C) shows that fibril formation is largely unaffected by increasing concentrations of hCC. At high stoichiometries of $[hCC]:[A\beta_{1-42}]$, the rate of fibril formation is slightly reduced. This shows that at these concentrations hCC is incapable of preventing fibril formation in low-binding microplates.

When compared to the normalised yields in polystyrene and glass microplates in figure 6.2(D), the yields in the low-binding microplates appear to be largely unaffected. This suggests that of the three surfaces tested, the low binding microplate is the only surface in which the amount of fibril formation is unaffected by hCC.

Figure 6.2 (E) however shows the half times of the reactions as the concentration of hCC increases relative to the half times of the reactions in the absence of hCC. Here, a value of 1 indicates that the half time of the reaction was the same as the half time of the reaction in the absence of hCC and a value of 2 indicates that the half time of the reaction was twice that of the half time in the absence of hCC and the reaction was therefore 2 times slower. In low-binding microplates, the half time for the reaction slowly increased as hCC was added with the reaction at $[hCC]:[A\beta_{1-42}]$ up to 1.5 times slower than in the absence of hCC. In glass, the introduction of hCC resulted in a drastic increase in half times. The reaction was on average between 5 and 6 times slower in the presence of half as much hCC as $A\beta_{1-42}$. In polystyrene however, the rate of fibril formation was largely unaffected by hCC.

6.3.3 LUVs do not impact upon hCC inhibition of fibril formation in glass

Since $A\beta_{1-42}$ fibril formation in glass is significantly different to that in polystyrene it was hypothesised that the inhibition by hCC might be different in the presence of these two surfaces. Figure 6.2 (D) shows that hCC inhibits fibril formation to a similar extent in glass and polystyrene however the mechanism may be different as figure 6.2 (E) shows that the rate of fibril formation is slower in the inhibited reactions in glass but not in polystyrene. As the mechanism of fibril formation and its inhibition are different in glass and polystyrene it was hypothesised that the interaction between hCC, $A\beta_{1-42}$ and LUVs would also be different in glass and polystyrene.

4 μ M $A\beta_{1-42}$ was therefore incubated with increasing concentrations of hCC in glass coated microplates with 50 μ g/ml of DOPC and 2% GM1, 33% cholesterol, 65% DOPC LUVs. Figure 6.3 (A) shows the time course of fibril formation for each reaction in the presence of DOPC LUVs and figure 6.3 (B) shows the same in the presence of the GM1/Chol/DOPC LUVs. In both cases, $A\beta_{1-42}$ was added last as this mimicked the conditions where inhibition was not observed in the polystyrene microplates. Inhibition

similar to that in the absence of LUVs was observed. When the normalised yields were plotted against the ratio of $[hCC]:[A\beta_{1-42}]$, (figure 6.3 (C)), the observed inhibition of fibril formation was similar in the presence and absence of DOPC and GM1/Chol/DOPC LUVs.

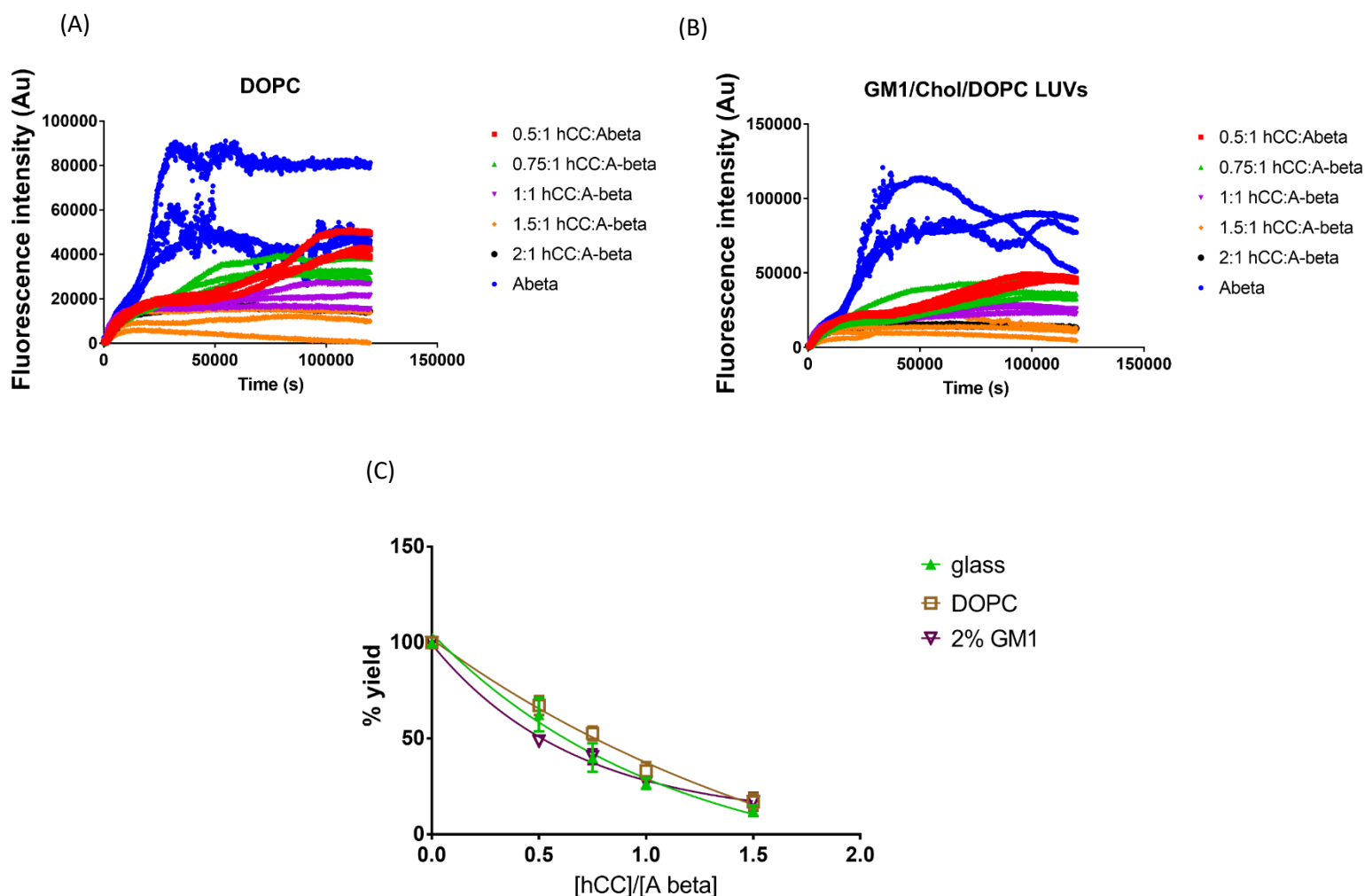


Figure 6.3 HCC inhibits fibril formation in glass independently of LUVs. $A\beta_{1-42}$ was incubated with increasing concentrations of hCC in the presence of DOPC and GM1/Chol/DOPC LUVs in glass coated microplates. Time courses of the reactions are shown in (A) (DOPC) and (B) (GM1/Chol/DOPC). The yields were normalised by taking an average of the fibril yields in the absence of hCC and calculating the percentage of this value for each of the yields in the presence of hCC (C). The error bars for the reactions with LUVs represent the standard error about the mean from 3 replicates per reaction.

6.3.4 HCC might stabilise the formation of films of A β ₁₋₄₂ on polystyrene

In chapter 3 (section 3.3.5), it was shown that A β ₁₋₄₂ forms a film on a polystyrene surface. It has also been reported previously that hCC binds strongly to A β ₁₋₄₂ after the A β ₁₋₄₂ had been incubated on a polystyrene surface for 16 hours¹⁵⁴. This tight binding has not been observed in other conditions¹⁵⁹. Therefore, it was hypothesised that hCC binds to the film of A β ₁₋₄₂ that is deposited when A β ₁₋₄₂ is incubated on polystyrene.

To investigate whether or not hCC binds to the film of A β ₁₋₄₂ on polystyrene, both hCC and A β ₁₋₄₂ were incubated at 11 μ M on a polystyrene surface that had been spin coated onto a silicon substrate. Figure 6.4(A) shows images of the film of A β ₁₋₄₂ that formed on the surface at progressing timepoints. Figure 6.4(B) shows a time course of surface roughness showing the height of the A β ₁₋₄₂ film in the presence and absence of hCC.

In the presence of hCC, an increase in the deposition of the film of A β ₁₋₄₂ was observed. The rate of film deposition was also increased in the presence of hCC. This suggests that hCC interacts with the film of A β ₁₋₄₂ potentially by binding to A β ₁₋₄₂ that is either incorporated into the film or is forming specific aggregates at the film. Either way this shows a potential mechanism by which hCC can be inhibiting fibril formation in polystyrene as it may be able to divert A β ₁₋₄₂ species towards a non-fibrillar species that is ultimately not present on the surface. However, this could be an anomalous result. This experiment would need to be repeated in order for that to be determined which due to time restrictions is outside the scope of this study at the time of writing.

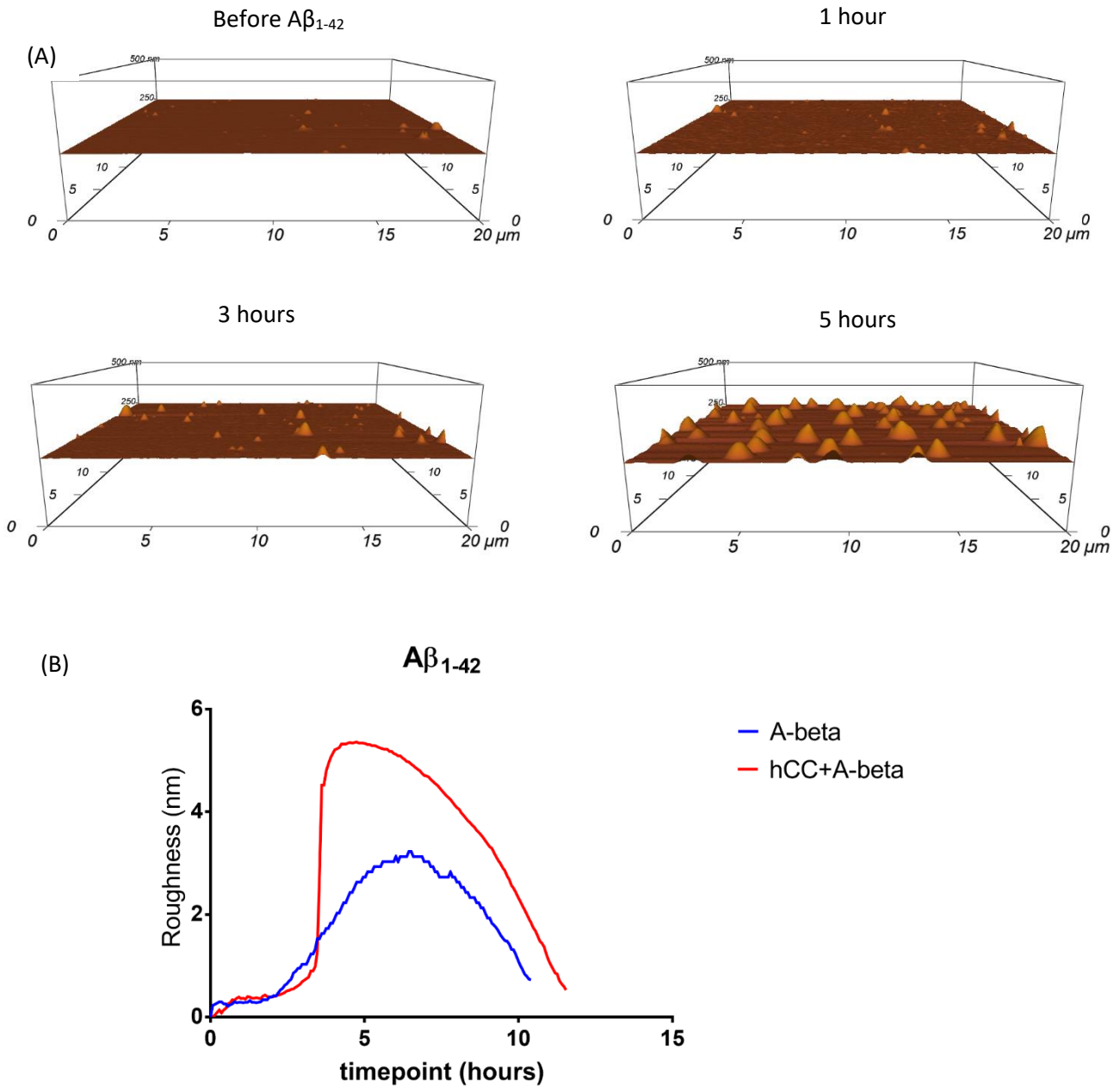


Figure 6.4 $A\beta_{1-42}$ film deposition and hCC. $A\beta_{1-42}$ and hCC were incubated on a polystyrene surface, the same 20 μm by 20 μm section of which which was then imaged by AFM every 4 minutes and 15 seconds. A selection of images at different timepoints (A) show the deposition of a film of $A\beta_{1-42}$. By taking a measurement of the surface roughness at each timepoint the average height of the film across the surface can be plotted as a function of time (B). When compared to the experiment in the absence of hCC, an increase in film deposition can be observed.

When compared to the data presented in chapter 3 (section 3.3.7), the morphology of the films formed were distinctly different here. This could be due to defects in the polystyrene surface. As the two polystyrene surfaces compared in figure 6.4 were made at the same time and the morphology of

the films observed was similar on those surfaces, these results were compared directly between each other but not to the result in chapter 3 (section 3.3.7).

6.3.5 HCC can inhibit the A β ₁₋₄₂ induced permeation of lipid bilayers.

It was hypothesised that since hCC can prevent A β induced toxicity in neuronal cells¹⁵³, it could also prevent A β ₁₋₄₂ induced permeation of lipid bilayers. Therefore, hCC was incubated with A β ₁₋₄₂ in the presence of both 100% DOPC and GM1/Chol/DOPC LUVs containing 50 mM carboxyfluorescein. Dye release was measured every 15 minutes for 16 hours. Figure 6.5 shows that hCC can prevent A β ₁₋₄₂ dye release from DOPC LUVs and that hCC can inhibit A β ₁₋₄₂ induced dye release from GM1 and cholesterol containing LUVs. Therefore, hCC can inhibit A β ₁₋₄₂ induced permeation of lipid bilayers indicating that this could be a mechanism by which hCC modulates A β ₁₋₄₂ toxicity *in vivo*.

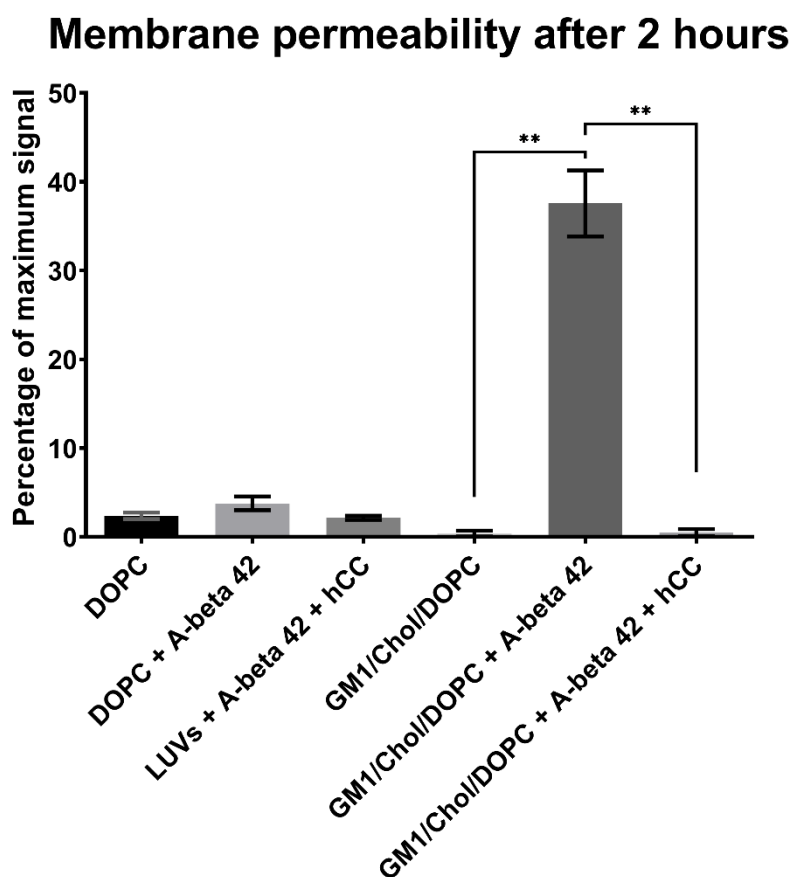


Figure 6.5 HCC can inhibit A β ₁₋₄₂ induced permeation of lipid bilayers. LUVs made with 100% DOPC and GM1/Chol/DOPC containing 50 mM carboxyfluorescein were incubated with 2 μ M hCC and 2 μ M A β ₁₋₄₂. In both cases after 2 hours in the presence of hCC, A β ₁₋₄₂ was inhibited from causing a significant increase in dye release although the DOPC LUVs did not significantly leak in the presence of A β ₁₋₄₂ in the presence or absence of hCC. Significance was determined using a Student's t-test where ** indicates that $p < 0.05$.

6.4 Discussion

6.4.1 HCC inhibits fibril formation by interactions with short lived oligomers of A β ₁₋₄₂

The ability of hCC to inhibit fibril formation has been displayed both here in figure 6.1 and figure 6.2 and in previous studies^{159,160,162}. One study concluded that hCC must be interacting with oligomeric A β ₁₋₄₂ when it inhibits fibril formation, in part due to an inability to observe hCC binding to A β ₁₋₄₂ monomers in solution by NMR¹⁵⁹. Figure 6.2 shows that in conditions where fibril formation is catalysed by low-binding microplates, hCC loses its ability to inhibit fibril formation. If hCC interacts with oligomeric species of A β ₁₋₄₂, then it could be suggested that in the presence of a low-binding surface these oligomers are either too short lived to be accessible to hCC or fibril formation is so rapid that these types of oligomers never form. In slower fibrillisation conditions such as glass, fibril formation is again inhibited by hCC suggesting that in these conditions the appropriate oligomers have time to form. In polystyrene, fibril formation is inhibited similarly to in glass suggesting that the same amount of A β ₁₋₄₂ material that binds hCC is formed. Kinetic analysis of the data in figure 6.2 shows that the rate of fibril formation is slower when concentrations of hCC are increased in glass which is not true in polystyrene. Reducing the pool of monomers for fibril formation in either case should result in relatively concentration independent rates of fibril formation as shown in chapter 3 (section 3.3.3).

An alternative mechanism by which hCC may be inhibiting the process is by binding to specific oligomers that are populated at a hydrophobic surface: fibrillisation on glass and polystyrene both depend on the presence of a hydrophobic surface, respectively the air water interface and the polystyrene surface.

6.4.2 HCC inhibits fibril formation in polystyrene by interacting with A β ₁₋₄₂ that deposits as a film.

A β ₁₋₄₂ fibril formation is concentration independent in polystyrene as it relies first on the deposition of a film of A β ₁₋₄₂ onto the surface discussed in chapter 3 (section 3.4.3). HCC inhibits fibril formation differently on polystyrene than on other surfaces as shown in figure 6.2. Figure 6.1 shows that when LUVs are incubated with A β ₁₋₄₂, the ability of hCC to inhibit fibril formation is diminished in polystyrene suggesting that oligomeric species that form in polystyrene, as a result of film deposition, don't form at the surface of DOPC LUVs. Furthermore, fibril formation is not inhibited by hCC when the microplates are agitated¹⁶² suggesting that hCC binds to the film which is disrupted by agitation. Alternately hCC could be binding to fibril ends which is an ineffective method of inhibition when the sample is agitated due to the observed increase in fragmentation creating new fibril ends²⁴¹. This is however a kinetic effect which wouldn't affect final yields. Figure 6.3 shows that hCC may interact with the film of A β ₁₋₄₂. If hCC was binding to the film the dissipation of the film would be expected to

be slower in the presence of hCC, but this is not observed. Therefore, it is more likely that hCC binds to a population of $A\beta_{1-42}$ on the film in a manner that promotes the eventual formation of non-fibrillar aggregates not observed on the film.

6.4.3 HCC modulates $A\beta_{1-42}$ by preventing the formation of lipid membrane permeating oligomers.

Figure 6.4 shows that hCC can inhibit $A\beta_{1-42}$ induced permeation of lipid bilayers. If hCC is interacting with an oligomeric species of $A\beta_{1-42}$ in such a manner as to not produce fibrils, it is also preventing them from forming other oligomeric species that result in the permeation of lipid bilayers. This activity could be a method by which hCC modulates $A\beta$ toxicity *in vivo* and may in part explain why it is upregulated in AD.

However, in a polystyrene microplate hCC was not effective at preventing fibril formation in the presence of LUVs. This could be due to hCC binding to the polystyrene surface prior to binding to $A\beta_{1-42}$ resulting in less interactions with $A\beta_{1-42}$ in the presence of LUVs. Alternatively, as $A\beta_{1-42}$ fibril formation is catalysed by LUVs in the presence of a polystyrene surfaces as shown in chapter 3 (section 3.3.7), $A\beta_{1-42}$ might form fibrils too quickly in these conditions for the species that binds hCC to form. This suggests that fibril formation is inhibited by hCC in a manner that is independent of the inhibition of $A\beta_{1-42}$ induced lipid bilayer permeation because DOPC LUVs were used in both sets of experiments. This separation between a pathway to membrane damage and one for fibrillisation was observed earlier in chapter 3 (section 3.4.2).

Chapter 7: The ionic strength dependency of amyloid fibril formation

7.1 Introduction

Amyloid fibril formation by $A\beta_{1-42}$ is one of the underlying mechanisms that occurs in patients with Alzheimer's disease²⁴²⁻²⁴⁴. A lot of research into the mechanisms by which $A\beta_{1-42}$ forms amyloid fibrils has revealed the existence of a plethora of prefibrillar aggregates that can be formed *in vitro*²⁴⁵⁻²⁴⁷. Many of these prefibrillar aggregates have been associated in some way or another with toxicity *in vivo*^{135,247,248}. There has also been research into the internal structure of $A\beta_{1-42}$ amyloid fibrils revealing again a range of structures and morphologies^{30,249}.

The polymorphism exhibited by amyloid fibrils is of interest when considering the differences in conditions between *in vitro* and *in vivo*. Differences in morphologies that can occur include twists along the longitudinal axis producing varied cross-over distances, different numbers of protofilaments making up the fibril and the length and width of the fibril³². Determining which morphologies are likely to exist *in vivo* is a major challenge that some are attempting to resolve using solid state NMR and cryo-TEM using fibril samples extracted from patients with Alzheimer's disease²⁴⁹⁻²⁵¹. The method used to determine these structures however, relies on forcing the sample into homogeneity by several rounds of seeding new fibrils from fresh pools of monomer. This method therefore eliminates some polymorphs found *in vivo* in favour of a single dominant polymorph that is favoured in a particular environment *in vitro*.

Polymorphism occurs due to differences in local conditions when new amyloid fibrils are formed. Changes in pH, temperature, the available surfaces and agitation may all result in different sets of polymorphs occurring in a given sample. Another factor that could affect polymorphism is the concentration of salt in solution. This could occur by Debye-Hückel screening²⁵² which could allow for interactions between monomers that would otherwise be prevented by unfavourable interactions elsewhere. Changing the salt concentration to observe how this affects polymorphism is therefore of interest.

In this chapter it will be shown that in extreme conditions, at high $A\beta_{1-42}$ concentrations it is possible to form exclusively small protofibril-like aggregates in a salt dependent manner. These protofibrils will be shown to have little regular cross- β structure. It will also be shown that the protofibrils can disrupt lipid bilayers thus displaying qualities associated with toxicity. Finally, the effects of salt concentrations on fibril length distributions will be investigated at lower, less extreme, concentrations of $A\beta$. It will

be shown that even then, high salt concentrations can induce the formation of smaller protofibril like aggregates. This will show that $A\beta_{1-42}$ experiences Debye-Hückel screening and this allows monomers to nucleate more rapidly by shielding otherwise unfavourable interactions with dissociated ions from the salt in solution. The impact of this is the creation of many short fibrils (nucleation far more rapid than elongation) as opposed to fewer long fibrils (elongation more rapid than nucleation) at low salt.

7.2 Methods

7.2.1 $A\beta_{1-42}$ preparation

$A\beta_{1-42}$ was prepared as per protocol 2 described in chapter 2 (section 2.2.2) with the caveat of using 10 mM NaOH as opposed to 50 mM NaOH to resuspend the lyophilised $A\beta_{1-42}$ unless otherwise stated.

7.2.2 Electron microscopy

$A\beta_{1-42}$ was diluted to a concentration of 22 μ M and incubated in either 50 mM sodium phosphate, 150 mM sodium chloride, 2 mM sodium azide, pH 7.4 or 20 mM sodium phosphate, 2 mM sodium azide, pH 7.4 at 37 °C for 3 hours.

$A\beta_{1-42}$ was also prepared exactly as per protocol 2 described in chapter 2 (section 2.2.2) and diluted to a concentration of 22 μ M and incubated in 100 mM sodium phosphate, 300 mM sodium chloride, 2 mM sodium azide, pH 7.4 at 37 °C for 3 hours.

TEM grids of all samples were prepared and imaged at 15000X magnification as per the protocol for negative stain EM described in chapter 2 (section 2.5).

The images were analysed using Gwyddion software ²⁵³ to determine the lengths and end to end values for both conditions.

7.2.3 AF4 MALS

22 μ M $A\beta_{1-42}$ was incubated for 3 hours in 50 mM sodium phosphate, 150 mM sodium chloride, 2mM sodium azide, pH 7.4 at 37°C. 50 μ l of sample was injected into the AF4 system. An initial cross flow of 4.5 ml/min was run for 5 minutes and then lowered over 20 minutes to 0 ml/min at which the system was ran for 5 minutes. The eluted sample was detected using UV absorbance at 280 nm and MALS as described in chapter 2 (section 2.7). This was repeated using 100 mM sodium phosphate and 300 mM sodium chloride and the sample was injected into the AF4 system after 30 minutes, 1 hour and 3 hours.

7.2.4 Circular Dichroism

A β_{1-42} was diluted to 22 μ M and incubated in either 50 mM sodium phosphate 150 mM sodium chloride 2 mM sodium azide pH 7.4 at 37 °C for 3 hours.

200 μ l was then injected into a 1 mm pathlength a quartz suprasil cuvette (Hellma, UK) and spectra were recorded immediately using a Jasco J-800 CD spectropolarimeter (Jasco, UK). 200 μ l of 50 mM sodium phosphate, 150 mM sodium chloride, 2 mM sodium azide, pH 7.4 was then added to the cuvette and another set of spectra were recorded.

7.2.5 Dye release

A solution of 50 mM carboxyfluorescein (sigma) was made by dissolving dry carboxyfluorescein in 70 mM phosphate buffer, pH 7.4 to 70 mM carboxyfluorescein. This was then diluted slowly into a solution of sodium chloride until the ionic strength of the solution matched a 50 mM phosphate 150 mM NaCl solution. The solution was then diluted in water to 50 mM carboxyfluorescein 50 mM phosphate pH 7.4.

LUVs were made using the protocol described in chapter 2 (section 2.10) with the exception that instead of buffer, the above carboxyfluorescein solutions were used to re-suspend the lipid film. This protocol includes removing any non-encapsulated carboxyfluorescein using a PD-10 desalting gel filtration column (GE Healthcare Life Sciences, UK) to purify the LUVs.

A β_{1-42} was diluted to 22 μ M and incubated in 50 mM sodium phosphate 150 mM sodium chloride 2 mM sodium azide pH 7.4 at 37 °C for 3 hours.

The A β_{1-42} sample was then mixed into a quartz cuvette with the carboxyfluorescein encapsulating LUVs and were incubated together for 1 hour at 37 °C. Measurements were taken every 5 minutes with excitation at 485 nm and emission recorded at 515 nm.

7.2.6 Thioflavin T

Thioflavin T was prepared as described in chapter 2 (section 2.9).

A β_{1-42} was diluted to 22 μ M and incubated in 50 mM sodium phosphate 150 mM sodium chloride 2 mM sodium azide pH 7.4 at 37 °C with 10 μ M thioflavin T. The mixture was aliquoted into 5 wells of a glass coated microplate (WebSeal Plate +, Thermo Scientific, USA). The process was repeated using 20 mM sodium phosphate 2 mM sodium azide pH 7.4. The microplate was covered with a clear plastic cover. The microplate was then incubated in an Omega fluostar fluorescence plate reader (BMG Labtech, UK) at 37 °C, with shaking for 4 seconds at 100 rpm before measurements. Measurements were taken every 2 minutes with excitation at 445 nm and emission recorded at 485 nm.

7.3 Results

7.3.1 TEM reveals a salt dependent change in morphology in amyloid fibrils

TEM is a useful method of measuring heterogeneity in fibrils formed under different conditions as the single molecule approach allows for the individual characterisation of each fibril. Polymorphism in amyloid fibrils can and has been revealed by TEM³³. TEM is however, most effective when there is a lot of material to observe. Therefore, in order to obtain the most information about fibril polymorphs that exist in different conditions, high concentrations of $A\beta_{1-42}$ must be used as opposed to more physiologically relevant low concentrations⁷⁷.

22 μM $A\beta_{1-42}$ was incubated for 3 hours at 37 °C in a glass coated microplate. Grids for negative stain TEM were then prepared and imaged. Figure 7.1 (A) shows that, when incubated in 50 mM phosphate buffer with 150 mM NaCl, the $A\beta_{1-42}$ mostly formed short aggregates. Comparatively, when incubated in 20 mM phosphate buffer with no NaCl shown in figure 7.1 (B), the $A\beta_{1-42}$ forms fewer but almost exclusively long amyloid fibrils. A simple interpretation for this would be that, at physiological concentrations of salt, $A\beta_{1-42}$ nucleates rapidly compared with elongation and many amyloids form but do not elongate much as the monomer population becomes depleted. In contrast, at lower salt concentrations, amyloids nucleate more rarely allowing more elongation of a smaller number of fibrils. This would imply that the nucleation of amyloid fibrils from $A\beta_{1-42}$ is salt dependent. In other words, the presence of salt results in more favourable conditions for the nucleation of $A\beta_{1-42}$ fibrils. Physiological salt concentrations allow for Debye-Hückel screening of unfavourable electrostatic interactions and surrounding exposed charged residues with dissociated ions in solution. This would allow $A\beta_{1-42}$ monomers to get close enough to one another to form favourable interactions allowing for nucleation to occur.

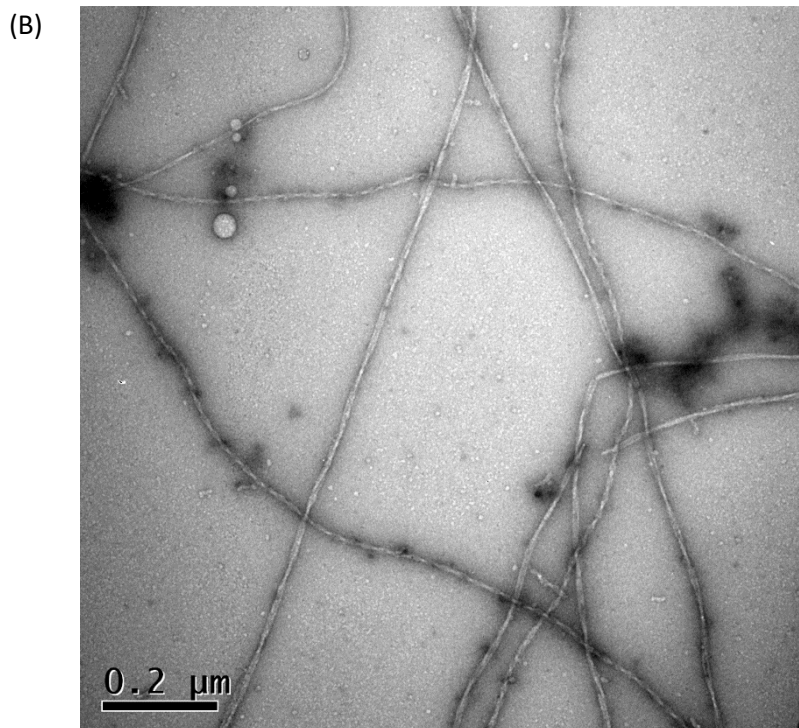
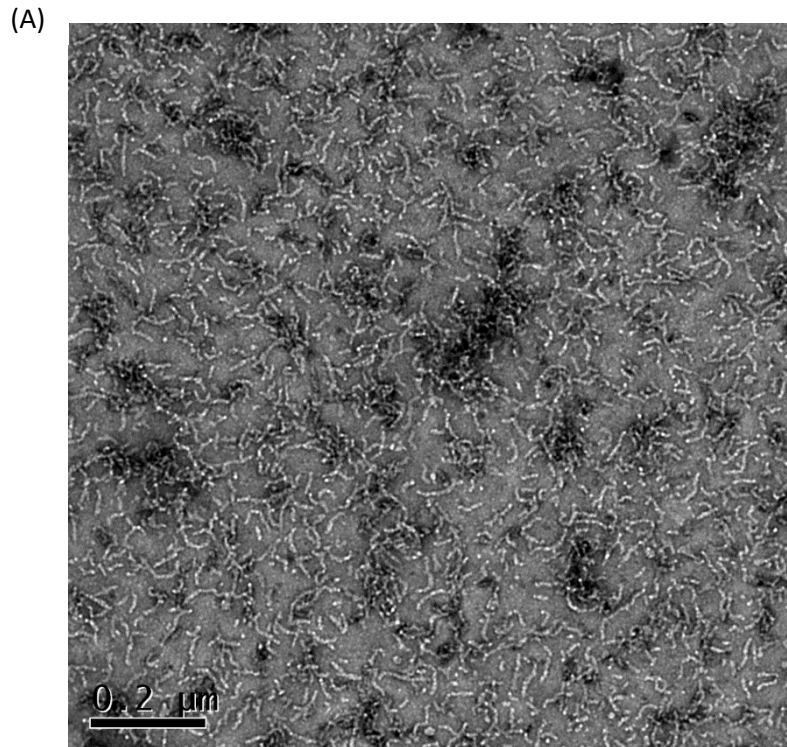


Figure 7.1: Salt dependent fibril morphology. $A\beta_{1-42}$ was incubated at $22\ \mu\text{M}$ in a high (50 mM phosphate 150 mM NaCl) and low (20 mM phosphate) salt buffer. Grids for EM were made for both conditions after 3 hours incubation at $37\ ^\circ\text{C}$. (A) shows a representative image of the results from the physiological buffer and (B) shows a representative image of the results from the low salt buffer. The fibrils observed in (B) are much longer than the shorter aggregates observed in (A). The physiological salt concentration in (A) results in a higher rate of nucleation resulting in many short fibrils as opposed to the slower nucleation and elongation observed in (B) at low salt.

Due to the length of the fibrils observed in figure 7.1 (B) the length of a given fibril was not discernible due to the inability to reliably track a single fibril across its entire length. However, 8 separate images were analysed for the fibrils observed in figure 7.1 (A) with clearly defined individual aggregates covering most of each section of grid. A length distribution was obtained by using multiple line segments to measure along the length of each protofibril. Figure 7.2 shows the resulting distribution.

Size distribution in physiological salt

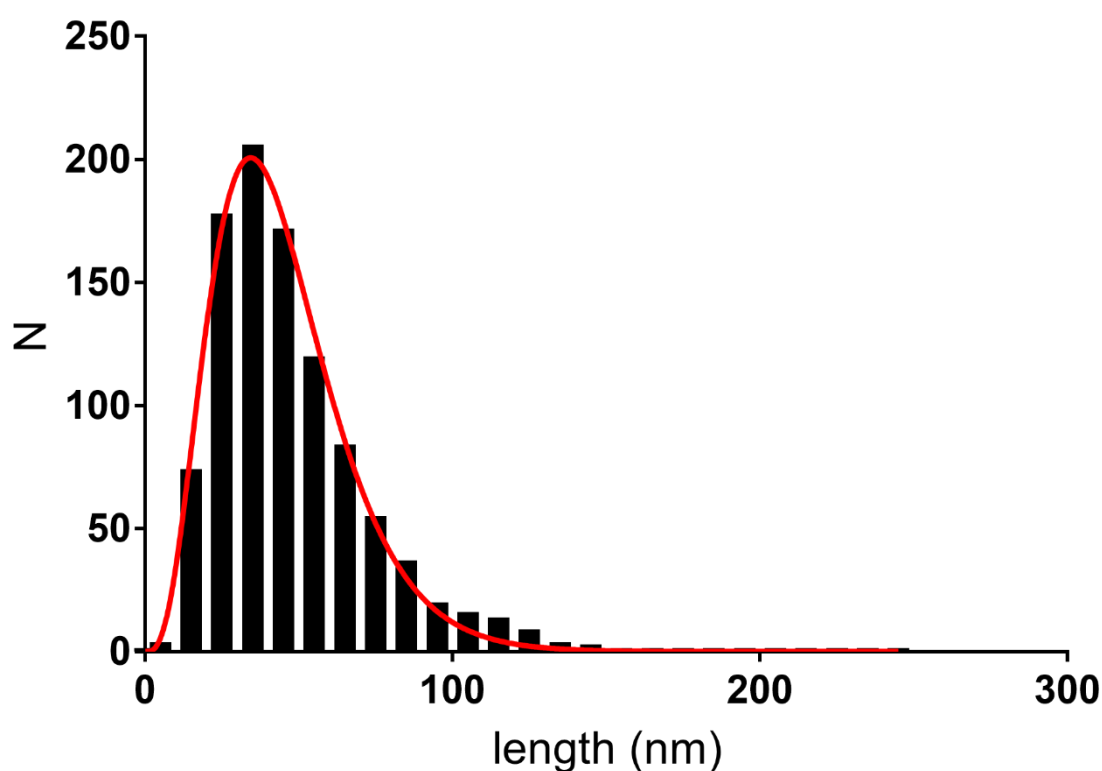


Figure 7.2: Salt induced protofibrils are less than 100 nm in length. 1000 protofibrils from 3 samples made in the conditions seen in figure 7.1 (B) were analysed by measuring multiple line segments along the length of each individual protofibril. These values were plotted on a histogram which was fitted to a Hill distribution ²⁵⁴. The majority of the protofibrils measured were less than 100 nm in length and almost all of them were less than 200 nm in length. Each bar represents a bin size of 10 nm (the first bar being 0-9 nm the second bar 10-19 nm etc).

The majority of the protofibrils measured were less than 100 nm in length and only one protofibril was measured above 200 nm in length. The histogram shown in figure 7.2 was fitted to a distribution and, as described by Hill ²⁵⁴, the degrees of freedom regarding each protofibril was calculated. The degrees of freedom of an individual molecule are reduced at a surface compared to in solution as a result of a molecule adsorbing onto a surface ²⁵⁵. As these experiments are all performed in glass microplates there isn't an expected impact of the surface except for the air water interface as discussed in chapter 3 (sections 3.3.3 and 3.3.4) although the relative surface area here is small.

For more detailed analysis of the protofibrils formed at physiological salt concentrations and the fibrils formed at low salt concentrations, the "end to end" lengths were analysed by using a single line segment to measure the distance from one end of the aggregate to another as opposed to tracking the length of the entire aggregate using multiple line segments. These values were then plotted against the actual length of the aggregates measured as before using multiple line segments. This was possible for the longer fibrils, as even though the whole length of the fibrils was not often obtainable, the length of a segment of fibril could be measured. The direct "end to end" length of the fibril could also be measured across such a segment by measuring the direct distance from one end of the segment to the other. Figure 7.3 shows the difference between the "end to end" length of a fibril segment and the "actual length" of a fibril segment.

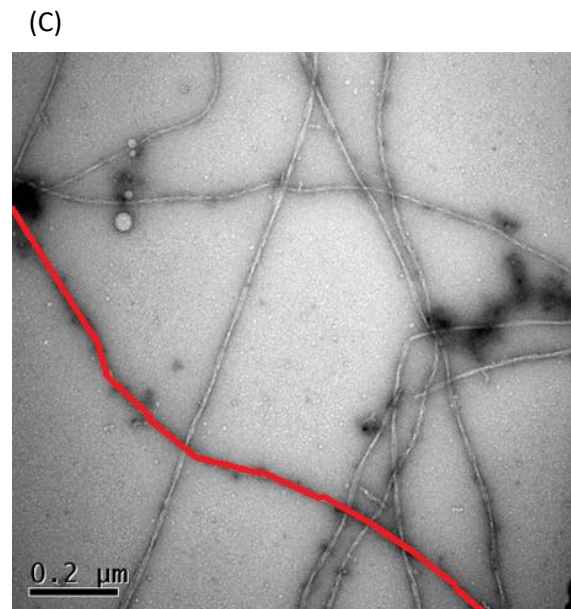
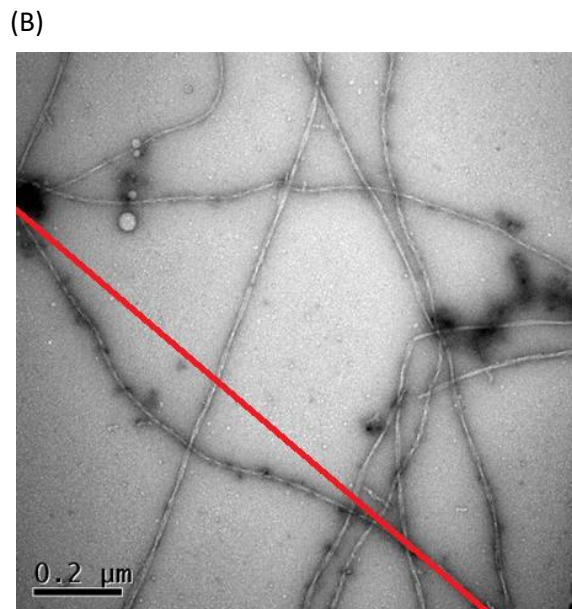
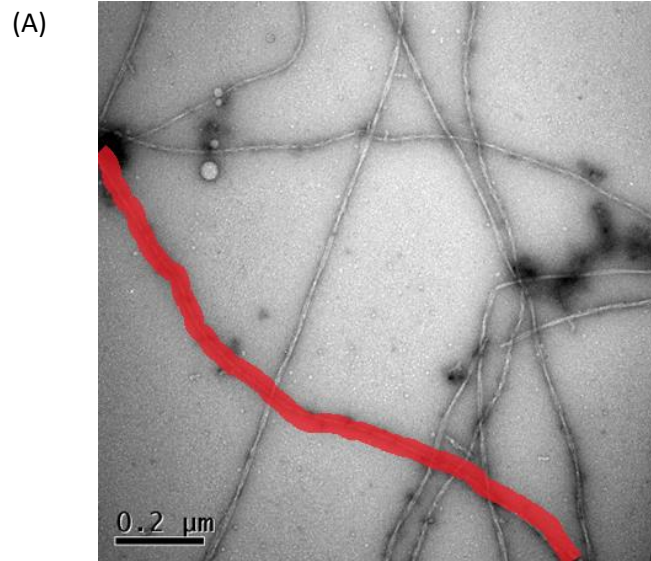


Figure 7.3: Method for measuring the “end to end” length and the actual length of a fibril. The amyloid fibrils and protofibrils were analysed by comparing the “end to end” length with the “actual length”. Image A highlights the shape of a fibril segment used for this analysis. Image B shows the method of measuring the “end to end” length of the fibril segment by using a straight line from one end of the segment to another. Image C shows the method of measuring the actual length of the fibril segment by using multiple small straight lines to measure multiple distances across the fibril segment and summing the lengths of all of these lines.

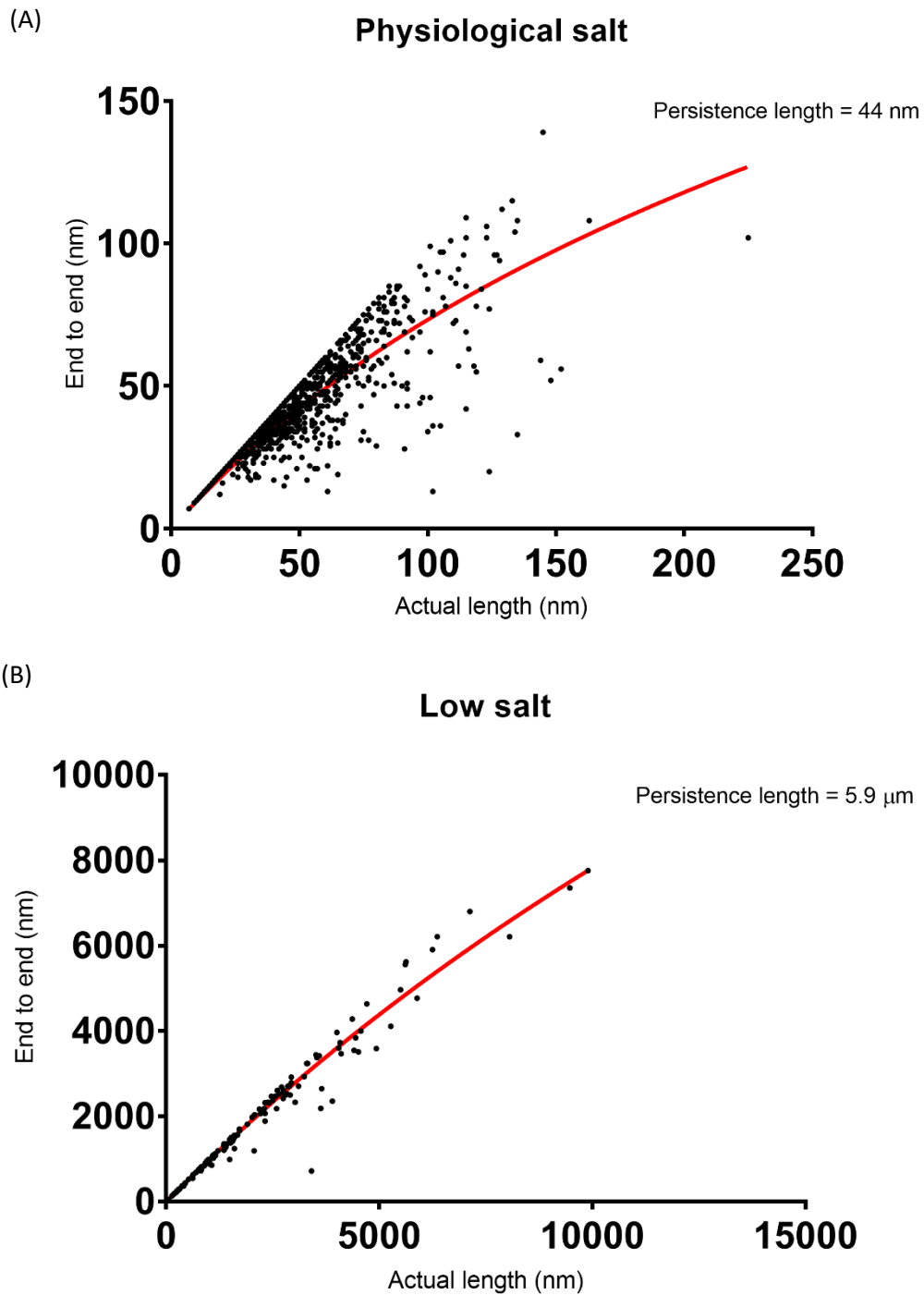


Figure 7.4: Protofibrils are 2 orders of magnitude less stiff than fibrils. The amyloid fibrils and protofibrils were analysed by comparing the “end to end” length with the “actual length”. These data were then fit to a model that calculates the persistence length of the aggregate which provides information about the stiffness of the aggregate. Graph (A) shows the “end to end” length of the protofibrils formed at physiological salt conditions against the actual length. The calculated persistence length of the protofibrils is 44 nm. Graph (B) shows the data for the fibrils formed in low salt and reveals a persistence length of 5.9 μm .

Figure 7.4 shows the comparisons between the “end to end” values and the “actual length” values for both the protofibrils formed at physiological salt concentrations and the fibrils formed at low salt. These data were then fit to a worm like chain model that calculates the persistence length of the aggregates ²⁵⁶. The persistence length is a measure of the stiffness of the amyloid. The higher the persistence length the more of the amyloid that behaves like a stiff beam. For lengths of amyloid above its persistence length it is more likely to have “random walk” characteristics, rather than appear as a straight line it will bend. As shown by Knowles *et al* ²⁵⁷ the bending rigidity of amyloids can be calculated from the persistence length and the height distributions for a given sample. Unfortunately, negative stain TEM is not conducive to calculating height distributions. However, a rough estimate of the width of the amyloid can be measured and compared to the data from Knowles *et al* ²⁴⁷.

The A β ₁₋₄₂ protofibrils formed at physiological salt concentrations however, have a much lower binding rigidity and fall into the same range as fibrils formed from α -lactalbumin. As it is predicted that a high rate of nucleation of A β ₁₋₄₂ is what results in these particular structures, it could be inferred that the reason α -lactalbumin forms similar structures is that it has a higher propensity to nucleate. However, in Knowles *et al* ²⁴⁷ the fibrillisation conditions involved incubating α -lactalbumin at pH 2 for 5 hours at 50 °C with constant shaking. In order to determine whether or not the rate of nucleation could be adjusted to result in different α -lactalbumin fibril morphologies this would need to be repeated in conditions that changed the rate of nucleation.

The persistence lengths of the fibrils formed in low salt are 2 orders of magnitude higher than the persistence lengths of the protofibrils formed at physiological salt concentrations. This suggests that there is some level of structure that allows the fibrils formed at low salt to be more rigid and have a higher Young’s modulus than the protofibrils formed at physiological salt concentrations.

7.3.2 AF4-MALS confirms the size distributions for A β ₁₋₄₂ aggregates formed at physiological salt concentrations

The TEM data suggest that in a physiological buffer the aggregates formed were all below 200 nm in length. However, there is a potential for unintentional bias in the acquisition and analysis of TEM data. Even with 1000 measured protofibrils only the aggregates that were observed can be included in the analysis. There is also the possibility that some aggregates formed in solution but did not adsorb onto the grid.

AF4 is a useful technique for quantifying the size distribution of samples such as the aggregates formed at physiological salt concentrations.

A β_{1-42} was incubated in the physiological buffer for 3 hours at 37 °C at 22 μ M. 50 μ l was then injected into the AF4 system. A lot of the sample eluted sterically meaning that it did not fractionate but instead eluted immediately. This was potentially due to the method used which included a step where the sample volume was reduced significantly in the AF4. This could have resulted in a higher than expected concentration and the formation of extremely large aggregates. Some of the sample did elute after the cross flow had been reduced. Figure 7.5 (A) shows a time course of absorbance at 280 nm showing the elution profile of the aggregates over time. A region of interest was determined and the distribution of the species that were eluted in this region is shown in figure 7.5 (B). The eluted species fit to a random coil model and 90% of the eluted sample had a radius of gyration of between 20 and 60 nm. This confirms that a majority if not all of the aggregates formed in physiological buffer really were distributed as shown in figure 7.2.

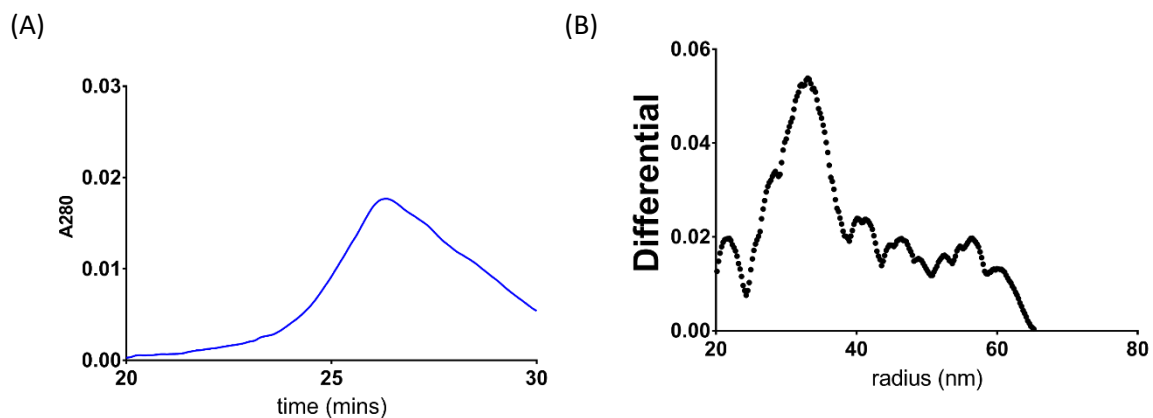


Figure 7.5 Quantification of aggregates formed at physiological salt concentrations reflects the distribution observed by TEM. A β_{1-42} was incubated at 22 μ M for 3 hours and injected into the AF4 system. As the cross flow was reduced to almost 0 ml/min some of the sample began to elute which can be seen when the absorbance at 280 nm is plotted against time (A). The eluting sample was measured for 30 minutes. The region of eluted sample was analysed by MALs (B) which shows a distribution of species that, when the data were fit to a random coil model, had radii of gyration ranging from 20 nm to 60 nm. This reflects the size distributions measured in figure 7.2.

7.3.3 Salt induced protofibrils have β -structure

Once it had been established that physiological salt conditions resulted in protofibrils, investigating their structure became an obvious next step. Circular dichroism can provide information about the

secondary structure of proteins and has been used to analyse the β structures displayed by amyloid fibrils²⁵⁸. It has also been used to differentiate between $A\beta$ oligomers that have been shown to display α and β structures and even transition between the two²⁵⁹. Samples were prepared as before in both the low salt and physiological conditions and, after incubation, CD spectra were obtained and are shown in figure 7.6. The protofibrils formed in the physiological conditions produced a negative CD band at 217 nm that indicates the presence of a β structure. In order to confirm that the signal observed was not an artefact, the sample was diluted and re-measured. The signal of the diluted sample was the same as the un-diluted sample when the signal was corrected for the different concentrations. The fibrils formed at low salt concentrations were also observed. These displayed a 10 times larger signal suggesting significantly more β structure.

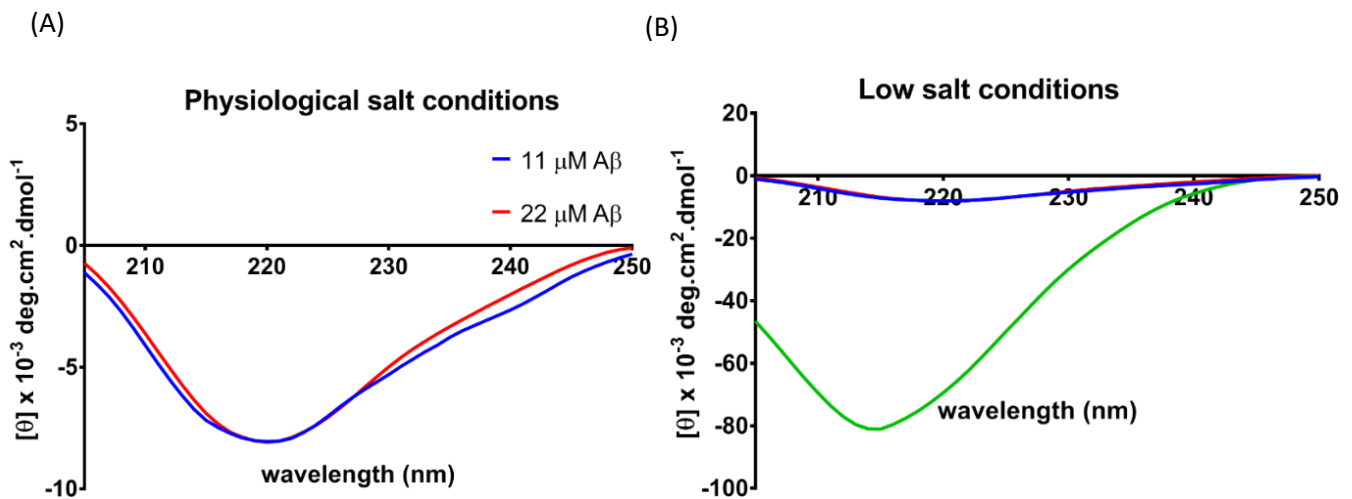


Figure 7.6: Protofibrils have a β signal by CD. A sample of protofibrils was made and CD spectra were obtained, the average of these is shown above (red). The signal obtained appeared to resemble the signal obtained from samples with β structures (A). The sample was also diluted to 11 μM (blue) to ensure that the signal was concentration dependent and not an artefact. When the signal was corrected for concentration there was little difference between the two samples indicating that the signal observed was not an artefact. The protofibrils therefore have some β structure. The fibrils formed at low salt concentration displayed 10 times the signal (B) (green line) of the protofibrils formed in physiological conditions. For comparison the red and blue lines indicate the sample from the physiological buffer. Each measurement represents the mean value of 5 replicate measurements.

7.3.4 Protofibrils can disrupt lipid bilayers

The toxicity of many $A\beta_{1-42}$ aggregates has been investigated^{60,64,173}. A useful indicator of this toxicity is the ability of the aggregate to disrupt a lipid bilayer as discussed in chapter 1 (section 1.3.1). A dye release assay discussed in chapter 2 (section 2.9) allows for the quantification of disruption to lipid bilayers. A sample of protofibrils formed in physiological conditions was prepared as before.

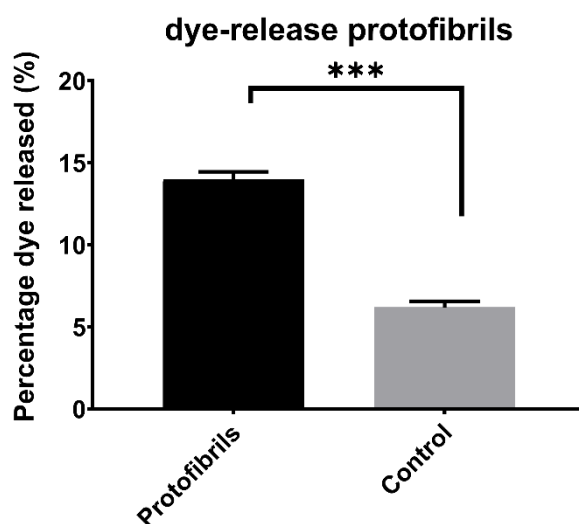


Figure 7.7: Protofibrils can disrupt LUVs. A sample of protofibrils was made and these were incubated with carboxyfluorescein encapsulating LUVs. After 1 hour of incubation at 37 °C the fluorescence from the samples containing protofibrils was twice the signal observed in a control with the LUVs alone showing that the protofibrils are capable of disrupting LUVs to the point where the carboxyfluorescein dye could leak out. Error bars represent the standard error about the mean for 3 repeats. The difference was determined to be significant using a Student's t-test where *** indicates that $P < 0.005$.

These were then incubated with dye encapsulating LUVs at 37 °C for 1 hour. Figure 7.7 shows that, when compared to a control of LUVs alone, the protofibrils were able to cause significant dye release. This suggests that the protofibrils can in fact contribute to the toxicity observed when levels of $A\beta_{1-42}$ are increased. *In vivo* conditions rarely exist without salt and therefore the rapid nucleation of $A\beta_{1-42}$ might produce protofibrils that are capable of membrane damage before the eventual formation of larger amyloids. The idea of protofibril structures displaying qualities associated with toxicity has been previously presented²⁶⁰ although, where in previous studies the relative toxicity has been compared to other oligomeric species, here, only the fact that protofibrils are capable of inducing permeation in lipid bilayer is presented.

7.3.5 High salt concentrations are required to form protofibrils when monomeric $A\beta_{1-42}$ is diluted to neutral pH from high pH

In the experiments discussed so far in this chapter, the $A\beta_{1-42}$ all came from the same batch and was prepared in the same way, by resuspending the lyophilised monomeric sample in 10 mM NaOH to 220 μM , then diluting into a sample buffer to the final pH and concentration. Taylor et al.²⁶¹ provides insight into the variability of samples prepared this way. Briefly, the expected pH of 12 is seldom attained when resuspending in 10 mM NaOH because the lyophilised sample vials often contain significant amounts of counter ion. Upon resuspension in 10 mM NaOH, the samples were often at pH 10 and occasionally even as low as pH 8. $A\beta_{1-42}$ is capable of aggregating at pH 10 and can therefore

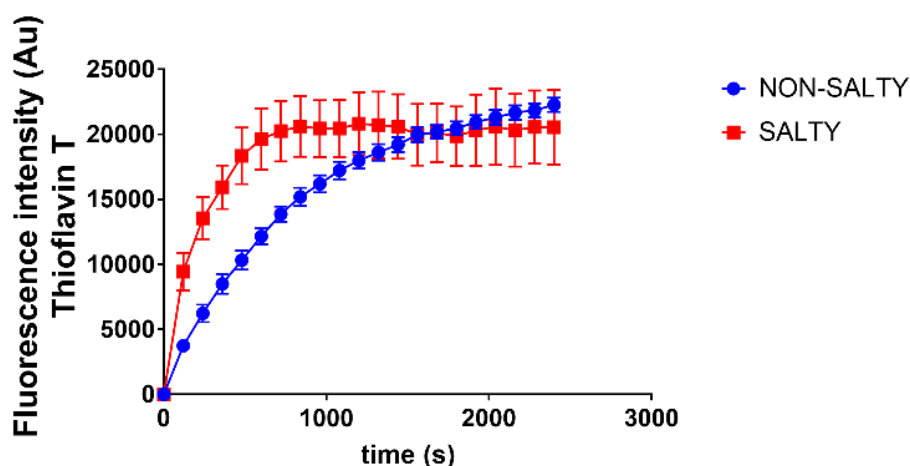


Figure 7.8: When the sample is prepared in 10 mM NaOH there is no lag phase for the reaction. Monomeric $A\beta_{1-42}$ was received in glass vials as a lyophilised film. The film was resuspended in 10 mM NaOH to a concentration of 220 μM . The $A\beta_{1-42}$ was then diluted to 22 μM and pH 7.4 in the high (red) and low (blue) salt buffers discussed previously. These solutions were incubated with 10 μM thioflavin T which upon binding to amyloid aggregates displays an increase in fluorescence. In both conditions no lag phase for the increase in signal is observed suggesting that these reactions are seeded. At high salt concentrations, the reaction is significantly faster than at low salt concentrations. Error bars represent the standard error about the mean from 2 repeats.

form amyloid seeds in these conditions. Indeed, when the sample used in the previous experiments was diluted to 22 μM at pH 7.4 with 10 μM thioflavin T, an increase in fluorescence was seen immediately (figure 7.8) with no lag phase. This strongly suggests that the reaction was seeded. This is also true for the reaction at the low salt concentration even if the reaction at the physiological salt concentration is more rapid. This further supports the hypothesis that there was rapid nucleation (albeit perhaps not primary nucleation) that led to a large number of small protofibrils in physiological conditions. In contrast, at the lower salt concentration, the nuclei that already existed elongated to form few but large amyloid fibrils.

Due to the inconsistencies observed when preparing samples using 10 mM NaOH, a sample was prepared using 50 mM NaOH which has now been shown to be reliable at producing monomeric $A\beta_{1-42}$.

⁴² samples by Taylor *et al.*²⁶¹. The previously used method for forming protofibrils at the physiological concentration did not yield protofibrils observable by TEM. However, when the salt in the buffer was increased to 100 mM sodium phosphate and 300 mM NaCl, protofibrils were observed after 30 minutes (figure 7.9). This shows that large quantities of protofibrils can be formed from a clean preparation of initially monomeric A β ₁₋₄₂.

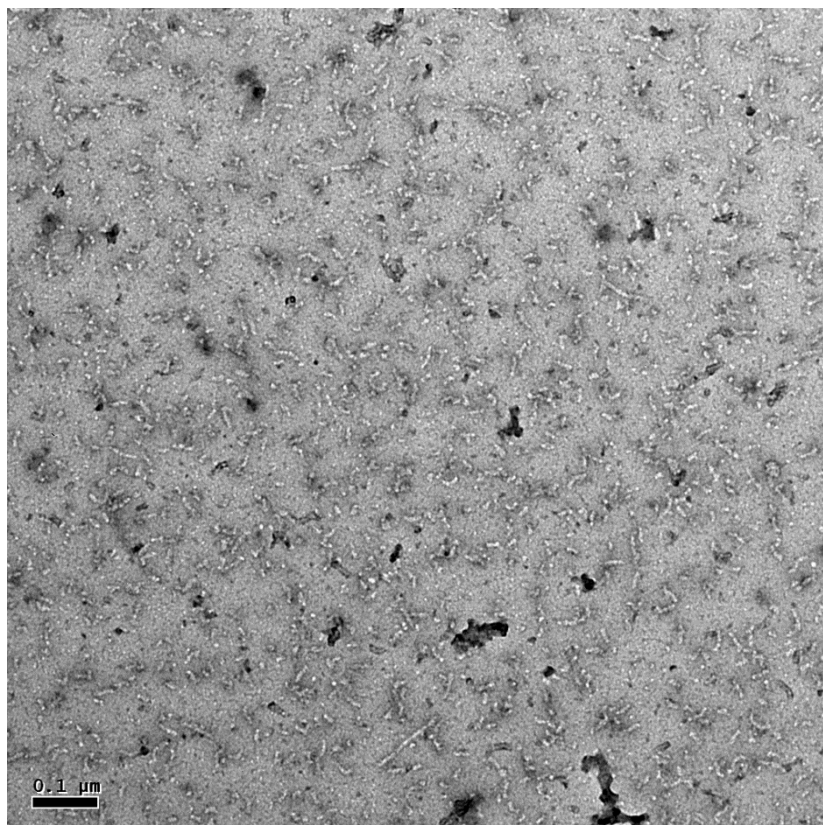


Figure 7.9 Protofibrils form after 30 minutes in high salt conditions. A sample of A β ₁₋₄₂ was incubated in a buffer containing 300 mM NaCl for 30 minutes. This sample was imaged by TEM and the resulting protofibrils are shown above.

In order to quantify the amount of protofibrils present at different time points, A β ₁₋₄₂ in the high salt buffer was injected into the AF4 system multiple times. An evaluation of the entire sample by MALs revealed two populations of species (figure 7.10 (A)). 60% of the eluted sample fit to a random coil model with radii of gyration distributed about 100 nm indicating that these protofibrils are larger than those observed in figures 7.2 and 7.5. The remainder of the eluted sample fit to a random coil model with radii of gyration distributed around 500 nm indicating that these are larger aggregates, possibly more similar to fibrils than protofibrils. After 1 hour, protofibrils were no longer observed and the larger aggregates had radii of gyration distributed around 650 nm indicating that these were growing

aggregates, most likely elongating fibrils (figure 7.10 (B)). After 3 hours, many populations of large aggregates were observed with radii of gyration ranging from 600 nm to over 1000 nm (figure 7.10 (C)). By comparing the size distributions of all of three time points, (figure 7.10 (D)) it was observed that the transition between protofibril-sized species to fibril-sized species was more rapid than the transition between fibril-sized species to larger fibrils indicating that the process involved in transitioning between small aggregates and fibrils is generally faster than elongation (although it might take longer depending on the conditions governing nucleation of fibrils).

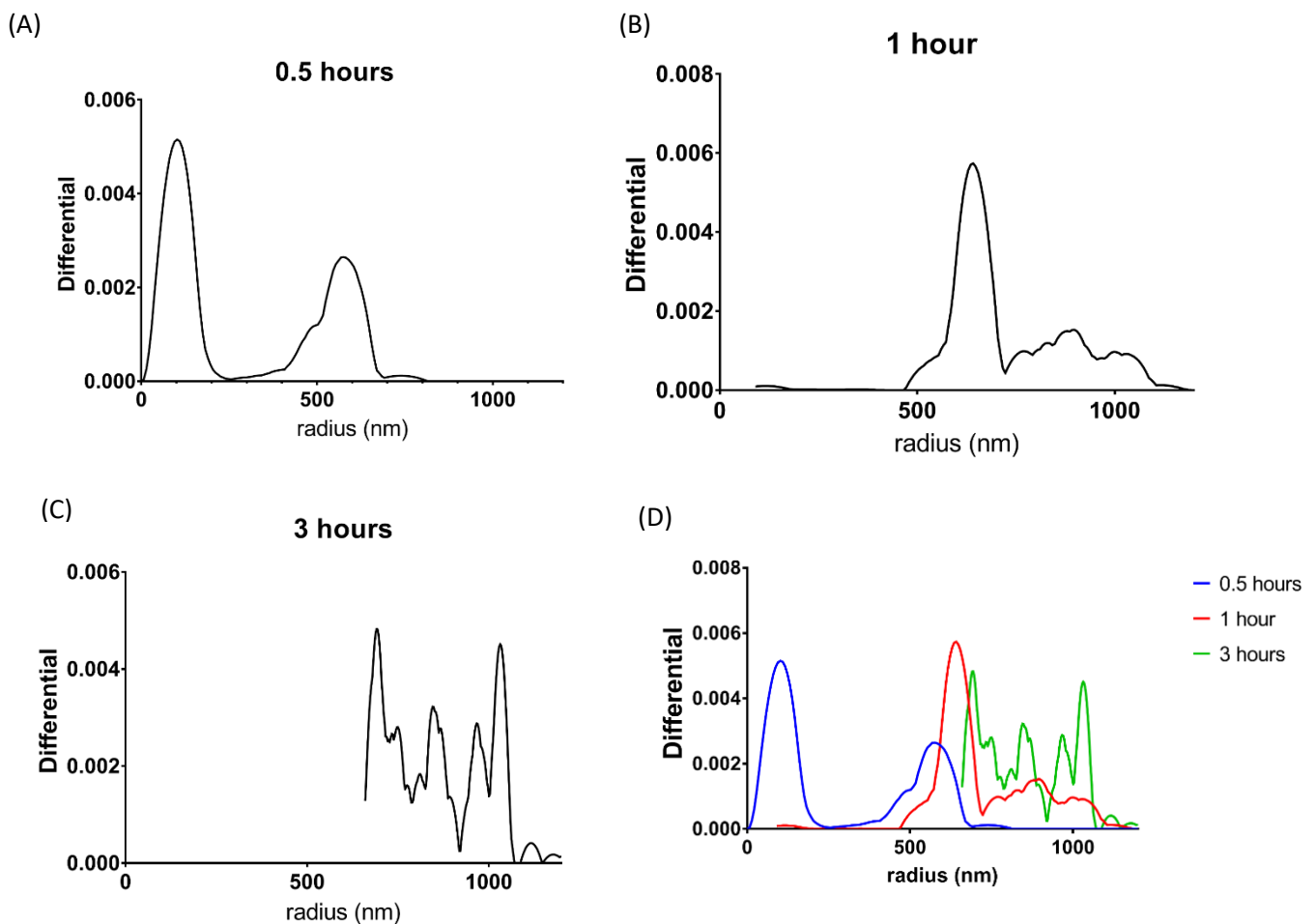
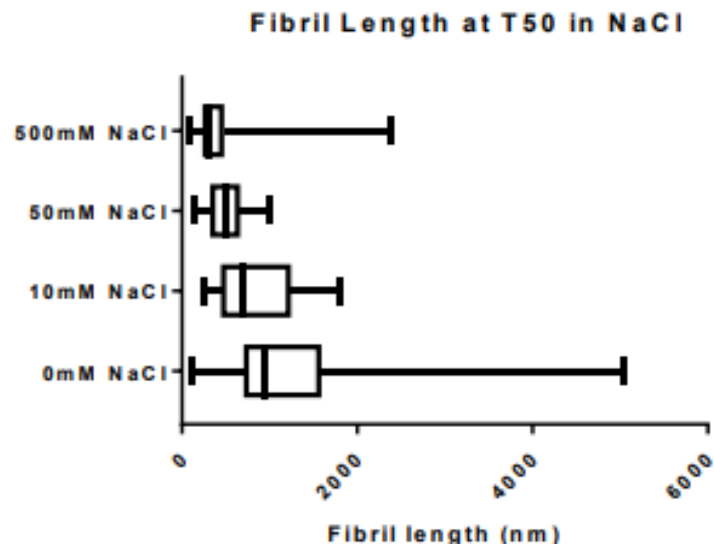


Figure 7.10 A time course of fibril formation detected by MALS. $A\beta_{1-42}$ was incubated for 3 hours in a high salt buffer. The sample was injected into the AF4 system after 30 minutes (A), 1 hour (B) and 3 hours (C). The size distributions of the eluted samples were measured by MALS. Protofibrils sized aggregates were observed after 30 minutes but disappeared after 1 hour. When plotted together (D) the progression of small aggregates to large as time progressed was observed.

7.3.6 Salt concentrations can affect the size of amyloid fibrils

The formation of protofibrils at an $A\beta_{1-42}$ concentration of 22 μM and exclusively at high salt concentrations is an interesting phenomenon, however, *in vivo* it is unlikely that $A\beta_{1-42}$ will exist at close to this concentration of peptide. 22 μM is also well above a reported critical micellar concentration of 17.6 μM ²⁶² which results in the formation of micelle-like aggregates and can affect the mechanism of fibrillisation. Therefore, the effect that salt concentrations have on lower concentrations of amyloid becomes relevant. As part of an investigation into the potential effects of the Hofmeister series on the fibrillisation of $A\beta_{1-42}$, one of our Masters students, Caitlin Bone, confirmed that the lengths of amyloid fibrils were longer when formed in the absence of salt ²⁶³. Amyloid fibrils were formed at 4 μM from stocks that had been prepared using 50 mM NaOH. EM grids were prepared at time points corresponding to half time and peak time (the point at which the thioflavin T signal reaches its maximum) of a thioflavin T time course. The lengths of the amyloid fibrils were measured using the method outlined in figure 7.3 (C). Figure 7.11 shows that at low concentrations of salt the amyloid fibrils formed are mostly longer than those formed at higher salt concentrations. This shows that at lower concentrations of monomer the rate of nucleation is still enhanced by high concentrations of salt.

(A)



(B)

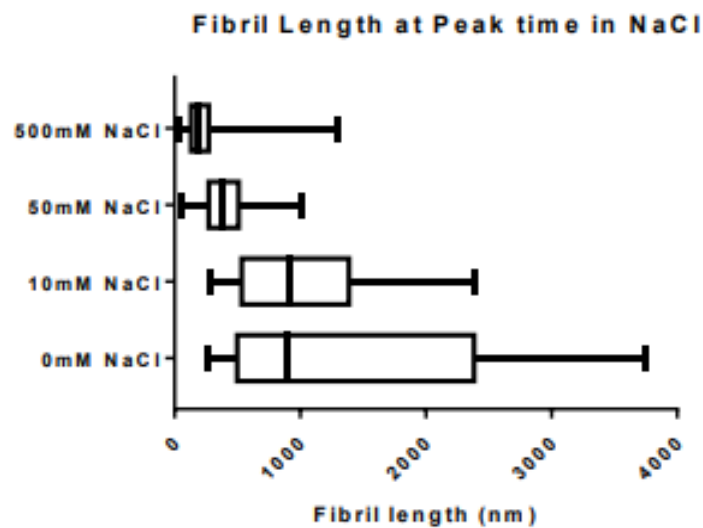


Figure 7.11: Amyloid fibrils formed at low salt are larger than those at high salt. 4 μM of monomeric $\text{A}\beta_{1-42}$ was incubated at 37 °C in 20 mM phosphate buffer at pH 8 and varying NaCl concentrations. TEM grids were prepared of each sample at times corresponding to the half time (A) and peak time (B) of a thioflavin T time course. The length of the fibrils observed in each condition was measured. The data above shows the mean, 25th and 75th percentiles and the maximum and minimum values for each data set. A trend of larger to smaller fibrils can be seen moving from low salt to high salt at both the half time of the reaction and the peak time of the reaction. (Taken with permission from Bone, 2018 ²⁶³)

7.4 Discussion

7.4.1 $\text{A}\beta_{1-42}$ nucleates fibrils and protofibrils in a salt dependent manner

Fibril formation by A β ₁₋₄₂ has been studied in a wide range of conditions^{32,33,35,68,96}. In many of these studies, properties of fibril formation have been observed, such as different rates of fibril formation or fibril morphology, that are different to those properties in other studies. This is rarely mentioned as direct comparisons are only made within a given study rather than from study to study in order to determine the overall effects of the different conditions used between the different studies.

Different salt concentrations were used to determine whether or not salt might impact upon fibril formation, as different buffer conditions are common between studies. Figures 7.1, 7.2 and 7.5 show that at physiological salt concentrations and high concentrations of A β ₁₋₄₂ it was possible to exclusively produce small protofibril-like aggregates. When the salt concentration was reduced, full length fibrils were observed. This shows that at least one step in the fibril formation process is dependent on salt concentrations. This is most likely to be the nucleation process as Debye-Hückel screening will allow for favourable interactions and shield unfavourable interactions between monomers or small oligomers. In conditions where the rate of nucleation is faster than the rate of elongation, many small aggregates would be expected and this is observed in figure 7.1. If this is true, then if these small aggregates were to be transferred into a lower salt concentration, then an eventual progression to larger fibrils, similar to that observed in figure 7.10, would occur at the same rate as the progression to larger fibrils if the aggregates were left at high salt concentrations. This is because the rate of both monomer dissociation from the protofibrils and elongation of those monomers onto the largest fibrils are expected to occur at the same rate independently of salt concentration. This has not been verified here but would form a useful part of further work.

7.4.2 Monomeric A β ₁₋₄₂ reacts less strongly to salt than small oligomers of A β ₁₋₄₂

Reactions involving A β ₁₋₄₂ prepared using 10 mM NaOH produced different results to those using A β ₁₋₄₂ prepared using 50 mM NaOH. The most likely explanation for this is that 10 mM NaOH was not sufficient to ensure that the A β ₁₋₄₂ was stored at a high pH due to variations in the amount of counter ions found in batches of A β ₁₋₄₂. In contrast, 50 mM NaOH consistently resulted in A β ₁₋₄₂ being stored above pH 12. The most likely result of this is that in the 50 mM NaOH stocks the A β ₁₋₄₂ remained mostly monomeric whereas in the 10 mM NaOH stocks the A β ₁₋₄₂ produced a range of small oligomers²⁶¹.

The contrast between physiological salt concentrations and low salt concentrations is greatest when the 10 mM NaOH stocks were used. When the 50 mM NaOH stocks were used, high salt concentrations were required to observe the salt dependent reaction and even then, the reaction rapidly progressed to normal fibril formation. This indicates that interactions between monomers are not affected by salt concentrations but interactions between small oligomers appear to be.

It was shown in chapter 3 (section 3.3.4) that a surface is required for fibril formation to occur. The experiments performed in this chapter were performed in a glass coated microplate with access to the air water interface. An investigation into the impact of salt concentrations on the interaction between $A\beta_{1-42}$ and lipid bilayers would be a physiologically relevant study.

Chapter 8: Conclusions and future work

8.1 Vesicles and the low-binding microplates

Previous work has shown that polyethylene glycol (PEG) can be used as a substrate for forming supported lipid bilayers²⁶⁴. Low-binding microplates (Corning 3686) are coated with a polyethylene oxide “like” substance²²² which is chemically similar to PEG. In chapter 3 (section 3.3.1), it was shown that in the low-binding microplates 100% of the vesicles that were added ruptured within minutes. It was therefore hypothesized that LUVs were forming an SLB on the surface of the microplate. The ability to coat microplate surfaces with SLBs would allow for reactions to occur in the absence of 3rd party surfaces (except for the air water interface). In chapter 4 therefore, the formation of possible SLBs on the low-binding microplate surface was investigated. It was shown that multiple additions of vesicles, with wash steps in between, resulted in profiles of dye release time courses that suggested SLB formation in which lipids were exchanged between vesicles and the SLB. However, when these experiments were repeated with a second batch of microplates, the results after the wash steps were not consistently reproducible suggesting that in some batches of microplates, the vesicles ruptured without seeming to form a SLB. Furthermore, when A β ₁₋₄₂ was incubated in microplates potentially coated with SLBs, it was observed that the reactions were indistinguishable from the reactions that occurred in the microplate alone. Therefore, at least in the batches of microplates tested, there is insufficient evidence that SLBs coat the surfaces of low-binding microplates. This could potentially be resolved using a quartz crystal microbalance or AFM or fluorescence microscopy (in particular FRAP) experiments. The difficulties in performing these experiments stems from both an inability to easily determine the exact surface chemistry of the low-binding microplates and an inability to easily dismantle the microplates to create a surface flat enough or small enough to accommodate these techniques.

8.2 A β fibril formation and lipid bilayer permeation are surface dependent processes

In chapter 3 (section 3.3.1), it was determined that A β ₁₋₄₂ was not able to induce lipid bilayer permeation in a polystyrene microplate. This was despite the formation of amyloid fibrils in the same conditions. It was also shown that A β ₁₋₄₂ was able to induce lipid bilayer permeation in a quartz glass cuvette.

When the fibrillar yield from a set of thioflavin T assay data was analysed it was observed in chapter 3 (section 3.3.2) that fibril formation in polystyrene resulted in a loss of 1 μ M of monomeric A β ₁₋₄₂ with regard to fibril formation. This is because when the yields were plotted against the initial monomer concentration and the data were fit to a linear regression model, the x-intercept of the data in the

polystyrene microplates was 1 μM . This was an unexpected result as the minimum concentration requirement for forming amyloid fibrils was expected to be negligibly small compared to the concentration of monomers used, therefore the x-intercept was expected to be much closer to 0. The most likely explanation for this was that 1 μM of $\text{A}\beta_{1-42}$ remained bound to the surface.

Further analysis of the thioflavin T assay data showed that fibril formation was concentration independent with respect to the rate of the reaction in the polystyrene microplates, but concentration dependent in the low binding microplates (chapter 3 section 3.3.3). As fibril formation is a self-assembly reaction, if it were completely homogenous then it would always be concentration dependent as concentration independence suggests that a process involved in the rate determining step of the reaction is in some way saturable. Therefore, since 1 μM $\text{A}\beta_{1-42}$ was found to remain adhered to the microplate, the most likely explanation for this was that the polystyrene microplate was catalysing the fibril formation reaction and above a concentration of 1 μM , the catalytic surface was saturated.

The result in section 3.3.1 of chapter 3, in which lipid bilayer permeation was not observed in polystyrene, was therefore quite unexpected. In that experiment, 11 μM of $\text{A}\beta_{1-42}$ was used. If only 1 μM of that remained bound to the surface then, at some point during the reaction, 10 μM was not bound to the surface. AFM in chapter 3 (section 3.3.5) revealed that large films were deposited onto the polystyrene surface which subsequently deteriorated as fibrils were forming. This suggested that the nucleation of fibrils occurred heterogeneously at the polystyrene surface and that $\text{A}\beta_{1-42}$ was then recruited for elongation and further nucleation of fibrils. Therefore, in the dye release assay, the $\text{A}\beta_{1-42}$ species were either adhered to the surface as part of the film or in the form of an amyloid fibril. Therefore, at no point in the reaction was the $\text{A}\beta_{1-42}$ able to interact with the LUVs.

In the low-binding microplates, the reaction was concentration dependent (chapter 3 section 3.3.3). However, when the same reaction was performed in glass or quartz glass microplates, the reaction was an order of magnitude slower. Therefore, the reaction in the low-binding microplates was also catalysed by the surface of the microplates. In comparable AFM conditions (chapter 3 section 3.3.6), using a hydrophilic mica substrate, bursts of interactions with the surface were observed. As the concentration of monomer was increased, these bursts were likely to be more frequent resulting in more rapidly catalysed reactions. Therefore, the reaction was concentration dependent. This would predict that at extremely high concentrations of $\text{A}\beta_{1-42}$, fibril formation would become concentration independent as the frequency of transient interactions with the surface would become so high that all of the surface would always be interacting with the $\text{A}\beta_{1-42}$, effectively saturating the surface.

The reactions observed in the glass and quartz glass microplates were also concentration independent (chapter 3 section 3.3.3). This suggested that in these conditions, there was a saturable property in the rate determining step of the fibril formation reaction. AFM (chapter 3 section 3.3.6) revealed that there was no interaction between the $A\beta_{1-42}$ and the quartz glass surface. However, in section 3.3.5 of chapter 3, when the air water interface was removed fibril formation was inhibited. Therefore, the rate of fibril formation in the glass and quartz glass microplate was dependent on the air water interface which was saturated at all concentrations of $A\beta_{1-42}$ that were tested. If the air water interface could be removed permanently, then the rate of fibril formation in truly homogeneous conditions could be measured assuming that heterogeneous surfaces are not a requirement for fibril formation.

8.3 Human Cystatin C can inhibit $A\beta_{1-42}$ induced lipid bilayer permeation and also inhibits fibril formation in a surface dependent manner

It was shown in chapter 6 (section 6.3.5) that hCC can inhibit $A\beta_{1-42}$ induced lipid bilayer permeation independently of the lipid bilayer composition. This suggests that one of the mechanisms by which hCC has protective properties *in vivo*^{148,153,265} includes preventing $A\beta$ induced lipid bilayer permeation.

When incubated at increasing concentrations with $A\beta_{1-42}$ in glass and polystyrene microplates, hCC can inhibit fibril formation as shown in chapter 6 (section 6.3.2). In low-binding microplates however, hCC cannot inhibit fibril formation. Chapter 3 (sections 3.3.3 to 3.3.7) shows that fibril formation in these microplates is catalysed in different ways. In polystyrene microplates, hCC can inhibit fibril formation as $A\beta_{1-42}$ is adhered to the surface of the microplate as shown in chapter 6 (section 6.3.4). In low-binding microplates, the reaction is fast and the interactions with the surface are transient suggesting that the reason that hCC cannot inhibit fibril formation in these conditions is that it interacts with a species that exists transiently. Therefore, when the reaction is rapid interactions between hCC and transient $A\beta_{1-42}$ species are not favourable. In glass coated microplates, the reaction is slow and transient species may exist for longer. Therefore, in these conditions hCC can inhibit fibril formation.

8.4 LUVs catalyse seeded fibril formation reactions and unseeded reactions differently

Chapter 5 (sections 5.3.1, 5.3.2 and 5.3.3) shows that LUVs can catalyse seeded fibril formation reactions. In these reactions, the effect of adding LUVs is to catalyse the reaction in a manner where, at low concentrations of LUVs, the overall rate of the reactions was dependent on the LUVs and therefore the rate of a reaction was dependent on both the concentration of LUVs and the concentration of $A\beta_{1-42}$. At high concentrations of LUVs, a competing, concentration independent process became rate determining giving the impression that LUVs were catalysing fibril formation in a concentration independent manner.

In an unseeded reaction, albeit in polystyrene microplates, the rate of fibril formation was reduced in the presence of LUVs (chapter 3 section 3.3.7). Specifically, the lag phase of the reaction was reduced, and combined EM images showed fibrils forming in association with the LUVs suggesting that LUVs were specifically catalysing nucleation of amyloid fibrils. This contradicts the explanation for the observed lack of A β ₁₋₄₂ induced lipid bilayer permeation from section 8.2. The most likely explanation for this data therefore becomes that the formation of lipid bilayer permeating species is a part of a different pathway to the pathways observed. The observed pathways are fibril formation and most of the A β ₁₋₄₂ being recruited to films on the surface. The nucleation of fibrils being promoted by LUVs and the formation of films results in the formation of lipid bilayer permeating species being drastically reduced.

Further analysis of fibril formation in the presence of LUVs but the absence of 3rd party surfaces is required, especially to determine the impact of lipid bilayer compositions on the fibril formation reaction.

8.5 A β ₁₋₄₂ forms differently sized aggregates when nucleation is increased or decreased by the presence of different ionic strength buffers.

When physiological salt buffers were compared with low salt buffers in a seeded reaction in chapter 5 (section 5.3.2), it was observed that the rate and concentration dependence of the reaction was increased at the physiological salt concentration. This suggested that in these conditions a competing elongation process, which was promoted by salt, was occurring. In these seeded conditions nucleation is likely to have a negligible effect as the elongation process should be dominant with regard to the increase in fibrillar mass. An example of a competing elongation process, that would be salt dependent, could be elongation by dimer addition. Alternately, despite the reaction being seeded, the nucleation rate could outcompete the rate of elongation at higher salt concentrations.

In chapter 7 the role of salt was further investigated. TEM revealed that at physiological concentrations of salt, in a seeded reaction, many short fibrils were formed. Comparatively, in low salt conditions fewer but much larger fibrils were observed. This suggests that nucleation was increased at physiological salt concentrations resulting in a rapid reduction in the concentration of monomer in solution before elongation could take over. At the low salt concentration, nucleation was reduced, resulting in fewer nuclei that were able to elongate before the monomer concentration was significantly depleted. It was then shown that these two types of aggregate had different physical properties stemming from a difference in structure. The fibrils formed at low salt concentrations were shown to have higher order β -structures than the smaller aggregates formed at the physiological salt concentration. The less structured species formed in the physiological conditions was capable of

inducing lipid bilayer permeation. This was not true of the fibrils formed at low salt concentrations which is consistent with previous studies suggesting that fibrils cannot induce lipid bilayer permeation⁶. Therefore, the structural state of amyloid fibrils and aggregates may be related to their ability to induce lipid bilayer permeation.

References

- 1 Alzheimer's Society's view on demography, <<https://www.alzheimers.org.uk/about-us/policy-and-influencing/what-we-think/demography>> (2018).
- 2 What are the most common symptoms for Alzheimer's disease?, <<https://www.alzheimers.org.uk/about-dementia/types-dementia/alzheimers-disease-symptoms#content-start>> (2018).
- 3 Drug treatments for Alzheimer's disease. (2018).
- 4 Honig, L. S. *et al.* Trial of Solanezumab for Mild Dementia Due to Alzheimer's Disease. *N. Engl. J. Med.* **378**, 321-330, doi:10.1056/NEJMoa1705971 (2018).
- 5 Petsko, G. in *BBS 2016*.
- 6 Chiti, F. & Dobson, C. M. in *Annual Review of Biochemistry* Vol. 75 *Annual Review of Biochemistry* 333-366 (Annual Reviews, 2006).
- 7 Goate, A. *et al.* Segregation of a missense mutation in the amyloid precursor protein gene with familial alzheimers-disease. *Nature* **349**, 704-706, doi:10.1038/349704a0 (1991).
- 8 Vassar, R. *et al.* beta-secretase cleavage of Alzheimer's amyloid precursor protein by the transmembrane aspartic protease BACE. *Science* **286**, 735-741, doi:10.1126/science.286.5440.735 (1999).
- 9 Jankowsky, J. L. *et al.* Mutant presenilins specifically elevate the levels of the 42 residue beta-amyloid peptide in vivo: evidence for augmentation of a 42-specific gamma secretase. *Hum. Mol. Genet.* **13**, 159-170, doi:10.1093/hmg/ddh019 (2004).
- 10 Storey, E. & Cappai, R. The amyloid precursor protein of Alzheimer's disease and the A beta peptide. *Neuropathol. Appl. Neurobiol.* **25**, 81-97 (1999).
- 11 Von Koch, C. S. *et al.* Generation of APLP2 KO mice and early postnatal lethality in APLP2/APP double KO mice. *Neurobiol. Aging* **18**, 661-669, doi:10.1016/s0197-4580(97)00151-6 (1997).
- 12 Small, S. A. & Petsko, G. A. Retromer in Alzheimer disease, Parkinson disease and other neurological disorders. *Nat. Rev. Neurosci.* **16**, 126-132, doi:10.1038/nrn3896 (2015).
- 13 Portelius, E. *et al.* Mass spectrometric characterization of brain amyloid beta isoform signatures in familial and sporadic Alzheimer's disease. *Acta Neuropathologica* **120**, 185-193, doi:10.1007/s00401-010-0690-1 (2010).
- 14 Hong, L. *et al.* Structure of the protease domain of memapsin 2 (beta-secretase) complexed with inhibitor. *Science* **290**, 150-153, doi:10.1126/science.290.5489.150 (2000).
- 15 Esler, W. P. *et al.* Transition-state analogue inhibitors of gamma-secretase bind directly to presenilin-1. *Nat. Cell Biol.* **2**, 428-434 (2000).
- 16 Ling, D. J., Song, H. J., Garza, D., Neufeld, T. P. & Salvaterra, P. M. Abeta42-Induced Neurodegeneration via an Age-Dependent Autophagic-Lysosomal Injury in Drosophila. *PLoS One* **4**, 11, doi:10.1371/journal.pone.0004201 (2009).
- 17 Huang, X. D. *et al.* Cu(II) potentiation of Alzheimer A beta neurotoxicity - Correlation with cell-free hydrogen peroxide production and metal reduction. *J. Biol. Chem.* **274**, 37111-37116, doi:10.1074/jbc.274.52.37111 (1999).
- 18 Selkoe, D. J. J., Hardy. The amyloid hypothesis of Alzheimer's disease at 25 years. *EMBO Mol Med* **8**, 595-608 (2016).
- 19 Glenner, G. G. & Wong, C. W. Alzheimers-disease - initial report of the purification and characterization of a novel cerebrovascular amyloid protein. *Biochem. Biophys. Res. Commun.* **120**, 885-890, doi:10.1016/s0006-291x(84)80190-4 (1984).
- 20 Selkoe, D. J. The molecular pathology of alzheimers-disease. *Neuron* **6**, 487-498, doi:10.1016/0896-6273(91)90052-2 (1991).

- 21 Hardy, J. & Selkoe, D. J. Medicine - The amyloid hypothesis of Alzheimer's disease: Progress and problems on the road to therapeutics. *Science* **297**, 353-356, doi:10.1126/science.1072994 (2002).
- 22 De Strooper, B. *et al.* Deficiency of presenilin-1 inhibits the normal cleavage of amyloid precursor protein. *Nature* **391**, 387-390, doi:10.1038/34910 (1998).
- 23 Fernandez, M. A., Klutkowski, J. A., Freret, T. & Wolfe, M. S. Alzheimer Presenilin-1 Mutations Dramatically Reduce Trimming of Long Amyloid beta-Peptides (A beta) by gamma-Secretase to Increase 42-to-40-Residue A beta. *J. Biol. Chem.* **289**, 31043-31052, doi:10.1074/jbc.M114.581165 (2014).
- 24 Glenner, G. G. & Wong, C. W. Alzheimers-disease and Downs-syndrome - sharing of a unique cerebrovascular amyloid fibril protein. *Biochem. Biophys. Res. Commun.* **122**, 1131-1135, doi:10.1016/0006-291x(84)91209-9 (1984).
- 25 Rovelet-Lecrux, A. *et al.* APP locus duplication causes autosomal dominant early-onset Alzheimer disease with cerebral amyloid angiopathy. *Nature Genet.* **38**, 24-26, doi:10.1038/ng1718 (2006).
- 26 Mullan, M. *et al.* A PATHOGENIC MUTATION FOR PROBABLE ALZHEIMERS-DISEASE IN THE APP GENE AT THE N-TERMINUS OF BETA-AMYLOID. *Nature Genet.* **1**, 345-347, doi:10.1038/ng0892-345 (1992).
- 27 Nilsberth, C. *et al.* The 'Arctic' APP mutation (E693G) causes Alzheimer's disease by enhanced A beta protofibril formation. *Nat. Neurosci.* **4**, 887-893, doi:10.1038/nn0901-887 (2001).
- 28 Jonsson, T. *et al.* A mutation in APP protects against Alzheimer's disease and age-related cognitive decline. *Nature* **488**, 96-99, doi:10.1038/nature11283 (2012).
- 29 Sunde, M. *et al.* Common core structure of amyloid fibrils by synchrotron X-ray diffraction. *J. Mol. Biol.* **273**, 729-739, doi:10.1006/jmbi.1997.1348 (1997).
- 30 Gremer, L. *et al.* Fibril structure of amyloid-beta(1-42) by cryo-electron microscopy. *Science* **358**, 116-+, doi:10.1126/science.aao2825 (2017).
- 31 Petkova, A. T. *et al.* A structural model for Alzheimer's beta-amyloid fibrils based on experimental constraints from solid state NMR. *Proc. Natl. Acad. Sci. U. S. A.* **99**, 16742-16747, doi:10.1073/pnas.262663499 (2002).
- 32 Schmidt, M. *et al.* Comparison of Alzheimer A beta(1-40) and A beta(1-42) amyloid fibrils reveals similar protofilament structures. *Proc. Natl. Acad. Sci. U. S. A.* **106**, 19813-19818, doi:10.1073/pnas.0905007106 (2009).
- 33 Meinhardt, J., Sachse, C., Hortschansky, P., Grigorieff, N. & Fandrich, M. A beta(1-40) Fibril Polymorphism Implies Diverse Interaction Patterns in Amyloid Fibrils. *J. Mol. Biol.* **386**, 869-877, doi:10.1016/j.jmb.2008.11.005 (2009).
- 34 Xiao, Y. L. *et al.* A beta(1-42) fibril structure illuminates self-recognition and replication of amyloid in Alzheimer's disease. *Nat. Struct. Mol. Biol.* **22**, 499-U497, doi:10.1038/nsmb.2991 (2015).
- 35 Cohen, S. I. A. *et al.* Proliferation of amyloid-beta 42 aggregates occurs through a secondary nucleation mechanism. *Proc. Natl. Acad. Sci. U. S. A.* **110**, 9758-9763, doi:10.1073/pnas.1218402110 (2013).
- 36 Young, L. J., Schierle, G. S. K. & Kaminski, C. F. Imaging A beta(1-42) fibril elongation reveals strongly polarised growth and growth incompetent states. *Phys. Chem. Chem. Phys.* **19**, 27987-27996, doi:10.1039/c7cp03412a (2017).
- 37 Gillam, J. E. & MacPhee, C. E. Modelling amyloid fibril formation kinetics: mechanisms of nucleation and growth. *J. Phys.-Condes. Matter* **25**, 20, doi:10.1088/0953-8984/25/37/373101 (2013).
- 38 Kalapothakis, J. M. D. *et al.* A Kinetic Study of Ovalbumin Fibril Formation: The Importance of Fragmentation and End-Joining. *Biophys. J.* **108**, 2300-2311, doi:10.1016/j.bpj.2015.03.021 (2015).

- 39 Lee, J., Culyba, E. K., Powers, E. T. & Kelly, J. W. Amyloid-beta forms fibrils by nucleated conformational conversion of oligomers. *Nat. Chem. Biol.* **7**, 602-609, doi:10.1038/nchembio.624 (2011).
- 40 Buell, A. K. *et al.* Detailed Analysis of the Energy Barriers for Amyloid Fibril Growth. *Angew. Chem.-Int. Edit.* **51**, 5247-5251, doi:10.1002/anie.201108040 (2012).
- 41 Hellstrand, E., Boland, B., Walsh, D. M. & Linse, S. Amyloid beta-Protein Aggregation Produces Highly Reproducible Kinetic Data and Occurs by a Two-Phase Process. *ACS Chem. Neurosci.* **1**, 13-18, doi:10.1021/cn900015v (2010).
- 42 Stefani, M. & Dobson, C. M. Protein aggregation and aggregate toxicity: new insights into protein folding, misfolding diseases and biological evolution. *J. Mol. Med.* **81**, 678-699, doi:10.1007/s00109-003-0464-5 (2003).
- 43 Seilheimer, B. *et al.* The toxicity of the Alzheimer's beta-amyloid peptide correlates with a distinct fiber morphology. *J. Struct. Biol.* **119**, 59-71, doi:10.1006/jsbi.1997.3859 (1997).
- 44 Kakio, A., Nishimoto, S., Yanagisawa, K., Kozutsumi, Y. & Matsuzaki, K. Interactions of amyloid beta-protein with various gangliosides in raft-like membranes: Importance of GM1 ganglioside-bound form as an endogenous seed for Alzheimer amyloid. *Biochemistry* **41**, 7385-7390, doi:10.1021/bi0255874 (2002).
- 45 Kaye, R. *et al.* Common structure of soluble amyloid oligomers implies common mechanism of pathogenesis. *Science* **300**, 486-489, doi:10.1126/science.1079469 (2003).
- 46 Mucke, L. *et al.* High-level neuronal expression of A beta(1-42) in wild-type human amyloid protein precursor transgenic mice: Synaptotoxicity without plaque formation. *J. Neurosci.* **20**, 4050-4058 (2000).
- 47 Yang, T., Li, S. M., Xu, H. X., Walsh, D. M. & Selkoe, D. J. Large Soluble Oligomers of Amyloid beta-Protein from Alzheimer Brain Are Far Less Neuroactive Than the Smaller Oligomers to Which They Dissociate. *J. Neurosci.* **37**, 152-163, doi:10.1523/jneurosci.1698-16.2017 (2017).
- 48 Klein, W. L. A beta toxicity in Alzheimer's disease: globular oligomers (ADDLs) as new vaccine and drug targets. *Neurochem. Int.* **41**, 345-352, doi:10.1016/s0197-0186(02)00050-5 (2002).
- 49 Gnanakaran, S., Nussinov, R. & Garcia, A. E. Atomic-level description of amyloid beta-dimer formation. *J. Am. Chem. Soc.* **128**, 2158-2159, doi:10.1021/ja0548337 (2006).
- 50 Jang, H. B., Zheng, J., Lal, R. & Nussinov, R. New structures help the modeling of toxic amyloid beta ion channels. *Trends Biochem.Sci.* **33**, 91-100, doi:10.1016/j.tibs.2007.10.007 (2008).
- 51 Lambert, M. P. *et al.* Diffusible, nonfibrillar ligands derived from A beta(1-42) are potent central nervous system neurotoxins. *Proc. Natl. Acad. Sci. U. S. A.* **95**, 6448-6453, doi:10.1073/pnas.95.11.6448 (1998).
- 52 Miller, Y., Ma, B. & Nussinov, R. Polymorphism in Alzheimer A beta Amyloid Organization Reflects Conformational Selection in a Rugged Energy Landscape. *Chem. Rev.* **110**, 4820-4838, doi:10.1021/cr900377t (2010).
- 53 Lin, H., Bhatia, R. & Lal, R. Amyloid beta protein forms ion channels: implications for Alzheimer's disease pathophysiology. *Faseb J.* **15**, 2433-2444, doi:10.1096/fj.01-0377com (2001).
- 54 Strodel, B., Lee, J. W. L., Whittleston, C. S. & Wales, D. J. Transmembrane Structures for Alzheimer's A beta(1-42) Oligomers. *J. Am. Chem. Soc.* **132**, 13300-13312, doi:10.1021/ja103725c (2010).
- 55 Davis, C. H. & Berkowitz, M. L. Interaction Between Amyloid-beta (1-42) Peptide and Phospholipid Bilayers: A Molecular Dynamics Study. *Biophys. J.* **96**, 785-797, doi:10.1016/j.bpj.2008.09.053 (2009).
- 56 Mattson, M. P. *et al.* Beta-amyloid peptides destabilize calcium homeostasis and render human cortical-neurons vulnerable to excitotoxicity. *J. Neurosci.* **12**, 376-389 (1992).

- 57 Curtin, C. C. *et al.* Metal ions, pH, and cholesterol regulate the interactions of Alzheimer's disease amyloid-beta peptide with membrane lipid. *J. Biol. Chem.* **278**, 2977-2982, doi:10.1074/jbc.M205455200 (2003).
- 58 Wong, P. T. *et al.* Amyloid-beta Membrane Binding and Permeabilization are Distinct Processes Influenced Separately by Membrane Charge and Fluidity. *J. Mol. Biol.* **386**, 81-96, doi:10.1016/j.jmb.2008.11.060 (2009).
- 59 Valincius, G. *et al.* Soluble Amyloid beta-Oligomers Affect Dielectric Membrane Properties by Bilayer Insertion and Domain Formation: Implications for Cell Toxicity. *Biophys. J.* **95**, 4845-4861, doi:10.1529/biophysj.108.130997 (2008).
- 60 Lasagna-Reeves, C. A., Glabe, C. G. & Kaye, R. Amyloid-beta Annular Protofibrils Evade Fibrillar Fate in Alzheimer Disease Brain. *J. Biol. Chem.* **286**, 22122-22130, doi:10.1074/jbc.M111.236257 (2011).
- 61 Gillman, A. L. *et al.* Activity and Architecture of Pyroglutamate-Modified Amyloid-beta (A beta(pE3-42)) Pores. *J. Phys. Chem. B* **118**, 7335-7344, doi:10.1021/jp5040954 (2014).
- 62 Schauerte, J. A. *et al.* Simultaneous Single-Molecule Fluorescence and Conductivity Studies Reveal Distinct Classes of A beta Species on Lipid Bilayers. *Biochemistry* **49**, 3031-3039, doi:10.1021/bi901444w (2010).
- 63 Klein, A. M., Kowall, N. W. & Ferrante, R. J. in *Oxidative/Energy Metabolism in Neurodegenerative Disorders* Vol. 893 *Annals of the New York Academy of Sciences* (eds J. P. Blass & F. H. McDowell) 314-320 (New York Acad Sciences, 1999).
- 64 Bode, D. C., Baker, M. D. & Viles, J. H. Ion Channel Formation by Amyloid-beta(42) Oligomers but Not Amyloid-beta(40) in Cellular Membranes. *J. Biol. Chem.* **292**, 1404-1413, doi:10.1074/jbc.M116.762526 (2017).
- 65 Jang, H. *et al.* Misfolded Amyloid Ion Channels Present Mobile beta-Sheet Subunits in Contrast to Conventional Ion Channels. *Biophys. J.* **97**, 3029-3037, doi:10.1016/j.bpj.2009.09.014 (2009).
- 66 Petkova, A. T., Yau, W. M. & Tycko, R. Experimental constraints on quaternary structure in Alzheimer's beta-amyloid fibrils. *Biochemistry* **45**, 498-512, doi:10.1021/bi051952q (2006).
- 67 Zhang, H. Y., Rochet, J. C. & Stanciu, L. A. Cu(II) promotes amyloid pore formation. *Biochem. Biophys. Res. Commun.* **464**, 342-347, doi:10.1016/j.bbrc.2015.06.156 (2015).
- 68 Viles, J. Metal ions and amyloid fiber formation in neurodegenerative diseases. Copper, zinc and iron in Alzheimer's, Parkinson's and prion diseases. *COORDINATION CHEMISTRY REVIEWS* **256**, 2271-2284, doi:10.1016/j.ccr.2012.05.003 (2012).
- 69 Matheou, C. J., Younan, N. D. & Viles, J. H. Cu²⁺ accentuates distinct misfolding of A beta((1-40)) and A beta((1-42)) peptides, and potentiates membrane disruption. *Biochem. J.* **466**, 233-242, doi:10.1042/bj20141168 (2015).
- 70 Ji, Z. S. *et al.* Apolipoprotein E4 potentiates amyloid beta peptide-induced lysosomal leakage and apoptosis in neuronal cells. *J. Biol. Chem.* **277**, 21821-21828, doi:10.1074/jbc.M112109200 (2002).
- 71 Sciacca, M. F. M. *et al.* Two-Step Mechanism of Membrane Disruption by A beta through Membrane Fragmentation and Pore Formation. *Biophys. J.* **103**, 702-710, doi:10.1016/j.bpj.2012.06.045 (2012).
- 72 Tofoleanu, F. & Buchete, N. V. Molecular Interactions of Alzheimer's A beta Protofilaments with Lipid Membranes. *J. Mol. Biol.* **421**, 572-586, doi:10.1016/j.jmb.2011.12.063 (2012).
- 73 Friedman, R., Pellarin, R. & Caflich, A. Amyloid Aggregation on Lipid Bilayers and Its Impact on Membrane Permeability. *J. Mol. Biol.* **387**, 407-415, doi:10.1016/j.jmb.2008.12.036 (2009).
- 74 Demuro, A. *et al.* Calcium dysregulation and membrane disruption as a ubiquitous neurotoxic mechanism of soluble amyloid oligomers. *J. Biol. Chem.* **280**, 17294-17300, doi:10.1074/jbc.M500997200 (2005).

- 75 Demuro, A., Smith, M. & Parker, I. Single-channel Ca²⁺ imaging implicates A beta 1-42 amyloid pores in Alzheimer's disease pathology. *J. Cell Biol.* **195**, 515-524, doi:10.1083/jcb.201104133 (2011).
- 76 Lacor, P. N. *et al.* Synaptic targeting by Alzheimer's-related amyloid beta oligomers. *J. Neurosci.* **24**, 10191-10200, doi:10.1523/jneurosci.3432-04.2004 (2004).
- 77 Walsh, D. M. *et al.* Naturally secreted oligomers of amyloid beta protein potently inhibit hippocampal long-term potentiation in vivo. *Nature* **416**, 535-539, doi:10.1038/416535a (2002).
- 78 Walsh, D. M., Tseng, B. P., Rydel, R. E., Podlisny, M. B. & Selkoe, D. J. The oligomerization of amyloid beta-protein begins intracellularly in cells derived from human brain. *Biochemistry* **39**, 10831-10839, doi:10.1021/bi001048s (2000).
- 79 Lauren, J., Gimbel, D. A., Nygaard, H. B., Gilbert, J. W. & Strittmatter, S. M. Cellular prion protein mediates impairment of synaptic plasticity by amyloid-beta oligomers. *Nature* **457**, 1128-U1184, doi:10.1038/nature07761 (2009).
- 80 Citron, M. *et al.* Mutation of the beta-amyloid precursor protein in familial alzheimers-disease increases beta-protein production. *Nature* **360**, 672-674, doi:10.1038/360672a0 (1992).
- 81 Gimbel, D. A. *et al.* Memory Impairment in Transgenic Alzheimer Mice Requires Cellular Prion Protein. *J. Neurosci.* **30**, 6367-6374, doi:10.1523/jneurosci.0395-10.2010 (2010).
- 82 Hu, N. W. *et al.* mGlu5 receptors and cellular prion protein mediate amyloid-beta-facilitated synaptic long-term depression in vivo. *Nat. Commun.* **5**, 13, doi:10.1038/ncomms4374 (2014).
- 83 Renner, M. *et al.* Deleterious Effects of Amyloid beta Oligomers Acting as an Extracellular Scaffold for mGluR5. *Neuron* **66**, 739-754, doi:10.1016/j.neuron.2010.04.029 (2010).
- 84 Salazar, S. V. & Strittmatter, S. M. Cellular prion protein as a receptor for amyloid-beta oligomers in Alzheimer's disease. *Biochem. Biophys. Res. Commun.* **483**, 1143-1147, doi:10.1016/j.bbrc.2016.09.062 (2017).
- 85 Shankar, G. M. *et al.* Natural oligomers of the Alzheimer amyloid-beta protein induce reversible synapse loss by modulating an NMDA-type glutamate receptor-dependent signaling pathway. *J. Neurosci.* **27**, 2866-2875, doi:10.1523/jneurosci.4970-06.2007 (2007).
- 86 Snyder, E. M. *et al.* Regulation of NMDA receptor trafficking by amyloid-beta. *Nat. Neurosci.* **8**, 1051-1058, doi:10.1038/nn1503 (2005).
- 87 Ferreira, I. L. *et al.* Amyloid beta peptide 1-42 disturbs intracellular calcium homeostasis through activation of GluN2B-containing N-methyl-D-aspartate receptors in cortical cultures. *Cell Calcium* **51**, 95-106, doi:10.1016/j.ceca.2011.11.008 (2012).
- 88 Kam, T. I., Gwon, Y. & Jung, Y. K. Amyloid beta receptors responsible for neurotoxicity and cellular defects in Alzheimer's disease. *Cell. Mol. Life Sci.* **71**, 4803-4813, doi:10.1007/s00018-014-1706-0 (2014).
- 89 Deane, R. *et al.* LRP/amyloid beta-peptide interaction mediates differential brain efflux of A beta isoforms. *Neuron* **43**, 333-344, doi:10.1016/j.neuron.2004.07.017 (2004).
- 90 Sagare, A. P., Deane, R. & Zlokovic, B. V. Low-density lipoprotein receptor-related protein 1: A physiological A beta homeostatic mechanism with multiple therapeutic opportunities. *Pharmacol. Ther.* **136**, 94-105, doi:10.1016/j.pharmthera.2012.07.008 (2012).
- 91 Deane, R., Wu, Z. H. & Zlokovic, B. V. RAGE (Yin) versus LRP (Yang) balance regulates Alzheimer amyloid beta-peptide clearance through transport across the blood-brain barrier. *Stroke* **35**, 2628-2631, doi:10.1161/01.STR.0000143452.85382.dl (2004).
- 92 Takuma, K. *et al.* RAGE-mediated signaling contributes to intraneuronal transport of amyloid-beta and neuronal dysfunction. *Proc. Natl. Acad. Sci. U. S. A.* **106**, 20021-20026, doi:10.1073/pnas.0905686106 (2009).

- 93 Simons, M. *et al.* Cholesterol depletion inhibits the generation of beta-amyloid in hippocampal neurons. *Proc. Natl. Acad. Sci. U. S. A.* **95**, 6460-6464, doi:10.1073/pnas.95.11.6460 (1998).
- 94 Kim, J., Basak, J. M. & Holtzman, D. M. The Role of Apolipoprotein E in Alzheimer's Disease. *Neuron* **63**, 287-303, doi:10.1016/j.neuron.2009.06.026 (2009).
- 95 Bhatia, N. & Hall, G. F. Untangling the role of tau in Alzheimer's disease: A unifying hypothesis. *Transl. Neurosci.* **4**, 115-133, doi:10.2478/s13380-013-0114-5 (2013).
- 96 Fitzpatrick, A. W. P. *et al.* Cryo-EM structures of tau filaments from Alzheimer's disease. *Nature* **547**, 185+, doi:10.1038/nature23002 (2017).
- 97 Xu, L., Zheng, J., Margittai, M., Nussinov, R. & Ma, B. Y. How Does Hyperphosphorylation Promote Tau Aggregation and Modulate Filament Structure and Stability? *ACS Chem. Neurosci.* **7**, 565-575, doi:10.1021/acschemneuro.5b00294 (2016).
- 98 Bennett, R. E. *et al.* Enhanced Tau Aggregation in the Presence of Amyloid beta. *Am. J. Pathol.* **187**, 1601-1612, doi:10.1016/j.ajpath.2017.03.011 (2017).
- 99 Bierer, L. M. *et al.* Neocortical neurofibrillary tangles correlate with dementia severity in alzheimers-disease. *Arch. Neurol.* **52**, 81-88, doi:10.1001/archneur.1995.00540250089017 (1995).
- 100 Bolmont, T. *et al.* Induction of tau pathology by intracerebral infusion of amyloid-beta-containing brain extract and by amyloid-beta deposition in APP x tau transgenic mice. *Am. J. Pathol.* **171**, 2012-2020, doi:10.2353/ajpath.2007.070403 (2007).
- 101 Hurtado, D. E. *et al.* A beta Accelerates the Spatiotemporal Progression of Tau Pathology and Augments Tau Amyloidosis in an Alzheimer Mouse Model. *Am. J. Pathol.* **177**, 1977-1988, doi:10.2353/ajpath.2010.100346 (2010).
- 102 Perez, M. *et al.* Characterization of a double (amyloid precursor protein-tau) transgenic: Tau phosphorylation and aggregation. *Neuroscience* **130**, 339-347, doi:10.1016/j.neuroscience.2004.09.029 (2005).
- 103 Ribe, E. M. *et al.* Accelerated amyloid deposition, neurofibrillary degeneration and neuronal loss in double mutant APP/tau transgenic mice. *Neurobiol. Dis.* **20**, 814-822, doi:10.1016/j.nbd.2005.05.027 (2005).
- 104 Saul, A., Sprenger, F., Bayer, T. A. & Wirths, O. Accelerated tau pathology with synaptic and neuronal loss in a novel triple transgenic mouse model of Alzheimer's disease. *Neurobiol. Aging* **34**, 2564-2573, doi:10.1016/j.neurobiolaging.2013.05.003 (2013).
- 105 Ittner, A. *et al.* Site-specific phosphorylation of tau inhibits amyloid-beta toxicity in Alzheimer's mice. *Science* **354**, 904-908, doi:10.1126/science.aah6205 (2016).
- 106 Kondo, T. *et al.* Modeling Alzheimer's Disease with iPSCs Reveals Stress Phenotypes Associated with Intracellular A beta and Differential Drug Responsiveness. *Cell Stem Cell* **12**, 487-496, doi:10.1016/j.stem.2013.01.009 (2013).
- 107 Oddo, S. *et al.* Triple-transgenic model of Alzheimer's disease with plaques and tangles: Intracellular A beta and synaptic dysfunction. *Neuron* **39**, 409-421, doi:10.1016/s0896-6273(03)00434-3 (2003).
- 108 Yu, C. J., Nwabuisi-Heath, E., Laxton, K. & LaDu, M. J. Endocytic pathways mediating oligomeric A beta 42 neurotoxicity. *Mol. Neurodegener.* **5**, 11, doi:10.1186/1750-1326-5-19 (2010).
- 109 Manczak, M. *et al.* Mitochondria are a direct site of A beta accumulation in Alzheimer's disease neurons: implications for free radical generation and oxidative damage in disease progression. *Hum. Mol. Genet.* **15**, 1437-1449, doi:10.1093/hmg/ddl066 (2006).
- 110 Demuro, A. & Parker, I. Cytotoxicity of Intracellular A beta(42) Amyloid Oligomers Involves Ca²⁺ Release from the Endoplasmic Reticulum by Stimulated Production of Inositol Trisphosphate. *J. Neurosci.* **33**, 3824-3833, doi:10.1523/jneurosci.4367-12.2013 (2013).

- 111 Strittmatter, W. J. *et al.* Apolipoprotein-e - high-avidity binding to beta-amyloid and increased frequency of type-4 allele in late-onset familial alzheimer-disease. *Proc. Natl. Acad. Sci. U. S. A.* **90**, 1977-1981, doi:10.1073/pnas.90.5.1977 (1993).
- 112 Wisniewski, T. & Frangione, B. Apolipoprotein-e - a pathological chaperone protein in patients with cerebral and systemic amyloid. *Neurosci. Lett.* **135**, 235-238, doi:10.1016/0304-3940(92)90444-c (1992).
- 113 Christensen, D. Z., Schneider-Axmann, T., Lucassen, P. J., Bayer, T. A. & Wirths, O. Accumulation of intraneuronal A beta correlates with ApoE4 genotype. *Acta Neuropathologica* **119**, 555-566, doi:10.1007/s00401-010-0666-1 (2010).
- 114 Puglielli, L., Tanzi, R. E. & Kovacs, D. M. Alzheimer's disease: the cholesterol connection. *Nat. Neurosci.* **6**, 345-351, doi:10.1038/nn0403-345 (2003).
- 115 Refolo, L. M. *et al.* Hypercholesterolemia accelerates the Alzheimer's amyloid pathology in a transgenic mouse model. *Neurobiol. Dis.* **7**, 321-331, doi:10.1006/nbdi.2000.0304 (2000).
- 116 Bodovitz, S. & Klein, W. L. Cholesterol modulates alpha-secretase cleavage of amyloid precursor protein. *J. Biol. Chem.* **271**, 4436-4440 (1996).
- 117 Abad-Rodriguez, J. *et al.* Neuronal membrane cholesterol loss enhances amyloid peptide generation. *J. Cell Biol.* **167**, 953-960, doi:10.1083/jcb.200404149 (2004).
- 118 Cordy, J. M., Hussain, I., Dingwall, C., Hooper, N. M. & Turner, A. J. Exclusively targeting beta-secretase to lipid rafts by GPI-anchor addition up-regulates beta-site processing of the amyloid precursor protein. *Proc. Natl. Acad. Sci. U. S. A.* **100**, 11735-11740, doi:10.1073/pnas.1635130100 (2003).
- 119 Fong, L. K. *et al.* Full-length amyloid precursor protein regulates lipoprotein metabolism and amyloid- clearance in human astrocytes. *J. Biol. Chem.* **293**, 11341-11357, doi:10.1074/jbc.RA117.000441 (2018).
- 120 Wood, W. G., Schroeder, F., Igbavboa, U., Avdulov, N. A. & Chochina, V. V. Brain membrane cholesterol domains, aging and amyloid beta-peptides. *Neurobiol. Aging* **23**, 685-694, doi:10.1016/s0197-4580(02)00018-0 (2002).
- 121 Subasinghe, S. *et al.* Cholesterol is necessary both for the toxic effect of A beta peptides on vascular smooth muscle cells and for A beta binding to vascular smooth muscle cell membranes. *J. Neurochem.* **84**, 471-479, doi:10.1046/j.1471-4159.2003.01552.x (2003).
- 122 Fernandez-Perez, E. J. *et al.* Effect of Cholesterol on Membrane Fluidity and Association of A beta Oligomers and Subsequent Neuronal Damage: A Double-Edged Sword. *Front. Aging Neurosci.* **10**, 14, doi:10.3389/fnagi.2018.00226 (2018).
- 123 Avdulov, N. A. *et al.* Lipid binding to amyloid beta-peptide aggregates: Preferential binding of cholesterol as compared with phosphatidylcholine and fatty acids. *J. Neurochem.* **69**, 1746-1752 (1997).
- 124 Fantini, J., Yahi, N. & Garmy, N. Cholesterol accelerates the binding of Alzheimer's beta-amyloid peptide to ganglioside GM1 through a universal hydrogen-bond-dependent sterol tuning of glycolipid conformation. *Front. Physiol.* **4**, 10, doi:10.3389/fphys.2013.00120 (2013).
- 125 Kakio, A., Nishimoto, S., Yanagisawa, K., Kozutsumi, Y. & Matsuzaki, K. Cholesterol-dependent formation of GM1 ganglioside-bound amyloid beta-protein, an endogenous seed for Alzheimer amyloid. *J. Biol. Chem.* **276**, 24985-24990, doi:10.1074/jbc.M100252200 (2001).
- 126 Opazo, C. *et al.* Metalloenzyme-like activity of Alzheimer's disease beta-amyloid - Cu-dependent catalytic conversion of dopamine, cholesterol, and biological reducing agents to neurotoxic H₂O₂. *J. Biol. Chem.* **277**, 40302-40308, doi:10.1074/jbc.M206428200 (2002).
- 127 Kakio, A., Nishimoto, S. I., Kozutsumi, Y. & Matsuzaki, K. Formation of a membrane-active form of amyloid beta-protein in raft-like model membranes. *Biochem. Biophys. Res. Commun.* **303**, 514-518, doi:10.1016/s0006-291x(03)00386-3 (2003).

- 128 Matsuzaki, K. How Do Membranes Initiate Alzheimer's Disease? Formation of Toxic Amyloid Fibrils by the Amyloid beta-Protein on Ganglioside Clusters. *Accounts Chem. Res.* **47**, 2397-2404, doi:10.1021/ar500127z (2014).
- 129 Okada, T., Ikeda, K., Wakabayashi, M., Ogawa, M. & Matsuzaki, K. Formation of toxic A beta(1-40) fibrils on GM1 ganglioside-containing membranes mimicking lipid rafts: Polymorphisms in A beta(1-40) fibrils. *J. Mol. Biol.* **382**, 1066-1074, doi:10.1016/j.jmb.2008.07.072 (2008).
- 130 Mozes, E., Hunya, A., Posa, A., Penke, B. & Datki, Z. A novel method for the rapid determination of beta-amyloid toxicity on acute hippocampal slices using MTT and LDH assays. *Brain Res. Bull.* **87**, 521-525, doi:10.1016/j.brainresbull.2012.02.005 (2012).
- 131 He, Y. *et al.* Soluble oligomers and fibrillar species of amyloid beta-peptide differentially affect cognitive functions and hippocampal inflammatory response. *Biochem. Biophys. Res. Commun.* **429**, 125-130, doi:10.1016/j.bbrc.2012.10.129 (2012).
- 132 Matsubara, T. *et al.* Size and Shape of Amyloid Fibrils Induced by Ganglioside Nanoclusters: Role of Sialyl Oligosaccharide in Fibril Formation. *Langmuir* **33**, 13874-13881, doi:10.1021/acs.langmuir.7b02091 (2017).
- 133 Matsubara, T. *et al.* Responsibility of lipid compositions for the amyloid beta assembly induced by ganglioside nanoclusters in mouse synaptosomal membranes. *Polym. J.* **50**, 745-752, doi:10.1038/s41428-018-0041-y (2018).
- 134 Chan, R. B. *et al.* Comparative Lipidomic Analysis of Mouse and Human Brain with Alzheimer Disease. *J. Biol. Chem.* **287**, 2678-2688, doi:10.1074/jbc.M111.274142 (2012).
- 135 Dong, X. W., Sun, Y. X., Wei, G. H., Nussinov, R. & Ma, B. Y. Binding of protofibrillar A beta trimers to lipid bilayer surface enhances A beta structural stability and causes membrane thinning. *Phys. Chem. Chem. Phys.* **19**, 27556-27569, doi:10.1039/c7cp05959k (2017).
- 136 Korshavn, K. J. *et al.* Reduced Lipid Bilayer Thickness Regulates the Aggregation and Cytotoxicity of Amyloid- beta. *J. Biol. Chem.* **292**, 4638-4650, doi:10.1074/jbc.M116.764092 (2017).
- 137 Kotler, S. A., Walsh, P., Brender, J. R. & Ramamoorthy, A. Differences between amyloid-beta aggregation in solution and on the membrane: insights into elucidation of the mechanistic details of Alzheimer's disease. *Chem. Soc. Rev.* **43**, 6692-6700, doi:10.1039/c3cs60431d (2014).
- 138 Butterfield, S. M. & Lashuel, H. A. Amyloidogenic Protein Membrane Interactions: Mechanistic Insight from Model Systems. *Angew. Chem.-Int. Edit.* **49**, 5628-5654, doi:10.1002/anie.200906670 (2010).
- 139 Sokolov Y, K. J., Kaye R, Chanturiya A, Glabe C, Hall JE. Soluble amyloid oligomers increase bilayer conductance by altering dielectric structure. *J Gen Physiol.* **6**, 637-647 (2006).
- 140 Sayre, L. M. *et al.* 4-hydroxynonenal-derived advanced lipid peroxidation end products are increased in Alzheimer's disease. *J. Neurochem.* **68**, 2092-2097 (1997).
- 141 Negre-Salvayre, A. *et al.* Pathological aspects of lipid peroxidation. *Free Radic. Res.* **44**, 1125-1171, doi:10.3109/10715762.2010.498478 (2010).
- 142 Beranova, L., Cwiklik, L., Jurkiewicz, P., Hof, M. & Jungwirth, P. Oxidation Changes Physical Properties of Phospholipid Bilayers: Fluorescence Spectroscopy and Molecular Simulations. *Langmuir* **26**, 6140-6144, doi:10.1021/la100657a (2010).
- 143 Perrin, R. J. *et al.* Identification and Validation of Novel Cerebrospinal Fluid Biomarkers for Staging Early Alzheimer's Disease. *PLoS One* **6**, 23, doi:10.1371/journal.pone.0016032 (2011).
- 144 Villarreal, A. *et al.* *Application of biomarkers to finding new drug therapies for treatment of Alzheimer's disease.* (OmniScience, 2014).
- 145 Potdar, P. D. & Shetti, A. U. Molecular Biomarkers for Diagnosis & Therapies of Alzheimer's Disease. *AIMS Neurosci.* **3**, 433-453, doi:10.3934/Neuroscience.2016.4.433 (2016).

- 146 Hansson, S. F. *et al.* Reduced Levels of Amyloid-beta-Binding Proteins in Cerebrospinal Fluid
from Alzheimer's Disease Patients. *J. Alzheimers Dis.* **16**, 389-397, doi:10.3233/jad-2009-
0966 (2009).
- 147 Kaeser, S. A. *et al.* Cystatin C modulates cerebral beta-amyloidosis. *Nature Genet.* **39**, 1437-
1439, doi:10.1038/ng.2007.23 (2007).
- 148 Mi, W. *et al.* Cystatin C inhibits amyloid-beta deposition in Alzheimer's disease mouse
models. *Nature Genet.* **39**, 1440-1442, doi:10.1038/ng.2007.29 (2007).
- 149 Crawford, F. C. *et al.* A polymorphism in the cystatin C gene is a novel risk factor for late-
onset Alzheimer's disease. *Neurology* **55**, 763-768, doi:10.1212/wnl.55.6.763 (2000).
- 150 Finckh, U. *et al.* Genetic association of a cystatin C gene polymorphism with late-onset
Alzheimer disease. *Arch. Neurol.* **57**, 1579-1583, doi:10.1001/archneur.57.11.1579 (2000).
- 151 Deng, A., Irizarry, M. C., Nitsch, R. M., Growdon, J. H. & Rebeck, G. W. Elevation of cystatin C
in susceptible neurons in Alzheimer's disease. *Am. J. Pathol.* **159**, 1061-1068,
doi:10.1016/s0002-9440(10)61781-6 (2001).
- 152 Nagai, A., Ryu, J. K., Kobayashi, S. & Kim, S. U. in *Alzheimer's Disease: Vascular Etiology and
Pathology* Vol. 977 *Annals of the New York Academy of Sciences* (eds J. C. DeLaTorre, R.
Kalaria, K. Nakajima, & K. Nagata) 315-321 (New York Acad Sciences, 2002).
- 153 Tizon, B., Ribe, E. M., Mi, W. Q., Troy, C. M. & Levy, E. Cystatin C Protects Neuronal Cells
from Amyloid-beta-induced Toxicity. *J. Alzheimers Dis.* **19**, 885-894, doi:10.3233/jad-2010-
1291 (2010).
- 154 Sastre, M. *et al.* Binding of cystatin C to Alzheimer's amyloid beta inhibits in vitro amyloid
fibril formation. *Neurobiol. Aging* **25**, 1033-1043, doi:10.1016/j.neurobiolaging.2003.11.006
(2004).
- 155 Ghidoni, R. *et al.* Cystatin C is released in association with exosomes: A new tool of neuronal
communication which is unbalanced in Alzheimer's disease. *Neurobiol. Aging* **32**, 1435-1442,
doi:10.1016/j.neurobiolaging.2009.08.013 (2011).
- 156 Perlenfein, T. J. & Murphy, R. M. Expression, purification, and characterization of human
cystatin C monomers and oligomers. *Protein Expr. Purif.* **117**, 35-43,
doi:10.1016/j.pep.2015.09.023 (2016).
- 157 Perlenfein, T. J., Mehlhoff, J. D. & Murphy, R. M. Insights into the mechanism of cystatin C
oligomer and amyloid formation and its interaction with beta-amyloid. *J. Biol. Chem.* **292**,
11485-11498, doi:10.1074/jbc.M117.786558 (2017).
- 158 Otzen, D. E. Protein unfolding in detergents: Effect of micelle structure, ionic strength, pH,
and temperature. *Biophys. J.* **83**, 2219-2230, doi:10.1016/s0006-3495(02)73982-9 (2002).
- 159 Williams, A. *Cystatin C and Alzheimer's disease* Doctor of Philosophy thesis, University of
Sheffield, (2014).
- 160 Selenica, M. L., Wang, X., Ostergaard-Pedersen, L., Westlind-Danielsson, A. & Grubb, A.
Cystatin C reduces the in vitro formation of soluble A beta 1-42 oligomers and protofibrils.
Scand. J. Clin. Lab. Invest. **67**, 179-190, doi:10.1080/00365510601009738 (2007).
- 161 Staniforth, R. (2018).
- 162 Al-Jaff, S. *Natural modulators of amyloid formation in Alzheimer's disease* Doctor of
Philosophy thesis, University of Sheffield, (2016).
- 163 Yanagisawa, K. GM1 ganglioside and Alzheimer's disease. *Glycoconjugate J.* **32**, 87-91,
doi:10.1007/s10719-015-9579-5 (2015).
- 164 Sambrook, J., Fritsch, E. F. & Maniatis, T. Vol. vols. 1 2 and 3. (1989).
- 165 Postnova. *AF2000 AT - Ambient Temperature Flow FFF*, 2018).
- 166 Carlred, L. *et al.* Simultaneous Imaging of Amyloid-beta and Lipids in Brain Tissue Using
Antibody-Coupled Liposomes and Time-of-Flight Secondary Ion Mass Spectrometry. *J. Am.
Chem. Soc.* **136**, 9973-9981, doi:10.1021/ja5019145 (2014).
- 167 Mao, Y. L. *et al.* Surface-induced phase separation of a
sphingomyelin/cholesterol/ganglioside GM1-planar bilayer on mica surfaces and

- microdomain molecular conformation that accelerates A beta oligomerization. *Biochim. Biophys. Acta-Biomembr.* **1798**, 1090-1099, doi:10.1016/j.bbamem.2010.03.003 (2010).
- 168 Matsuzaki, K., Kato, K. & Yanagisawa, K. A beta polymerization through interaction with membrane gangliosides. *Biochim. Biophys. Acta Mol. Cell Biol. Lipids* **1801**, 868-877, doi:10.1016/j.bbalip.2010.01.008 (2010).
- 169 Relini, A., Marano, N. & Gliozzi, A. Probing the interplay between amyloidogenic proteins and membranes using lipid monolayers and bilayers. *Adv. Colloid Interface Sci.* **207**, 81-92, doi:10.1016/j.cis.2013.10.015 (2014).
- 170 Williams, T. L., Day, I. J. & Serpell, L. C. The Effect of Alzheimer's A beta Aggregation State on the Permeation of Biomimetic Lipid Vesicles. *Langmuir* **26**, 17260-17268, doi:10.1021/la101581g (2010).
- 171 Sciacca, M. F. M., Monaco, I., La Rosa, C. & Milardi, D. The active role of Ca²⁺ ions in Ab-mediated membrane damage. *Chem. Commun.* **54**, 3629-3631, doi:10.1039/c8cc01132j (2018).
- 172 Lockhart, C. & Klimov, D. K. Cholesterol Changes the Mechanisms of A beta Peptide Binding to the DMPC Bilayer. *J. Chem Inf. Model.* **57**, 2554-2565, doi:10.1021/acs.jcim.7b00431 (2017).
- 173 Arispe, N. Architecture of the Alzheimer's A beta P ion channel pore. *J. Membr. Biol.* **197**, 33-48, doi:10.1007/s00232-003-0638-7 (2004).
- 174 Kandel, N., Zheng, T. Y., Huo, Q. & Tatulian, S. A. Membrane Binding and Pore Formation by a Cytotoxic Fragment of Amyloid beta Peptide. *J. Phys. Chem. B* **121**, 10293-10305, doi:10.1021/acs.jpcc.7b07002 (2017).
- 175 Yanagisawa, K. Pathological significance of ganglioside clusters in Alzheimer's disease. *J. Neurochem.* **116**, 806-812, doi:10.1111/j.1471-4159.2010.07006.x (2011).
- 176 Yu, X., Wang, Q. M., Pan, Q. F., Zhou, F. M. & Zheng, J. Molecular interactions of Alzheimer amyloid-beta oligomers with neutral and negatively charged lipid bilayers. *Phys. Chem. Chem. Phys.* **15**, 8878-8889, doi:10.1039/c3cp44448a (2013).
- 177 Sarell, C. J., Wilkinson, S. R. & Viles, J. H. Substoichiometric Levels of Cu²⁺ Ions Accelerate the Kinetics of Fiber Formation and Promote Cell Toxicity of Amyloid-beta from Alzheimer Disease. *J. Biol. Chem.* **285**, 41533-41540, doi:10.1074/jbc.M110.171355 (2010).
- 178 Cohen, S. I. A., Vendruscolo, M., Dobson, C. M. & Knowles, T. P. J. From Macroscopic Measurements to Microscopic Mechanisms of Protein Aggregation. *J. Mol. Biol.* **421**, 160-171, doi:10.1016/j.jmb.2012.02.031 (2012).
- 179 Eden, K., Morris, R., Gillam, J., MacPhee, C. E. & Allen, R. J. Competition between Primary Nucleation and Autocatalysis in Amyloid Fibril Self-Assembly. *Biophys. J.* **108**, 632-643, doi:10.1016/j.bpj.2014.11.3465 (2015).
- 180 Choi, S. H. *et al.* in *Stem Cell Technologies in Neuroscience* Vol. 126 *Neuromethods* (eds A. K. Srivastava, E. Y. Snyder, & Y. D. Teng) 1-18 (Humana Press Inc, 2017).
- 181 Eimer, W. A. *et al.* Alzheimer's Disease-Associated beta-Amyloid Is Rapidly Seeded by Herpesviridae to Protect against Brain Infection. *Neuron* **99**, 56+, doi:10.1016/j.neuron.2018.06.030 (2018).
- 182 Hellstrand, E., Sparr, E. & Linse, S. Retardation of A beta Fibril Formation by Phospholipid Vesicles Depends on Membrane Phase Behavior. *Biophys. J.* **98**, 2206-2214, doi:10.1016/j.bpj.2010.01.063 (2010).
- 183 Jean, L., Lee, C. F. & Vaux, D. J. Enrichment of Amyloidogenesis at an Air-Water Interface. *Biophys. J.* **102**, 1154-1162, doi:10.1016/j.bpj.2012.01.041 (2012).
- 184 Milanesi, L. *et al.* Direct three-dimensional visualization of membrane disruption by amyloid fibrils. *Proc. Natl. Acad. Sci. U. S. A.* **109**, 20455-20460, doi:10.1073/pnas.1206325109 (2012).

- 185 Habchi, J. *et al.* Cholesterol catalyses A beta 42 aggregation through a heterogeneous nucleation pathway in the presence of lipid membranes. *Nat. Chem.* **10**, 673-683, doi:10.1038/s41557-018-0031-x (2018).
- 186 Sackmann, E. Supported membranes: Scientific and practical applications. *Science* **271**, 43-48, doi:10.1126/science.271.5245.43 (1996).
- 187 Suresh, S. Biomechanics and biophysics of cancer cells. *Acta Biomater.* **3**, 413-438, doi:10.1016/j.actbio.2007.04.002 (2007).
- 188 Yang, X. G., Askarova, S. & Lee, J. C. M. Membrane Biophysics and Mechanics in Alzheimer's Disease. *Mol. Neurobiol.* **41**, 138-148, doi:10.1007/s12035-010-8121-9 (2010).
- 189 Sturgis, J. N., Tucker, J. D., Olsen, J. D., Hunter, C. N. & Niederman, R. A. Atomic Force Microscopy Studies of Native Photosynthetic Membranes. *Biochemistry* **48**, 3679-3698, doi:10.1021/bi900045x (2009).
- 190 Zhang, Y. M. & Rock, C. O. Membrane lipid homeostasis in bacteria. *Nat. Rev. Microbiol.* **6**, 222-233, doi:10.1038/nrmicro1839 (2008).
- 191 Prenner, E. J., Lewis, R. & McElhaney, R. N. The interaction of the antimicrobial peptide Gramicidin S with lipid bilayer model and biological membranes. *Biochim. Biophys. Acta-Biomembr.* **1462**, 201-221, doi:10.1016/s0005-2736(99)00207-2 (1999).
- 192 Koch, A. L. The biophysics of the gram-negative periplasmic space. *Crit. Rev. Microbiol.* **24**, 23-59, doi:10.1080/10408419891294172 (1998).
- 193 Lombard, J. Once upon a time the cell membranes: 175 years of cell boundary research. *Biol. Direct* **9**, 35, doi:10.1186/s13062-014-0032-7 (2014).
- 194 Simons, K. & Ikonen, E. Functional rafts in cell membranes. *Nature* **387**, 569-572, doi:10.1038/42408 (1997).
- 195 Simons, K. & Gerl, M. J. Revitalizing membrane rafts: new tools and insights. *Nat. Rev. Mol. Cell Biol.* **11**, 688-699, doi:10.1038/nrm2977 (2010).
- 196 Bliss, T. V. P. & Collingridge, G. L. A SYNAPTIC MODEL OF MEMORY - LONG-TERM POTENTIATION IN THE HIPPOCAMPUS. *Nature* **361**, 31-39, doi:10.1038/361031a0 (1993).
- 197 van Meer, G., Voelker, D. R. & Feigenson, G. W. Membrane lipids: where they are and how they behave. *Nat. Rev. Mol. Cell Biol.* **9**, 112-124, doi:10.1038/nrm2330 (2008).
- 198 Simons, K. & Vaz, W. L. C. Model systems, lipid rafts, and cell membranes. *Annu. Rev. Biophys. Biomolec. Struct.* **33**, 269-295, doi:10.1146/annurev.biophys.32.110601.141803 (2004).
- 199 Esterbauer, H., Gebicki, J., Puhl, H. & Jurgens, G. THE ROLE OF LIPID-PEROXIDATION AND ANTIOXIDANTS IN OXIDATIVE MODIFICATION OF LDL. *Free Radic. Biol. Med.* **13**, 341-390, doi:10.1016/0891-5849(92)90181-f (1992).
- 200 Dathe, M. *et al.* Peptide helicity and membrane surface charge modulate the balance of electrostatic and hydrophobic interactions with lipid bilayers and biological membranes. *Biochemistry* **35**, 12612-12622, doi:10.1021/bi960835f (1996).
- 201 Garrigues, A., Nugier, J., Orłowski, S. & Ezan, E. A high-throughput screening microplate test for the interaction of drugs with P-glycoprotein. *Anal. Biochem.* **305**, 106-114, doi:10.1006/abio.2002.5650 (2002).
- 202 Magalhaes, L. M. *et al.* High-throughput microplate assay for the determination of drug partition coefficients. *Nat. Protoc.* **5**, 1823-1830, doi:10.1038/nprot.2010.137 (2010).
- 203 Hong, S. P. *et al.* Interaction of poly(amidoamine) dendrimers with supported lipid bilayers and cells: Hole formation and the relation to transport. *Bioconjugate Chem.* **15**, 774-782, doi:10.1021/bc049962b (2004).
- 204 Tamm, L. K. & Tatulian, S. A. Infrared spectroscopy of proteins and peptides in lipid bilayers. *Q. Rev. Biophys.* **30**, 365-429, doi:10.1017/s0033583597003375 (1997).
- 205 Richter, R. P. & Brisson, A. R. Following the formation of supported lipid bilayers on mica: A study combining AFM, QCM-D, and ellipsometry. *Biophys. J.* **88**, 3422-3433, doi:10.1529/biophysj.104.053728 (2005).

- 206 Cremer, P. S. & Boxer, S. G. Formation and spreading of lipid bilayers on planar glass supports. *J. Phys. Chem. B* **103**, 2554-2559, doi:10.1021/jp983996x (1999).
- 207 Keller, C. A. & Kasemo, B. Surface specific kinetics of lipid vesicle adsorption measured with a quartz crystal microbalance. *Biophys. J.* **75**, 1397-1402 (1998).
- 208 Mennicke, U. & Salditt, T. Preparation of solid-supported lipid bilayers by spin-coating. *Langmuir* **18**, 8172-8177, doi:10.1021/la025863f (2002).
- 209 Naumann, C. A. *et al.* The polymer-supported phospholipid bilayer: Tethering as a new approach to substrate-membrane stabilization. *Biomacromolecules* **3**, 27-35, doi:10.1021/bm0100211 (2002).
- 210 Dufrene, Y. F. & Lee, G. U. Advances in the characterization of supported lipid films with the atomic force microscope. *Biochim. Biophys. Acta-Biomembr.* **1509**, 14-41, doi:10.1016/s0005-2736(00)00346-1 (2000).
- 211 Terrettaz, S., Stora, T., Duschl, C. & Vogel, H. PROTEIN-BINDING TO SUPPORTED LIPID-MEMBRANES - INVESTIGATION OF THE CHOLERA-TOXIN GANGLIOSIDE INTERACTION BY SIMULTANEOUS IMPEDANCE SPECTROSCOPY AND SURFACE-PLASMON RESONANCE. *Langmuir* **9**, 1361-1369, doi:10.1021/la00029a033 (1993).
- 212 Mariappan, M. *et al.* A ribosome-associating factor chaperones tail-anchored membrane proteins. *Nature* **466**, 1120-U1138, doi:10.1038/nature09296 (2010).
- 213 Gowrishankar, K. *et al.* Active Remodeling of Cortical Actin Regulates Spatiotemporal Organization of Cell Surface Molecules. *Cell* **149**, 1353-1367, doi:10.1016/j.cell.2012.05.008 (2012).
- 214 Blobel, C. P. Adams: Key components in EGFR signalling and development. *Nat. Rev. Mol. Cell Biol.* **6**, 32-43, doi:10.1038/nrm1548 (2005).
- 215 Moradpour, D. & Penin, F. in *Hepatitis C Virus: From Molecular Virology to Antiviral Therapy* Vol. 369 *Current Topics in Microbiology and Immunology* (ed R. Bartenschlager) 113-142 (Springer-Verlag Berlin, 2013).
- 216 Falanga, A. *et al.* Biophysical Characterization and Membrane Interaction of the Two Fusion Loops of Glycoprotein B from Herpes Simplex Type I Virus. *PLoS One* **7**, 15, doi:10.1371/journal.pone.0032186 (2012).
- 217 Hardy, G. J., Nayak, R. & Zauscher, S. Model cell membranes: Techniques to form complex biomimetic supported lipid bilayers via vesicle fusion. *Curr. Opin. Colloid Interface Sci.* **18**, 448-458, doi:10.1016/j.cocis.2013.06.004 (2013).
- 218 Lind, T. K. & Cardenas, M. Understanding the formation of supported lipid bilayers via vesicle fusion-A case that exemplifies the need for the complementary method approach (Review). *Biointerphases* **11**, 12, doi:10.1116/1.4944830 (2016).
- 219 Merritt, E. A. *et al.* CRYSTAL-STRUCTURE OF CHOLERA-TOXIN B-PENTAMER BOUND TO RECEPTOR G(M1) PENTASACCHARIDE. *Protein Sci.* **3**, 166-175 (1994).
- 220 Abrami, L., Liu, S. H., Cosson, P., Leppla, S. H. & van der Goot, F. G. Anthrax toxin triggers endocytosis of its receptor via a lipid raft-mediated clathrin-dependent process. *J. Cell Biol.* **160**, 321-328, doi:10.1083/jcb.200211018 (2003).
- 221 Heath, G. R. *et al.* Layer-by-Layer Assembly of Supported Lipid Bilayer Poly-L-Lysine Multilayers. *Biomacromolecules* **17**, 324-335, doi:10.1021/acs.biomac.5b01434 (2016).
- 222 Dana Craig Bookbinder, E. J. F., Jr. James Arthur Griffin, Frances M. Smith, David L. Tennent Low protein-binding polymer product produced using low HLB number non-ionic surfactant. USA patent (1996).
- 223 LeVine, H. Quantification of beta-sheet amyloid fibril structures with thioflavin T. *Methods Enzymol.* **309**, 274-284 (1999).
- 224 Hsiao, K. *et al.* Correlative memory deficits, A beta elevation, and amyloid plaques in transgenic mice. *Science* **274**, 99-102, doi:10.1126/science.274.5284.99 (1996).
- 225 Phillips, R., Kondev, J., Theriot, J., Garcia, H. G. *Physical Biology of the Cell*. 2 edn, 31 (Garland Science, Taylor and Francis Group, LLC, 2013).

- 226 Dimitrievski, K. & Kasemo, B. Simulations of lipid transfer between a supported lipid bilayer and adsorbing vesicles. *Colloid Surf. B-Biointerfaces* **75**, 454-465, doi:10.1016/j.colsurfb.2009.09.019 (2010).
- 227 Kunze, A., Svedhem, S. & Kasemo, B. Lipid Transfer between Charged Supported Lipid Bilayers and Oppositely Charged Vesicles. *Langmuir* **25**, 5146-5158, doi:10.1021/la802758h (2009).
- 228 Drazenovic, J., Ahmed, S., Tuzinkiewicz, N. M. & Wunder, S. L. Lipid Exchange and Transfer on Nanoparticle Supported Lipid Bilayers: Effect of Defects, Ionic Strength, and Size. *Langmuir* **31**, 721-731, doi:10.1021/la503967m (2015).
- 229 Jang, H. *et al.* in *Protein Amyloid Aggregation: Methods and Protocols* Vol. 1345 *Methods in Molecular Biology* (ed D. Eliezer) 251-268 (Humana Press Inc, 2016).
- 230 Canale, C. *et al.* Different effects of Alzheimer's peptide A beta(1-40) oligomers and fibrils on supported lipid membranes. *Biophys. Chem.* **182**, 23-29, doi:10.1016/j.bpc.2013.07.010 (2013).
- 231 Biancalana, M. & Koide, S. Molecular mechanism of Thioflavin-T binding to amyloid fibrils. *BBA-Proteins Proteomics* **1804**, 1405-1412, doi:10.1016/j.bbapap.2010.04.001 (2010).
- 232 Yip, C. M., Elton, E. A., Darabie, A. A., Morrison, M. R. & McLaurin, J. Cholesterol, a modulator of membrane-associated A beta-fibrillogenesis and neurotoxicity. *J. Mol. Biol.* **311**, 723-734, doi:10.1006/jmbi.2001.4881 (2001).
- 233 Simons, M., Keller, P., Dichgans, J. & Schulz, J. B. Cholesterol and Alzheimer's disease - Is there a link? *Neurology* **57**, 1089-1093 (2001).
- 234 Williamson, M. P., Suzuki, Y., Bourne, N. T. & Asakura, T. Binding of amyloid beta-peptide to ganglioside micelles is dependent on histidine-13. *Biochem. J.* **397**, 483-490, doi:10.1042/bj20060293 (2006).
- 235 Williams, T. L. & Serpell, L. C. Membrane and surface interactions of Alzheimer's A beta peptide - insights into the mechanism of cytotoxicity. *Febs J.* **278**, 3905-3917, doi:10.1111/j.1742-4658.2011.08228.x (2011).
- 236 Bucciantini, M. *et al.* Toxic effects of amyloid fibrils on cell membranes: the importance of ganglioside GM1. *Faseb J.* **26**, 818-831, doi:10.1096/fj.11-189381 (2012).
- 237 Thomaier, M. *et al.* High-Affinity Binding of Monomeric but Not Oligomeric Amyloid-beta to Ganglioside GM1 Containing Nanodiscs. *Biochemistry* **55**, 6662-6672, doi:10.1021/acs.biochem.6b00829 (2016).
- 238 Nicolson, G. L. The Fluid-Mosaic Model of Membrane Structure: Still relevant to understanding the structure, function and dynamics of biological membranes after more than 40 years. *Biochim. Biophys. Acta-Biomembr.* **1838**, 1451-1466, doi:10.1016/j.bbamem.2013.10.019 (2014).
- 239 Cohen, S. I. A. *et al.* Nucleated polymerization with secondary pathways. I. Time evolution of the principal moments. *J. Chem. Phys.* **135**, 16, doi:10.1063/1.3608916 (2011).
- 240 Wang, X. F. *et al.* Cystatin C Shifts APP Processing from Amyloid-beta Production towards Non-Amyloidgenic Pathway in Brain Endothelial Cells. *PLoS One* **11**, 16, doi:10.1371/journal.pone.0161093 (2016).
- 241 Grigolato, F., Colonabo, C., Ferrari, R., Rezabkova, L. & Arosio, P. Mechanistic Origin of the Combined Effect of Surfaces and Mechanical Agitation on Amyloid Formation. *ACS Nano* **11**, 11358-11367, doi:10.1021/acsnano.7b05895 (2017).
- 242 Selkoe, D. J. Alzheimer's disease: Genes, proteins, and therapy. *Physiol. Rev.* **81**, 741-766 (2001).
- 243 Lorenzo, A. & Yankner, B. A. BETA-AMYLOID NEUROTOXICITY REQUIRES FIBRIL FORMATION AND IS INHIBITED BY CONGO RED. *Proc. Natl. Acad. Sci. U. S. A.* **91**, 12243-12247, doi:10.1073/pnas.91.25.12243 (1994).

- 244 Naslund, J. *et al.* Correlation between elevated levels of amyloid beta-peptide in the brain and cognitive decline. *JAMA-J. Am. Med. Assoc.* **283**, 1571-1577, doi:10.1001/jama.283.12.1571 (2000).
- 245 Sakono, M. & Zako, T. Amyloid oligomers: formation and toxicity of A beta oligomers. *Febs J.* **277**, 1348-1358, doi:10.1111/j.1742-4658.2010.07568.x (2010).
- 246 Caughey, B. & Lansbury, P. T. Protofibrils, pores, fibrils, and neurodegeneration: Separating the responsible protein aggregates from the innocent bystanders. *Annu. Rev. Neurosci.* **26**, 267-298, doi:10.1146/annurev.neuro.26.010302.081142 (2003).
- 247 Bucciantini, M. *et al.* Prefibrillar amyloid protein aggregates share common features of cytotoxicity. *J. Biol. Chem.* **279**, 31374-31382, doi:10.1074/jbc.M400348200 (2004).
- 248 Stefani, M. Biochemical and biophysical features of both oligomer/fibril and cell membrane in amyloid cytotoxicity. *Febs J.* **277**, 4602-4613, doi:10.1111/j.1742-4658.2010.07889.x (2010).
- 249 Qiang, W., Yau, W. M., Lu, J. X., Collinge, J. & Tycko, R. Structural variation in amyloid-beta fibrils from Alzheimer's disease clinical subtypes. *Nature* **541**, 217-+, doi:10.1038/nature20814 (2017).
- 250 Lu, J. X. *et al.* Molecular Structure of beta-Amyloid Fibrils in Alzheimer's Disease Brain Tissue. *Cell* **154**, 1257-1268, doi:10.1016/j.cell.2013.08.035 (2013).
- 251 Paravastu, A. K., Qahwash, I., Leapman, R. D., Meredith, S. C. & Tycko, R. Seeded growth of beta-amyloid fibrils from Alzheimer's brain-derived fibrils produces a distinct fibril structure. *Proc. Natl. Acad. Sci. U. S. A.* **106**, 7443-7448, doi:10.1073/pnas.0812033106 (2009).
- 252 Onsager, L. & Samaras, N. N. T. The Surface Tension of Debye-Huckel Electrolytes. *J. Chem. Phys.* **2**, 9, doi:10.1063/1.1749522 (1934).
- 253 Necas, D. & Klapetek, P. Gwyddion: an open-source software for SPM data analysis. *Cent. Eur. J. Phys.* **10**, 181-188, doi:10.2478/s11534-011-0096-2 (2012).
- 254 Hill, T. L. Length dependence of rate constants for end-to-end association and dissociation of equilibrium linear aggregates. *Biophys. J.* **44**, 285-288, doi:10.1016/s0006-3495(83)84301-x (1983).
- 255 Moores, B., Drolle, E., Attwood, S. J., Simons, J. & Leonenko, Z. Effect of Surfaces on Amyloid Fibril Formation. *PLoS One* **6**, 8, doi:10.1371/journal.pone.0025954 (2011).
- 256 Bouchiat, C. *et al.* Estimating the persistence length of a worm-like chain molecule from force-extension measurements. *Biophys. J.* **76**, 409-413, doi:10.1016/s0006-3495(99)77207-3 (1999).
- 257 Knowles, T. P. *et al.* Role of intermolecular forces in defining material properties of protein nanofibrils. *Science* **318**, 1900-1903, doi:10.1126/science.1150057 (2007).
- 258 Wood, S. J., MacKenzie, L., Maleeff, B., Hurle, M. R. & Wetzel, R. Selective inhibition of A beta fibril formation. *J. Biol. Chem.* **271**, 4086-4092 (1996).
- 259 Zhang, Y. *et al.* Morphology and structural dynamics of amyloid beta 42 assembly in vitro. *Neural Regen. Res.* **6**, 335-339, doi:10.3969/j.issn.1673-5374.2011.05.003 (2011).
- 260 O'Nuallain, B. *et al.* Amyloid beta-Protein Dimers Rapidly Form Stable Synaptotoxic Protofibrils. *J. Neurosci.* **30**, 14411-14419, doi:10.1523/jneurosci.3537-10.2010 (2010).
- 261 Taylor, A., Aubrey, L. D., Davis, P. & Staniforth, R. AF4 insights into the preparation of monomeric beta amyloid peptide. (manuscript in preparation).
- 262 Sabate, R. & Estelrich, J. Evidence of the existence of micelles in the fibrillogenesis of beta-amyloid peptide. *J. Phys. Chem. B* **109**, 11027-11032, doi:10.1021/jp050716m (2005).
- 263 Bone, C. *The Effect of Salt on the Structure and Formation of Amyloid-β (1-42) fibrils* MBiolSci Biochemistry and Genetics thesis, University of Sheffield, (2018).
- 264 Munro, J. C. & Frank, C. W. In situ formation and characterization of poly(ethylene glycol)-supported lipid bilayers on gold surfaces. *Langmuir* **20**, 10567-10575, doi:10.1021/la048378o (2004).

265 Sun, B. G. *et al.* Cystatin C-Cathepsin B Axis Regulates Amyloid Beta Levels and Associated Neuronal Deficits in an Animal Model of Alzheimer's Disease. *Neuron* **60**, 247-257, doi:10.1016/j.neuron.2008.10.001 (2008).